Allosteric Regulation and Functional Dynamics of CRY1 in the Mammalian Circadian Clock: Insights from Mutational and Small Molecule Interactions

by

ONUR ÖZCAN

A Dissertation Submitted to
the Graduate School of Sciences and Engineering
in Partial Fulfillment of the Requirements for
the Degree of

Doctor of Philosophy

in

Molecular Biology and Genetics

KOÇ ÜNİVERSİTESİ

January 20, 2025

Allosteric Regulation and Functional Dynamics of CRY1 in the Mammalian Circadian Clock: Insights from Mutational and Small Molecule Interactions

Koç University

Graduate School of Sciences and Engineering

This is to certify that I have examined this copy of a doctoral dissertation by

ONUR ÖZCAN

and have found that it is complete and satisfactory in all respects, and that any and all revisions required by the final examining committee have been made.

Committee Members:

Prof. İbrahim Halil Kavaklı (Advisor)

Prof. Nuri Öztürk

Prof. Mahmut Çalışkan

Asst Prof. Onur Öztaş

Asst.Prof. Serkan Kır

Date: **20.01.2025**

To my beloved family and
everyone who has been in this journey with me

ABSTRACT

Allosteric Regulation and Functional Dynamics of CRY1 in the Mammalian Circadian Clock: Insights from Mutational and Small Molecule Interactions

ONUR ÖZCAN

Doctor of Philosophy in Molecular Biology and Genetics

January 20, 2025

Cryptochromes (CRYs) are essential components of the molecular clock that governs circadian rhythms in mammals, functioning as inhibitors of BMAL1/CLOCK-driven transcription. While mammals possess two CRYs with distinct roles in the circadian clock, the mechanisms underlying their differential functions remain unclear. This study elucidates how a specific mutation in CRY1 allosterically alters its dynamic behavior. Molecular dynamics simulations were conducted on eight CRY1 mutants experimentally shown to exhibit reduced repressor activity. My findings reveal that mutations in CRY1 affect the dynamic behavior of the serine loop and the accessibility of the secondary pocket, changes not observed in CRY2. Further analysis highlights that the flexibility of the serine loop influences secondary pocket volume, with S44 and S45 playing crucial roles through their interactions with E382. Additionally, I explored the potential for small molecules to modulate CRY1 allosterically, demonstrating both in silico and in vitro that this regulation impacts CRY1's affinity to CLOCK. This discovery provides a promising avenue for developing therapeutics targeting CRY1, though it also raises concerns about unforeseen side effects of existing small molecules. To address this, virtual screening was performed to identify compounds targeting the CRY1 secondary pocket. Subsequent phenotypic analysis revealed five distinct effects on circadian rhythm, underscoring the complexity of this regulatory mechanism. This study offers critical insights into CRY1 dynamics, its interaction with CLOCK, and the potential for small-molecule modulation, paving the way for advancements in circadian biology and drug design.

ÖZETÇE

Targeting mammalian cryptochromes at their secondary pocket

ONUR ÖZCAN

Mooleküler Biyoloji ve Genetik, Doktora

January 20, 2025

Kriptokromlar (CRY'ler), memelilerde sirkadiyen ritimleri yöneten moleküler saatin temel bileşenleridir ve BMAL1/CLOCK tarafından yönlendirilen transkripsiyonun inhibitörleri olarak işlev görürler. Memeliler sirkadiyen saatte farklı rollere sahip iki CRY'ye sahip olsalar da, farklı işlevlerinin altında yatan mekanizmalar hala belirsizliğini korumaktadır. Bu çalışma, CRY1'deki belirli bir mutasyonun dinamik davranışını allosterik olarak nasıl değiştirdiğini açıklamaktadır. Deneysel olarak azaltılmış represör aktivitesi gösterdiği gösterilen sekiz CRY1 mutantı üzerinde moleküler dinamik simülasyonları yürütülmüştür. Bulgularım, CRY1'deki mutasyonların serin döngüsünün dinamik davranışını ve ikincil cebin erişilebilirliğini etkilediğini, CRY2'de gözlemlenmeyen değişiklikleri ortaya koymaktadır. Daha ileri analizler, serin döngüsünün esnekliğinin ikincil cep hacmini etkilediğini, S44 ve S45'in E382 ile etkileşimleri yoluyla önemli roller oynadığını vurgulamaktadır. Ek olarak, küçük moleküllerin CRY1'i allosterik olarak modüle etme potansiyelini araştırdım ve hem silico hem de in vitro olarak bu düzenlemenin CRY1'in CLOCK'a olan afinitesini etkilediğini gösterdim. Bu keşif, CRY1'i hedef alan terapötikler geliştirmek için umut verici bir yol sağlıyor, ancak aynı zamanda mevcut küçük moleküllerin öngörülemeyen yan etkileri konusunda endişeleri de artırıyor. Bunu ele almak için, CRY1 ikincil cebini hedef alan bileşikleri belirlemek için sanal tarama yapıldı. Daha sonraki fenotipik analiz, sirkadiyen ritim üzerinde beş farklı etki ortaya koyarak bu düzenleyici mekanizmanın karmaşıklığını vurguluyor. Bu çalışma, CRY1 dinamikleri, CLOCK ile etkileşimi ve küçük molekül modülasyonu potansiyeli hakkında kritik içgörüler sunarak sirkadiyen biyoloji ve ilaç tasarımında ilerlemeler için yol açıyor.

ACKNOWLEDGMENTS

I would like to express my gratitude and thank my advisor, Prof. İ. Halil Kavaklı, for his invaluable mentoring and scientific contributions on my studies, as well as continuous support as a person on me. Over the course of seven years, I had a lot of opportunities learn and grow, both scientifically and mentally. This growth made me overcome many obstacles I faced throughout my thesis study. Without him, none of this would be possible.

I would like to thank my thesis committee members Prof. Nuri Öztürk and Asst Prof. Onur Öztaş for their support. Not only for their contributions, but also opening their laboratories to us whenever we are in need of help. I enjoyed my time while working at there. Without them, not only this study but many would have struggle. I, also, would like to thank Prof. Mahmut Çalışkan and Asst. Prof. Serkan Kır for accepting to be in my thesis jury.

I would like to thank to KOÇ University and TUBITAK for their financial support. This study was supported by Tübitak 1001 122Z892.

I would like to thank Dr. İbrahim Barış and Assoc. Prof Şeref Gül. Their studies led to me to this thesis. Not only that, but also it was a joy to work with both. I learnt a lot from them in Kavaklı Lab.

I would like to thank Gizem Çağla Parlak and Elif Uyanık for their support and contributions to this study.

I would like to thank my family. They always believed in me and supported me through all these years. Figen, Zafer and Erdal Özcan, without you I couldn't carry out this study. Thank you for going through this with me.

I would like to thank all previous and current Kavaklı Lab members. It was a pleasure to work with you. Without you, this journey wouldn't be as adventurous. Barış, thank you for being amazing! It was the peak of amazingness the day you suit up. Melis, most likely no one else but you could have deal with the hardships you faced. Thank you for being an inspiring person and showing us the domain when we need it most. Gizem, you are joyful to a point that having a bad mood was challenging when you were around. Thank you singing for us when we want and even when we don't. Zeynep, it was pleasure to meet you and thank

you for everything. I hope one day we all can finish a movie before you fall asleep. Şafak, your unorthodox attitude towards the life was always heartwarming. I hope we can drink again one day while watching elections. Çisel, you are a great friend and the best colleague someone could ask for. I'll never forget the vegetable quiche; hope we can eat it again one day. Begüm, I really enjoyed working and hanging around with you. Thank you for your hospitality and dogs. And in my defense, that glass door was too clean. Bahar and Çağla, it was fun to work with you, lab meetings were never same without you. Onur and Ayşe, we couldn't work that long together but thank you for reminding me the old days of this lab again. Finally, I would like to thank Sticky's. Ayşegül and Erhan Batuk, thank you for welcoming me all these years. I truly appreciate it and felt at home. Without you, it would be a lot harder to deal with ups and downs of this journey.

TABLE OF CONTENTS

LIST OF FIGURES

LIST OF TABLES

CHAPTER 1
INTRODUCTION

In mammals, circadian clock is regulated by a transcriptional-translational feedback loop (TTFL). While the basic helix-loop-helix PER-ARNT-SIM (bHLH-PAS) domain-containing transcription factors BMAL1 and CLOCK heterodimer drives transcription of clock-controlled genes by binding their E-box including Cryptochromes (CRYs) and Periods (PERs). After translocating back to nucleus, CRY alone or CRY and PER heterodimer inhibits this transcription by blocking or displacing BMAL1-CLOCK heterodimer from E-box, respectively. Either type of inhibition of BMAL1-CLOCK heterodimer results in inhibits their transcription along with other clock-controlled genes.(Cao et al., n.d.; Gekakis et al., 1998; King et al., n.d.; Koike et al., 2012a; Kume et al., 1999) CRY and PER form a complex with group of casein kinases to translocate into nucleus.(Y. Lee et al., 2019) Heterodimerizing of CRYs with FBXL3, an E3 ubiquitin ligase, leads to their ubiquitination and proteasomal degradation.(Nangle et al., 2014; Schmalen et al., 2014; Xing et al., 2013) However, FBXL21, homolog of FBXL3, causes attenuated degradation of CRYs due to reduced ubiquitination, respectively. (Hirano et al., 2013; Yoo et al., 2013) Within core clock components, Cryptochromes (CRY1 and CRY2) have high sequence and tertiary structure similarities along with their mechanism of action in clock regulation. However, studies increasingly show their distinct functions in output pathways. *Cry1*$^{-/-}$ and *Cry2*$^{-/-}$ mice have shown that each Cryptochrome has unique regulation on the behavior. *Cry1* knock-out mice exhibits shortened period, yet *Cry2* knock-out mice exhibits lengthened period.(Horst et al., 1999a) Also, peak binding to chromatin of CRY1 and CRY2 occurs at different circadian time points.(Koike et al., 2012a) Clinical studies, in humans, related *Cry1* and *Cry2* gene alterations can result in delayed or advanced sleep phase disorders, respectively.(Hirano, Shi, et al., 2016; Patke et al., 2017) Despite high sequence and tertiary structure similarities between CRY1 and CRY2, a set of key amino acids have been identified for isoform specific behavior of CRY1 and CRY2. (Rosensweig et al., 2018a) However, significant amount of the sequence has yet to be studied. Thus, different characteristics of CRYs still remained elusive, regarding to sequence and function relationship.

Both cryptochromes have evolutionarily conserved photolyase homology region (PHR) which consists of a α/β domain followed by a α-helical domain and a variable intrinsically disordered C-terminal tail. C-terminal coiled-coil-like helix (CC helix) is a functional helix at the end of the α-helical domain, right before variable tail. CC-helix interacts with CRY-binding domain (CBD) of PER protein. Mutations within CC-helix can interrupt PER2 binding. CRYs C-terminal domain also interacts with transactivation domain (TAD) of BMAL1 by competing coactivator CBP/p300. (Czarna et al., 2013a; Michael et al., 2017; Ozber et al., 2010)

Two ancestral cavities within the PHR are flavin-adenine dinucleotide binding pocket (Primary) and a secondary pocket.(Czarna et al., 2013a; Nangle et al., 2014; Rosensweig et al., 2018a) In mammals, FBXL3 interacts with CRYs in their primary pocket. This interaction regulates CRYs half-life and length of circadian period. (Xing et al., 2013) Evidently, a mutation in FBXL3 has been reported to delay CRY1 degradation, therefore, lengthens the circadian period. (Godinho et al., 2007) Furthermore, loop regions that are gating primary pocket, P-loop and C-lid, serve as period determining regions in CRYs.(Ode et al., 2017) Thus, primary pocket of CRYs has been targeted to a great extend for discovery of small molecules, that modulates CRYs half-life indiscriminately or in an isoform specific manner. (S. Gul et al., 2022a; Hirota, Lee, st. John, et al., 2012; Kolarski et al., 2021; J. W. Lee et al., n.d.; Miller et al., 2021, 2022a; Oshima, Yamanaka, Kumar, Yamaguchi, Nishiwaki-Ohkawa, et al., 2015; Surme et al., 2023; Yagi et al., 2022)

Repressive phase of TTFL starts when CLOCK interacts with CRYs in their secondary pocket.(Michael et al., 2017; Nangle et al., 2014) One of the most notable differences between CRY1 and CRY2 is their differential affinity to CLOCK. Recent reports shed light on the critical amino acids and loop dynamics for the CRY-CLOCK binding.(Fribourgh et al., 2020) Serine loop differentially gates access to the secondary pocket of CRYs. CRY1 and CRY2 has two amino acid difference at serine loop, GLY43 and ASN46 in CRY1 is equivalent of ALA61 and SER64 in CRY2, respectively. They showed that CRY2 A61G/S64N mutant (CRY2 2M), when CRY2 serine loop is mutated to CRY1 serine loop, degree of flexibility at serine loop and volume of secondary pocket for CRY2 2M was in between CRY1 and CRY2. Also, CRY2 2M has shown around 4-fold affinity increase to

CLOCK-BMAL1 PAS domain core compared to wild type CRY2 which is again lower than CRY1 but higher than CRY2.

A previous study reported several CRY mutations that have reduced repression activity on CLOCK-BMAL1 dependent transactivation assay (McCarthy et al., 2009). In that experiment cDNA of *Clock* and *Bmal1*, with or without *Cry*s, and a plasmid expressing *luciferase* under the control of *Per2* promoter were transfected to cells. When CLOCK-BMAL1 complex binds to the *Per2* promoter, it initiates the transactivation, leading to the production of *luciferase*. Then repression of CLOCK-BMAL1 dependent transactivation by wild type or mutant CRYs were analyzed. Some CRY mutants caused loss of function and had attenuated repression activity which is controlled by the interaction between secondary pocket of CRYs and CLOCK. Also, in our previous study, an allosteric regulation between the Arg-293, which located in the primary pocket, and serine loop of CRY1 was identified. This rare variant changes the flexibility and conformation of serine loop, which in turn, causes weak interaction with CLOCK PAS-B domain through altered availability of secondary pocket.

In this this thesis, three SNPs (p.Gly144Val, p.Arg293His, and p.Arg348Cys) identified from 1000 Genomes project and Ensembl databases were characterized at biochemical level. Among these SNPs, the p.Arg293His CRY1 variant had a longer $t_{1/2}$ and weaker repression activity The period length of rhythm observed in p.Arg293His CRY1 rescue cell lines were shorter than (wild type) WT CRY1, but longer than CRY2. To understand all these changes mediated by Arg-293 within the structural context of CRY1, I performed molecular dynamic (MD) simulations. The MD studies of both mutant and WT CRY1 suggest that Arg-293 is involved in allosteric regulation of CLOCK binding by regulating the dynamicity of the serine loop adjacent to the secondary pocket. My further analysis revealed that the Arg-293 is highly conserved in both CRY1 and CRY2. Thus, I performed the molecular dynamics simulation to understand the role of Arg-311 in CRY2 (the homolog of Arg-293 in CRY1) in the allosteric regulation of the Ser-loop.

Next, I extensively analyzed dynamic effects of these deficient repression mutants in CRY1 and CRY2 alongside wild type CRY1, CRY2 and CRY1 R293H to see if they have any effect on flexibility of Serine loop and dynamics of the secondary pocket. Among those known mutations, four *CRY1* mutants (A217V/L218F, C259Y, E214K, G288R) and three

CRY2 mutants (A235T, E312K, G230R) are selected. Then, *in silico* models of aforementioned mutants subjected to MD simulations. These mutations selected based on their locations that is distant enough to ensure that they are not at close contact with serine loop. Collectively, approximately 2μs of simulation, six CRY1 and four CRY2 systems were analyzed. Our findings indicated that mutations in CRY1 affected the dynamicity of the serine loop, whereas mutations in CRY2 did not have a similar effect. I further demonstrated that the dynamicity of the CRY1 serine loop is regulated by residues S44 and S45, which form hydrogen bonds with E382. The mutations in CRY1 led to a reduction in the correlated motion of residues between the mutant positions and the serine loop, thereby disrupting the allosteric pathway. Consequently, this resulted in a loss of regulation on the serine loop that explain reduction in CRY1 repression activity.

To investigate whether the secondary pocket of CRY1 can be allosterically regulated via the primary pocket, I utilized known small molecules that interact with CRY1. Specifically, I focused on the CRY stabilizers KL001 and GO200, which have opposing effects on the circadian period (Oshima, Yamanaka, Kumar, Yamaguchi, Nishiwaki-Ohkawa, et al., 2015). These molecules were docked into the wild-type CRY1 homology model and subjected to molecular dynamics simulations. Interestingly, KL001 decreased the fluctuation of the serine loop, whereas GO200 increased the fluctuation of the C-lid. Notably, KL001 not only increased the secondary pocket volume but also enhanced the loop opening distance. Stabilized serine loops typically result in a closed-loop conformation, rendering the secondary pocket inaccessible. However, unlike mutations, KL001 stabilized the serine loop in an open-state conformation without causing the excessive fluctuations observed with the G288R mutation. This stabilization allowed for a consistently accessible secondary pocket, potentially influencing the affinity between CRY1 and CLOCK.

To test this hypothesis, co-immunoprecipitation (co-IP) assay performed to evaluate CLOCK's interaction with CRY1 in the presence of KL001. Surprisingly, KL001 significantly increased CLOCK's affinity for CRY1. These findings challenge existing paradigms regarding CRY1 stability and its effects on the interaction with CLOCK, shedding light on its implications for circadian phenotype and amplitude regulation.

However, this discovery raises additional questions. Many small molecules targeting CRY1 primarily modulate its half-life, which in turn impacts CRY1's roles in other pathways, such as gluconeogenesis. Understanding how these mechanisms intersect remains a critical avenue for future research.

To further explore the allosteric regulation of CRY1, I conducted a virtual screening study targeting its secondary pocket using Ambinter's library. Approximately 7 million molecules were filtered, and 1.2 million were docked into the CRY1 secondary pocket. Remarkably, I identified small molecules that induced five distinct phenotypes. Five molecules decreased amplitude and lengthened the circadian period, while four molecules increased amplitude and lengthened the period. Seven molecules increased amplitude without a dose-dependent effect on the period, one molecule slightly decreased the period without a dose-dependent effect on amplitude, and six molecules lengthened the period without a dose-dependent effect on amplitude.

Understanding the extent of communication between residues and the potential for allosteric regulation is critical for unraveling the differential regulation of CRY proteins. Beyond their roles in the circadian clock, CRYs are involved in various biological processes. Insights into their dynamic ensembles and allosteric mechanisms may reveal how different interaction partners influence their functions. Additionally, the discovery of a CRY1 antagonist that inhibits secondary pocket interactions could address challenges associated with small molecules targeting the primary pocket. Such an antagonist could provide a powerful tool for uncovering the underlying mechanisms of core clock protein interactions and their effects on circadian phenotypes, while also offering promising therapeutic opportunities.

CHAPTER 2
LITERATURE REVIEW

2.1. Circadian Rhythms

Circadian rhythm is simply overall response of an organism to diel (~24h) cycles of changes, that is governed by circadian clock and considered to be present in almost all organisms. This response mechanism evolved in a way that even in absence of external ques, free running of this clockwork still serves as a timekeeping mechanism. Oldest putative traces of life emerged nearly 3.5 billion years ago; majority of organisms have evolved under constant exposure to earths daily cycles. Only after approximately a billion year later Great Oxidation event occurred (GOE). Photosynthetic bacteria acquired the capacity for photo-dissociation of water(M. Wang et al., 2010). Which later resulted as decline of anaerobic life. To adept this, organisms gained a system to eliminate reactive oxygen species (ROS) which is Superoxide dismutase (SOD). SODs convert superoxide radicals to hydrogen peroxide. Subsequently, hydrogen peroxides handled by peroxiredoxin, which virtually all organisms have (Edgar et al., 2012). It has been shown that in several organisms (human, mice, green algea), hyper-oxidized form of peroxiredoxin (PRX-SO2/3) cycles with a period of ~24 h(O'neill et al., 2011; O'neill & Reddy, 2011). Later, peroxiredoxin oxidation is reported as a conserved circadian marker across phylogenetic domains(Edgar et al., 2012). Oldest known clockwork mechanism KaiABC cluster, circadian oscillations of phosphorylation, happen to co-evolved with peroxiredoxins (**Fig.2.1**). Yet, it has also been shown that deletion or inactivation of circadian oscillations persists. Which rather implies that redox oscillations are consequence of circadian rhythms (Amponsah et al., 2021).

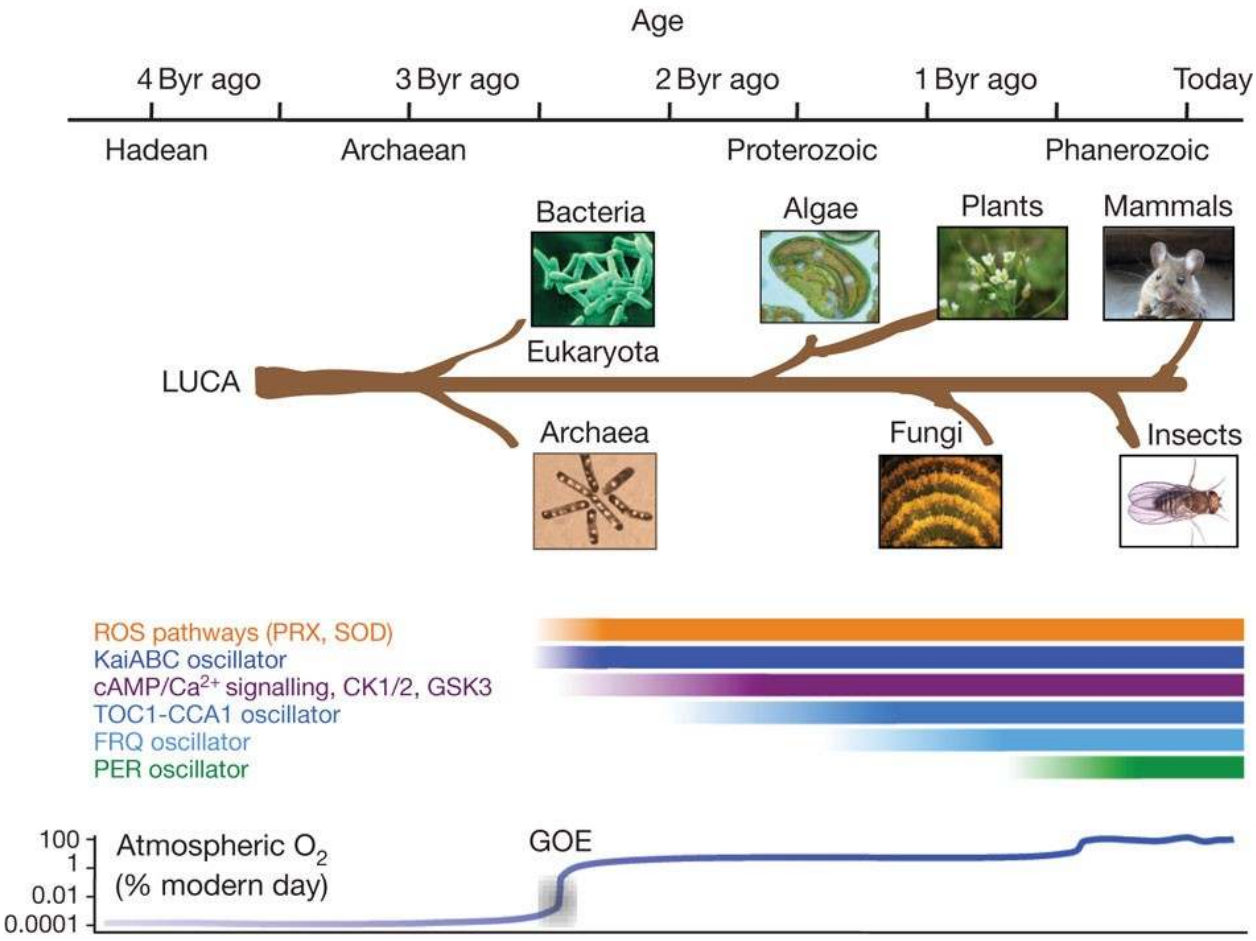

Figure 2.1. Phylogenetic origins of circadian oscillatory systems.

Figure adapted from (Edgar et al., 2012)A timeline is shown at the top of the schematic, with the geological era illustrated. A schematic phylogenetic tree shows the origins of each organism studied, stemming from the last universal common ancestor (LUCA). The putative epoch over which each oscillator systemhas existed is illustrated by the labelled bars. CK1/2, casein kinase 1 or 2; GSK3, glycogen synthase kinase 3; SOD, superoxide dismutase.

2.2. Prokaryotes

2.2.1. *Synechococcus elongatus*

Synechococcus elongatus one of the model organisms, a cyanobacteria, for studying oldest known circadian rhythms(E & S, 2015). Cyanobacteria known to utilize light as their energy

source, which in turn cellular processes are tightly tied to light cycles. Circadian clock mechanism in cyanobacteria mainly consists of KaiA, KaiB, and KaiC proteins **(Figure 2.2.1.1)**. KaiC protein has autokinase and phosphatase activity. State of the phosphorylation of KaiC is the determining factor. KaiA and KaiB proteins regulates these phosphatase and kinase activity. Time of day determined by the redox status of the cell in cyanobacteria instead of a photoreceptor. CikA (histidine kinase) and LdpA (iron-sulfur center-binding redox-active protein) some of the redox sensitive input pathways for circadian clock. (Schmitz et al., 2000). Regulatory response pathway consists of SasA(histidine kinase) and RpaA (transcription factor)(Iwasaki et al., 2000; Takai et al., 2006). Phosphorylation of RpaA enables the binding of this transcription factor to its targets which also promotes expression of KaiBC cluster.

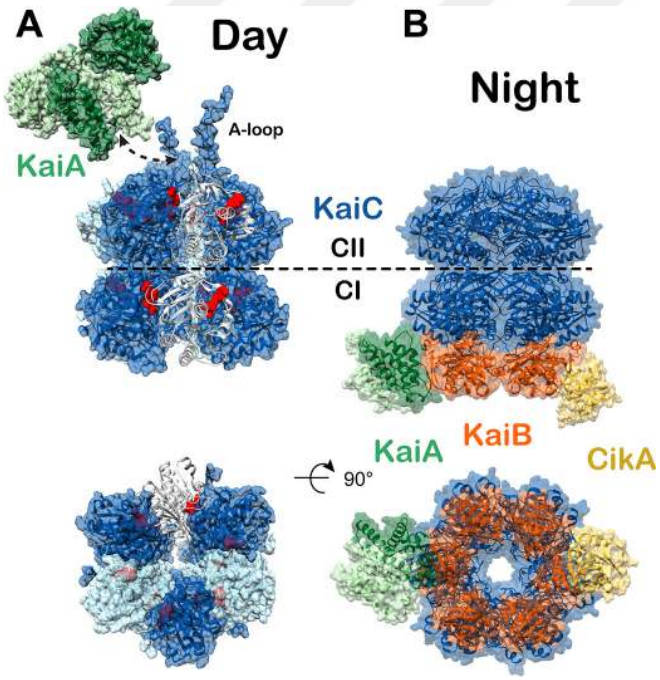

Figure 2.2.1.1 Day and night states of the cyanobacterial clock.

Figure adapted from (Swan et al., 2018) High-resolution models of the day and nighttime states of the core oscillator are compared. A) day complex. The CI and CII hexamers form stacked doughnuts (alternating subunits shown in light and dark blue for contrast, PDB code 3K0C). One subunit is shown in cartoon mode to highlight the nucleotide-binding sites (red)

at the subunit interfaces. Phosphorylation of KaiC residues Thr-426 and Ser-432 takes place near the CII nucleotide-binding sites. The KaiA dimer (light and dark green for contrast) binds to C-terminal A-loops of KaiC (white, shown in complex with KaiA PDB code 5C5E). The dashed arrow represents the point of connection between the KaiA–CII loop structure and the CII A-loop extensions shown on the right. B) night complex. The intermediate-resolution cryo-EM model (PDB code 5N8Y) is combined with higher resolution models from studies on indepen- dent subcomplexes. The S431E phosphomimetic of the pS/T state of KaiC binds six molecules of KaiB (PDB code 5JWQ). This results in the recruitment and sequestration of KaiA near the KaiB–CI interface (PDB code 5JWR). Output signaling occurs through interactions between KaiB and the C-terminal PsR domain of CikA (PDB code 5JYV), as well as through interactions between KaiC and SasA at dusk, although no high-resolution structure exists for the latter.

2.3. Eukaryotes

2.3.1. *Neurospora crassa*

Neurospora crassa, a type of red bread mold, is one of the model organisms for circadian clock studies in fungus. Circadian rhythm in eukaryotes results of transcriptional translational feedback loop (TTFL). Core clock mechanism in N.crassa consist of frequency (FRQ), White collar-1 (WC1), White collar-2 (WC2), vivid (VVD) proteins(Crosthwaite et al., 1995) (**Fig. 2.3.1.1**). WC1 and WC2 forms a heterodimer, which known as White collar complex (WCC). WCC promotes the transcription of *frq* gene. Although WC1 is not highly reactive to light, WC2 incorporation to clock box, in *frq* promoter, strictly dependent on light (Belden et al., 2007). When FRQ levels are peaked, FRQ downregulates its own transcription (K. Lee et al., 2000) by inhibiting WCC. Additionally, VVD protein also inhibits WWC. Thus, also inhibits its own transcription(Heintzen et al., 2001). Other than FRQ itself CK1 and CK2 also regulates binding of WC1 and WC2 to DNA(Belden et al., 2007). Stability of FRQ is also dependent on its phosphorylation. Phosphorylation of FRQ increases its affinity

for FWD-1 (subunit of SCF-type E3 ubiquitin ligase), which in turn leads to degradation of FRQ by proteasome(He et al., 2003).

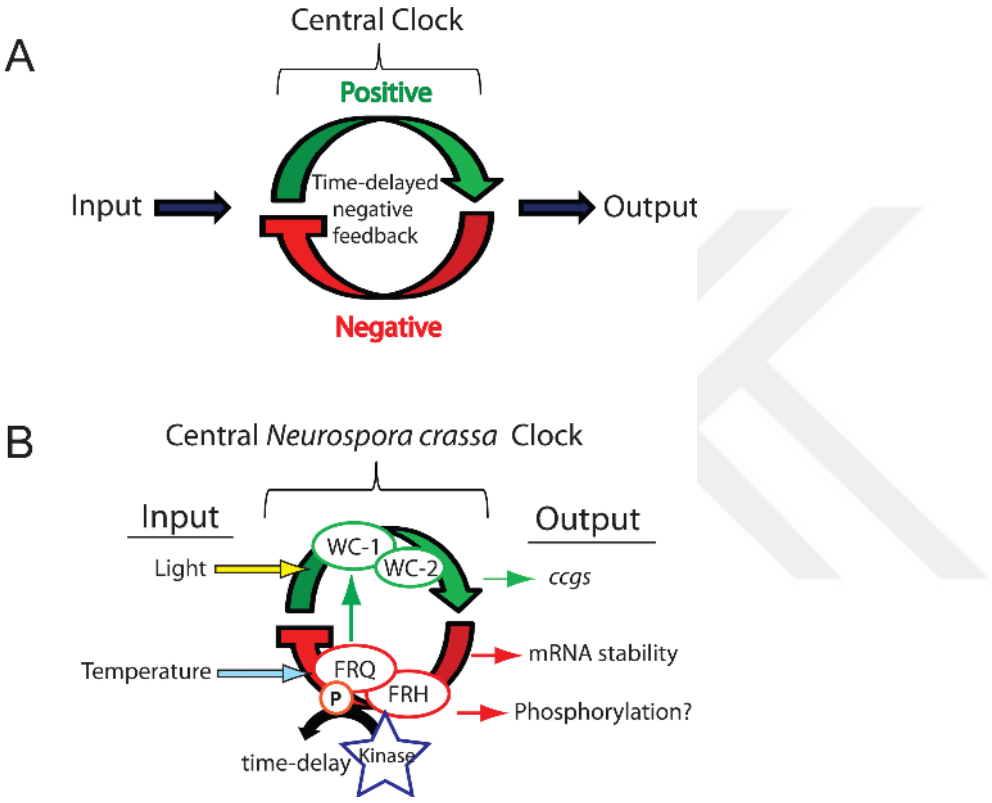

Figure 2.3.1.1. Oscillator model for the circadian clock

Figure adapted from (Baker et al., 2012). (A) Circadian systems comprise three essential elements: an endogenous self-sustaining oscillator, an ability to sense environmental time cues (Input), and physiological output tied to the oscillator at distinct phases. Environmental variables such as light and temperature can entrain or couple the core clock via input pathways. The central oscillator is based on the interplay between positive acting factors driving the expression of negative factors which feedback to inhibit the positive complex. A critical component to this feedback is a mechanism for time delay of the negative state variable that reflects the ~24-hour nature of the physiological rhythms. (B) The organization of molecular components of the feedback loop in *Neurospora crassa*. The entraining variables of light and temperature impact different parts of the oscillator, light acting through

the photoreceptor function of WC-1 to induce transcription of *frq* and temperature acting to modulate amounts of FRQ. WC-1 and WC-2 form the WCC complex. FRQ and FRH form the FFC complex. Rhythmic output is primarily generated through rhythmic expression of clock-controlled genes (*ccgs*) but can also be due to changes in mRNA stability and possibly phosphorylation. Kinases contribute to the time-delay by influencing the stability of FRQ.

2.3.2. *Arabidopsis thaliana*

In plants circadian clock is highly interlocked with temperature and light related pathways. Thus, it allows plants to be more responsive to light during the day, and growth during the night. Clock mechanism in *A.thaliana* involves the morning loop genes, *LATE ELONGATED HYPOCOTYL (LHY) and CIRCADIAN CLOCK-ASSOCIATED 1 (CCA1)*. LHY and CCA1 are repressors that binds to evening element (EE) in promoter region of clock-controlled genes which includes the evening loop gene *TIMING OF CAB EXPRESSION 1 (TOC1),* also known as *PRR1*. Other evening loop genes includes PRR5, PRR7, and PRR9. Which in turn PSEUDO-RESPONSE REGULATOR (PRR) genes, including *TOC1* later represses the *CCA1* and *LHY* genes(Alabadí et al., 2001; Nakamichi et al., 2010) (**Fig. 2.3.2.1)**. Light response is especially crucial in plants. Red light availability, in particular, assessed and responded by the phytochrome-signaling pathway(Oakenfull & Davis, 2017). PHYTOCHROME-INTERACTINGFACTORS (PIFs) are transcription factors that regulates with LHY and CCA1, hence, links circadian clock with light.

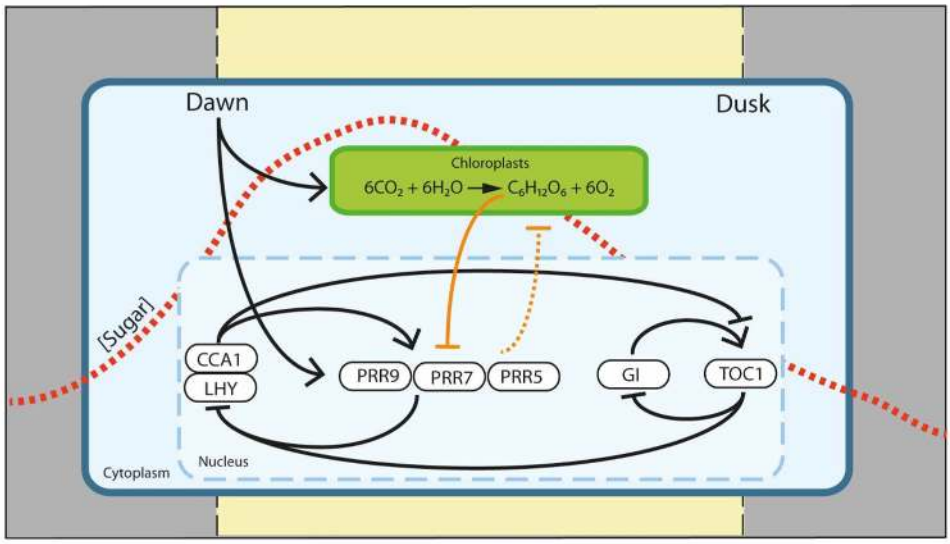

Figure 2.3.2.1. A model for entrainment of the A. thaliana circadian clock by photosynthetically derived sugars.

Figure adapted from (Haydon et al., 2013). From dawn, light activates PRR7and drives photosynthesis. The concentrations of simple sugars produced by photosynthesis accumulate within the plant during the day (red dashed line), peaking around 4–8 h after dawn. High endogenous sugar concentrations lead to suppression of thePRR7promoter, contributing to the phase ofPRR7rhythms. PRR7 is a transcriptional repressor of the circadian clock component CCA1. Thus, the rhythms of endogenous sugars derived from photosynthesis contribute to circadian entrainment through PRR7.

2.3.3. *Drosophila melanogaster*

D.melanogaster one of the most studied model organisms overall, and in circadian rhythms since 1970s with the identification of *period* (*per*) gene(Konopka & Benzer, 1971). Most advantageous aspect of *D.melanogaster* in circadian related research is, it is one of the most simplistic organisms which allows monitor of sleep and locomotor activity. In following years, *timeless (tim)*, *clock (clk)* and lastly, *cycle (cyc)* discovered (Allada et al., 1998; Rutila et al., 1998; Sehgal et al., 1994). Core clock mechanism in *D.melanogaster* consist of these four genes (*per, tim, clk and cyc*). Other regulatory elements of the circadian clock in *D.melanogaster* involves *cryptochrome (cry), the kinases double-time (dbt), and shaggy (sgg)*(Emery et al., 1998; Kloss et al., 1998; Martinek et al., 2001; Price et al., 1998; Stanewsky et al., 1998). PER and TIM are the repressors of feedback loop. They accumulate in cytoplasm and translocate into nucleus in heterodimer form. After translocating into nucleus, they inhibit CYC-CLK complex, which is the transcriptional activator complex. Which in turn inhibits their transcription alongside other clock-controlled genes. PER and TIM stability is controlled by their cyclic phosphorylation as well as their nuclear transport(Kloss et al., 1998; Price et al., 1998) by DBT (Casein Kinase 1ε homolog) and SSG.

Resembling suprachiasmatic nucleus in mammals, around 150 “clock neurons” in D.*melanogaster* brain co-expresses core clock components (HANDLER & KONOPKA, 1979). Pigment-dispersing factor (PDF) act as synchronizer within these neurons by binding PDF receptors (PDFR)(Lin et al., 2004). Entrainment of clock in *D.melanogaster* is mainly through light by CRY which act as a photoreceptor (Emery et al., 1998). As response to light CRY binds to TIM and promotes its degradation(Emery et al., 1998).

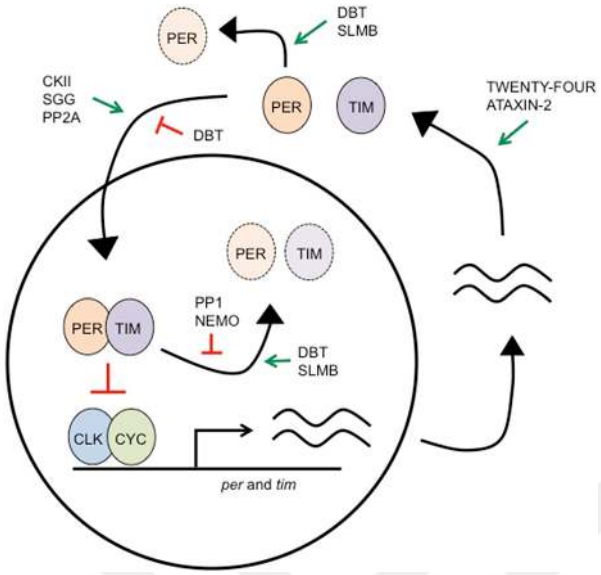

Figure 2.3.3.1. The molecular feedback loop is formed by the negative feedback of Period (PER) and Timeless (TIM) on their own transcription.

Figure adepted from (Dubowy & Sehgal, 2017). Delays exist between transcription of per and tim mRNA and the localization of these proteins in the nucleus, where they can interact with transcriptional activators Clock (CLK) and Cycle (CYC). These delays are thought to be important for allowing the molecular clock to cycle with a period of $24 hr. Critical regulators have been identified at several steps of the cycle that are necessary for accurate timing and strength of molecular rhythms. Degradation of PER and TIM allows the cycle to start anew. Not pictured is the second feedback loop formed by PDP1 and Vrille, which produces cycling of Clk mRNA. This secondary feedback loop is thought to reinforce molecular oscillations, although cycling of the CLK protein is not necessary for rhythms. CKII, Casein Kinase II; SGG, shaggy; PP2A, Protein Phosphatase 2A; PP1, Protein Phosphatase 1; DBT, doubletime.

2.3.4. Mammals

Circadian rhythm, which is governed by the circadian clock, is an internal process that cycles every 24 h (Roenneberg et al., 2003). The suprachiasmatic nucleus (SCN), master clock, is found in the hypothalamus of the brain and is made up of approximately 20,000 neuronal cells (Mieda, 2019). SCN receives light input from the environment and uses it to regulate the organism's circadian clock. In multicellular organisms, the peripheral tissues have their own clocks, called the peripheral clock, and the SCN synchronizes their rhythms via humoral and neural signals (Kavakli & Sancar, 2002; Roenneberg et al., 2003). It regulates several biochemical processes and, in turn, physiological variables such as blood pressure, body temperature, bowel movement, and hormonal production (Kavakli et al., 2017a; Roenneberg & Merrow, 2016). Mammals receive the light input via their eyes and transmit it to the SCN through the retinohypothalamic tract. The SCN relies on connections with the endocrine and autonomic nervous systems as well as a robust neuronal network to relay time signals to other hypothalamic and extra-hypothalamic nuclei in order to synchronize peripheral clocks (Astiz et al., 2019; Schibler & Sassone-Corsi, 2002). The SCN regulates hormone release rhythms and influences the autonomic nervous system, which in turn affects how sensitive peripheral tissues are to these hormones, thereby synchronizing other tissue clocks. Four core clock genes are necessary for the generation and maintenance of circadian rhythms at molecular level; Brain and Muscle Aryl Hydrocarbon Receptor Nuclear Translocator (ARNT)-like protein (Bmal1), Circadian Locomotor Output Cycle Kaput (Clock), Cryptochrome (Cry1 and Cry2), and Period (Per1, Per2, and Per3) (Allada & Bass, 2021; Bass & Lazar, 2016; Kavakli & Sancar, 2002; Takahashi, 2017). Circadian rhythm is generated as a result of these core clock proteins using transcriptional and translational feedback loops (TTFL) mechanisms (**Fig. 2.3.4.1**) (Allada & Bass, 2021). BMAL1 and CLOCK interact and then bind to the E-box (CACGTG) in the promoter region to initiate the transcription of clock-controlled genes (CCGs), which form the positive arm of TTFL (Allada & Bass, 2021; H. Gul et al., 2022; Sancar, 2003). CRYs and PERs are among the CCGs that accumulate within the time frame and then translocate into the cell nucleus with Casein Kinase 1ε/δ (CSKIε/δ), where they inhibit BMAL1/CLOCK-driven transcription via displacement or repression type mechanisms, forming the negative arm of

TTFL (Takahashi, 2017; R. Ye et al., 2014). CRYs are ubiquitinated and degraded via the SCF(Fbxl3) ubiquitin ligase complex and, in turn, initiate the cycle (Busino et al., 2007; Reischl et al., 2007). The second TTFL is the one that controls the transcription of Bmal1 in a circadian rhythm dependent manner. Bmal1 transcription is initiated by retinoid-related orphan receptors (RORs), whereas it is suppressed by nuclear receptor subfamily 1, member 1 (REV-ERB) (Sato et al., 2004). RORs are shown to be essential clock components in experiments on Rorα deficient mice and cells, which exhibited disrupted or dampened rhythmicity (Akashi & Takumi, 2005). Furthermore, several other proteins have been shown to either directly or indirectly regulate the activity of the core clock protein (Anafi et al., 2014; Cal-Kayitmazbatir et al., 2021; Honma et al., 2002; Mohawk et al., 2012). A more recent BioID study suggests that several candidate proteins interact with core clock proteins and possibly regulate the clock (H. Gul et al., 2022). Posttranslational modification (PTM) mechanisms play a significant role in regulating the different aspects of the molecular clock (Kavakli et al., 2022a; Okamoto-Uchida et al., 2019). It has been shown that different types of PTM, such as phosphorylation, acetylation, and SUMOylation, are required to control the stability of core clock proteins, their cellular distribution, the transcriptional activity, and communication with other pathways (Hirano, Fu, et al., 2016). The phosphorylation of the PERs is important to regulate circadian rhythms. CKIδ/ε phosphorylates PERs, targeting them for proteasomal degradation (Eide et al., 2005). Interfering with the phosphorylation of PERs alters the period length of circadian rhythm (Gallego & Virshup, 2007). In addition, the degradation and stability of CRYs are regulated by PTMs. Genetic studies showed two F-box-type E3 ligases (FBXL3 and FBXL21) bind CRYs and exhibit an opposite effect on their stability. CRYs are ubiquitinated by FBXL3 and are targeted for degradation (Busino et al., 2007) while FBXL21 competes with FBXL3 to ubiquitinate CRYs and, in turn, increases the stability of the CRYs (Hirano, Fu, et al., 2016; Yoo et al., 2013). This interaction is used in drug discovery to regulate the stability of the CRYs. KL001, which decreases the interaction between FBXL3 and CRYs, increases the stability of CRYs and has the potential to be used as an anti-diabetic drug. A more recent study identified small molecules that regulate CRYs stability (S. Gul et al., 2021; Kavakli et al., 2022b). M47, for example, selectively reduces CRY1 stability by increasing CRY1 and FBXL3 interaction and

increasing CRY1 ubiquitination. Further studies with mice suggest that M47 has a cancer-protective role.

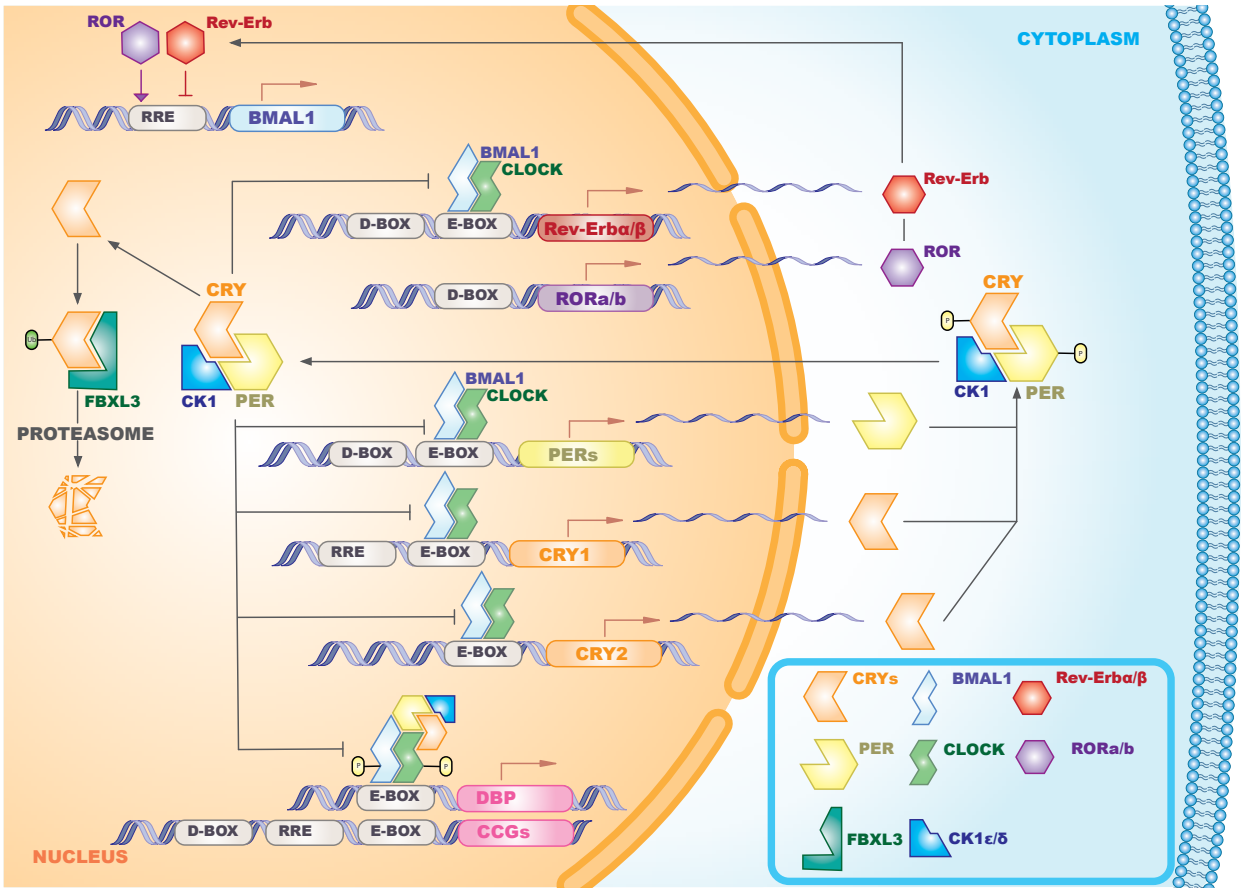

Figure 2.3.4.1 The core clock mechanism in mammalian cells.

Figure adapted from (Baris et al., 2023a). The circadian rhythm is governed by transcriptional and translational feedback loops (TTFL) mechanism. BMAL1 and CLOCK bind E-box element of the promotor region and initiate the transcription of clock-controlled genes including *Per*s and *Cry*s. PERs and CRYs form dimer and translocate to the nucleus along with Casein Kinase 1ε/δ (CK1ε/δ), where they repress the transcription of CCGs. The stability of both CRYs and PERs is regulated with different enzymes. In a second loop, the transcription of nuclear receptors REV-ERBα and REV-ERBβ is driven by CLOCK/BMAL1. Then REV-ERBα and REV-ERBβ compete with the retinoic acid-related orphan receptors (RORs) and, in turn, to regulate the Bmal1 transcription.

2.4. Single nucleotide polymorphisms (SNPs) in circadian genes: Impact on gene function and phenotype

2.4.1 The association of pathogenic circadian core clock gene variations with human diseases

Studies suggest that circadian dysregulation may affect the proper function of different organs (**Fig.2.4.1.1**). Such dysregulation can arise from either circadian misalignment with environmental factors such as nightshift work and jetlag or mutations in clock genes (Roenneberg & Merrow, 2016). There are several review articles about how environmental factors can result in disease through circadian misalignment ((Ingram, 2020; O'Donnell et al., 2020; Roenneberg & Merrow, 2016)). Here, the relationship between diseases and clock gene variations have discussed. Although circadian clock genes are highly polymorphic, few reported diseases are associated with pathogenic variants of the core clock genes in humans. To date, pathogenic variations in the CRY1, PER2, and PER3 genes have been linked to human diseases in the Online Mendelian Inheritance in Man (OMIM) database (https://omim.org), which is a repository for human gene-phenotype relationships, genetic disorders, and their characteristics. CRY1 gene variations are associated with delayed sleep phase disorder (DSPD; MIM 614163) (Patke et al., 2017) and attention deficit/hyperactivity disorder (Emre Onat et al., 2020a). Other variations are detected in both PER2 and PER3, which are related to familial advanced sleep phase syndrome types 1 and 3, respectively (FASPS1; MIM 604348 and FASPS3; MIM 616882). A variant in the CRY2 SNP, which is not listed in OMIM, is associated with the familial advanced sleep phase (FASP) (PMID 27529127) (Hirano, Fu, et al., 2016). Although they are not listed in ClinVar (a public archive that reports the relationships among human variations and phenotypes), two pathogenic variations in the CRY1 gene and a pathogenic variation in the CRY2 gene were found to be clinically relevant to human sleep disorders. There are not any identified pathogenic variations in CLOCK and BMAL1 genes related to human disease yet (OMIM 601851 and 602550).

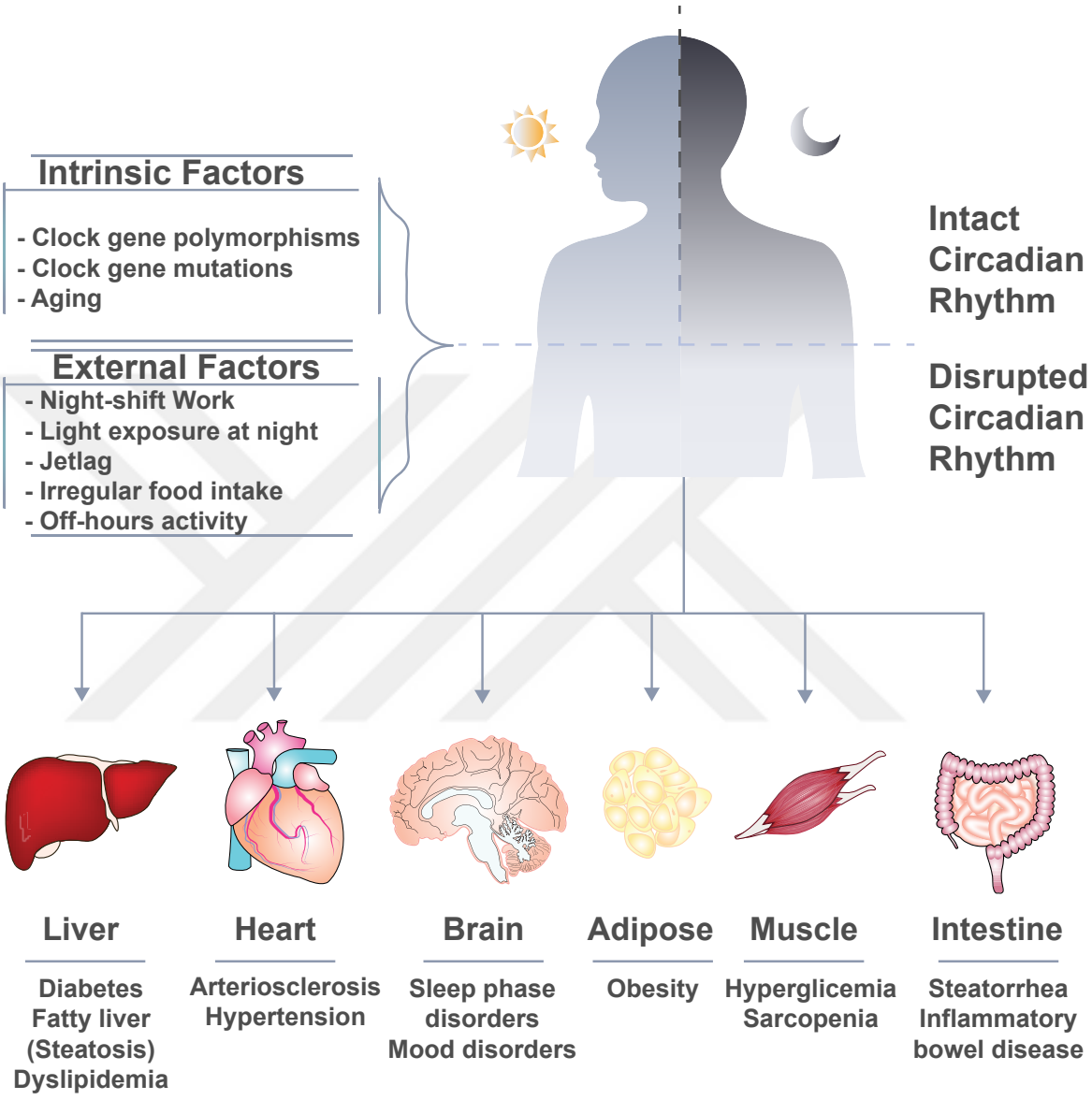

Figure 2.4.1.1 Representation of disruption of circadian clock in different organs in relation with human health.

Figure adapted from (Baris et al., 2023a). Circadian rhythms disruptions can occur by either intrinsic and/or extrinsic factors. Such disruptions may affect proper functions of organs.

2.4.2 The structure and function analyses of pathogenic variations

Human circadian clock-gene variations are associated with several behavioral and physiological diseases (Barnard & Nolan, 2008; Rijo-Ferreira & Takahashi, 2019). However, little is known about how clock gene variants affect the molecular clock and, and, in turn, cause diseases. Since the majority of the published variations are localized in noncoding regions of core clock genes such as intronic and promoter regions, it is hard to investigate their effects at the molecular level on circadian rhythm and phenotypes. Investigation of identified mutations help us to understand not only the role of variation in the pathogenesis of disorder but also the role of amino acids or domains for the function of protein. There are few published reports investigating the effect of mutations at molecular levels (Emre Onat et al., 2020b; S. Gul et al., 2020; Parlak et al., 2022a; Patke et al., 2017; Pellegrino et al., 2014). The PER2 gene is the first link discovered between pathogenic variation in the core clock gene and human disease. This variation in the PER2 gene (c.1984A > G; p.Ser662Gly) cosegregated with the familial advanced sleep phase syndrome-1 (FASPS1; 604348) in a 4-generation pedigree (Toh et al., 2001). Subsequent studies revealed that Ser-662 of the PER2 is being phosphorylated CSKIε, which regulates the stability and nuclear localization of the PER2 (Toh et al., 2001; J. T. Vanselow & Kramer, 2010; K. Vanselow et al., 2006). Also, this initiates a cascade of phosphorylation of several other residues within PER2. In fact, transgenic mice with the human PER2 Ser662Gly mutation recapitulated the human FASPS phenotype (Y. Xu et al., 2007). The PER2 Ser662Gly transgenic mice showed a ∼2 h period shorter than wild-type and a robust ∼4 h phase advance of activity rhythms in LD12:12. Further molecular characterization of this transgenic animal revealed that the level of both PER2 mRNA and protein decreased and CSNK1ε phosphorylates another region of PER2 as well. This sequential phosphorylation region of PER2 is modulated by another post-translational regulation, O-GlcNAcylation, demonstrating an interplay and competition between phosphorylation and O-GlcNAcylation of serine residues in this region (Kaasik et al., 2013). These studies revealed mechanistic insight into the regulation of PER2 and highlighted the important role of post-translational regulation of clock proteins in cellular function. These first findings proved that a mutation in the core clock protein may alter the

circadian period, affect human sleep behavior, and lead to a sleep disorder. Two rare variations in the PER3 gene were identified in humans with FASP, accompanied by higher Beck Depression Inventory and seasonality scores (Liu & Zhang, 2016). These two missense variations [c.1243 C > G (p.Pro415Ala) and c.1250 A > G (p.His417Arg)] are on the same allele (cisposition) and co-segregate with FASP and mood traits. These variations recapitulate circadian and mood phenotypes in transgenic mice expressing hPER3-P415A/H417R-Tg allele. Although Per3 knockout mice have a shortened period under LL, the period of hPER3-P415A/H417R-Tg mice was significantly longer than that of hPER3-WT (wild type)-Tg mice. hPER3-P415A/H417R-Tg mice has a 4 h phase delay in activity onset and offset time in 4 h light/20 h dark cycles, whereas hPER3-WT-Tg, WT, and Per3−/− mice have no phase delay. The authors suggested a dominant effect of PER3-P415A/H417R on the light-sensing pathway(s) in mice. Functional analyses revealed that PER3-P415A/H417R has reduced repressor activity and is less stable when compared to WT PER3. Although PER3 was shown to promote nuclear translocation of PER1 and PER2
(Yagita et al., 2000), PER1 levels were significantly reduced in cytoplasmic fractions, and PER2 levels were significantly lower in both the nuclear and cytoplasmic fractions of the hypothalamus from the hPER3-P415A/H417R-Tg mice. PER3-P415A/H417R has a reduced ability to stabilize PER1 and PER2. A missense mutation [c.778 G > A (p.Ala260Thr)] in the human CRY2 gene was identified in a family member with FASP (Hirano, Fu, et al., 2016; Xing et al., 2013). Ala260 residue is located in the primary pocket of CRY2, and it is highly conserved in CRY1 and CRY2 in various species. The authors generated a mouse expressing the hCRY2 p.Ala260Thr allele and observed an advanced phase of sleep-wake behavior in a light-dark cycle with a shortened circadian period in constant darkness in these animals. In vitro experiments showed that the nuclear CRY2 protein levels in the cell line were decreased by the Ala260Thr mutation and less stable than wild type CRY2, especially in the nucleus. They suggest that the p.Ala260Thr mutation affects the FBXL3-CRY2 interaction, thus altering the CRY2 stability. Analysis of this interaction showed that CRY2 p.Ala260Thr binds more strongly to FBXL3, which leads to faster degradation of mutant CRY2. FAD stabilizes CRY2 by structurally interfering with the interaction between FBXL3 and CRY2 (Xing et al., 2013). They showed that treating HEK293 cells with FAD increased CRY2 protein levels much more than CRY2 p.Ala260Thr, implying that the mutation

reduced CRY2 stabilization by FAD. This study emphasizes the significance of CRY2 protein post-translational regulation in the human circadian clock, which regulates the sleep-wake cycle. A variant in the CRY1 gene (c.1657 +3 A > C) is identified in familial delayed sleep phase disorder patients (DSPD) (Patke et al., 2017). The variation within the 5' splice site resulted in the skipping of exon 11 in the mRNA. The mutation resulted in deletion of exon 11 (CRY1 Δ11) with an in-frame deletion of 24 residues at the C-terminal region. c.1657 + 3 A > C variation showed dominant inheritance with a gain-of-function effect causing sleep disturbances, long-period behavioral and body temperature rhythms with diminished amplitudes. Expression of CRY1Δ11 cDNA in $Cry1^{-/-}/Cry2^{-/-}$ in a mouse embryonic fibroblast cell line (DKO MEF) restored circadian cycling but showed a lengthened period of molecular circadian rhythms in cells. In vitro experiments revealed that CRY1Δ11 has increased nuclear localization and enhanced interaction with CLOCK and BMAL1. Interestingly, ChipSeq results demonstrated that CRY1 exon 11 deletion specifically reduces the presence of clock gene proteins at target gene promoters, consistent with CRY1-mediated transcriptional regulation through displacement of CLOCK and BMAL1. The authors concluded that the CRY1 tail modulates transcriptional inhibition at defined stages of the circadian cycle. Another study identified CRY1c.825 + 1 G > A variant which segregated with Attention-deficit/hyperactivity disorder (ADHD) and delayed sleep phase disorder (DSPD) in the affected family members (Emre Onat et al., 2020a). c.825 + 1 G > A variant in the photolyase homology region (PHR) results in the skipping of exon 6 (loss of amino acid residues from 229 to 275 in the protein, CRY1Δ6). Further structure-function studies revealed that CRY1Δ6 variant is unable to rescue circadian rhythm and has reduced affinity to CLOCK. In fact, docking simulations suggest that Arg256 and Phe257, encoded by exon 6 of CRY1, are essential for the interaction with CLOCK. The CRY1Δ6 variant had a severe deficit in its ability to coimmunoprecipitate with the BMAL1/CLOCK heterodimer and showed less repressor activity on BMAL1/CLOCK transactivation. Interestingly, the half-life of CRY1Δ6 was significantly higher than that of WT CRY1. The authors concluded that residues coded by exon 6 are important for the repression activity of CRY1 via CLOCK interaction and its stability.

2.4.3 Circadian clock gene variations in relation to mental health

There are several psychiatric disorders, such as depression, schizophrenia, and obsessive–compulsive disorder, that are associated with sleep disruptions (Karatsoreos, 2014). Therefore, several genome-wide studies have been initiated to find an underlying genetic mechanism, including core clock genes. Several single nucleotide changes (SNPs) are found mainly in the non-coding region CLOCK gene (Schuch et al., 2018). Whether these SNPs have any functional effect on circadian rhythm is still not known. Molecular characterization of the CLOCK c .3111 T > C (rs1801260) SNP, located in 3′-untranslated region, indicates that it has altered mRNA stability. (Ozburn et al., 2016). The c.3111 T > C (rs1801260) SNP is associated different type of diseases including bipolar disorder, depression, sleep disturbances, insomnia, and Alzheimer disease (Emre Onat et al., 2020a; Valladares et al., 2015). Two recently identified pathogenic CRY1 variants, the CRY1Δ11 and CRY1Δ6, are linked to ADHD. CRY1Δ6 variant causes an arrhythmic phenotype, while CRY1Δ11 lengthens the circadian period at the cell-based circadian rescue assays. A genome-wide association study involving 9438 unrelated adults in Europe showed that c.1657 + 3 A > C (CRY1Δ11) was associated with major depressive disorder, insomnia, and anxiety. They did not observe a significant difference in the severity of ADHD in individuals carrying CRY1Δ11 or CRY1Δ6; however, more severe psychiatric symptoms were observed in CRY1Δ6 carriers with anxiety and oppositional defiant disorder. Several PER2 gene variations are associated with mental (Charrier et al., 2017). Different PER2 variations were found in 4 out of 5102 patients with autism spectrum disorder (ASD) (Hoang et al., 2021). A detailed clinical questionnaire revealed that these patients also have symptoms of sleep disturbances. A patient with c.2365 A > T (p.Lys789∗) had symptoms suggestive of FASPS1, two other patients, one of whom carries c.3738del (p.Leu1247∗) and the other c.1153del (p.Ile385Serfs) have a history of sleep disturbance. One patient with the de novo c.2191 G > A (p.Ala731Thr) variation did not have a sleep problem. They classified this missense variation as VUS (Variant of Uncertain Significance), whereas others are classified as nonsense or frameshift and are pathogenic. Yang et al. sequenced the coding region of 18 canonical clock genes, including PER2, and detected a missense c 0.3682 C > G (p.Pro1228Ala) variation in a Japanese patient with ASD and difficulty initiating sleep (Li et

al., 2016). This missense variation is classified as a VUS (Variant of Uncertain Significance). A maternally inherited frameshift c.1931del (p.Arg644fs) variation was identified in a female patient with ASD and her unaffected brother (unpublished data from the Simons Simplex Collection WGS database). All of these findings suggest that loss-of-function PER2 variations are not a common cause of ASD; however, patients with PER2 who have these pathogenic variations showed a broad range of sleep disturbances, but not necessarily a clinical sleep disorder.

2.4.4. The association of single nucleotide polymorphisms (SNPs) with human diseases

Human circadian core clock gene SNPs are associated with numerous behavioral and physiological diseases including cancer, neurological disorders, endocrine and metabolic disorders. Epidemiological studies revealed that majority of the clock-gene variations localize in noncoding regions (intergenic, UTR, promoter, or intron) and they have no or controversial effect on the phenotype. For example, A study suggest a significant association between CLOCK rs12649507/rs11932595 and long sleep duration (Allebrandt et al., 2010) whereas other study find no significant association with sleep duration (Lane et al., 2013). Also, in a European study, the minor allele T of BMAL1 rs11022775 was associated with a higher odds ratio of Type 2 diabetes mellitus (T2DM) than allele C in Asian populations, but the opposite association was observed in white European cohorts (Kelly et al., 2012). Studies on animals have provided a link between the metabolic syndromes and the disturbance of synchronous clock activity (Staels, 2006). ClockΔ19/Δ19 mutant animals become obese and have hyperglycemia, hyperinsulinemia, hepatic steatosis, and dyslipidemia (Turek et al., 2005). Additionally, the deletion of Bmal1 and/or Clock disrupts the diurnal variation in glucose, triglycerides and gluconeogenesis (Bass & Lazar, 2016; Bass & Takahashi, 2010; Kennaway et al., 2007; Rudic et al., 2004). The genome-wide association studies in humans suggest that a few of the SNPs are associated with metabolic disorders. A significant association between the CLOCK rs4580704 and CLOCK rs1801260 SNPs are found with

T2DM and obesity, respectively, was found (Valladares et al., 2015). BMAL1 rs7950226-rs11022775 showed a significant association between T2DM and hypertension in British individuals, as reported (Woon et al., 2007). In a study population of 1.715 nondiabetic German individuals, four CRY2 SNPs (rs3824872, rs10838524, rs11605924, and rs7933420) are associated with fasting glycaemia. Carriers of these SNPs minor alleles revealed elevated fasting glycaemia and reduced liver fat content (Machicao et al., 2016). Several behavioral and molecular studies suggest an important role for the circadian clock in neuronal function and in the regulation of the expression of neurogenic transcription factors (Kimiwada et al., 2009). Several circadian clock gene variations have been linked to the etiology of many psychiatric disorders, according to epidemiological studies. Among them, CLOCK gene rs1801260 (3111 T/C), rs3762836 (p.H542R), rs3805148, rs12504300, rs4864542, rs12649507, rs17777927, rs119325595, rs12648271, rs3805148, rs3736544, rs3749474, rs2412646, rs2412646, and rs6850524 are mostly investigated and found to be associated with autism, schizophrenia, substance use disorder, and anxiety disorder (Schuch et al., 2018). Furthermore, BMAL1 rs900147 variation was associated with Parkinson Disease; CRY1 gene rs10861688, rs2287161; and CRY2 gene rs10838524, rs7121611, rs7945565, rs1401419, rs10838524, rs3824872, rs7123390, rs2292910 variations were associated with major depression; PER1 gene rs2253820 was associated with Parkinson Disease; and PER3 gene rs228697 variation showed significant association with major depression (Jagannath et al., 2017). The intrinsic link between dysregulated circadian rhythms and cancer has been demonstrated by both epidemiological and experimental evidence. In different types of cancer, CRY2 expression is significantly reduced compared with matched normal tissues (Y. Ye et al., 2018). Additionally, after gamma radiation, mice deficient in the Per2 gene showed a marked increase in tumor development and reduced apoptosis in thymocytes (Fu et al., 2002). The deletions of Cry1 and Cry2 diminished tumor development in p53 null mice (J. H. Lee et al., 2013). A meta-analysis identified a significant association between PER3 rs1012477, CLOCK rs3749474, and rs11943456 variations and breast cancer (Benna et al., 2017). In another study, PER3 rs77404158 and BMAL1 rs142435152 variants were linked with breast and prostate cancers, respectively (Mocellin et al., 2018). Interestingly, both studies suggest that instead of single variations, there is a strong association between circadian genes and cancer risk, suggesting the additive effect of haplotypes (multiple SNPs).

3.1 The structure and function analyses of SNPs There are few studies investigating single nucleotide polymorphisms (SNPs) of the core clock gene at molecular levels. Developing tools both at the in vitro and in vivo levels to investigate the effect of SNPs on molecular clock mechanisms will provide valuable information. First, investigating the impact of clock gene SNPs will help us better understand the structure function relationship of clock proteins. Second, it will not only reveal the effects of these SNPs on the circadian rhythm but also contribute to the understanding of the relationship between circadian rhythm and disease. Our group has studied SNPs of CRY1 and CRY2, which are not associated with diseases (S. Gul et al., 2020; Parlak et al., 2022b). SNPs selected from the Ensembl database. SNPs were filtered based on homology conservation, location of the functional domain, and pathogenicity effect. After the prediction of deleterious SNPs using SIFT, PolyPhen, CADD, REVEL, MetaLR, MutationAssessor, and Mutation Taster tools, the selected CRY1 and CRY2 SNPs were further characterized by biochemical and genetic complementation assays. During the characterization of CRY1 SNPs, CRY1 p.Arg293His has enhanced stability and reduced repressor activity on CLOCK/BMAL1-driven transcription (S. Gul et al., 2020). Further characterization of this variant suggests that it causes a shortened circadian period and has a reduced affinity for CLOCK. CRY1's Arg293 is important for the dynamic regulation of the Ser-loop, which has been shown to play a critical role in CLOCK binding (Patke et al., 2017). Further analysis of MD simulations of both variant and wild type CRY1 in terms of the communication pathways suggested that p.Arg293His variation changes the path to the serine loop by allosteric regulation and such regulation is not observed for CRY2 (Ozcan et al., 2021a). Collectively, these studies provide direct evidence that allosterism in CRY1 is critical for the regulation of circadian rhythm. In a similar approach, different SNPs of CRY 2 from the Ensembl database are identified and studied in vitro (Parlak et al., 2022b). Three CRY2 variants (p.Pro123Leu, p.Asp406His, and p.Ser410Ile) are identified at the rim of the secondary pocket and showed reduced repressor activity on CLOCK/BMAL1 transactivation. Further biochemical studies indicate that all three variants' nuclear localizations are altered independently of PER2. Additionally, the CRY2 variants are unable to rescue the rhythm of $Cry1^{-/-}/Cry2^{-/-}$ mouse embryonic fibroblast cells (DKO-MEF) even in the presence of PER2 overexpression. Interestingly, although the CRY2 variants had comparable PER2 affinity, they could not translocate from the cytoplasm to the nucleus. It

shows that the rim of the secondary pocket of CRY2 plays a significant role in its nuclear localization independently of PER2 and in the intact circadian rhythm at the cellular level. Consistently, our group reported previously that Arg501 and Lys503 residues of mCRY2 within this C-terminal region abolish interaction with PER2, but the variant CRY2 proteins can still localize to the nucleus, supporting the PER2 independent localization of CRY2 (Chan et al., 2021; Ozber et al., 2010) investigated several somatic CRY2 variants identified in human cancers rather than germ-line-inherited variations. They selected CRY2 SNPs based on their predicted impacts on the interactions between CRY2, FBXL3, and c-MYC. Human CRY2 D347H and CRY2 S532L variants showed a reduced affinity for CLOCK and are unable to repress CLOCK/BMAL1-driven transcription. Mutants failed to suppress 2D colony growth in c-MYC–expressing fibroblasts. In $Cry2^{-/-}$ MEFs expressing CRY2 mutants, gene set enrichment analysis revealed a decrease in Tp53 mRNA and expression of TP53 target genes. These findings suggest that CRY2 influences P53 activity and cell growth. Notably, D347 is located on the edge of the secondary pocket of CRY2 that plays a critical role in the stable recruitment of CRYs to CLOCK/BMAL1. Together with our above findings (Parlak et al., 2022b), the D347H mutation represents another example of how the secondary pocket is important for CRY function in the clock mechanism.

CHAPTER 3
MATERIALS and METHODS

3.1 Selection of mutations and generation of initial models along wild type CRYs

The protein structures of CRY1 and CRY2 were obtained via homology modeling. Complete PHR domain sequences of CRY1 and CRY2 were obtained from UniProt (mouse CRY1(P97784), mouse CRY2(Q9R194)). Residues between 3-491 and 21-510 are used to model the PHR domain for CRY1 and CRY2. Sequences were submitted to the RaptorX web server to obtain protein structures for CRY1 and CRY2.(H. Wang et al., 2012) The structure of the G144V, R293H, and R348C CRY1 was also obtained by the same procedure. Cry2 R293H mutant protein structures were generated using VMD psfgen plugin using respective model. For repression deficient mutants, previously(McCarthy et al., 2009) described single or double mutants with deficient repression activity were mapped onto the average structure of the CRY1 wild type. Mutations that are not in close proximity (within 4Å) of the serine loop (G43), to prevent direct interaction, are selected for further characterization. For CRY1, alongside R293H, four mutants were selected (A217V/L218F, C259Y, E214K, and G288R), and three mutants (A235T, E312K, and G230R) were selected for CRY2. Mutant structures are generated from their respective wild type structures in PyMol.

3.2 Molecular Dynamics Simulation

All structures were protonated with PROPKA using the PDB2PQR webserver (Dolinsky et al., n.d.)**.** The CHARMM36m force field was used for simulations (Huang et al., 2017). All systems were configured as described previously (S. Gul et al., 2022b). Structures solvated using the TIP3P water model. 10Å of padding from the closest atom was added in all axes. Appropriate amounts of sodium and chloride ions were added to systems to neutralize and reach 0.15mM salt concentration. Periodic boundary conditions and Particle Mesh Ewald (PME) are used for full electrostatic interactions with a 12Å cutoff. All covalent

hydrogen bond lengths were constrained with the SHAKE algorithm with a time-step of 2 fs. Langevin dynamics, Langevin thermostats, and the modified Nose-Hoover method, applied to control the temperature and pressure of systems, respectively. All configurations were minimized for 50,000 steps with fixed backbone atoms and another 50,000 steps without any constraints. After minimization, all systems were stepwise heated to 310K. During equilibration, harmonic constraints 3kcal*mol^{-1}*A^{-2}, on CA atoms are gradually removed. After equilibration, for wild type CRY1/2 systems, 300ns of production runs were performed. In the same manner, for CRY1 mutants (R293H, A217V/L218F, C259Y, E214K, and G288R) and CRY2 mutants (A235T, E312K, and G230R, R311H), at least 150ns and 100ns of production runs were performed under NPT (constant number of atoms, constant pressure, and constant temperature) conditions, respectively. All production runs were performed at 310K and under 1atm pressure. All initial configurations were prepared and run in Visual Molecular Dynamics (VMD) and Nanoscale Molecular Dynamics (NAMD) software, respectively, using CHARMM c36m force fields. A total of more than two microseconds of molecular dynamics simulations were performed. The first 10ns of all trajectories are discarded before further analysis.

3.3 Post-analysis of trajectories

To verify integrity of systems, all trajectories aligned with the initial frame of the wild type CRY1 structure. Root mean square deviation (RMSD) values are calculated to confirm all systems reached an equilibrium state. Root mean square fluctuations (RMSF) profiles were calculated and compared to respective wild type system to explore possible flexibility differences in mutant systems. Number of hydrogen bonds that serine loop establishes were calculated to see whether it contributes to differential dynamics of the serine loop and residue interaction energies. All priori calculations performed in VMD v1.9.3. Evenly distributed ten frames for every nanosecond were extracted from every trajectory used for further analysis. Inter-residue distances were calculated to compare motions of the serine loop among wild type and mutant systems, with a custom Python script. Secondary pocket in CRYs serves as protein-protein interaction (PPI) interface for CLOCK-CRY heterodimer. Volume of this

pocket indicate its availability for this interaction. Therefore, I calculated cavity volume of the secondary pocket using POVME software. To understand if conformational differences arise from pairwise residue interaction differences, gRINN software was utilized with default parameters other than the residue selections, to calculate pairwise residue interaction energies (Sercinoglu & Ozbek, 2018). Suboptimal pathway length differences and involving residues may contribute to understand the underlying mechanism that how distantly located residues affects the dynamics of the secondary pocket. Therefore, command-line version of Weighted Implementation of Suboptimal Paths (WISP) software was used to calculate optimal and suboptimal pathways and pathway lengths between source and sink residues, with default parameters other than side chains included in node definition and the maximum number of paths set to 50 (Van Wart et al., 2014). To understand whether any conformational difference among systems predominantly observed, pairwise best-fit RMSD based method implemented in UCSF Chimera were used for clustering trajectories. Clusters that are representative of the most crowded clusters are used for visualization in PyMol. Clusters representative of the most crowded cluster in both CRY2WT and CRY2 mutants are used to dock the CLOCK-PASB domain (261-384) in the HADDOCK webserver. CLOCK-PASB domain extracted from the crystal structure (PDBID: 4F3L). Gly124, Arg127, Asp382, Glu383 are used as restrains for CRY2 and Gly332, His360, Gln361, Trp362, Glu367 are used as restrains in CLOCK. The rest of the docking was done with default parameters. Throughout the trajectory, u/w angles of the Serine loop (CRY1:38-48, Cry2:56-66) calculated via an in-house Python script. Plots were generated in R using ggplot2.

3.4 Molecular Docking Studies

Wild type CRY1 trajectory (300ns) subjected to pairwise best-fit RMSD based method implemented in UCSF Chimera for clustering analysis. Cluster representative of the most crowded cluster is taken as near psychological and most represented conformation. This structure further used for molecular docking studies. Current Ambinter catalogue for small molecules retrieved from Ambinter website (https://ambinter.com/catalogue/Ambinter_Screening_Library.sdf.tgz). Around 7 million

molecules subjected to preliminary filtering. CRY1 primary and secondary pocket volumes are drastically different. Ambinter catalogue is filtered mostly according to Lipinski's rule of five, Ghose filter, Veber's Rule with minor modifications with OpenBabel software. Most notably, molecular weight limit set to 300 Da considering DMRL, a known cofactor of photolyases in their secondary pocket. Around 1.2 million molecules were survived, then converted to 3D via OpenBabel software. Rectangular grid box, large enough to cover secondary pocket placed via visual inspection. Surviving molecules docked to the CRY1 secondary pocket via Autodock Vina. Then candidate molecules sorted according to their binding energies.

3.5 MTT Toxicity Assay

Cytotoxicity of small molecules tested U2OS *Bmal1:dLuc* and HEK293T cell lines. First, 4000 cells/well were seeded to clear 96-well plates (in triplicate). Cells grown for 48 h at 37°C 5% CO_2. Next, cells are treated with small molecules solvated in DMSO, at final concentration 20µM,10 µM and 5 µM doses without exceeding 0.5% DMSO as the final concentration. Molecules and cells were incubated for another 48 h. Since mitochondria convert tetrazolium dye 3-[4,5-dimethylthiazol-2-yl]−2,5 diphenyl tetrazolium bromide (MTT) to insoluble formazan (purple color), each well was treated with tetrazolium MTT to measure the cell viability. After incubating cells with MTT reagent for 4 h, the purple formazan was dissolved in DMSO:EtOH (1:1, v/v). The absorbance of solutions in wells was measured at 600 nm. As a negative control, cells treated with 5% final DMSO were evaluated. Experiment done as three biological replicates which each of them is average of 3 technical replicates.

3.6 LUC Degradation Assay

To test if small molecules affect luciferase half-life, I used *pCDNA-Luc* plasmid. *Luc* plasmid (5 ng) were transfected to HEK293T cells (4×10^4) in an opaque 96-well plate (flat bottom) by reverse transfection with polyethyleneimine (PEI). Following day, cells

treated with small molecules at their highest non-toxic dose, or an equivalent amount of DMSO as control group. After 24 h, luciferin (0.4 mM final) and HEPES (10 mM final, pH = 7.2) were added to the cells. Cells were treated with cycloheximide (CHX) (20 µg/ml final) after the addition of luciferin, to inhibit protein synthesis. Optically clear film was used to seal the plate. Synergy H1 recorded the bioluminescence readings at 32 °C every 10 min for 24 h. One-phase exponential decay function of GraphPad Prism v.5.0 software (CA, USA) was used to calculate the half-life of proteins. Experiment done as three biological replicates which each of them is average of 3 technical replicates.

3.7 Real-Time Bioluminescence Monitoring

Synergy H1 used for recording real-time bioluminescence at initial screening phase. U2OS cells stably expressing *Bmal1*-d*Luc* seeded in a 96-well plate at density of $4x10^4$ cell per well. The next day, cells were treated with dexamethasone (DXM) (0.1 µM final) for 2 h for resetting. After 2 h, the media of cells were replaced with bioluminescence recording media having DMEM powder (sigma D-2902, 10X 1 L), 0.35gr sodium bi-carbonate (tissue culture grade, sigma S5761), 3.5gr D(+) glucose powder (tissue culture grade, sigma G7021), 10 mL 1 M HEPES buffer (Gibco 15140-122), 2.5 mL Pen/Strep (100ug/ml), 50 mL 5% FBS (in 1 L). Luciferin (0.1 mM final) and small molecules at their highest non-toxic dose without exceeding 0.5% DMSO as the final concentration, were added fresh to the bioluminescence media. Optically clear film was used to seal the plate. Bioluminescence is recorded with Synergy H1.

LumiCycle (Actimetrics, Inc., Evanston, IL) was used for were used for high-resolution real-time bioluminescence assay. $4x10^5$ U2OS cells stably expressing *Bmal1*-d*Luc* per 35mm plate were seeded. The next day, cells were treated with dexamethasone (DXM) (0.1 µM final) for 2 h for resetting. After 2 h, the media of cells were replaced with bioluminescence recording media. Luciferin (0.1 mM final) and small molecules at 20µM, 10 µM and 5 µM doses, without exceeding 0.5% DMSO as the final concentration, were added fresh to the bioluminescence media. To prevent evaporation and gas exchange silicon grease was used to seal plates. Bioluminescence recorded for the following 7 days.

CHAPTER 4
RESULTS

4.1 Single Nucleotide Polymorphisms (SNPs)

Although high and low frequency SNPs are associated with different type of diseases, functional significance of rare missense mutations have yet to be explained. Therefore, single nucleotide polymorphisms (SNPs), that met the criteria, on *CRY1* gene identified from 1000 Genomes project and Ensembl databases(Auton et al., 2015; Zerbino et al., 2018). First, SNPs that are not in coding region or silent mutations were filtered out. From remaining 116 SNPs, focused was on the ones that is expected to effect Photolyase homology region (PHR) domain based on their position on tertiary protein structure which crucial for functional CRY1 protein(Khan et al., 2012a). Mutations that are predicted to be pathogenic according to SIFT, PolyPhen, and Provean scores are further investigated (**Table 4.1**). Remaining mutations are interpreted as "disease-causing" by MutationTaster (Schwarz et al., 2014). and the clinical effects of these variants. Although these variants were classified as "variant of uncertain significance-VUS", and all of them meet two pathogenic American College of Medical Genetics and Genomics criteria (guide- lines for interpretation of sequence variants)(Richards et al., 2015). None of these variants were reported in ClinVar. The p.Arg293His and p.Arg348Cys CRY1 variants were detected as heterozygous; the genotype of the p.Gly144Val was not reported in Ensembl. To analyze the degree of conservation of these SNPs, multiple sequence alignment was performed (**Fig. S1A**). The Arg-293 in CRY1 is conserved in all CRY1, whereas Gly-144 is conserved in all CRY1 proteins except for mosquito CRY1. Finally, Arg-348 is conserved in CRY1 from most organisms, but not in CRY1 from sponge, mosquito, housefly, green sea turtle, blowfly, and stony coral. WT amino acids in all three SNPs are highly conserved in the CRY1 across different organisms, which suggests a potential role in protein function. Thus, investigation of the effects of these variants at the molecular level performed.

Table 4. 1 The clinical features of selected CRY1 SNPs.

Adapted from (S. Gul et al., 2020)

dbSNP	Position in CDS (NM_004075.4)	Position in protein (NP_004066.1)	SIFT/PolyPhen/Provean	ACMG	gnomAD exom	ClinVar
rs78310335	c.431G.T	p.Gly144Val	0/0.999/damaging	VUS (PM2, PP3)	not detected	—
rs772585429	c.878G.A	p.Arg293His	0/1/damaging	VUS (PM2, PP3)	*f* = 0.00000797	—
rs749506981	c.1042C.T	p.Arg348Cys	0/0.989/damaging	VUS (PM2, PP3)	not detected	—

4.2 The effect of SNPs on CRY1 t1/2 and molecular clock function and interactions.

The functional characteristics of the selected rare missense variations were studied in detail using biochemical and cell-based assays. Mapping of SNPs onto the crystal structure of CRY1 indicated that these SNPs are located on functionally important domains. Gly-144 and Arg-348 are both exposed to solvent and are located on the loop between helices α5 and α6, or in helix α14, respectively (**Fig 4.1A**). Arg-293 is located within the FAD binding pocket and FBXL3 interaction site which is adjacent to the secondary pocket. Because FBXL3 is the E3 ligase responsible for ubiquitination of CRY1, mutations in this region of FBXL3 might change the stability of CRY1. We, therefore, investigated the effect of these mutations on the half-life ($t_{1/2}$) of CRY1

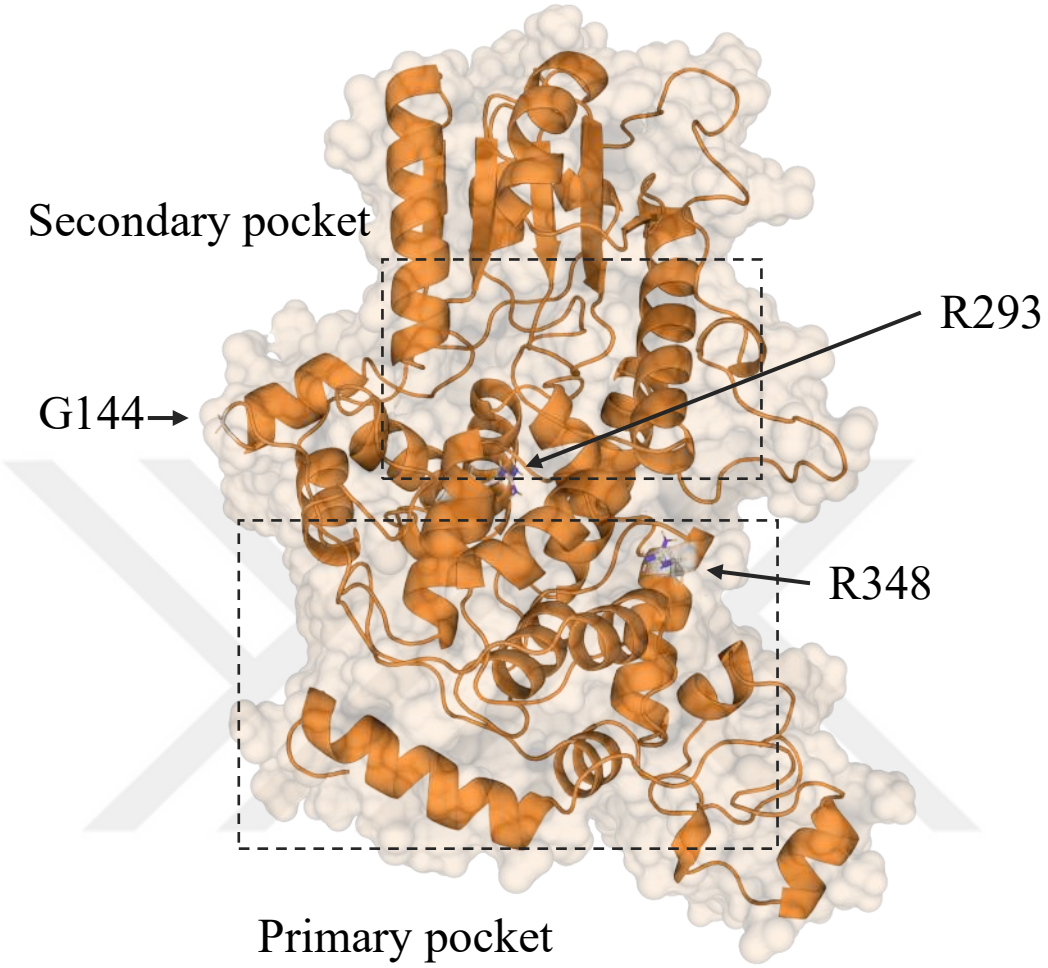

Figure 4. 1. Three rare SNPs affect highly conserved amino acid residues in CRY1.

Positions of SNPs were visualized in the mCRY1 structure using Pymol. The mCry1 protein structure is shown as a ribbon diagram and transparent surface representation, and the mutant residues are shown as sticks (Grey). Secondary pocket (FAD binding pocket) and primary pocket were indicated with dashed lines. Gly-144 and Arg-348 are exposed to solvent; Arg-293 is in the primary pocket facing the secondary pocket.

by monitoring the degradation of CRY1 fused to LUC (CRY1::LUC) at the C-terminal. After generating *Cry1* variants, plasmids were transiently transfected into HEK293T cells, which

were then treated with cycloheximide to inhibit protein synthesis. Luminescence was monitored to determine the $t_{1/2}$ of the proteins. Stability of the p.Arg348Cys CRY1 and p.Gly144Val CRY1 variants were found to be similar to WT CRY1 (**Fig. S2A**). However, the t1/2 of the p.Arg293His CRY1 variant was significantly longer than that of WT CRY1 and shorter than luciferase. Next, the effect of these variants on circadian clock function were determined. To do this, a complementation assay using *Cry1*$^{-/-}$ *Cry2* $^{-/-}$ mouse embryonic fibroblast cells (DKO-MEF) was employed. Plasmid constructs carrying WT Cry1 were shown to rescue circadian rhythms in DKO-MEF when expressed under the control of mCry1 promoter containing E/E9-box and D-box elements and the ROR/REV-ERB-binding element in the first intron (Ukai-Tadenuma et al., 2011). The Cry expression vector carrying either the variants or WT Cry1 and the mPer2-dLuc reporter plasmid were transiently expressed in DKO-MEF cells. Although WT and variants were able to restore the circadian rhythm, they had varying effects on period length. The period length for WT CRY1 was calculated as 26.3 h **(Fig 4.2A,B)**. Next, the effect of these variants on circadian clock function were determined. To do this, a complementation assay was employed using *Cry1*$^{-/-}$ *Cry2* $^{-/-}$ mouse embryonic fibroblast cells (DKO-MEF). Plasmid constructs carrying WT *Cry1* were shown to rescue circadian rhythms in DKO-MEF when expressed under the control of m*Cry1* promoter containing E/E'-box and D-box elements and the ROR/REV-ERB-binding element in the first intron(Ukai-Tadenuma et al., 2011). Thus, the p.Gly144Val, p.Arg293His, and p.Arg348Cys variants were introduced into the pMU2-Cry plasmid. The Cry expression vector carrying either the variants or WT Cry1 and the mPer2-dLuc reporter plasmid were transiently expressed in DKO-MEF cells. Bioluminescence for 5 days was monitored. Although WT and variants were able to restore the circadian rhythm, they had varying effects on period length. The period length for WT CRY1 was calculated as 26.3 h (**Fig 4.2A,B**). The p.Gly144Val and p.Arg348Cys CRY1 variants increased the period length to 27.8 and 27 h, respectively. Despite the longer t1/2 of the p.Arg293His CRY1 variant, the mutant caused a significantly shorter period length (23.8 h) and displayed weaker repressor activity based on higher luminescence intensities compared with WT CRY1. Because rhythm is generated as a result of interaction between core clock proteins, e.g. CRY1, PER2, BMAL1, and CLOCK, this intriguing observation on p.Arg293His mutant led us to analyze binding properties of these mutants to the core clock proteins.

To assess binding of each CRY1 variants to CLOCK and BMAL1, HEK293T cells were transiently transfected with expression plasmids coding for CLOCK, Bmal1, and either WT or Cry1 variants. The CRY1-myc-His (variants or WT) containing protein complexes were then precipitated using Ni-NTA agarose, and the samples were probed for the presence of CLOCK and BMAL1 by Western blot analysis as described previously. To assess the binding of CLOCK properly, comparable amount of the CRYs were used in pulldown assay. The p.Gly144Val and p.Arg348Cys CRY1 variants exhibited similar affinities to BMAL1/CLOCK compared with WT CRY1, whereas the p.Arg293His CRY1 variant exhibited significantly less affinity to BMAL1/CLOCK (**Fig. S3A**). A similar experiment was performed in the presence and absence of PER2 to investigate the possibility that PER2 is required for proper binding. All three CRY1 variants and WT CRY1 bound similar

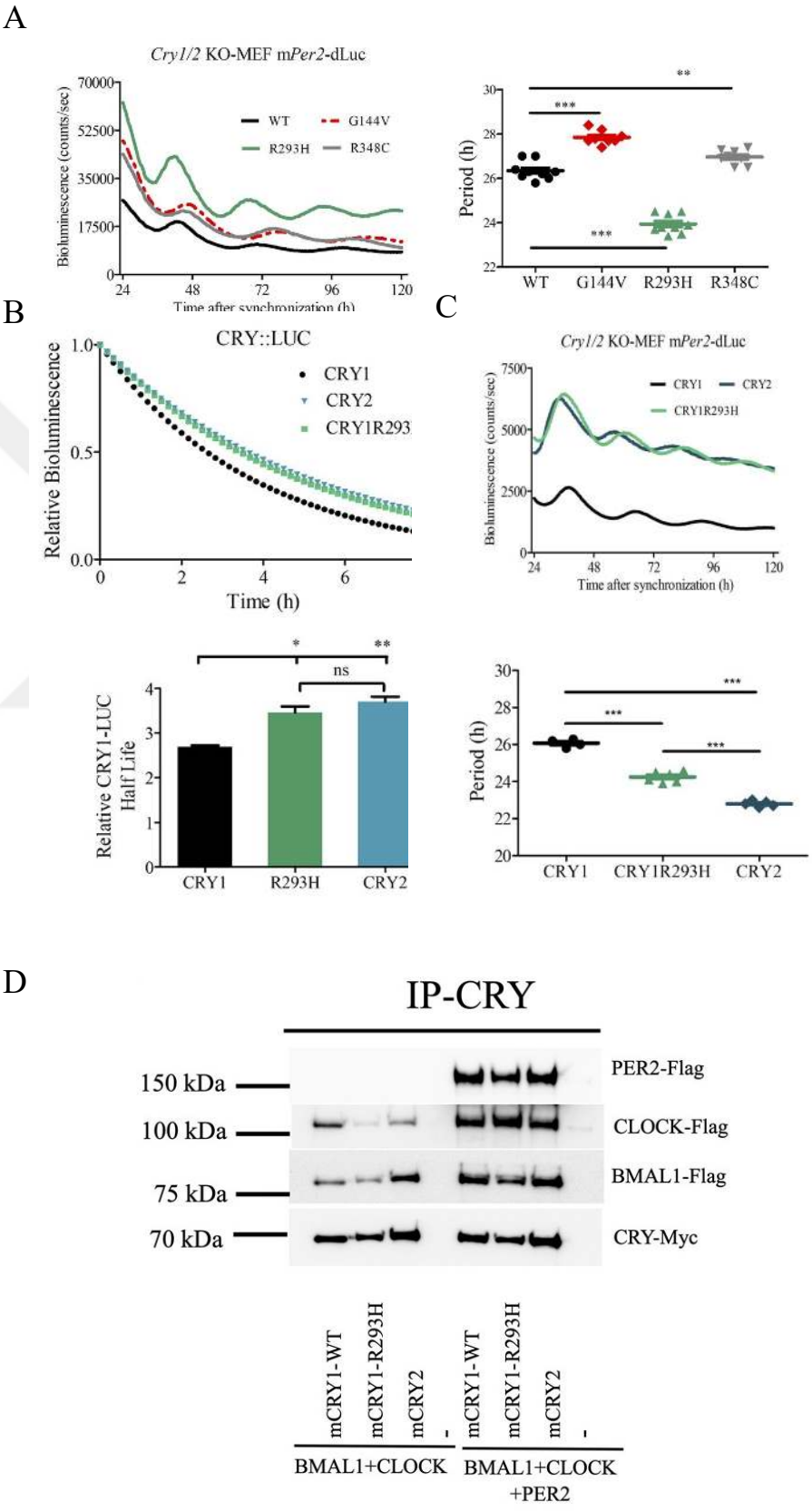
A
Cry1/2 KO-MEF mPer2-dLuc
Bioluminescence (counts/sec)
WT
G144V
R293H
R348C
Time after synchronization (h)
Period (h)
B
CRY::LUC
Relative Bioluminescence
CRY1
CRY2
CRY1R293
Time (h)
Relative CRY1-LUC Half Life
ns
C
Cry1/2 KO-MEF mPer2-dLuc
Bioluminescence (counts/sec)
CRY1R293H
Time after synchronization (h)
Period (h)
D
IP-CRY
150 kDa
100 kDa
75 kDa
70 kDa
PER2-Flag
CLOCK-Flag
BMAL1-Flag
CRY-Myc
mCRY1-WT
mCRY1-R293H
mCRY2
BMAL1+CLOCK
BMAL1+CLOCK +PER2

Figure 4. 2. Effects of CRY1 variants on circadian phenotype and clock interaction.

Adapted from (S. Gul et al., 2020) A) WT or variant CRY rescued circadian rhythms in *Cry1*$^{-/-}$ *Cry2*$^{-/-}$ MEF cells with varying effects on period and amplitude. DKO MEF cells transiently transfected with pGL3-Per2-dLuc and Cry rescue plasmids (WT or variant). After 72 h, cells were synchronized with dexamethasone (0.1 mM) and luminescence values were recorded for 5 days. CRY1 rhythm was representative bioluminescence of four independent experiments with eight plates. The circadian period from all plates were determined. Statistical analysis was per- formed using an unpaired t test with a Welch's correction (***, p , 0.0001; **, p , 0.005; *, p , 0.05; G144V, p , 0.0001; R293H, p , 0.0001; R348C, p , 0.0044). B) Average t1/2 values 6 S.E. from three independent experiments (with triplicate samples) relative to WT CRY1::dLUC were reported (left panel). Statistical analysis was performed using an unpaired t test with a Welch's correction (***, p , 0.0001; **, p , 0.005; *, p , 0.05; WT CRY1 versus R293H, p = 0.0226; WT CRY1 versus CRY2, p = 0.0034; R293H CRY1 versus CRY2, p = 0.4854). Degradation of WT CRY1 and R293H CRY1 was analyzed by immunoblot using anti-Myc for CRYs and anti-b-actin for loading controls (right panel). Degradation of LUC was compared with WT and R293H CRY1::LUC. C) pArg293His CRY1 and CRY2 rescued the rhythm similarly, although periods are still significantly different. Representative rhythms of three in- dependent experiments are shown. Periods and amplitudes of all plates were reported (4-WT, 6-R293H CRY1, and 6-CRY2). Significance analysis was per- formed using unpaired t test with Welch's correction (***, p , 0.0001; **, p , 0.005; *, p , 0.05; WT CRY1 versus R293H, p , 0.0001; WT CRY1 versus CRY2, p , 0.0001; R293H CRY1 versus CRY2, p , 0.0001). D, pulldown analysis of WT or pArg293His CRY1, CRY2 with BMAL1, CLOCK, and PER2. HEK293T cells were transfected with plasmids expressing Bmal1-FLAG, CLOCK-FLAG, and Cry-His-Myc. Proteins were pull downed with Ni-NTA agarose resin and analyzed with Western blotting. This blot is the representation of three independent experiments.

amounts of PER2. Nevertheless, the p.Arg293His CRY1 variant was to bind less BMAL1/ CLOCK in the absence of PER2 (**Fig. S3B**). Biochemical binding analysis showed that

reduced repression by the p.Arg293His variant of CRY1 is most likely caused by attenuated binding to the BMAL1/CLOCK dimer. However, the p.Gly144Val and p.Arg348Cys variants retained binding activity to the BMAL1/CLOCK dimer. Overall, the p.Arg293His CRY1 variant had longer t1/2, rescued circadian rhythms with shorter period in a weakly repressed state in DKO-MEF cells (**Fig. S3B**) and exhibited reduced affinity for the BMAL1/CLOCK dimer even in the presence of PER2 (**Fig. S3**). These features of the p.Arg293His CRY1 variant reported here are very similar to those reported for

CRY2(Khan et al., 2012b; Rosensweig et al., 2018b), which led us to perform additional studies. p.Arg293His CRY1 variant exhibits similar characteristics to CRY2

The secondary pocket of CRY1 is critical for its interaction with CLOCK. Subtle changes in this pocket can result in substantial differences in periodicity in cycling cells(Fribourgh et al., 2020; Michael et al., 2017). For example, differential rhythms driven by CRY1 and CRY2 are the result of these changes(Rosensweig & Green, 2020). To directly compare p.Arg293His CRY1 and WT CRY2, their half- lives and effects on circadian rhythms were measured using DKO-MEF cells. Both the pArg293His CRY1 variant and WT CRY2 exhibited similar half-lives (**Fig 4.2B**). It has been shown that CRY2 can rescue circadian rhythms when the pMU2 plasmid with Cry2 cDNA is transfected in DKO-MEFs (Rosensweig et al., 2018b; Ukai-Tadenuma et al., 2011). Therefore, Cry2 cDNA into the pMU2 plasmid were cloned and transfected this construct into DKO-MEF to see whether it rescues circadian rhythms. Compared with CRY1, CRY2 was able to rescue circadian rhythms with a shorter period, which was consistent with a previous study(Rosensweig et al., 2018b). Our results showed that cells expressing CRY2 had higher overall luminescence intensity than cells expressing CRY1, suggesting higher BMAL1/CLOCK activity, again consistent with a previously published report (22). Interestingly, cells expressing the p.Arg293His CRY1 or CRY2 had similar luminescence level (**Fig 4.2C**). In the complementation assay, DKO-MEF cells expressing WT CRY1 or CRY2 had circadian periods of 26.2 and 22.9 h, respectively. Cells expressing the p.Arg293His CRY1 variant had a period length of 24.1 h, which is shorter than that of WT CRY1 and longer than CRY2.

Finally, the amplitude of the circadian rhythm was higher in cells expressing p.Arg293His CRY1 variant and CRY2 than WT CRY1.

To compare the ability of p.Arg293His CRY1 and CRY2 to repress BMAL1/CLOCK trans- activation, an mPer1-dLuc assay using *Cry1*$^{-/-}$ *Cry2* $^{-/-}$ MEF cells was utilized. These results indicated that both CRY2 and p.Arg293His CRY1 had comparable levels of repressor activity that was dose-dependent and statistically significantly different from that of WT CRY1 (**Fig. S4C**). Additionally, binding of WT and p.Arg293His CRY1 and CRY2 to BMAL1, CLOCK, and PER2 were analyzed side by side (**Fig 4.2D**). Pulldown assay in the absence and presence of PER2 was performed to assess the binding ability of WT CRY1, CRY2, and p.Arg293His CRY1 to CLOCK. All CRYs tested in this study had comparable binding to CLOCK in the presence of PER2. However, CRY2 and p.Arg293His CRY1 had attenuated binding to CLOCK compared with WT CRY1 in the absence of the PER2.

Collectively, our results suggested that the p.Arg293His CRY1 variant possesses similar properties to CRY2 in terms of stability, binding to core clock components, repression activity and rescuing circadian rhythms in DKO-MEF, except p.Arg293His CRY1 generated longer rhythm than CRY2.

4.3 Understanding the role of Arg-293 in CRY1 function

Although p.Arg293His CRY1 variant exhibits CRY2-like in vitro properties, the conservation of this amino acid residue in all mammalian CRY1s suggests that it might play an important role, such as regulation of CLOCK binding to the secondary pocket of CRY1. To investigate this, I employed MD simulations using CRY1 structural data. Recently, it has been shown that CRYs bind to the CLOCK PASB domain through the secondary pocket, and this is regulated by the serine loop(Fribourgh et al., 2020). I, therefore, explored possible dynamical differences between WT CRY1 and p.Arg293His CRY1 around the secondary pocket via MD simulations. p.Gly144Val CRY1 and p.Arg348Cys CRY1 structures were also simulated as controls. For this purpose, I utilized mouse CRY1 crystal structure to generate a complete PHR domain of the individual variants. Each protein was sampled for 300 ns, and the root mean square deviation (RMSD) values were determined to show that

simulations reached equilibrium (**Fig 4.3A**). To investigate the dynamics of each residue, root mean square fluctuation (RMSF) values were assessed (**Fig 4.3B**). I observed differences in the RMSF values of residues in the serine loop (residues 38–48). When compared with WT CRY1, the residues in p.Arg293His CRY1 simulations showed minimal dynamism/fluctuation (**Fig 4.3B**). Because the serine loop regulates the volume and access to the secondary pocket, I analyzed the volume of the secondary pocket using POVME 3.0 software. Analysis showed that simulations of p.Arg293His CRY1 sampled significantly smaller secondary pocket volume than WT CRY1. Secondary pocket volume of p.Gly144Val CRY1 was comparable to WT CRY1. Interestingly, p.Arg348Cys CRY1 simulation sampled a larger secondary volume pocket. Because secondary pocket volume of WT CRY1 allows CLOCK binding, I do not expect larger pocket volume will affect CLOCK binding to p.Arg348Cys CRY1. In fact, rescue assays (**Fig 4.2A**) and BMAL1/CLOCK binding analysis to CRY1 variants (**Fig. S3**) confirmed that p.Arg348Cys mutation did not change the binding of CRY1 to CLOCK. To further examine the relative internal dynamics of the loop, I analyzed the distance between the Ca atoms of Gly-43 located on the loop and Phe-105 (**Fig 4.3D**

A

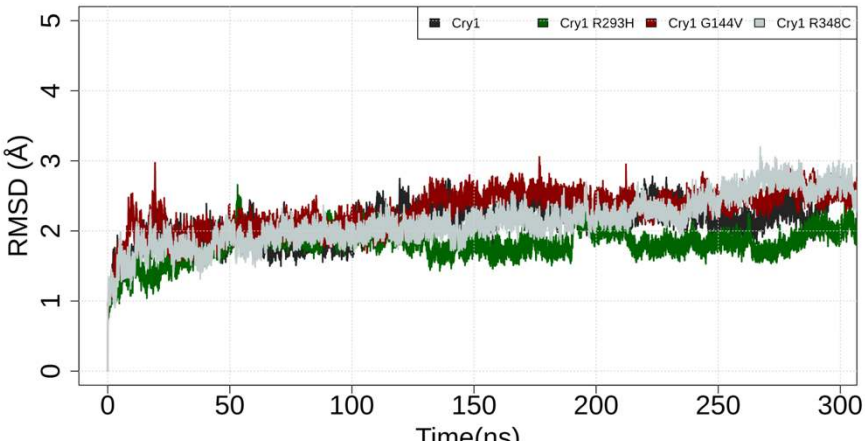
Cry1
Cry1 R293H
Cry1 G144V
Cry1 R348C
RMSD (Å)
0
1
2
3
4
5
0
50
100
150
200
250
300
Time(ns)

B

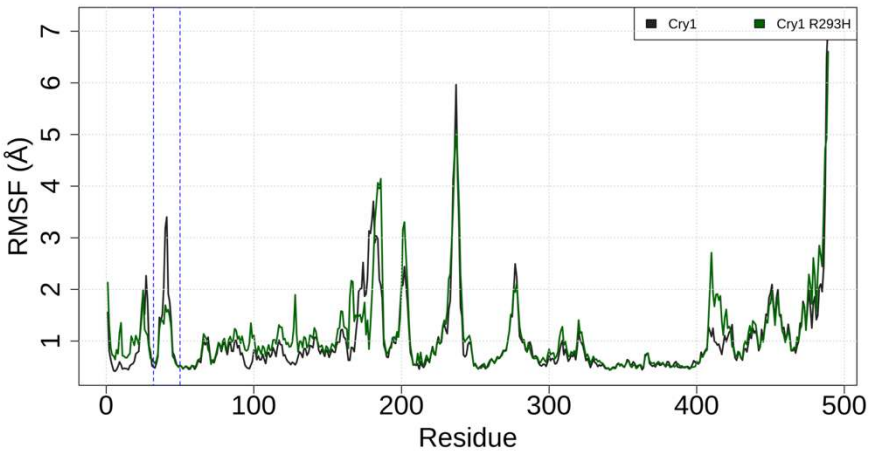
Cry1
Cry1 R293H
RMSF (Å)
1
2
3
4
5
6
7
0
100
200
300
400
500
Residue

C

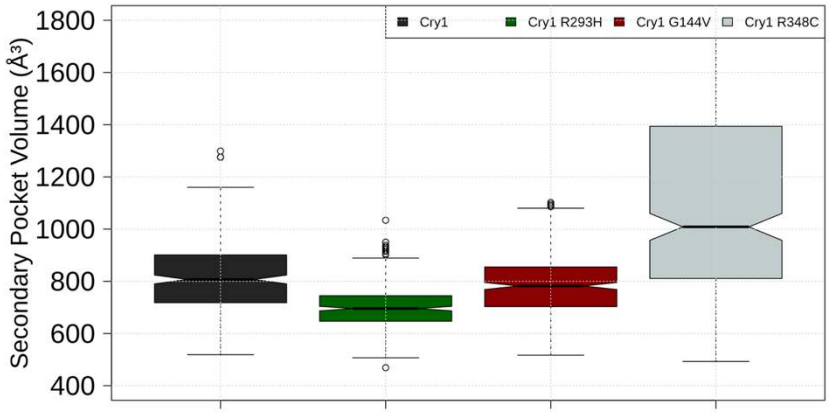
Cry1
Cry1 R293H
Cry1 G144V
Cry1 R348C
Secondary Pocket Volume (Å³)
400
600
800
1000
1200
1400
1600
1800

D

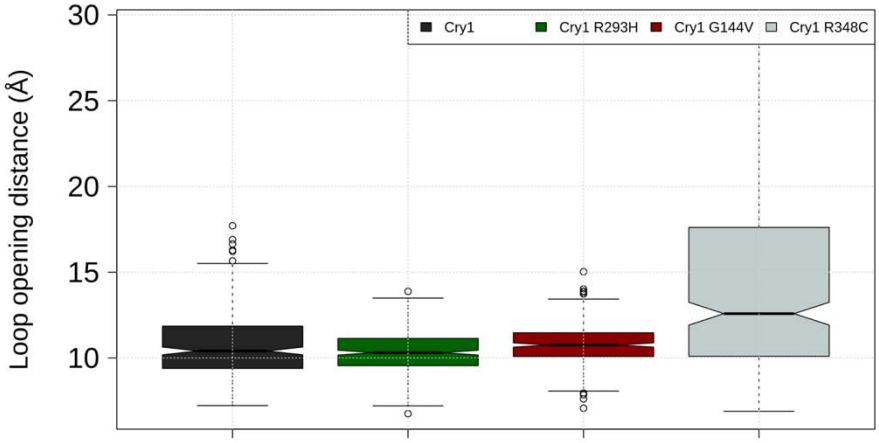
Cry1
Cry1 R293H
Cry1 G144V
Cry1 R348C
Loop opening distance (Å)
30
25
20
15
10

E

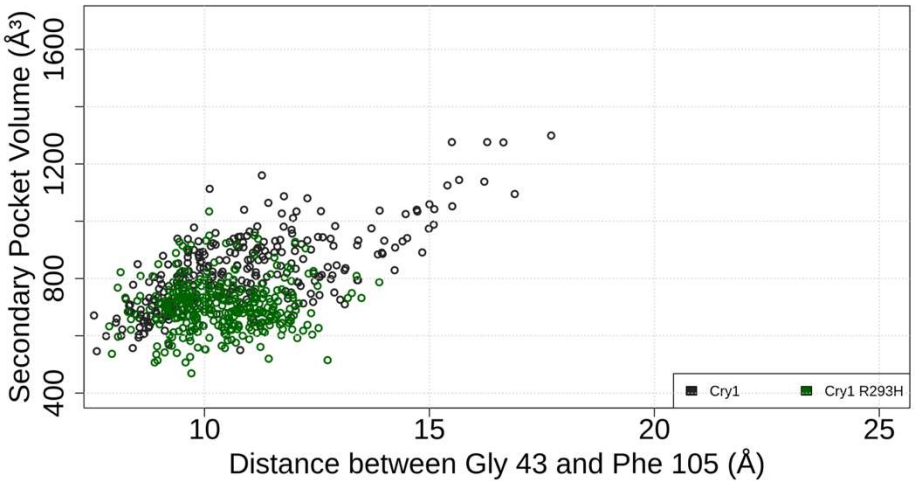
Secondary Pocket Volume (Å³)
1600
1200
800
400
Cry1
Cry1 R293H
10
15
20
25
Distance between Gly 43 and Phe 105 (Å)

F

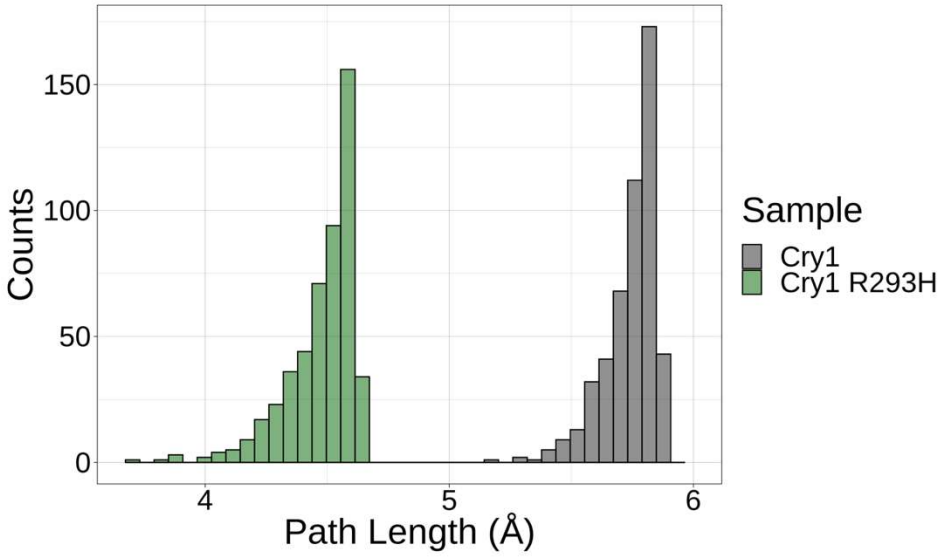
150
100
50
0
Counts
4
5
6
Path Length (Å)
Sample
Cry1
Cry1 R293H

G

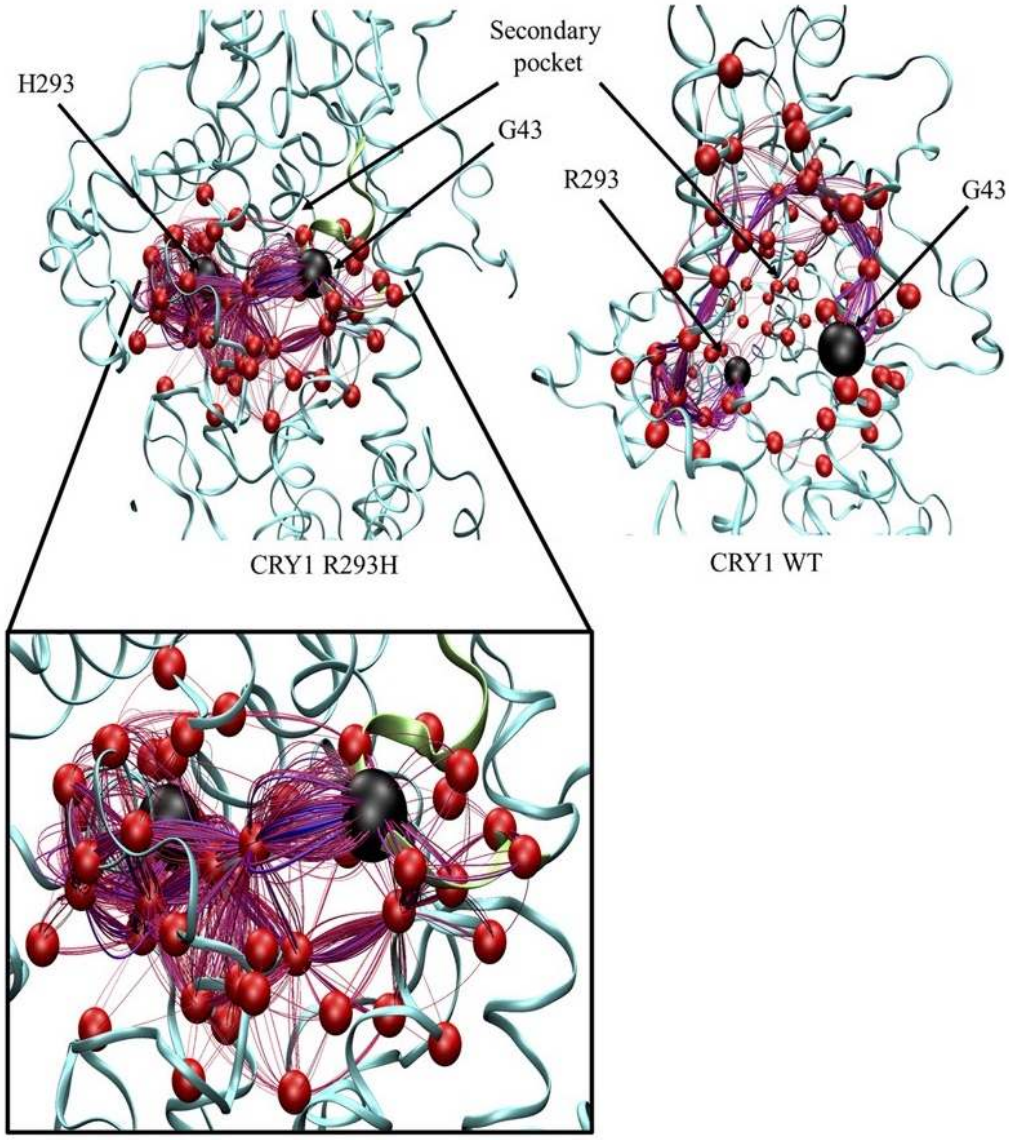

Figure 4. 3. Molecular dynamic simulation studies of mutant and WT CRY1.

Adapted from (S. Gul et al., 2020) A) RMSD of CRY1 WT, G144V, R293H, and R348C CRY1 simulations. B) RMSF of CRY1 WT and pArg293His CRY1. Residue numbering is according to CRY1. Residues between two dashed lines belong to the serine loop. C) Box plot representation of the secondary pocket volume sampled throughout the simulations. Wilcoxon rank sum test was applied (*, p ,0.0001). D) box plot representation of the loop

distance produced by measuring the distance between Ca atoms of Gly-43 and Phe-105. Distance between Gly-43(on loop) and Phe-105 was calculated with a custom Python script. The same multi-frame PDB files extracted from the trajectories were used to calculate the secondary pocket volume and loop distances. Statistical analysis between variances of loop distances of CRY1 and CRY1R293H simulations was calculated by the Levene's test (p , 0.001). E) scatter plot of the loop distance against the secondary pocket volume in WT and R293H CRY1 simulations. F) Histogram representation of the 500 pathways' lengths calculated by WISP. G) WISP analysis of the 500 pathways for CRY1 WT and CRY1R293H simulations. Red spheres represent the nodes participating in the communication pathway between residues 293 and 43 in CRY1. Each node corresponds to a residue. Residues Arg-293 or His-293 and Gly-43 were shown as black spheres.

and E). The average loop distances of CRY1 and p.Arg293His CRY1 were not significantly different. However, the variance of loop distances sampled throughout the simulations were significantly different (Levene's test). To compare the scatter of loop distance and its correlation with the volume of the secondary pocket, I plotted loop distance against the secondary pocket volume (**Fig 4.3E**). My analysis of secondary pocket volume and loop distance showed that p.Arg293His CRY1 behaved similarly to WT CRY1 (**Fig 4.3C–E**). Despite this similarity between CRY1 and p.Arg293His CRY1 simulations, p.Arg293His CRY1 only sampled a fraction of the space explored by WT CRY1. In line with secondary pocket volume analysis, p.Gly144Val sampled similar loop distance to WT CRY, p.Arg348Cys sampled longer loop distance. These observations in MD simulations implied that the dynamics of the serine loop in CRY1 and p.Arg293His CRY1 are regulated differently. Although the serine loop in WT CRY1 is more dynamic, reduced dynamicity of this loop in p.Arg293His CRY1 might explain the attenuated binding of p.Arg293His CRY1 to CLOCK. To explain this differential regulation on the serine loop in detail, I analyzed possible communication pathways between Arg-293 and the serine loop by using Weighted Implementation of the Suboptimal Paths (WISP) software as described before(Ozdemir et al., 2018). The WISP algorithm can calculate both optimal and suboptimal (longer) communication pathways between nodes (residues). Residue 293 was used as a source residue, and several possible residues on the serine loop (Gly-43, Ser-44, Ser-45, Asn-46)

were used as a sink to determine promising pairs for communicating pathways. A total of 500 pathways between residues Arg-293 and Gly-43 for each WT and p.Arg293His CRY1 were calculated. The shortest pathway length for p.Arg293His CRY1 was calculated as 3.26 Å. The shortest communicating pathway involves the His-293, Ile-392, Ser-391, Trp-390, Gly-43 residues. However, the length of shortest pathway for WT CRY1 was calculated as 5.19 Å, which involves the Arg-293, Phe-296, Ala-300, Pro-104, Gly-106, Arg-109, Trp-8, Ile-36, Asp- 38, Gly-43 residues (**Fig 4.3F and G**). Not only is the shortest pathway changed, but also the suboptimal pathways sampled longer lengths in p.Arg293His CRY1 (**Fig 4.3F**). Residues involved more than 200 suboptimal paths between Arg-293/ His-293 and Gly-43 are Asp-38, Pro-104, Gly-106, Ile-36, Ala-300, Arg-109, Phe-296, Trp-8, and Ala-299 for WT CRY1; Glu-382, Phe-296, Gln-393, and Ile-392 for p.Arg293His CRY1. Both representation of pathways and histogram of pathway lengths showed that the mutation introduced new communicating pathways between His-293 and Gly-43. Taken together, these computational findings suggest that the serine loop is allosterically regulated by residue Arg-293 in CRY1 and reduces the dynamicity of the serine loop, keeping it in a closed conformation.

4.4 Comparison of the role of Arg-293(Arg 311) in CRY1 and CRY2 dynamics

Our previous work showed that p.Arg293His CRY1 variant exhibits CRY2-like in vitro properties(S. Gul et al., 2020). My further molecular dynamic simulation revealed that the Arg-293 is responsible for allosteric regulation of the Ser-loop, which plays an important role in CLOCK-CRY1 binding. The multiple sequence alignment with other CRYs from different organisms showed the conservation of this residue, including mammalian CRY2. To understand the role of Arg-311 (homolog of Arg-293 of CRY1) in allosteric regulation of CRY2 I employed molecular dynamics (MD) simulations using CRY1, CRY1-R293H, CRY2, and CRY2-R311H structures for MD simulations. All structures were modeled, protonated, and solvated as described in (S. Gul et al., 2020) and then, CRY2 and CRY2 R311H simulated near physiological conditions for a total of 400 ns. I calculated root-mean-square deviation (RMSD) values for each structure to show that simulations reached

equilibrium (**Fig 4.4A**). I compared the dynamics of CRY1 and CRY2 by plotting root-mean-square fluctuation (RMSF) of each amino acid residue in CRYs. Overall, the dynamicity of both CRYs is different, especially loop regions, namely, Ser-loop and P-loop (**Fig 4.4B**). Ser-loop in CRY1 was found to be highly dynamic compared to Ser-loop of CRY2. I then compared RMSF plot of CRY2-R311H with CRY2 to evaluate change in the dynamicity of both structures. Results demonstrated that Ser-loop dynamicity are very similar in both structures. However, the P-loop behavior was greatly affected by the mutation in CRY2 (**Fig 4.4B, C, D**). Contrary to effects differential of R293H mutation on Ser-loop, on C-lid increased the dynamicity in both CRY1 and CRY2. Collectively, my data suggested that the highly conserved Arg amino acid residue in CRY1 and CRY2 has differential effects on the CRYs.

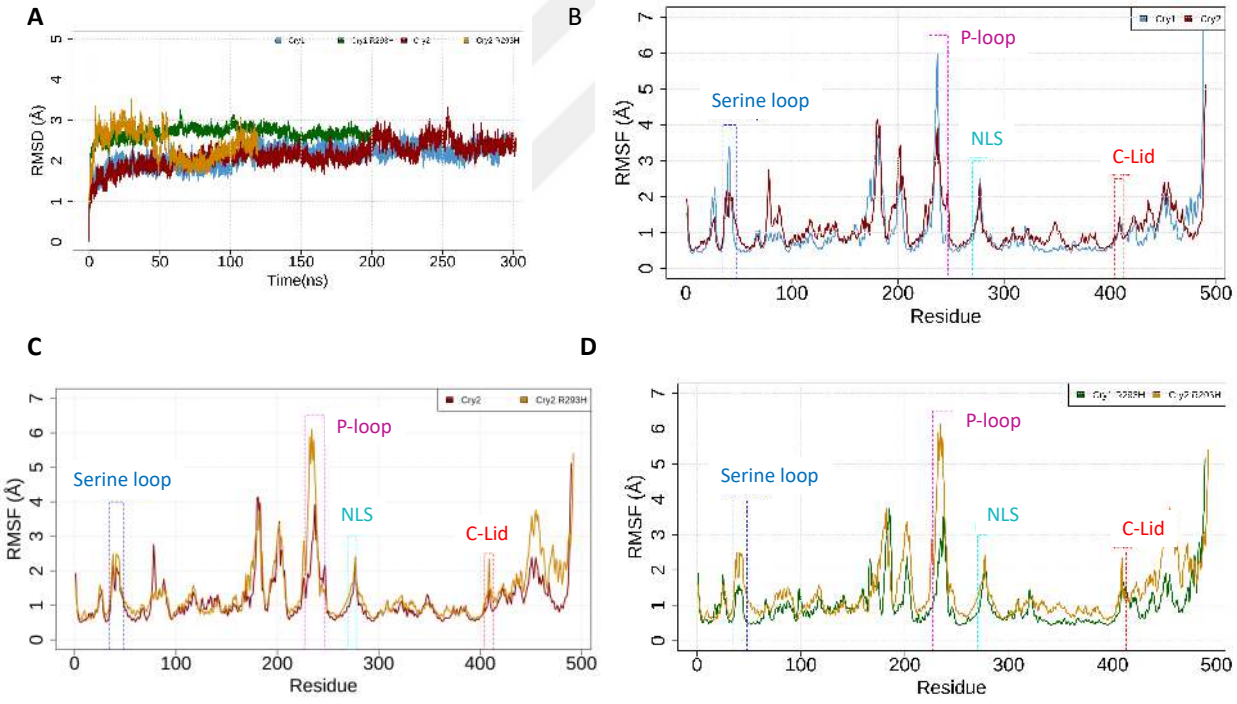

Figure 4. 4. Dynamics of CRY1 R293H and CRY2 R293H

A) Root mean square deviation (RMSD) of all simulations (CRY1, CRY1-R293H, CRY2, CRY2-R311H). Root mean square fluctuation (RMSF) of **B)** CRY1 and CRY2; **C)** CRY2 and CRY2-R311H; **D)** CRY1-R293H and CRY2-R311H. For the sake of figure clarity, residue numbering in CRY1 was followed. The critical and functional parts of CRYs were shown between dashed lines. NLS: Nuclear localization signal.

I then calculated the secondary pocket volumes (SPV) of CRY1, CRY1-R293H, CRY2 and CRY2-R311H to analyze the effect of mutations, where CLOCK binds. The SPV of the CRY2-R311H was quite larger than both CRY1 and CRY1-R293H and comparable to CRY2 (**Fig 4.5A**). Unlike Arg-293 mutation to His in CRY1, Arg-311 mutation in CRY2 did not affect the SPV. The distances between the secondary pocket and Ser-loop for CRY1 is correlated with SPV results. The distance between the serine loop and secondary pocket was not affected in CRY2-R311H, however, the same distance was affected in CRY1- R293H (**Fig 4.5B**). Finally, the number of H-bonds were calculated between the Ser-loop and the rest of the protein. The decreased distance between Ser-loop and secondary pocket in CRY1-R293H can be explained by more hydrogen bonds formation throughout the simulation compared to CRY1. Amount of hydrogen bonds that present per frame were similar in CRY2 and CRY2-R311H. H-bond analysis suggests that effect of Arg-311 mutation in CRY2 has a different effect on CRY2 than that of its homolog mutation in CRY1 (**Fig 4.5C**). To address the effect of R311H mutation on the allosteric regulation of Ser-loop in CRY2, I investigated the allosteric paths between Ser-loop and Arg-311 using WISP. The shortest lengths of the allosteric paths between Ser-loop and residue 293 in CRY1 and CRY1-R293H were 5.2 Å and 3.0 Å, respectively. These values (between Ser-loop and residue 311) in CRY2 and CRY2-R311H were 3.4 Å and 2.2 Å, respectively. Other suboptimal paths to Ser loop were quite different in CRYs (**Fig 4.5D**). WISP analysis showed that: 1) CRY1 and CRY2 path lengths are changing in different magnitudes, implying that allosteric regulations between Arg293/311 and Ser-loop in CRY1 and CRY2 are different; 2) while Arg293His mutation changed the shortest path length dramatically in CRY1, Arg311His mutation in CRY2 had less effect on the path length. To note, SPV mainly affected by the position of highly dynamic unstructured Ser-loop in CRY1, however, Ser-loop in CRY2 has a turn of alpha helix that increases its rigidity. Because of the rigidity of Ser-loop in CRY2, effect of mutation might not alter its dynamics as drastically as in the CRY1.

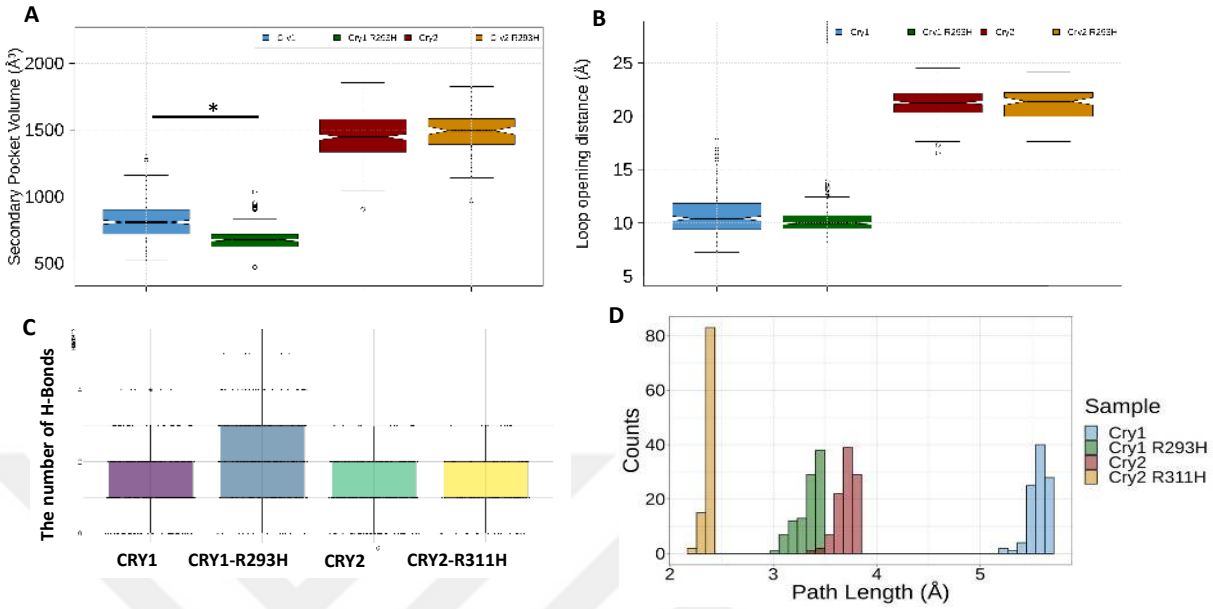

Figure 4. 5. Secondary pocket dynamics of CRY1 R293H and CRY2 R293H

Box-plot representation of the A) secondary pocket volume (Wilcoxon rank sum test *: p <0.0001); B) loop distance between Ser-loop (Gly43/Ala61) and Phe 105/123 (first residue number is for CRY1, second for CRY2), C) number of H-bonds between Ser-loop and rest of the protein per frame. The same number of PDB files were used for each calculation. D) Histogram representation of pathways' length calculated by using WISP.

4.5 CRYs loops and secondary pocket dynamics on WT and repression deficient mutants

CRY mutants were selected from experimental studies that demonstrated a decrease in repressor activity on CLOCK:BMAL1 transactivation and a subsequent decrease in their affinity to these proteins (S. Gul et al., 2020; McCarthy et al., 2009). In a prior study by (McCarthy et al., 2009) multiple mutations in CRYs were reported, resulting in diminished repression activity on CLOCK:BMAL1 transactivation(**Fig. S5**). To generate these mutants, they subjected the cDNAs of *Cry1* and *Cry2* to random mutagenesis and selected those with altered repressor activities using the Per2:dLuc assay. The study identified CRY mutants that exhibited loss of function and attenuated repression activity, primarily governed by the

interaction between the secondary pocket of CRYs and CLOCK. I subsequently pinpointed the following mutations in the modeled structures of CRYs: R293H, A217V/L218F, C259Y, E214K, and G288R in CRY1, and A235T, E312K, and G230R in CRY2. These mutant structures were then subjected to molecular dynamics simulations (MD) for a total of 2 μs (**Fig 4.6A**). To confirm each configuration reached equilibrium, I first determined the root mean square (RMSD) value of each mutant and wild type CRYs (**Fig 4.7A,B**). After achieving equilibrium in each protein, I analyzed the effect of each mutation on the flexibility of the serine loop and dynamics of the secondary pocket by plotting the root mean square fluctuations (RMSF) of all amino acids. Overall, the RMSF values obtained from the simulations of wild type CRY1 and CRY2 were consistent with previous studies indicates the reliability of our calculations (Fribourgh et al., 2020; Miller et al., 2021; Ozcan et al., 2021b). Notably, the CRY1 mutants showed distinct patterns in the flexibility of amino acids within the serine and P-loops, whereas no significant difference was observed in CRY2 compared to their respective wild type CRYs (**Fig 4.6B,C**). The significance of the P- loop in protein half-life and phosphorylation of CRYs has been well established (Ode et al., 2017). We, therefore, focused on the serine loop behaviors to probe reduced repressor activities of CRYs (Carlo et al., n.d.; S. Gul et al., 2020). The model serine loop had a flexible conformation in CRY1 while the serine loop preserved its fold with a single turn of the a-helix in CRY2 throughout the simulation (**Fig 4.6D and 7C**). Such structural differences can be attributed to two amino acid differences (Gly43 and Asn46 in CRY1 vs Ala61 and Ser64 in CRY2) in their serine loops (**Fig 4.7D**). Among the simulated CRY1 mutants, all mutations had different effects on the dynamic fluctuation of the serine loop (**Fig 4.6B**). The serine loop of G288R CRY1 exhibited a higher root mean square fluctuation (RMSF) value compared to the wild type CRY1, reaching a peak of 4.25Å at G43. On the other hand, the E214K, R293H, and C259Y CRY1 mutants showed lower RMSF values than the wild type, with peaks of 2.1Å, 1.5Å, and ~0.6Å at G43, respectively. A217V/L218F CRY1 mutant exhibited similar RMSF value compared to wild type peaked at A42 having 2.7Å (**Fig 4.6B**).

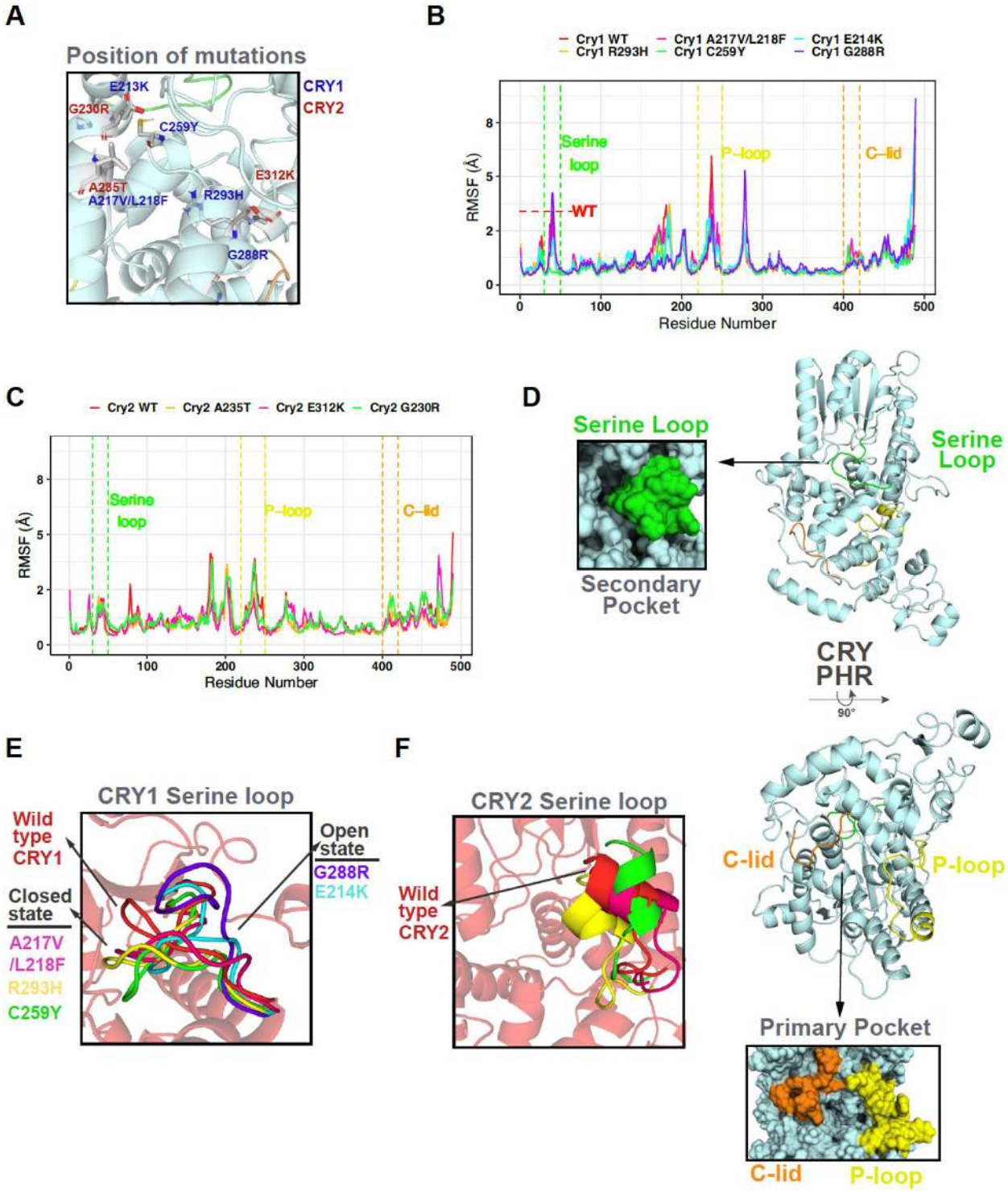
A
Position of mutations
E213K
G230R
C259Y
E312K
A235T
A217V/L218F
R293H
G288R
CRY1
CRY2
B
Cry1 WT
Cry1 R293H
Cry1 A217V/L218F
Cry1 C259Y
Cry1 E214K
Cry1 G288R
Serine loop
P-loop
C-lid
WT
RMSF (Å)
Residue Number
C
Cry2 WT
Cry2 A235T
Cry2 E312K
Cry2 G230R
Serine loop
P-loop
C-lid
RMSF (Å)
Residue Number
D
Serine Loop
Secondary Pocket
Serine Loop
CRY PHR
90°
C-lid
P-loop
Primary Pocket
C-lid
P-loop
E
CRY1 Serine loop
Wild type CRY1
Closed state
A217V
/L218F
R293H
C259Y
Open state
G288R
E214K
F
CRY2 Serine loop
Wild type CRY2

Figure 4. 6. Figure 4.6. Effects of mutations on mutant and wild type CRY PHR domains.

(a) Position of mutations represented on the CRY1 PHR domain (cyan) Green, yellow, and orange regions correspond to serine loop, P-loop, and C-lid residues, respectively. Mutant residues highlighted in blue and red correspond to CRY1 and CRY2, respectively. Root mean square fluctuation values of Ca atoms from MD simulations in (b) CRY1 systems and (c) CRY2 systems for each residue. Dashed lines correspond to the range of serine loop(green), P-loop(yellow), C-lid(orange) residues and the peak RMSF value of wild type CRY1(red). for all systems, residue numbering in CRY1 is used for RMSF plots for consistency. (d) A cluster representative of the most crowded cluster in the wild type CRY1 trajectory is used as a representative structure. Serine loop, P-loop, and C-lid residues are highlighted in green, yellow, and orange, respectively. Insets are a surface view of the primary pocket and secondary pocket. Green, yellow, and orange surfaces correspond to serine loop, P-loop, and C-lid residues, respectively. Cluster representatives of the most crowded cluster in (e) CRY1 systems and in (f) CRY2 systems superpositioned with their respective wild type. Serine loop residues of wild type CRY1 and CRY2 are colored in red. The rest of the respective wild type structure is represented in the background as a semi-transparent cartoon. For mutant systems, only serine loop residues are represented in their respective colors.

In contrast, the analysis of wild type and mutant CRY2 showed no differences in RMSF values (**Fig 4.6C**). To gain further insight into the conformational states of the CRY1 serine loop, I performed clustering analysis using a pairwise best-fit root mean square deviation (RMSD) method on all trajectories. From each mutant simulation, I selected the cluster representative of the most populated cluster and aligned it with the representative structure obtained from the wild type CRY1 simulation (**Fig 4.6E**). The serine loop in the representative structures of CRY1 mutants showed two distinct conformations, referred to as the open and closed states, compared to the wild type Specifically, the A217V/L218F, R293H, and C259Y CRY1 mutants adopted closed-state serine loop conformations, while the G288R and E214K CRY1 mutants exhibited open-state serine loops. In contrast, there

were no differences observed in the conformations of the mutants and wild type CRY2 (**Fig 4.6F**). To ensure that the observed serine loop conformations were representative, I also calculated and visualized the averaged coordinates of backbone atoms (**Fig 4.7E**). As a summary, CRY1 mutants with reduced repressor activities exhibited altered serine loop conformations, while CRY2 mutants displayed a similar phenotype without distinct changes in their serine loop. Since wild type and mutant CRY2 systems had relatively low fluctuations

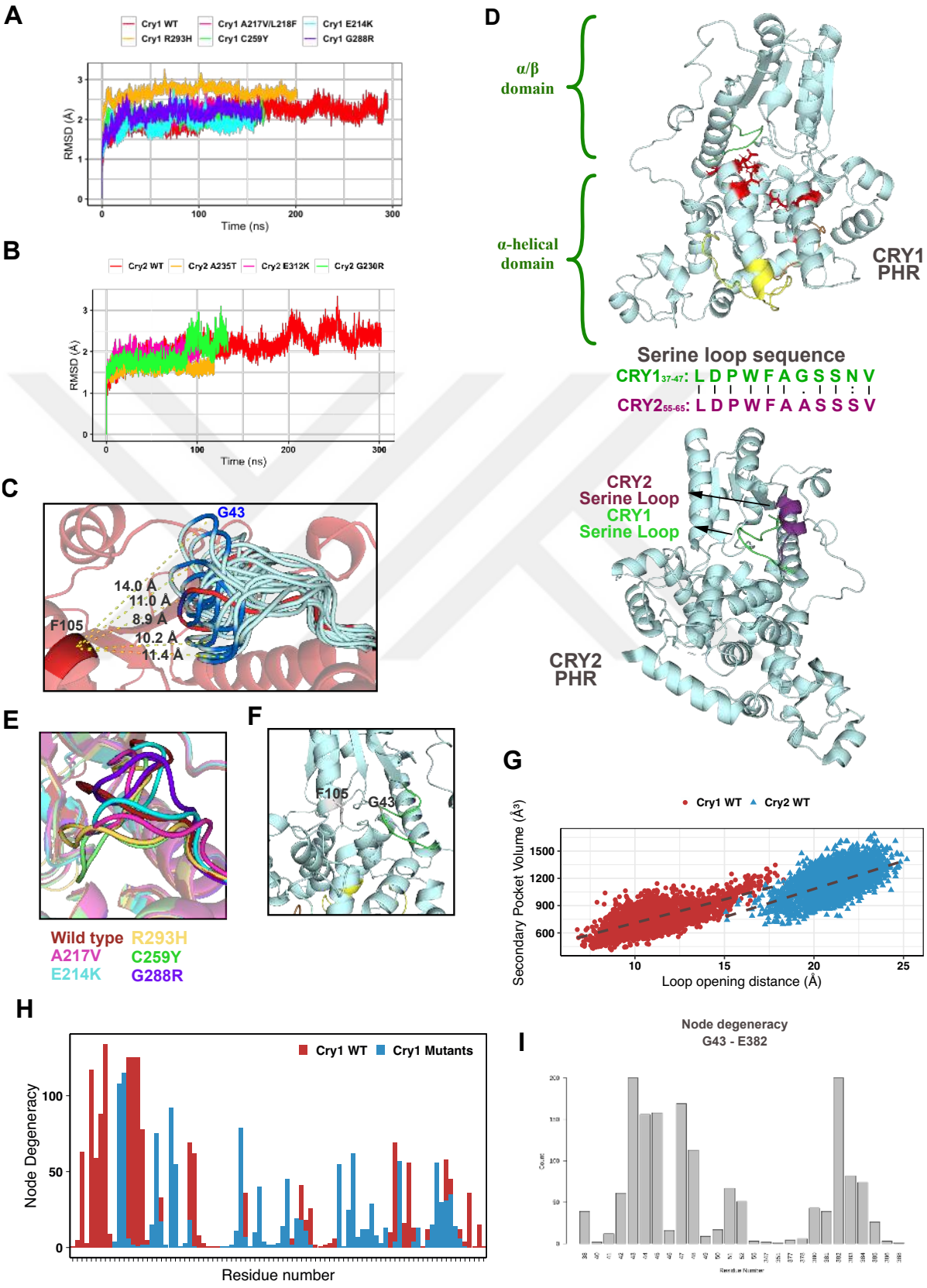
A
Cry1 WT
Cry1 R293H
Cry1 A217V/L218F
Cry1 C259Y
Cry1 E214K
Cry1 G288R
RMSD (Å)
Time (ns)
B
Cry2 WT
Cry2 A235T
Cry2 E312K
Cry2 G230R
RMSD (Å)
Time (ns)
C
G43
14.0 Å
11.0 Å
8.9 Å
10.2 Å
11.4 Å
F105
D
α/β domain
α-helical domain
CRY1 PHR
Serine loop sequence
CRY1 37-47: L D P W F A G S S N V
CRY2 55-65: L D P W F A A S S S V
CRY2 Serine Loop
CRY1 Serine Loop
CRY2 PHR
E
Wild type
R293H
A217V
C259Y
E214K
G288R
F
F105
G43
G
Cry1 WT
Cry2 WT
Secondary Pocket Volume (Å³)
Loop opening distance (Å)
H
Cry1 WT
Cry1 Mutants
Node Degeneracy
Residue number
I
Node degeneracy
G43 - E382
Count

Figure 4. 7.

Root mean square deviation values of **(A)** CRY1 systems and **(B)** CRY2 systems. **(C)** Conformational ensemble of the serine loop (cyan) in wild type CRY1 throughout trajectory. F105 and G43 are highlighted in red and blue, respectively. Distances for different conformations are shown in dashed lines with their respective values. **(D)** Modeled structures of PHR domain CRY1 and CRY2, which are further divided into α/β domain and α-helical domain. Mutant residues shown as stick representation colored in red. The serine loop, c-lid and p-loop highlighted. **(E)** Average structure of the serine loop in wild type and mutant CRY1s. **(F)** Position of F105 and G43 in the CRY1 PHR domain. **(G)** Scatter plot representation of pocket volume versus loop opening distance in wild type CRY1 and CRY2. **(H)** The frequency of the residues in the merged suboptimal pathways among wild type and mutant CRY1. **(I)** The frequency of the residues in fifty suboptimal pathways between G43 and E382.

in their serine loops, such conformers might be masked by other flexible regions while clustering. To explore that, I carried out additional studies in detail in the following sections.

4.6 Investigating the state of serine loop of mutant CRYs with deficient repression

Since I observed that the serine loop of CRY1 mutants acquires open and closed conformations in representative structures, I then calculated the Ca distance between G43 (A61 in CRY2) and F105 in CRY1 (F123 in CRY2) throughout the trajectories as previously described (**Fig 4.7F**). The distance between G43 and F105 was not normally distributed (Shapiro-Wilk's test, $p<0.05$). Thus, the median and quartiles were reported as median (Q1–Q3). The median distance between G43 and F105 was calculated as 10.4 (9.4–11.8) Å for wild type CRY1, while the same distance between corresponding amino acid residues was calculated as 21.3 (20.2– 22.1) Å for CRY2 (**Fig. 8A, B**). I analyzed serine loop states of the E214K and G288R CRY1 mutants compared to wild type CRY1 by measuring the serine loop opening distance. E214K and G288R CRY1 mutants, which exhibit open- state serine loop structures, demonstrated a greater opening distance compared to wild type CRY1

(pairwise Wilcoxon rank sum test with Benjamini and Hochberg correction, p=1.7E-15 and p<2.0E-15, respectively). The closed-state mutants, however, displayed a similar or even larger loop distance compared to the wild type CRY1. Moreover, the serine loop in the wild type CRY1 exhibited a high level of flexibility and adopted various conformations (**Fig 4.7C**). Based on these analyses, it became evident that there was no correlation between the opening distance of the loop and its state. Therefore, I hypothesized that the primary determinant for distinguishing between the open and closed states of CRY1 might be the volume changes within the secondary pocket of the mutants compared to wild type. To test this hypothesis, I proceeded with the calculation of the secondary pocket volumes in both the wild type CRY1 and its mutant variants.

Consistent with a previous study, my calculations demonstrated a positive correlation between the state of the serine loop and the volumes of the secondary pockets in wild type CRYs (**Fig 4.7G**)(Fribourgh et al., 2020). The R2 values were 0.49 for CRY1 and 0.31 for CRY2, indicating a stronger effect of the loop position on the pocket volume in CRY1

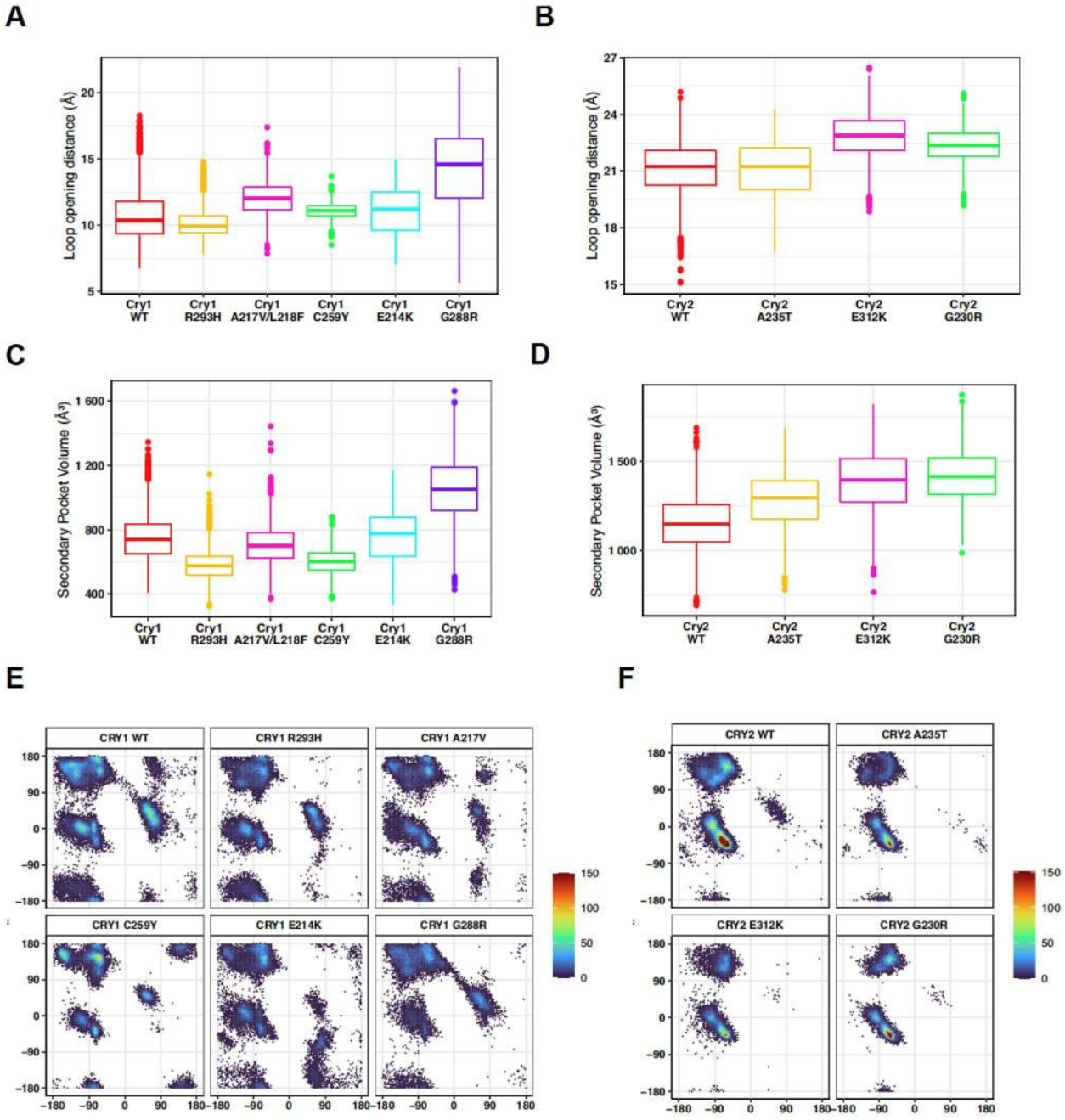

Figure 4. 8 Dynamic of the serine loop and secondary pocket in wild type (WT) and mutant CRYs.

Evenly distributed ten frames for every nanosecond of trajectory extraction for all systems were used for the rest of the calculations. Loop opening distance (distance between F105-G43 and F123-A61 in CRY1 and CRY2, respectively) in (a) CRY1 systems and (b) CRY2 systems is represented as boxplots. In CRY1, all mutants have significantly different loop

opening distances compared to wild type (pairwise Wilcoxon rank sum test with pvalue adjusted with the Benjamini and Hochberg method. WT vs mutant adjusted pvalue are 1.20E-15, <2.00E- 16, <2.00E-16, 1.70E-15 and <2.00E-16 in their respective order in figure). the median values for WT, R293H, A217V/L218F, C259Y, E214K and G288R CRY1 are 10.38, 9.97, 12.04, 11.10, 11.23 and 14.61Å respectively. The median values for wild type, A235T, E312K, and G230R CRY2 are 21.25, 21.24, 22.88, and 22.36Å respectively. All CRY2 mutants except A235T CRY2, have significantly different loop opening distances compared to wild type CRY2 (pairwise Wilcoxon rank sum test with pvalue adjusted with the Benjamini and Hochberg method, WT vs mutant adjusted pvalue are 0.34, <2.00E-16 and <2.00E-16 in their respective order in figure). secondary pocket volumes of (c) CRY1 systems and (d) CRY2 systems are represented as boxplots. The median values for wild type, R293H, A217V/L218F, C259Y, E214K, and G288R CRY1 are 741, 576, 702, 602, 778, and 1054 Å3 respectively. In CRY1, all mutants have significantly different secondary pocket volumes compared to wild type (pairwise Wilcoxon rank sum test with pvalue adjusted with the Benjamini and Hochberg method. WT vs mutant adjusted pvalue are <2.00E-16, <2.00E-16, <2.00E-16, 0.00093 and <2.00E-16 in their respective order in figure). the median values for wild type, A235T, E312K and G230R CRY2 are 1146, 1295, 1394 and 1414Å respectively. In CRY2, all mutants have significantly different secondary pocket volumes compared to wild type (pairwise Wilcoxon rank sum test with pvalue adjusted with the Benjamini and Hochberg method, WT vs mutant adjusted pvalue are <2.00E-16, <2.00E-16 and <2.00E-16 in their respective order in figure). backbone dihedral angles, u and w, for each residue in a serine loop are calculated with hundred picosecond intervals throughout the trajectory for (e) CRY1 systems and (f) CRY2 systems.

compared to CRY2. Further analysis of CRY1 mutants revealed significant differences (Wilcoxon rank-sum test, $p<0.05$) in their secondary pocket volumes compared to the wild type CRY1 (**Fig 4.8C**). The secondary pocket volumes were not normally distributed in wild type and CRY1 mutants (Shapiro-Wilk's test, $p<0.05$). The wild type CRY1 median secondary pocket volume was calculated as 741 (652–834) $Å^3$ (median (Q1–Q3)). However, the secondary pocket volumes of R293H, A217V/L218F, and C259Y CRY1 were calculated

as 576 (521–636), 702 (625–785) and 602 (550–657) $Å^3$, respectively. Since the secondary pocket volumes in CRY1 mutants were significantly smaller than those in the wild type, I concluded that the serine loop in these three mutants is indeed in a closed state. In contrast, the secondary pocket volumes for the open-state mutants E214K and G288R CRY1 were calculated as 778 (634–876) $Å^3$ and 1054 (919–1188) $Å^3$, respectively, which are larger than the secondary pocket volume of wild type CRY1. In summary, our findings indicate that the volumes of the secondary pockets correlate with the state of the loop in CRY1. In CRY2 mutants, the secondary pocket volumes were larger compared to the wild type CRY2 (**Fig 4.8D**). The secondary pocket volume for wild type CRY2 was 1146 (1049–1256) $Å^3$, while the volumes for A235T, E312K, and G230R CRY2 were 1295 (1175–1391) $Å^3$, 1394 (1273–1513) $Å^3$, and 1414 (1312– 1518) $Å^3$, respectively. Considering that CRY2 has a rigid serine loop, the primary cause of the volume change might be local alterations in the side chain conformations within the pocket.

I performed detailed analyses by plotting the backbone dihedral angles (Φ/Ψ) of the serine loop residues (37th—47th and 55th–65th amino acids for CRY1 and CRY2, respectively) throughout simulations for each system. Overall, in CRY1 closed state mutants (R293H, A217F/L218V, C259Y), the serine loop mostly stabilized in the fraction of conformational space sampled by the serine loop in wild type. In open-state CRY1 mutants, mostly in E214K and to some degree in G288R, serine loops sampled additional conformations. However, differences in CRY2 systems were minor (**Fig 4.8E,F**). All these results suggested that the state of the serine loop in CRY1 is a major parameter that affects the secondary packet volume, but not in CRY2.

4.7 Residue interactions of serine loop in CRY1

Since mutations in CRY1 caused two different serine loop states, I hypothesized that these differences may be due to the different interaction energies between serine loop and the nearby amino acids. To test this, I calculated the interaction energies, which encompassed both van der Waals and electrostatic interactions. Specifically, I calculated the sum of interaction energies between each residue in the serine loop and with other residues within a distance of 14Å. My analysis revealed significant changes in the interaction energies between

the serine loop and the nearby polar or charged amino acids, namely D38, S44, S45, and N46. Notably, the changes in interaction energies for S44 and S45 exhibited a strong correlation with the loop state (**Table 2**). In the case of the R293H, C259Y, and A217V/L218F CRY1 mutants, S44 and S45 demonstrated stronger interactions with the nearby amino acids, resulting in a closed state of the serine loop. Conversely, in the E214K and G288R CRY1 mutants, these amino acid residues displayed weaker interactions, leading to an open state of the serine loop. It is important to note that while D38 of the serine loop in the wild type CRY1 exhibited the highest affinity for the nearby residues, it did not correlate with the state of the serine loop (**Table 2**).

Table 4. 2 Total interaction energies (kcal/mol) of residues in serine loop.

Interaction energies of residues in the serine loop with other residues are calculated, and the sum of these interaction energies, excluding other loop residues, is reported. ΔSer column represents the difference between the sum of the interaction energies of Ser44 and Ser45 in each system compared to wild type. The state of the serine loop in given systems is given in the loop state column.

	Asp 38	Ser 44	Ser 45	Asn 46	DSer	Loop state
CRY1WT	–68.07	1.39	–13.6	–8.7	0	–
CRY1 R293H	–85.87	–17.37	–20.02	12.37	–25.18	Closed
CRY1 A217V	–53.15	–9.48	–13.13	2.61	–10.4	Closed
CRY1 C259Y	–69.43	–42.87	–44.91	18.77	–75.57	Closed
CRY1 E214K	–46.73	0.46	–6.32	–16.25	6.35	Open
CRY1 G288R	–48.4	1.49	–5.11	–8.09	8.59	Open

I performed a detailed analysis of the decomposition of total interaction energies per residue to determine the individual contributions of nearby amino acid residues to the overall interaction energies of S44 and S45. My findings revealed that E382 of CRY1 made the largest contribution to the interaction energies of S44 and S45. Given that glutamate can form hydrogen bonds, I further investigated the occurrence of hydrogen bond throughout the trajectories for each system. Across all CRY1 systems, I observed that E382 and/or E383 were frequently involved (**Table 4.3**). In the closed-state mutants (R293H, C259Y, and A217V/L218F CRY1), E382 and/or E383 exhibited a significantly higher frequency of hydrogen bonding with either S44 or S45 compared to wild type CRY1, with a two-fold and five-fold increase, respectively (**Table 4.3**). Conversely, in the open state of the serine loop, G288R CRY1 displayed similar results to wild type CRY1, with the most frequent hydrogen bond formation occurring between G48 and E383 (**Table 4.3**). These findings suggest that E382 of CRY1 plays a crucial role in determining the state of the loop.

Table 4. 3 Frequency of hydrogen bonds.

B and R donates for backbone and side chain, respectively. Hydrogen bonds between the serine loop and the rest of the residues are calculated throughout the trajectory and reported for each CRY1 system. B and R donate for the backbone and side chain, respectively. The occupancy column represents the frequency of the frames that a given hydrogen bond observed.

	Donor	Acceptor	Occupancy
CRY1 WT	GLY48 (B)	GLU383 (B)	17.20%
	GLN79 (R)	ASP38 (R)	16.09%
	SER45 (R)	GLU382 (R)	14.02%
CRY1 R293H	SER44 (B)	GLU382 (R)	38.87%
	GLY48 (B)	GLU383 (B)	31.88%
	SER45 (R)	GLU382 (R)	25.78%
	SER45 (B)	GLU382 (R)	25.14%

	GLU103 (R)	ALA42 (B)	22.36%
CRY1 A217V	GLY48 (B)	GLU383 (B)	12.97%
	GLY43 (B)	GLU382 (R)	12.53%
	SER45 (R)	GLU383 (R)	10.10%
	SER45 (R)	GLU382 (R)	9.91%
	ARG51 (R)	PHE41 (B)	8.85%
	SER44 (B)	GLU382 (R)	4.99%
CRY1 C259Y	SER45 (R)	GLU382 (R)	75.64%
	ARG51 (R)	ALA42 (B)	42.99%
	TYR35 (R)	ASP38 (R)	30.15%
	GLY48 (B)	GLU383 (B)	25.49%
	SER45 (B)	GLU382 (R)	23.88%
	SER44 (B)	GLU382 (R)	11.94%
	TRP52 (B)	GLY48 (B)	5.91%
CRY1 E214K	GLY48 (B)	GLU383 (B)	34.59%
	TRP52 (R)	ASN46 (R)	30.06%
	SER44 (B)	GLU382 (R)	14.68%
	SER45 (R)	GLU382 (R)	13.98%
	SER45 (B)	GLU382 (R)	7.91%
	LYS379 (R)	SER44 (R)	7.66%
	GLN79 (R)	ASP38 (R)	5.49%
CRY1 G288R	GLY48 (B)	GLU383 (B)	17.82%
	TRP52 (R)	ASN46 (R)	9.82%
	TRP52 (B)	GLY48 (B)	8.42%
	GLN79 (R)	ASP38 (R)	4.73%

4.8 Dynamical network analysis between mutant residues and the serine loop

All these findings indicate that distantly located mutants have an impact on the dynamic behavior of the serine loop in CRY1, suggesting a potential common mechanism underlying their effects on serine loop dynamics. To investigate the communication between distant mutations and the serine loop, I employed a dynamical network analysis. In each CRY1 system, I designated the mutation positions as source residues, and G43 in CRY1 (or A61 in CRY2) as the sink residue, as it exhibited the highest root mean square fluctuation (RMSF) value within the loop. Another compelling rationale for selecting this residue as a sink is its central positioning within the loop, minimizing the likelihood of interactions with neighboring amino acids due to its absence of side chain atoms. Consequently, any allosteric signal is more likely to propagate through the nearest functional residues situated either at the C-terminal or N-terminal of G43. Pathways were defined between the source and sink residues, traversing through residues with correlated motion. The lengths of the fifty pathways between the mutation positions and G43 were calculated for each CRY1 mutant. Additionally, corresponding pathways were calculated for the wild type CRY1 using the same source and sink positions (**Fig 4.9A-E, left**), and the average conformations of the serine loop for each mutant and the wild type CRY1 were superimposed (**Fig 4.9A–E, right**). All mutations resulted in a shift in the lengths of the pathways, including the shortest pathway, suggesting the presence of allosteric effects. **Table 4.4** provides the shortest pathways between the source and sink residues for both mutants and wild type CRY1. Interestingly, common amino acid residues were observed in the shortest pathways across different source and sink residues. For instance, amino acid residues R256, F257, F41, and A42 were shared in the shortest pathways between R293- G43 in wild type CRY1 and C259-G43 in mutant C259Y CRY1. Similarly, L13, Y35, L37, and D38 residues were common between L218-G43 and E214-G43 in wild type CRY1 (**Table 4.4**).

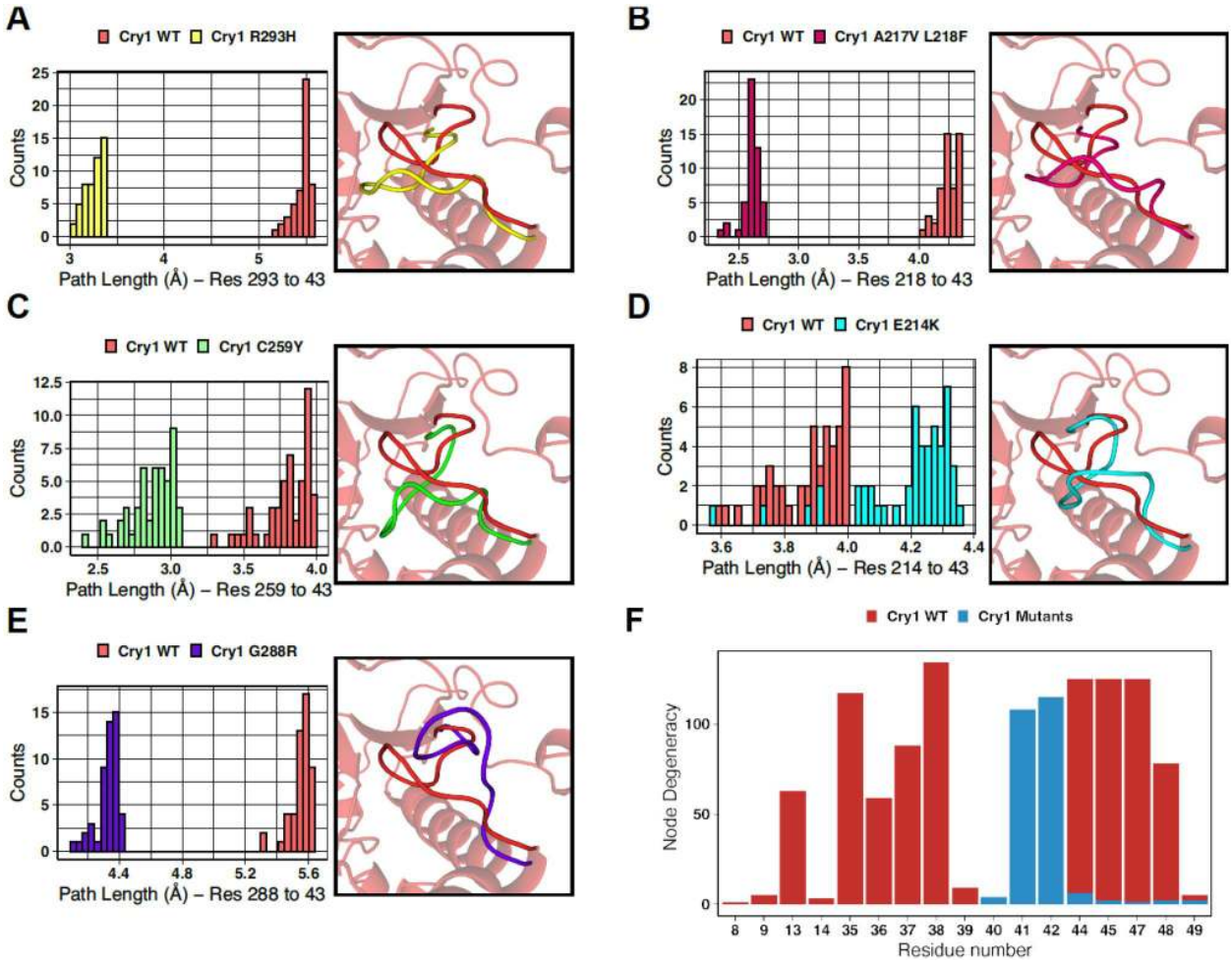

Figure 4. 9. Signaling pathway distribution in wild type and mutant CRY1s.

The top fifty pathways for each source and sink residue pair are calculated. In mutant structures, mutation position is used as source residue and G43 used as sink residue. Corresponding positions of mutant residues in wild type are used as source residues. The length of calculated pathways for (a, left) R/H293, (b, left) L/F218 (c, left) C/Y259, (d, left) E/K214 and (e, left) G/R288 represented as histograms. Each pair's serine loop positions are shown on the right. (f) Pathways between different source and sink residues are merged, excluding source and sink residues for wild type and mutant organisms. The frequency of occurrences of residues in merged pathways is calculated and represented as a bar plot.

To further explore the communication pathways, I calculated the pooled node degeneracy for both wild type and CRY1 mutants. In this analysis, suboptimal pathways

between all source and sink residue pairs were pooled together, excluding the source and sink residues themselves. Additionally, the suboptimal pathways for different mutants were aggregated as CRY1 mutants (**Fig 4.9F and 7H; Table 4.5**). The analysis revealed a significant difference in the pathways between wild type and mutants CRY1, particularly in the region surrounding the serine loop. In wild type CRY1, amino acids at positions 13, 35, 36, 37, 38, 41, 42, 44, 45, 47, and 48 exhibited high node degeneracy, indicating their involvement in multiple communication pathways. However, in CRY1 mutants, the node degeneracy for these residues was generally decreased, except for residues 41 and 42, which showed an increase in node degeneracy. Notably, a similar analysis was conducted for E382, a key contributor to hydrogen bonds and interaction energies, and a participant in the shortest pathway in the G288R CRY1 mutant. The node degeneracy analysis for the 200 suboptimal pathways between E382 (source) and G43 (sink) in wild type CRY1 confirmed the importance of S44, S45, and V47 in the communication network (**Fig 4.7I**). This further emphasizes the role of communication between S44/45 and E382 in influencing the dynamicity of the serine loop. In contrast, a similar network analysis performed for CRY2 indicated minor changes between wild type and mutants (**Fig 4.10A–C**). The repetitive occurrences of residues suggest the existence of an allosteric regulatory mechanism between the a/b domain and the a-helical domain in CRY1. Collectively, these findings strongly support the notion that the serine loop is highly regulated by allosteric mechanisms

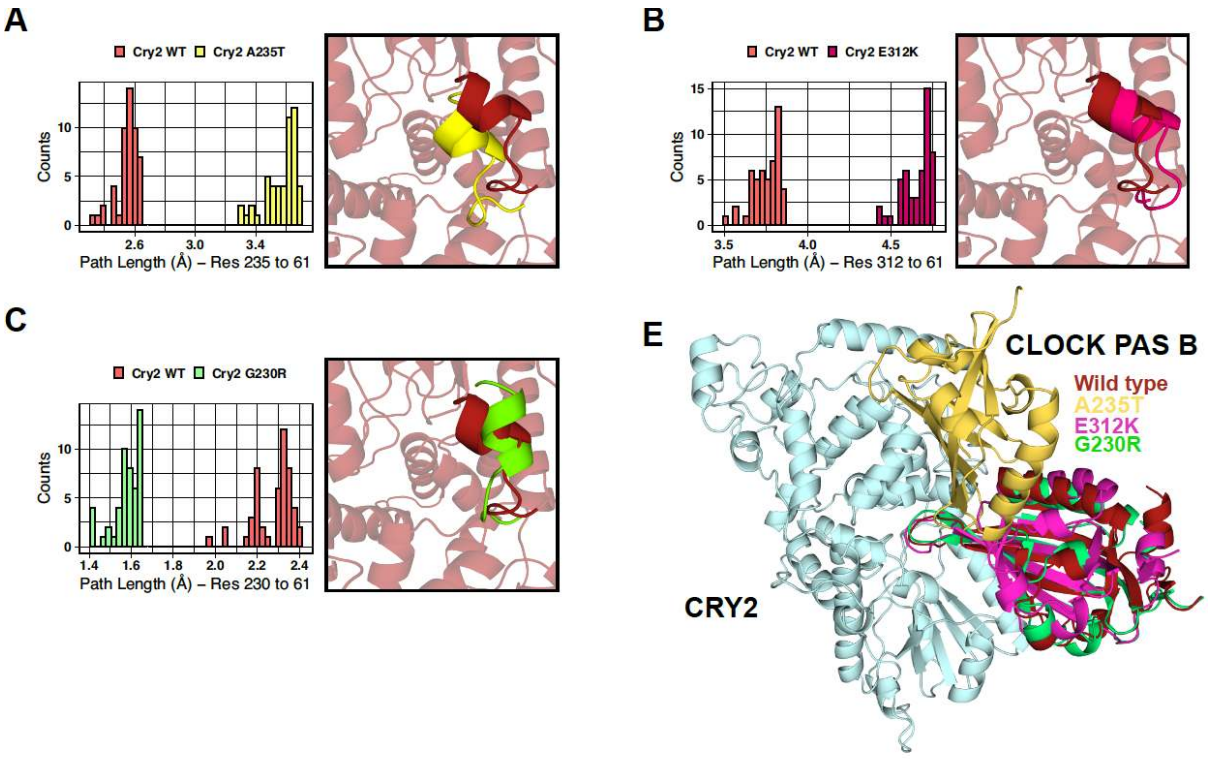

Figure 4. 10 Signaling pathway distribution in wild type and mutant CRY2s.

The top fifty pathways for each source and sink residue pair are calculated. In mutant structures, mutation position is used as source residue and A61 used as sink residue. Corresponding positions of mutant residues in wild type are used as source residues. Length of calculated pathways for (A, left) A/T235, (B, left) E/K312 and (C, left) G/R230 represented as histograms. Each pair's serine loop positions are shown on the right. (D) CLOCK PASB domain docked into the secondary pocket of wild type and mutant CRY2s. Wild type CRY2 PHR domain (cyan) is used as a representative. CLOCK PASB domain docked for each mutation and wild type represented.

Table 4. 4 Shortest pathway between source and sink residues respective to wild type. The shortest (optimal) pathway between the source (mutation position) and sink (G43) is calculated. Length column is the distance of the shortest pathway for a given source and sink residue pair in wild type and corresponding mutant CRY1. Nodes are the residues that the shortest pathway traverses in that order.

CRY1	Source-sink	Length (A)	Nodes							
WT	293-43	5.19	Arg293	Arg256	Phe257	Phe41	Ala42	Gly43		
R293H		3.02	His293	Phe296	Ala300	Trp390	Gly43			
WT	218-43	4.03	Leu218	Glu214	Leu13	Tyr35	Leu37	Asp38	Gly43	
A217V/L218F		2.37	Phe218	Val217	Gly213	Cys58	Leu55	Phe41	Gly43	
WT	259-43	3.31	Cys259	Phe257	Phe41	Ala42	Gly43			
C259Y		2.4	Tyr259	Phe257	Arg256	Ala42	Gly43			
WT	214-43	3.56	Glu214	Leu13	Tyr35	Leu37	Asp38	Gly43		
E214K		3.57	Lys214	Gly213	Phe54	Arg51	Ala42	Gly43		
WT	288-43	5.32	Gly288	Trp292	Trp399	Trp397	Phe381	Leu384	Gly48	Val47
			Ser45	Ser44	Gly43					
G288R		4.12	Arg288	Trp292	Ile392	Asn393	Glu382	Phe41	Ala42	Gly43

Table 4. 5 Node degeneracy of pooled pathways.

Node degeneracy of the residues in merged suboptimal pathways among wild type and mutant CRY1s for each observed residue. WT and MUT corresponds to frequency of the given residue in wild type and mutant merged pathways.

	Frequency			Frequency			Frequency			Frequency	
Resid	**WT**	**MUT**	**Resid**	**WT**	**MUT**	**Resid**	**WT**	**MUT**	**Resid**	**WT**	**MUT**
8	1	0	56	0	1	254	10	45	381	69	4
9	5	0	57	0	3	255	6	2	382	3	57
13	63	0	58	69	18	256	9	19	383	16	0
14	3	0	59	62	1	257	41	18	384	56	0
35	117	0	75	8	0	258	18	11	385	13	4
36	59	0	76	3	0	259	26	2	386	0	13
37	88	0	104	1	0	260	2	0	387	1	0
38	134	0	106	1	0	262	1	0	388	12	5
39	9	0	109	1	0	265	2	0	389	10	15
40	0	4	150	0	1	290	3	0	390	0	56
41	41	108	210	0	1	291	6	0	391	2	30
42	85	115	211	1	2	292	45	55	392	58	31
44	125	6	212	11	11	294	0	1	393	45	35
45	125	2	213	57	79	295	7	25	394	2	14
47	125	1	214	36	7	296	51	62	395	12	6
48	78	2	215	0	1	297	0	7	396	4	1
49	5	2	216	0	10	298	0	12	397	36	0
50	5	15	217	27	40	299	1	12	398	1	0
51	15	75	219	0	4	300	1	29	399	15	0
52	33	17	220	0	2	306	0	8	401	1	0
53	0	2	221	0	2	307	0	3			
54	40	92	251	0	3	378	0	13			
55	13	55	253	1	14	380	10	0			

4.9 Determination of conformational states of the residues in pathways

To further analyze the conformational changes of amino acids involved in the shortest pathways and those participating in hydrogen bond formation, I superimposed the cluster representatives of the three most populated clusters for CRY1 proteins (**Fig 4.11**). Predominant conformational changes in top three most crowded clusters were observed in specific residues, while others remained relatively stable. In the cases of R293H and A217V/L218F CRY1, the residues involved in the shortest pathways did not exhibit predominant conformational changes. However, in wild type CRY1, R256 extended towards the serine loop with a χ1 angle of 60°, whereas in C259Y CRY1, the same residue moved away from the serine loop with a χ1 angle of -90° (**Fig 4.11A**). This conformational change enabled the serine loop to adopt a closed-state fold without causing steric clashes with R256. The conformation of F41 differed between G288R and wild type CRY1. In wild type CRY1, F41 was buried towards the secondary pocket, while in G288R CRY1, it occupied a position between S44 of the loop and E382. This conformational change results as increase in the distance between E382 and S44, expanding from 12.8Å to 15.3Å in top three representative frames, which, in turn, interferes with the hydrogen bond formation between these two residues. (**Fig 4.11B**). Interestingly, F41 has the potential to engage in a lone pair- p (lp–p) interaction with E382 (within 4Å), which could stabilize this conformation (**Fig 4.11B, inset**). Furthermore, N46 exhibited a conformational change in E214K CRY1, potentially allowing for an additional hydrogen bond with W52 compared to wild type CRY1 (**Fig 4.11BC**). These findings shed light on the specific conformational changes of amino acids involved in the shortest pathways and their potential role in modulating the structural dynamics of the serine loop in CRY1.

Next, I analyzed the dihedral angle distributions of the residues involved in frequent hydrogen bonds. The χ1 and χ2 dihedral angles of E383 were similar between wild type and CRY1 mutants. Regarding E382, there were no noticeable differences in the v1 dihedral angles correlating with the serine loop state in both wild type and CRY1 mutants (**Fig 4.12A**). However, the χ2 dihedral angles showed differences between wild type and mutants

depending on the loop state (**Fig 4.11D**). In wild type CRY1, the v2 dihedral angle of E382 sampled two conformers: plus (+60°) and trans (±180°). In the closed-state mutants, C259Y and R293H CRY1, the χ2 dihedrals remained stable in the trans (±180°) conformation. Conversely, the open-state mutant, G288R CRY1, predominantly sampled the minus (-60°) conformation and did not exhibit the trans (±180°) conformation. A217V/L218F CRY1, which closely resembled the wild type in terms of the serine loop conformation, mainly adopted the trans (±180°) conformer rather than the plus (+60°) conformer. E214K CRY1 exhibited multiple conformations to some extent without a dominant conformation. In summary, the analysis of the χ2 dihedral angle of E382 revealed that the trans (±180°) conformations were favored in the closed-state loop, while the minus (-60°) and plus (+60°) conformations were primarily favored in the open- state conformations.

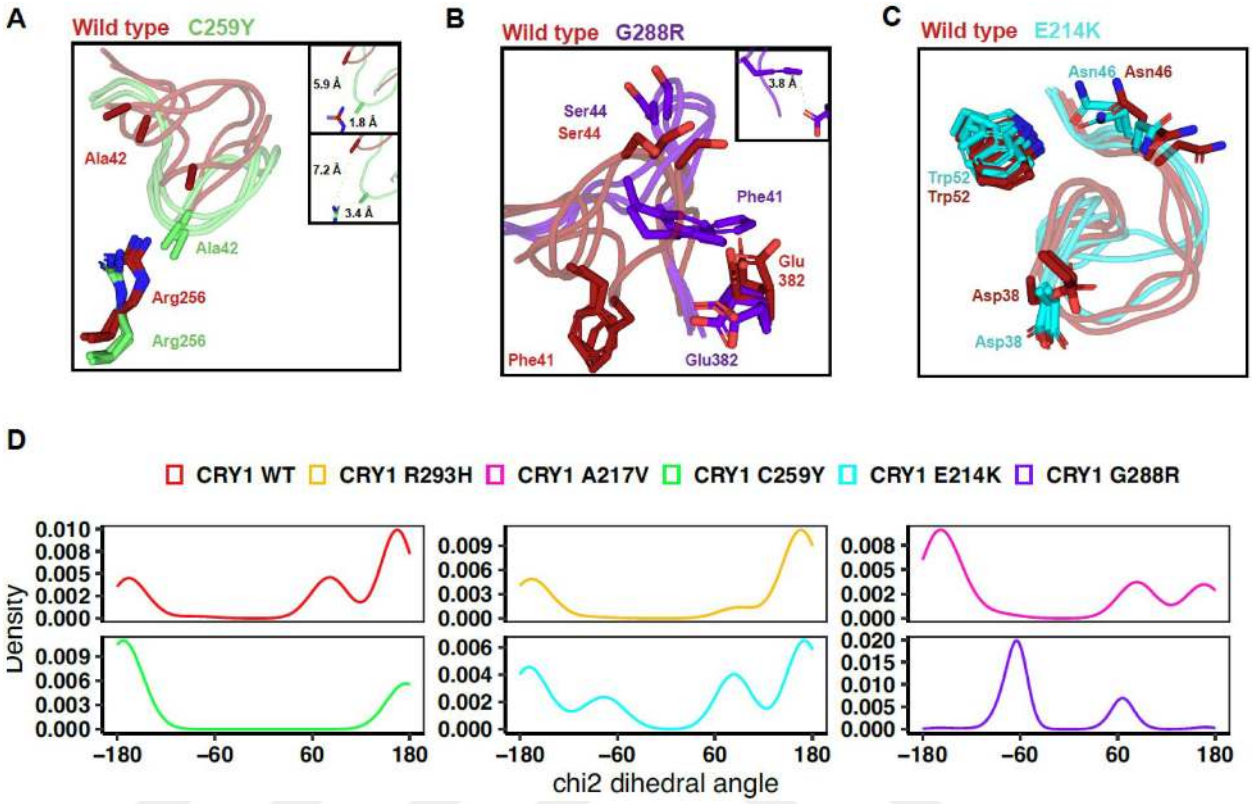

Figure 4. 11. Conformations of the residues involved in the shortest pathways or hydrogen bonding. Cluster representatives of top three most crowded clusters superpositined.

(a) In C259Y CRY1, R256 side conformation was predominantly different compared to the wild type (-90˝˘and 60˝˘, respectively). (b) In G288R CRY1, the conformation of F41 was predominantly different compared to the wild type. In wild type, F41 was buried toward the secondary pocket. However, in G288R CRY1, it extends toward the rim of the secondary pocket. (c) In E214K CRY1, N46 sampled different conformations compared to wild type, most likely, due to hydrogen bonding with W52. (d) The distribution of side chain conformations (v2) at E382 was distinct between the open and closed states of the serine loop. Trans (±180˝˘) conformations were observed more in closed state loop mutants (R293H, A217V/L218F, C259Y), while mainly minus (-60˝˘) and plus (+60˝˘) conformations were observed more in open state loop mutants (E214K CRY1 and G288R).

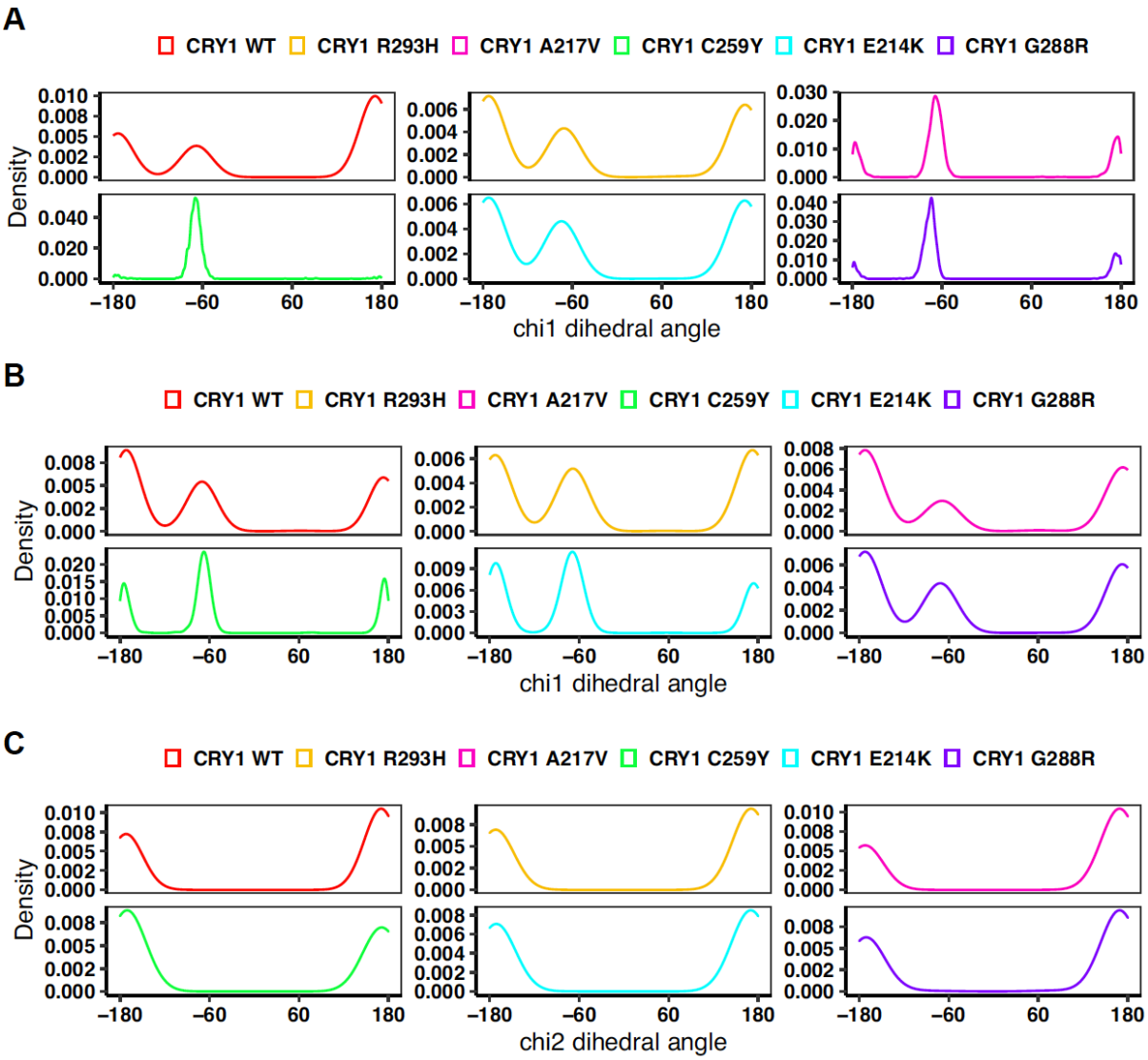

Figure 4. 12. Dihedral angels of E382 and E383 in all CRYs

(A) Distribution of χ1 dihedral of E382, **(B)** χ1 dihedral of E383 and **(C)** χ2 dihedral of E383 are represented for all CRY1 systems. None of the angles showed a distinct distribution depending on loop state.

4.10 Interactions of CRY2 with CLOCK-PASB domain

Interestingly, I not only did not observe any changes in serine loop dynamics but also found that the secondary pocket volume is significantly larger in both wild type and mutant CRY2 (**Fig 4.6C, 7, and 10**). Since the serine loop gates CRYs-CLOCK interaction our data collectively suggest that the binding mechanism between CRY2 and CLOCK may involve a different mechanism. To explore this further, I conducted a detailed investigation of the interactions between CLOCK and CRY2 mutants. Using the HADDOCK webserver, I docked cluster representatives of CRY2 with the CLOCK-PASB domain, and the results were consistent with previously published findings (**Fig 4.10E**) (Emre Onat et al., 2020c; Michael et al., 2017). In the first clusters, the conformations of G230R and E312K CRY2 were similar to those of the wild type CRY2 when docked with CLOCK. However, when A235T CRY2 was docked with CLOCK, CLOCK adopted different conformations compared to the other mutants in all three top clusters. Additionally, I calculated the binding energies between CRY2 mutants and CLOCK-PAS-B. Except for A235T CRY2, all mutants exhibited very similar binding energies to the CLOCK-PAS-B domain (**Table 4.6**). Overall, these results indicate that there are no significant changes in the serine loop of CRY2 and its affinity to the CLOCK PAS-B domain.

Table 4. 6 Interaction energies between CRY2 systems and CLOCK (Pas-B domain). CLOCK PASB domain docked to secondary pocket of wild type and mutant CRY2 systems. ΔG column represents the calculated binding free energy of the representative structure of most crowded cluster.

Protein-protein complex	ΔG (kcal mol-1)
CRY2 WT - CLOCK(PASB)	-9.5
CRY2 A235T- CLOCK(PASB)	-7.5
CRY2 E312K- CLOCK(PASB)	-9.2
CRY2 G230R- CLOCK(PASB)	-9.4

4.11 Allosteric regulation of serine loop in CRY1 with small molecules

Previously it has been shown that small molecules that are targeting primary pocket can exhibit both period lengthening and shortening circadian phenotypes(Oshima, Yamanaka, Kumar, Yamaguchi, Nishiwaki-Ohkawa, et al., 2015). While KL001 increases the period approximately 2 hours and decreases the amplitude, GO200 shortens the period about 0.6 hours. Given that both molecules occupy primary pocket and lengthens the half-life of CRY1 protein, underlying mechanism of how they exhibit opposite effects is yet to be explained. To further investigate this phenomenon, I subjected CRY1-KL001 and CRY1-GO200 systems for total of 800 ns molecular dynamic simulations. To confirm each configuration reached equilibrium, I first determined the root mean square (RMSD) value of each mutant and wild type CRYs (**Fig 4.13A**). After achieving equilibrium in each protein, I analyzed the effect of each mutation on the flexibility of the serine loop and dynamics of the secondary pocket by plotting the root mean square fluctuations (RMSF) of all amino acids (**Fig 4.13B**). When compared with Apo-CRY1, I observed differences in the RMSF values

of residues in the serine loop (residues 38–48) in halo systems. The serine loop in CRY1-KL001 simulations showed less fluctuation compared to apo system (**Fig 4.13B**) similar to R293H CRY1. Because the serine loop regulates the volume and access to the secondary pocket, I analyzed the volume of the secondary pocket using POVME 3.0 software. Interestingly, analysis showed that simulations of CRY1-KL001 sampled significantly larger secondary pocket volume than apo-CRY1 unlike R293H CRY1 (**Fig 4.13C**). This means serine loop stabilized on a slightly open conformation. To further examine the relative internal dynamics of the loop, I analyzed the distance between the Ca atoms of Gly-43 located on the loop and Phe-105 (**Fig 4.13D**). The mean loop distances of apo-CRY1 and CRY1-GO200 were similar although CRY1-KL001 showed larger loop opening distance. This means serine loop stabilized on a slightly open conformation. These observations in MD simulations implied that the dynamics of the serine loop in apo-CRY1 and CRY1-KL001 are regulated differently. Although the serine loop in apo-CRY1 is more dynamic, stable open conformation of this loop in CRY1-KL001 and might affect binding of CRY1-KL001 to CLOCK.

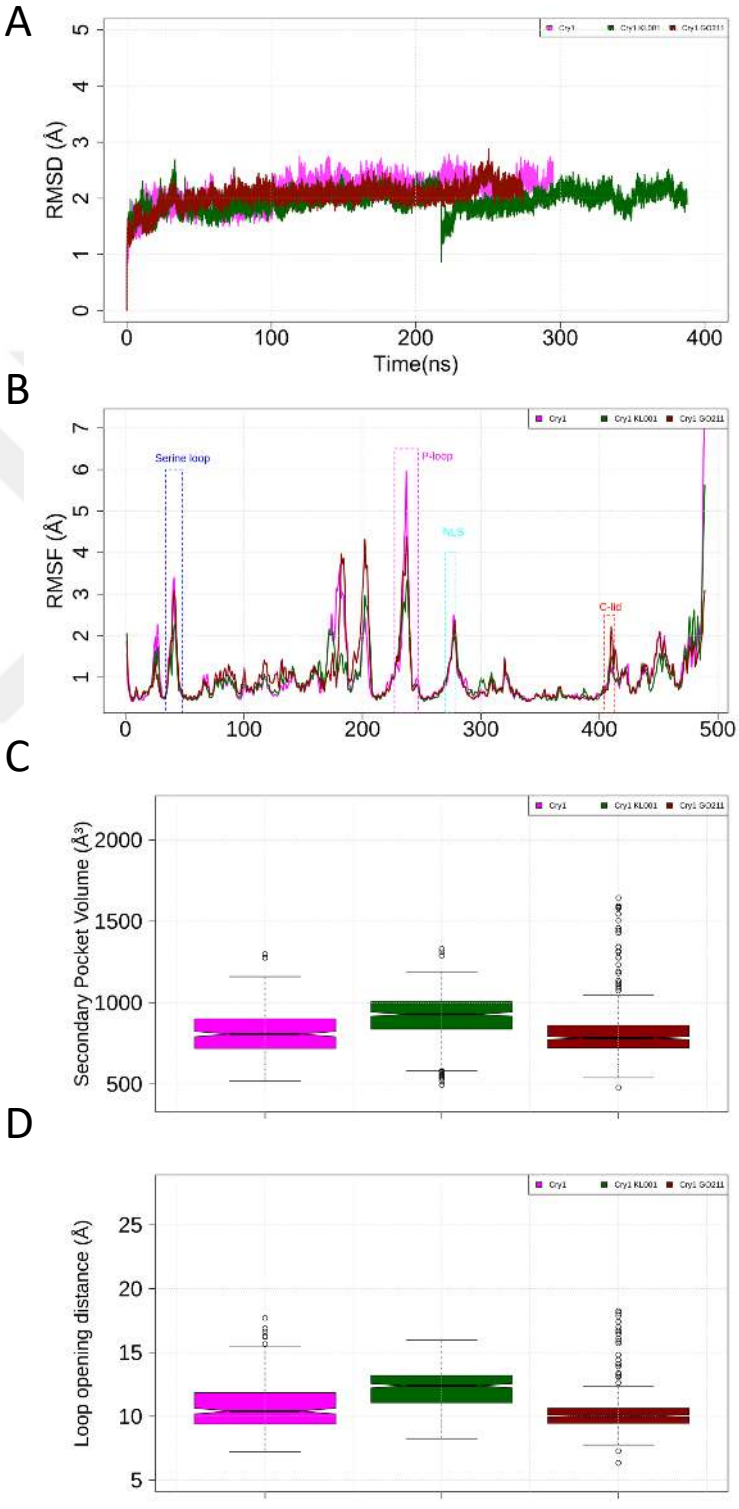
A
RMSD (Å)
Time(ns)
B
RMSF (Å)
Serine loop
P-loop
NLS
C-lid
C
Secondary Pocket Volume (Å³)
D
Loop opening distance (Å)

Figure 4. 13. Molecular dynamic simulation studies of Apo-CRY1, CRY1-KL001 and CRY1-GO200 halo systems.

A) RMSD of Apo-CRY, CRY1-KL001, CRY1-GO200 simulations. B) RMSF of Apo-CRY, CRY1-KL001, CRY1-GO200. Residues between two dashed lines belong to the serine loop. C) Box plot representation of the secondary pocket volume sampled throughout the simulations. Wilcoxon rank sum test was applied (*, p ,0.0001). D) box plot representation of the loop distance produced by measuring the distance between Ca atoms of Gly-43 and Phe-105. Distance between Gly-43(on loop) and Phe-105 was calculated with a custom Python script. The same multi-frame PDB files extracted from the trajectories were used to calculate the secondary pocket volume and loop distances. Statistical analysis between variances of loop distances of CRY1 and CRY1R293H simulations was calculated by the Levene's test (p, 0.001).

4.12 CLOCK binding to CRY1 is enhanced in presence of KL001

Since I observed that KL001 affects serine loop dynamics in molecular dynamics simulations, to assess binding of CRY1 to CLOCK and BMAL1 with presence of KL001, HEK293T cells were transiently transfected with expression plasmids coding for CLOCK-flag, BMAL1, and CRY1. The CRY1-myc-His containing protein complexes were then precipitated using Anti-DYKDDDDK Affinity resin, and the samples were probed for the presence of CLOCK and CRY1 by Western blot analysis. CLOCK affinity to CRY1 and CRY1-KL001 was significantly different (**Fig 4.14**). When KL001 is present, CLOCK affinity to CRY1-KL001 complex increased. Previously, (Hirota, Lee, st. John, et al., 2012) discussed that CRY1 stabilization through KL001 leads to circadian period lengthening up to 6 hours. However, (Rosensweig et al., 2018b) also discussed that Rescue vector dosage does not underlie period differences in *Cry1/Cry2* rescues(Rosensweig et al., 2018b). *Cry1*$^{-/-}$ *Cry2* $^{-/-}$ MEFs transfected with increasing amount of rescue vectors for *Cry1* and *Cry2*. Increasing the amount of transfected rescue vector for either *Cry1* or *Cry2* resulted period shortening in a dose dependent manner. Although exact mechanism is not clear, there might

be another aspect of how CRYs regulate period. Increasing affinity of CLOCK to CRY1-KL001 complex may help to explain this mechanism.

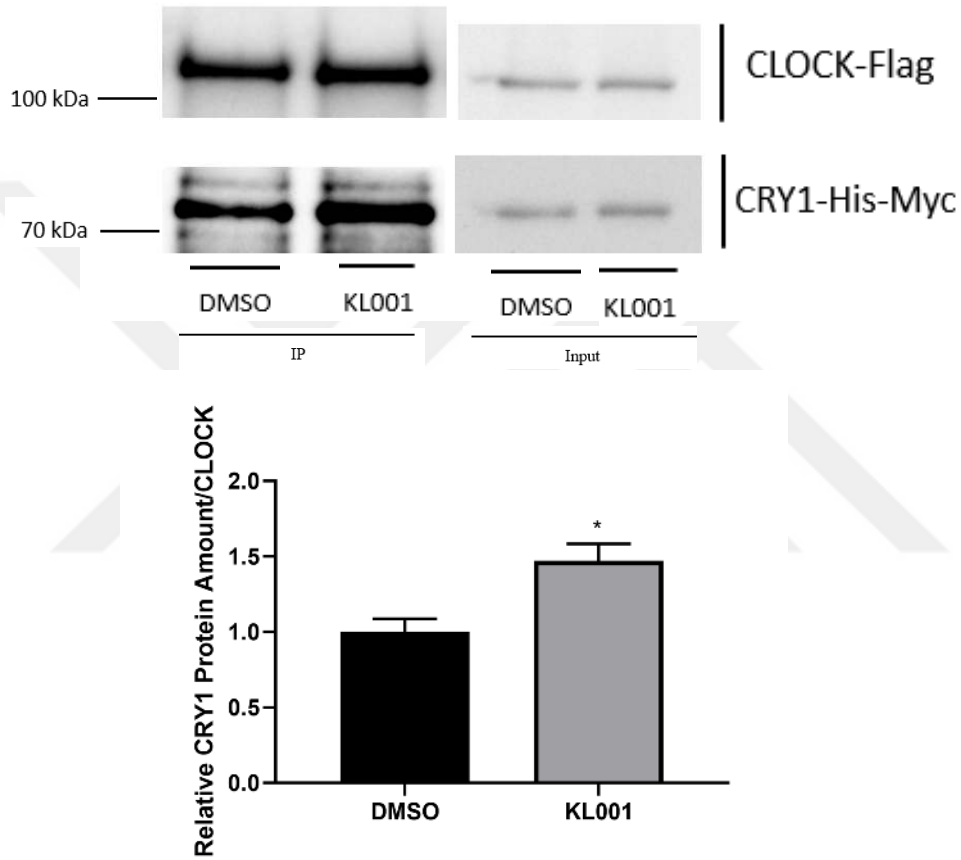

Figure 4. 14. Co-IP of CLOCK with CRY1 in presence of KL001.

Co-immunoprecipitation of CLOCK with CRY1, CRY1-KL001. HEK293T cells were transfected with plasmids expressing CLOCK-FLAG, CRY1-His/myc. CLOCK were co-immunoprecipitated with anti-flag resin and analyzed with Western blotting. This blot is the representation of three independent experiments.

4.13 In silico drug design: Targeting mammalian CRYs in their secondary pocket

Known small molecule modulators of CRYs target their primary pocket. Which results in modified half-life of CRYs (KL001, GOxxx, THxxx, etc.)(S. Gul et al., 2022b; Hirota, Lee, st. John, et al., 2012; Oshima, Yamanaka, Kumar, Yamaguchi, Nishiwaki-Ohkawa, et al., 2015). I have shown that how targeting CRYs at their primary pocket may have unforeseeable effects. Mammalian CRYs also have wide range of interaction partners in circadian clock mechanism as well as other pathways such gluconeogenesis (**Fig 4.15**)(Surme et al., 2023; Zhang et al., 2010). Therefore, targeting interaction between CRYs and CLOCK without disrupting CRYs half-life is essential to minimize off target effects of drug candidates. To address this, I did a virtual screening of small molecules that are targeting secondary pocket of mammalian CRY1.

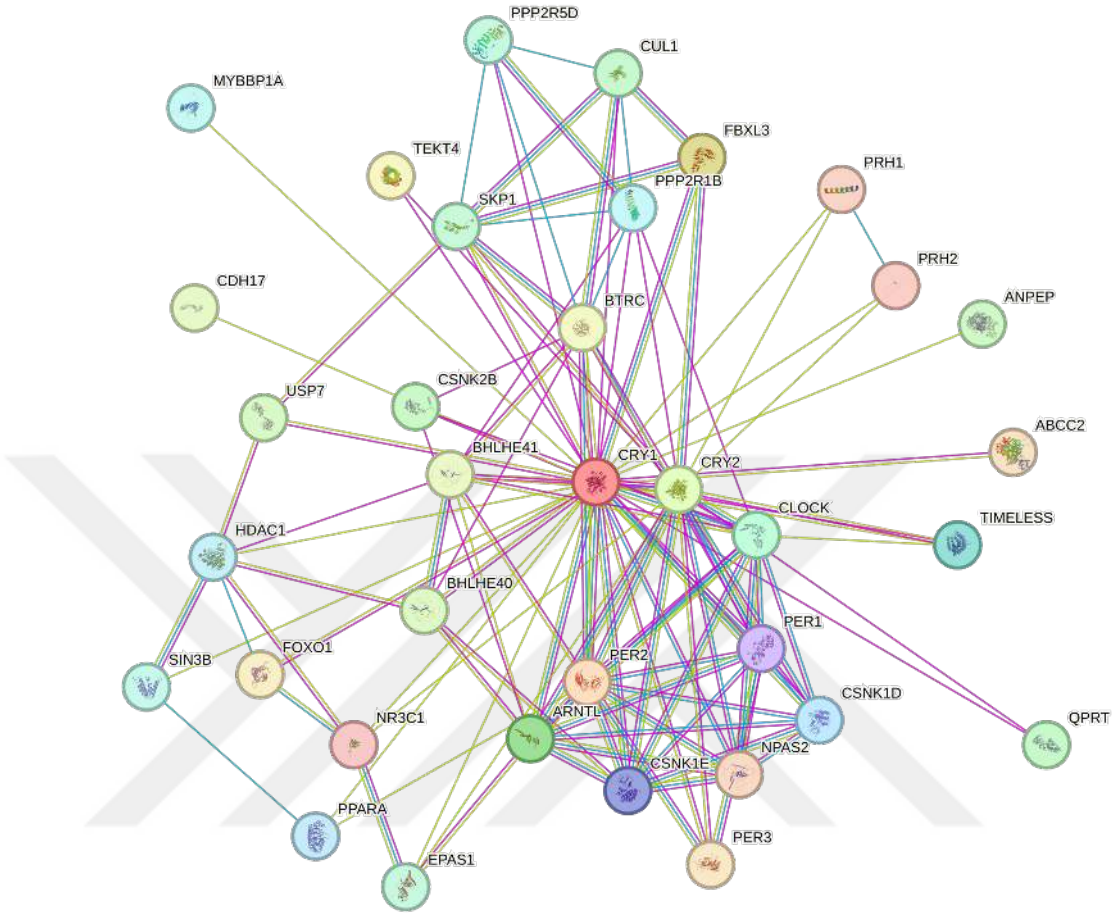

Figure 4. 15. Interaction partners of human CRY1.

Interactions limited to physical network and max interactors at first shell limited to 50.

I generated homology model of mouse CRY1 PHR domain. Sequences of PHR domain, sequence between starting and ending residue of Cry1 crystal structure (PDB ID:4k0r), retrieved from Uniprot (P97784) and submitted to RaptorX web server. I ran 300 ns molecular dynamics simulation for wild type Apo-CYR1 model, under NPT conditions and 310K(**Fig 4.4.16A**). Next, trajectory subjected to pairwise best-fit RMSD based method implemented in UCSF Chimera for clustering analysis. Cluster representative of the most crowded cluster is taken as near psychological and most represented conformation (**Fig 4.16B**). This structure further used for molecular docking studies.

Current Ambinter catalogue for small molecules retrieved from Ambinter website (https://ambinter.com/catalogue/Ambinter_Screening_Library.sdf.tgz). Around 7 million molecules subjected to preliminary filtering. CRY1 primary and secondary pocket volumes are drastically different (**Fig 4.16C**). While pocket volumes fluctuate throughout trajectory, CRY1 primary pocket volume has average of 1314.811 $Å^3$ while CRY1 secondary pocket volume has average of 817.1044 $Å^3$. Considering this difference and size of known interacting molecules for primary pocket, I filtered small molecule catalogue accordingly. Ambinter catalogue is filtered mostly according to Lipinski's rule of five, Ghose filter, Veber's Rule with minor modifications. Most notably, molecular weight limit set to 300 Da considering DMRL, a known cofactor of photolyases in their secondary pocket. Around 1.2 million molecules were survived and docked to the CRY1 secondary pocket(**Fig 4.16D**). When candidate molecules sorted according to their binding energies of top 75 ranked molecules ranged from -10.2 Kcal/mol to -9.6 Kcal/mol. Ambinter accession codes of available molecules and interacting residues top 30 ranking molecules were given in Appendix (**Table S7 and Table S7.1**). Molecules renamed to shorter abbreviations for sake of ease; name conversion table also given in Appendix (**Table S8**). Due to various reasons such as not being commercially available at the time of purchase number of ordered haven't molecules arrived. Additionally some of the molecules haven't used for in vitro experiments due to poor solubility in DMSO (C3,C7,,D4,D6,D12,E1).

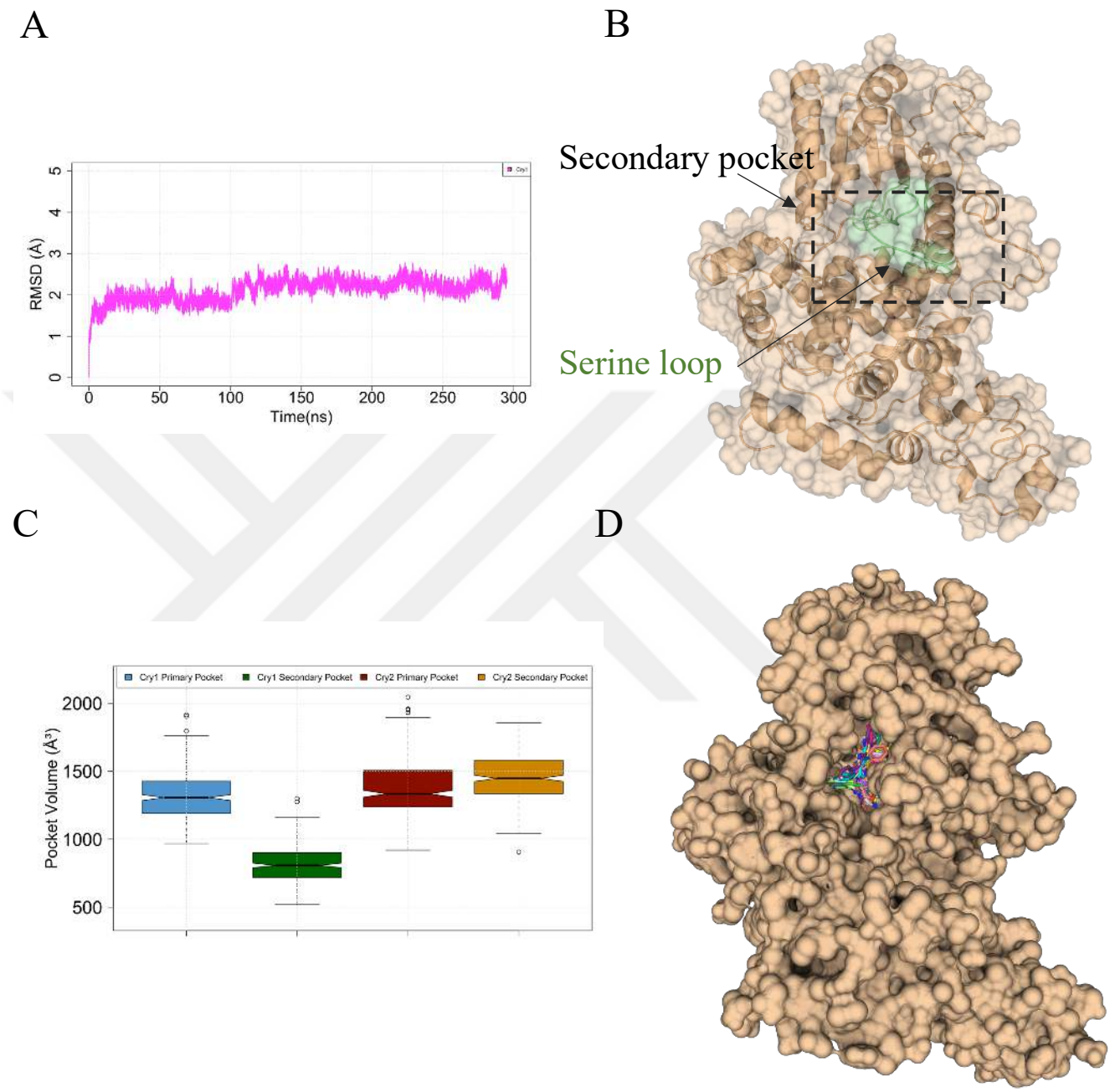

Figure 4. 16. In vitro screening of CRY1

A) RMSD values of 300ns Apo-CRY1. B) Cluster representative of most crowded cluster. Serine loop (green) and secondary pocket (dashed lines) indicated on semitransparent surface representation on top of cartoon representation. C) Box plot representation of primary and secondary pocket volumes of CRY1 and CRY2 throughout trajectory. D) Top 30 molecules after molecular docking according to their binding affinity shown in secondary pocket.

4.14 Cytotoxicity assessment of small molecules

In order to determine toxicity of these molecules at given doses, I used MTT (3-[4,5-dimethylthiazol-2-yl]-2,5 diphenyl tetrazolium bromide) test in U2OS and HEK293T cell lines. MTT is a colorimetric assay which is used to detect mitochondrial activity. Mitochondrial activity is an acceptable indicator of viable cells in a population. For all drugs doses are arranged between 20μM and 5 μM. Drugs tested in The toxicity of selected molecules was, first, assessed using human osteosarcoma (U2OS Bmal1-dLuc where the destabilized form of Luciferase (Luc) gene fused with Bmal1 promoter) since this cell line further used in other experiments. Out of 39 tested small molecules 25,4 and 1 were nontoxic at 20μM, 10μM and 5μM, respectively (**Table 4.7, Fig 4.17-18-19**). 9 of them were toxic at every dose above 5μM. Next, I used HEK293T cell line to further confirm small molecules are non-toxic at given doses in different genetic background. Highest non-toxic dose at U2OS cells of small molecules were used to treat HEK293T cells (**Fig 4.20**). Other than E3 molecule, none of the small molecules significantly affected cell viability.

Table 4. 7 Highest non-toxic doses of small molecules on U2OS *Bmal1:dLuc* cells

Name	MTT Non-Toxic Dose (uM)	Name	MTT Non-Toxic Dose (uM)
A1	10	C1	20
A2	20	C2	20
A3	20	C4	20
A4	T	C5	20
A5	20	C6	20
A6	10	C8	20
A7	20	C10	20
A8	10	C11	20
A9	20	C12	20
A10	20	D1	T
A11	20	D2	20
B1	20	D3	T
B2	T	D5	T
B3	T	D7	T
B4	20	E2	20
B5	T	E3	5
B6	T	E4	20
B7	20	E5	20
B8	20		
B9	20		
B10	T		

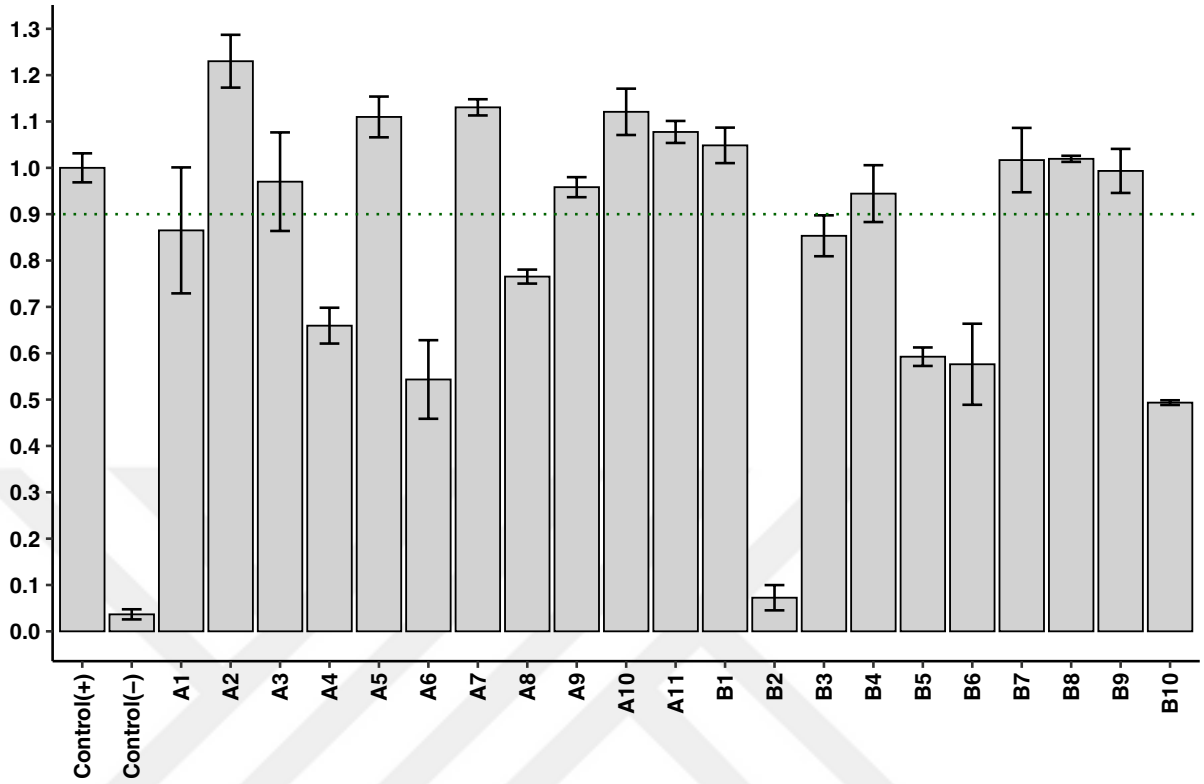
1.3
1.2
1.1
1.0
0.9
0.8
0.7
0.6
0.5
0.4
0.3
0.2
0.1
0.0
Control(+)
Control(−)
A1
A2
A3
A4
A5
A6
A7
A8
A9
A10
A11
B1
B2
B3
B4
B5
B6
B7
B8
B9
B10

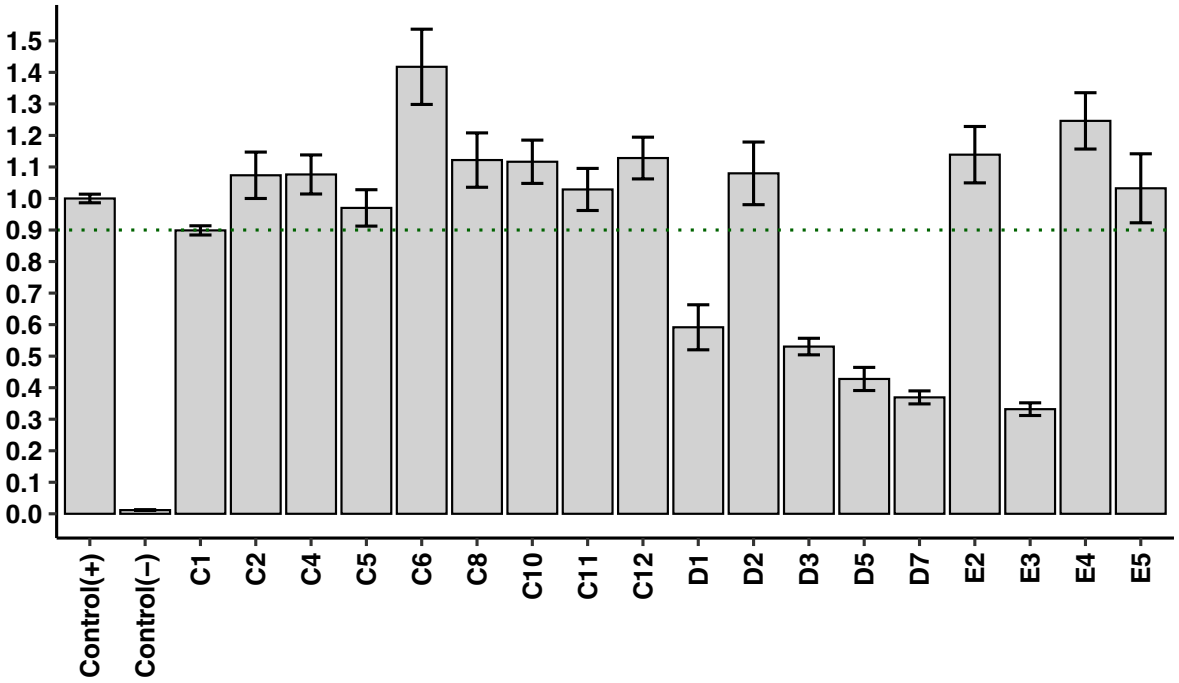
1.5
1.4
1.3
1.2
1.1
1.0
0.9
0.8
0.7
0.6
0.5
0.4
0.3
0.2
0.1
0.0
Control(+)
Control(−)
C1
C2
C4
C5
C6
C8
C10
C11
C12
D1
D2
D3
D5
D7
E2
E3
E4
E5

Figure 4. 17. Cytotoxicity of small molecues on U2OS cell line.

U2OS *Bmal1:dLuc* cells were seeded in 96 well plates as triplicates. After treatment with 20 μM of small molecules for 48h, cell viability assessed with MTT assay. Mean indicates average of three independent biological replicates. ANOVA with Dunnett's post hoc test used to evaluate statistical difference between control group (DMSO) and treatment. (* indicates that p-val < 0.05)

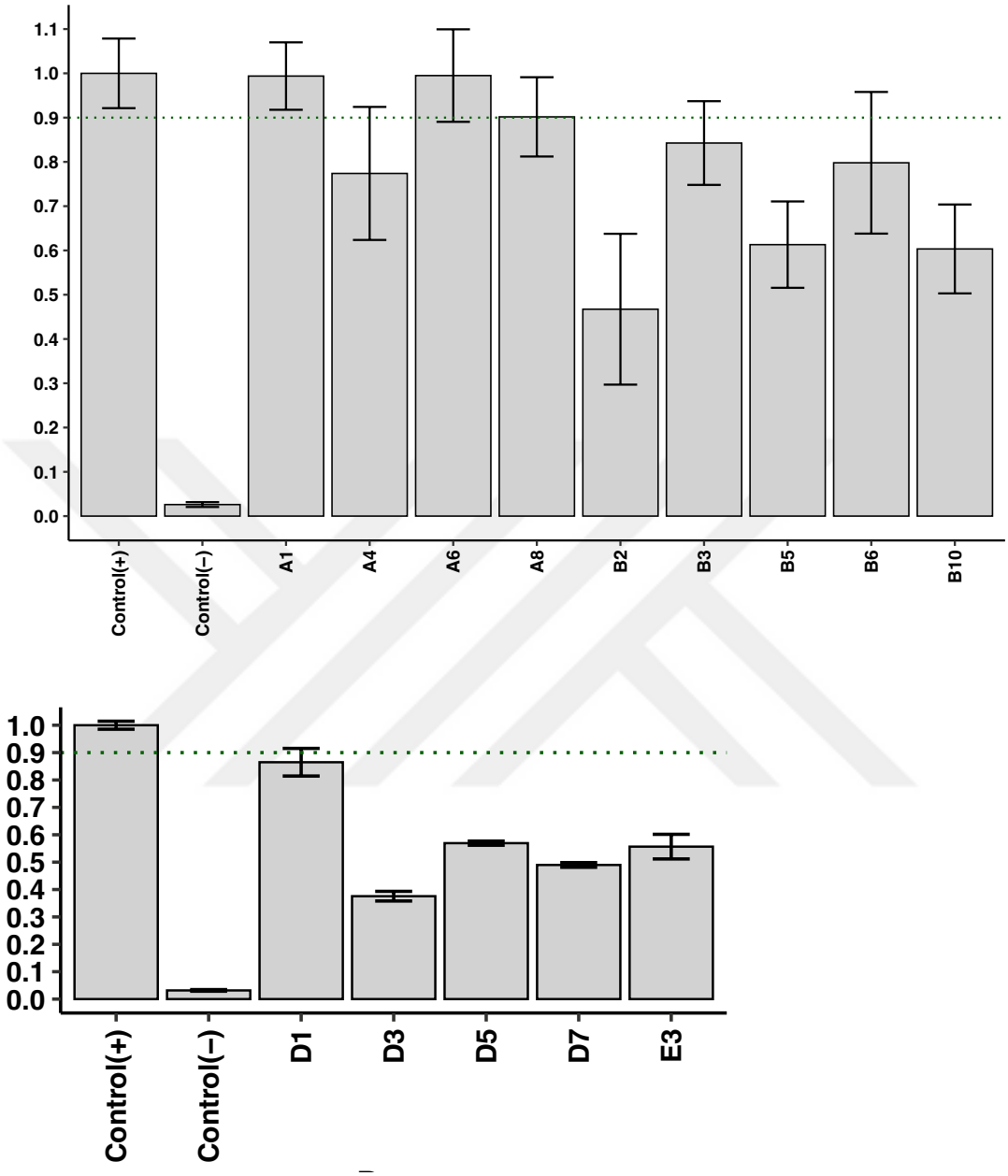

Figure 4. 18 Cytotoxicity of small molecules on U2OS cell line.

U2OS *Bmal1:dLuc* cells were seeded in 96 well plates as triplicates. After treatment with 10 uM of small molecules for 48h, cell viability assessed with MTT assay. Mean indicates average of three independent biological replicates. ANOVA with Dunnett's post hoc test used to evaluate statistical difference between control group (DMSO) and treatment. (* indicates that p-val < 0.05)

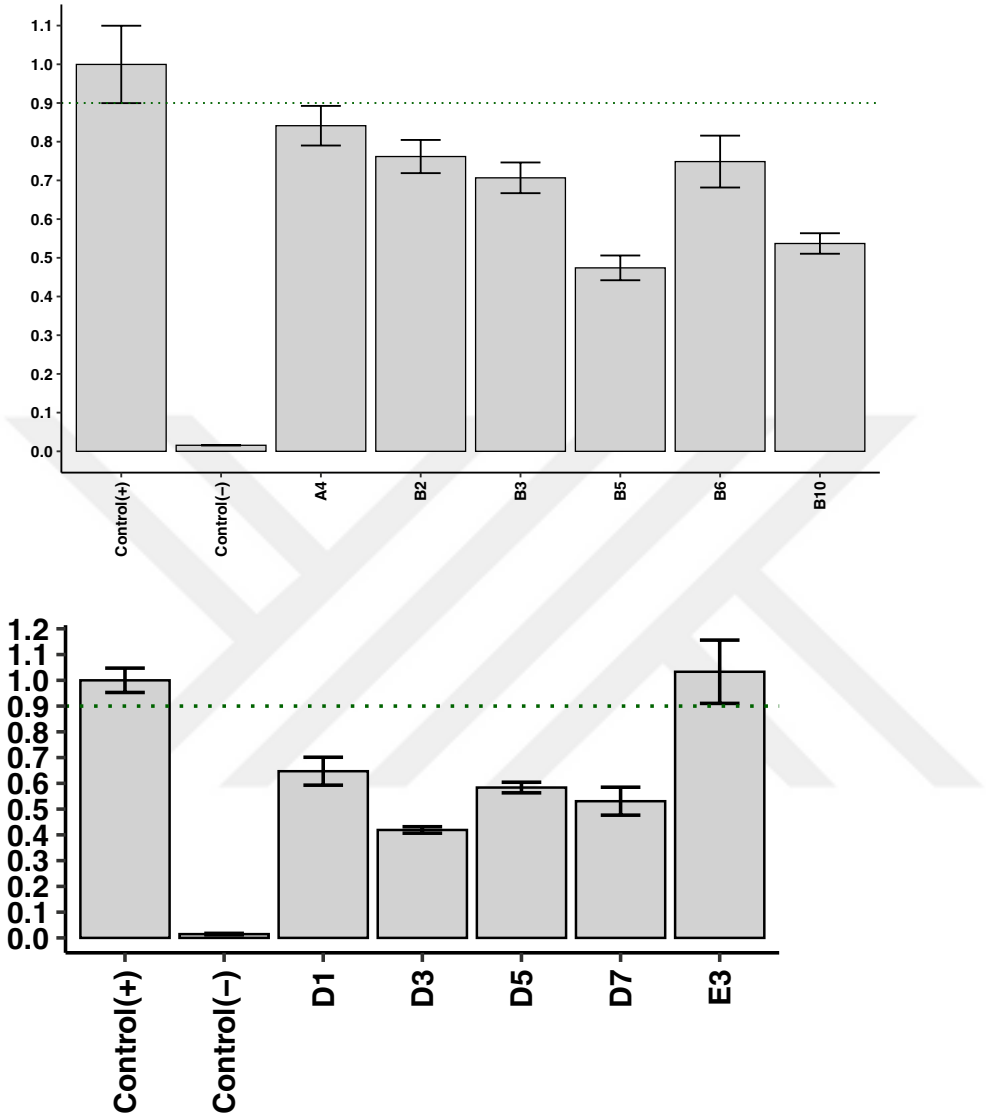

Figure 4. 19 Cytotoxicity of small molecules on U2OS cell line.

U2OS *Bmal1:dLuc* cells were seeded in 96 well plates as triplicates. After treatment with 5 uM of small molecules for 48h, cell viability assessed with MTT assay. Mean indicates average of three independent biological replicates. ANOVA with Dunnett's post hoc test used to evaluate statistical difference between control group (DMSO) and treatment. (* indicates that p-val < 0.05)

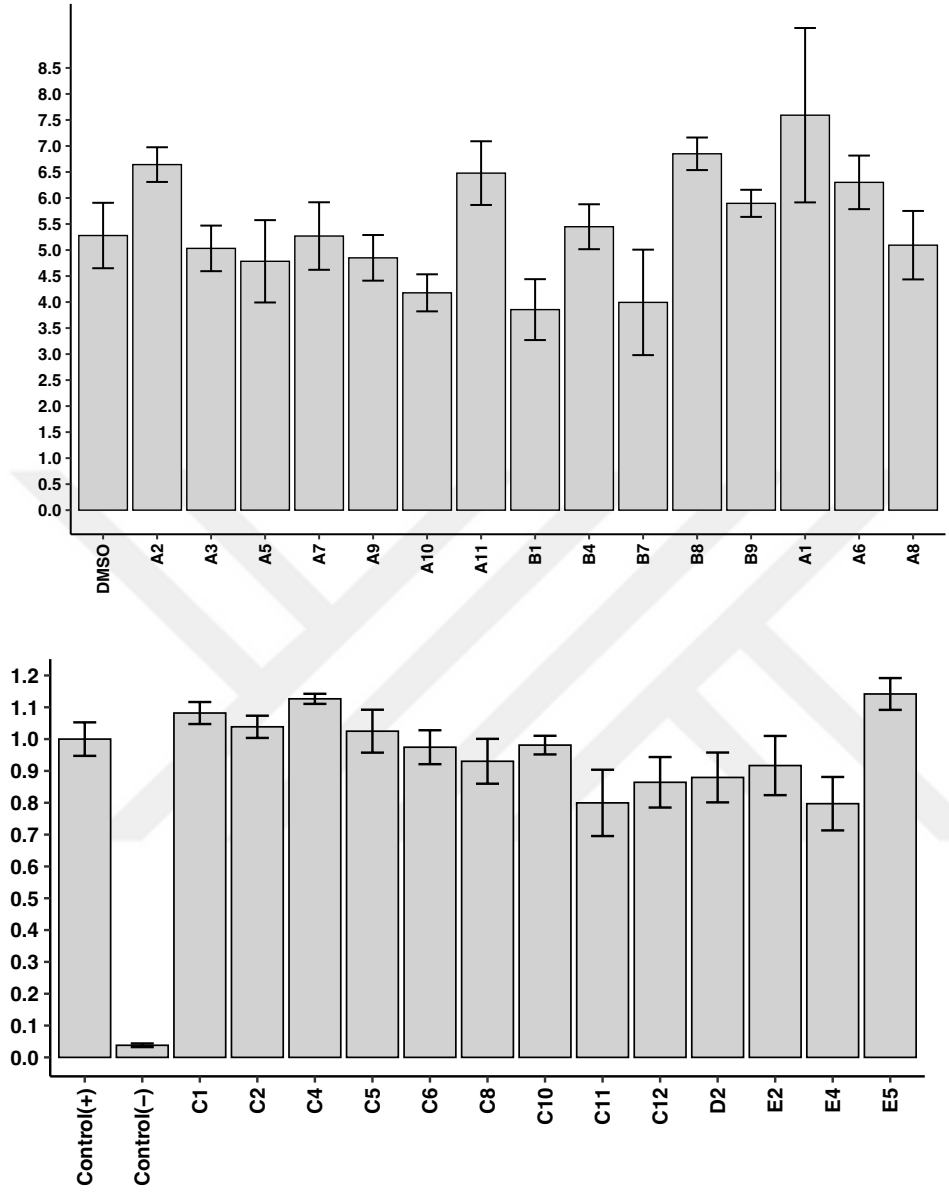

Figure 4. 20. Cytotoxicity of small molecues on HEK293T cell line.

HEK293T cells were seeded in 96 well plates as triplicates. After treatment with maximum non-toxic dose of small molecules on US2OS cells for 48h, cell viability assessed with MTT assay. Mean indicates average of three independent biological replicates. ANOVA with Dunnett's post hoc test used to evaluate statistical difference between control group (DMSO) and treatment. (* indicates that p-val < 0.05)

4.15 Determination of effect of small molecules in LUC half-life

To assess if any of the molecules affect luciferase half-life, HEK293T cells transfected with pCDNA-*Luc* vector. Cells were treated with each small molecules highest non-toxic dose for 24 hours. After that protein synthesis terminated with cycloheximide treatment and luminescence is recorded for 48h via Synergy H1. None of the small molecules other than E3 significantly affect luciferase half-life. All other small molecules further used for characterization.

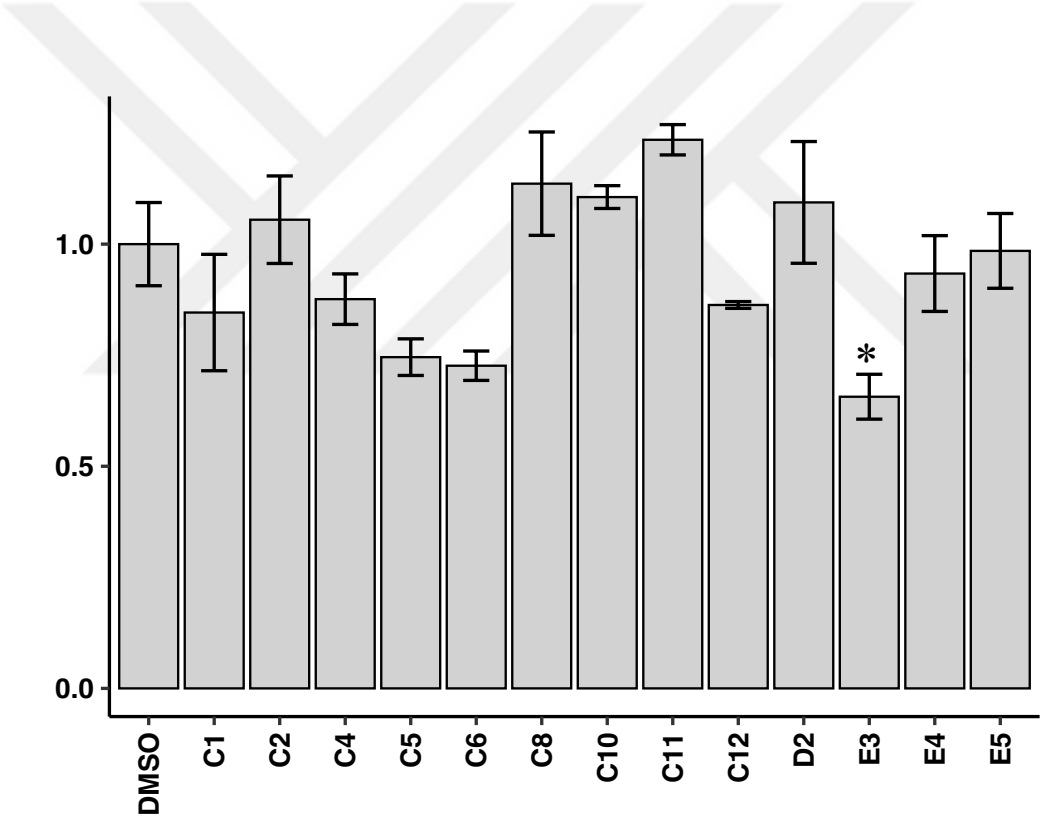

Figure 4. 21 Figure 4.21. Relative luciferase hallflife upon small molecule treatment on HEK293T cell line with highest non toxtic dose.

HEK293T cells were seeded in 96 well plates as triplicates reserves transfected with pcDNA-*Luc* vector. After treatment with maximum non-toxic dose of small molecules, cells are treated with cycloheximide. Bioluminescence recorded with Synergy H1 for 48 hours. Mean indicates average of three independent biological replicates. ANOVA with Dunnett's post

hoc test used to evaluate statistical difference between control group (DMSO) and treatment. (* indicates that p-val < 0.05)

4.16 Effect of Small molecules on circadian phenotype

To see effect of small molecules I further characterized candidate molecules that has a non-toxic dose between 20 µM-5µM and doesn't affect luciferase half-life. First, human osteosarcoma (U2OS Bmal1-dLuc where the destabilized form of Luciferase (Luc) gene fused with Bmal1 promoter) cells seeded in a 96 well plate. Next day, cells were treated with small molecules at their highest non-toxic dose and luciferase luminescence recorded with Synergy H1 for seven days. After data collection circadian period and amplitude assessed via Biodare webserver (https://biodare2.ed.ac.uk). Most of the drugs lengthened circadian period although they had variable effects on amplitude (**Fig 4.22, Fig S6**).

Since I saw that most of the small molecules were effective at their higher non-toxic does at the initial screening, I deployed a more sensitive method. Cells were seeded to 35mm well plates and treated with small molecules with dose dependent manner. Next, bioluminescence recorded with Lumicycle which has more precise and frequent recording compared to Synergy. Overall, molecules exhibited 5 different phenotypes (**Fig 4.23, Table 4.8**). Five molecules, decreased amplitude and lengthen the period. 4 molecules increased amplitude and lengthen the period. Seven molecules increased amplitude without a dose dependent effect on period. One molecule slightly decreased the period without a dose dependent effect on amplitude. Six molecules lengthen the period without a dose dependent effect on amplitude. Individual bioluminescence, amplitude and periods of drugs were given at **Appendix D**.

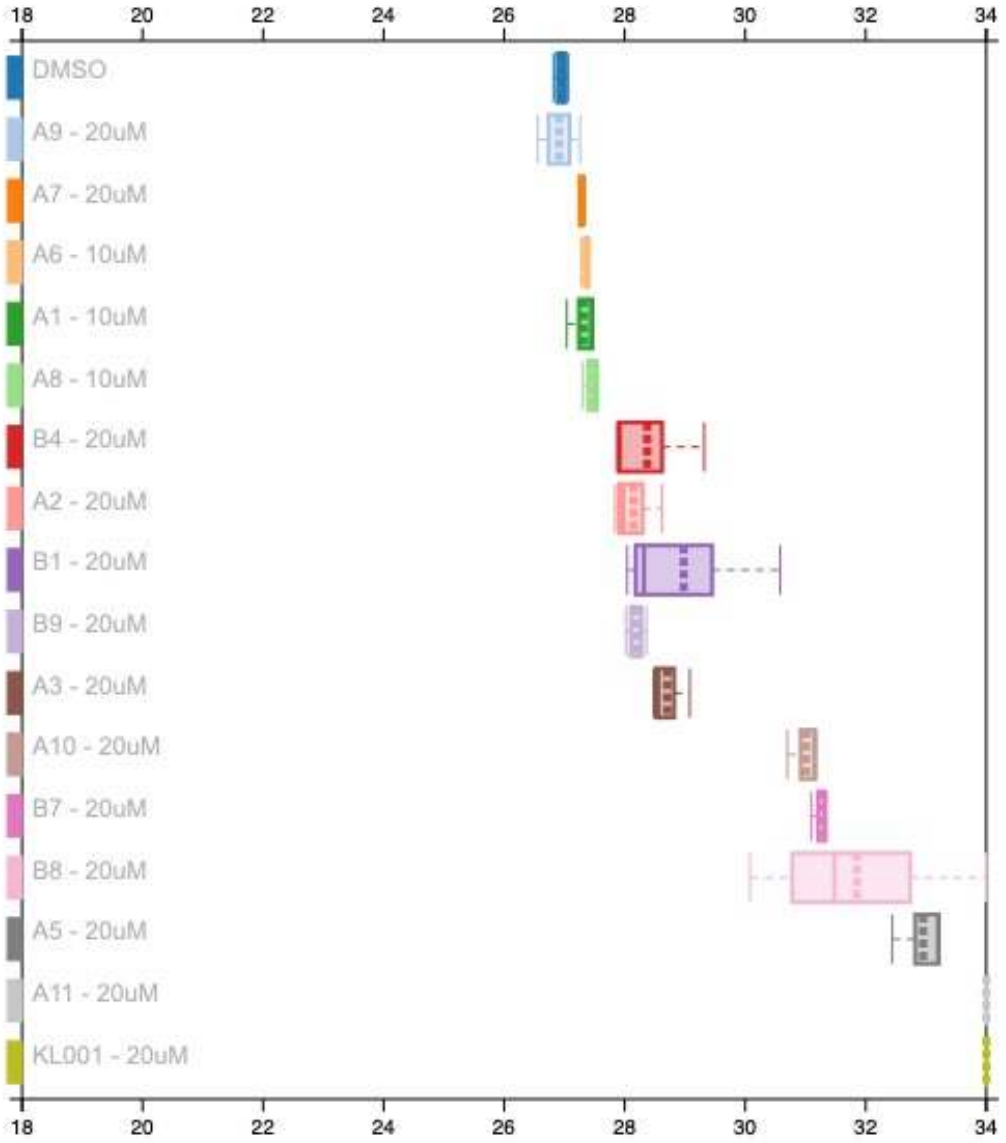

Figure 4. 22. Circadian period of U2OS Bmal1:dLuc upon drug treatment.

U2OS *Bmal1:dLuc* cells seeded in 96 well plate. After 24h, synchronized with dexamethasone and bioluminescence recorded for 7 days in Synergy H1. Circadian period calculations performed via Biodare webserver.

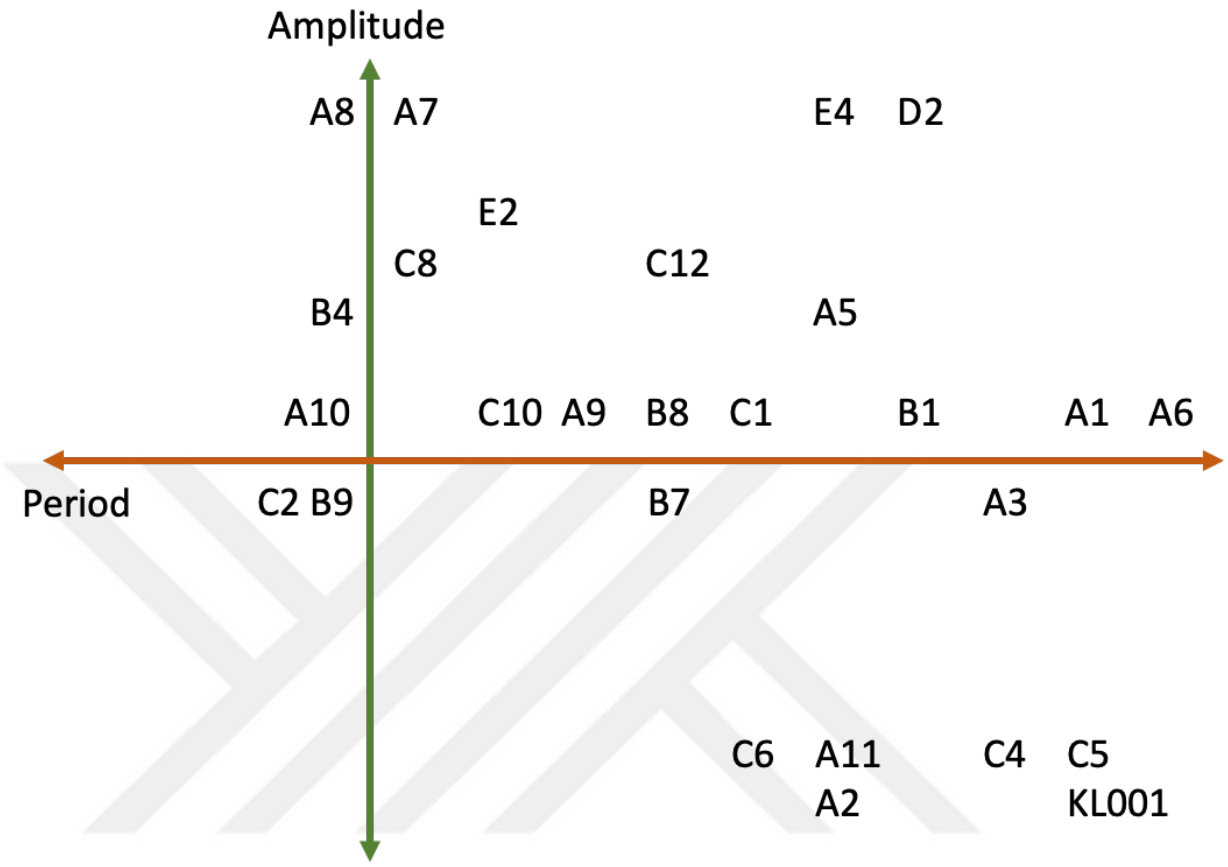

Figure 4. 23 Effects of all small molecules on circadian amplitude and period relative its magnitude.

Effect of small molecules on the bioluminescence rhythm of U2OS cells stably expressing *Bmal1*-d*Luc* seeded in 35 mm plates. After 24h cells are synchronized with dexamethasone treated with small molecules in a dose dependent manner. Luciferase luminescence recorded in Lumicycle for 7 days. Circadian period calculations performed via Biodare webserver.

Table 4. 8 Effects of small molecules on circadian amplitude and period.

Name	Amplitude	Period
A2	**-**	+
A11	**-**	+
C4	**-**	+
C5	**-**	+
C6	**-**	+
E4	+	+
A5	+	+
C12	+	+
E2	+	+
D2	+	**NA**
B8	+	**NA**
A7	+	**NA**
A8	+	**NA**
B4	+	**NA**
B9	+	**NA**
C8	+	**NA**
C2	**NA**	**-**
A1	**NA**	+
A6	**NA**	+
A3	**NA**	+
B1	**NA**	+
B7	**NA**	+
C1	**NA**	+
A10	**NA**	**NA**
A9	**NA**	**NA**
C10	**NA**	**NA**

CHAPTER 5
DISCUSSION

Mammalian CRYs are integral components of the circadian clock mechanism and are strong transcriptional repressors of BMAL1/CLOCK transactivation (Sato et al., 2006; Ueda et al., 2005) Several genetic studies have highlighted the relationship between CRY variants and different types of diseases. For example, CRY1 variants have been associated with depression and mood disorders (Hua et al., 2014; Kovanen et al., 2015; Soria et al., 2010), elevated blood pressure and hypertension, and insulin resistance (Dashti et al., 2014; Kovanen et al., 2016). This clinical heterogeneity implies a variety of different functions for CRY1 potentially caused by different functional domains of the protein. Despite the high primary and tertiary structure similarities of CRY1 and CRY2, several studies suggest that they have different affinities to CLOCK (Horst et al., 1999b; Koike et al., 2012b; Thresher et al., 1998; Vitaterna et al., 1999). Although rare CRY1 variants have been previously shown to be associated with several disorders, the underlying mechanisms are yet to be characterized. Here, not only the potential functional impact of rare nonsynonymous SNPs on the function of CRY1 was investigated but I also revealed the allosteric regulation between primary and secondary pockets of CRY1 by characterizing one of the rare mutants. The three variants, which map to important domains of the CRY1 and are predicted to affect its function, were selected from Ensembl and the 1000 Genomes project. Arg-348 and Gly-144 residues map to the surface; Arg-293 is located within the primary pocket (**Fig. 4.1**). The effect of mutations on the $t_{1/2}$ CRY1 protein using the CRY1::dLUC degradation assay was analyzed. p.Arg348Cys and p.Gly144Val CRY1 variants had no effect on the stability of CRY1, whereas the p.Arg293His variant significantly increased the stability compared with WT CRY1 (Fig. 2A). Next, a cell-based rescue assay in *Cry1*$^{-/-}$ *Cry2* $^{-/-}$ MEF cells with a special Cry1 rescue plasmid was utilized to identify their effects on the circadian rhythm. Surprisingly, p.Arg293His CRY1 variant had longer t1/2 than the WT CRY1 and caused shorter period length with enhanced luminescence. This implies less repression activity (Fig. 2B), which is the indicator of weak binding of mutant CRY1 to BMAL1/CLOCK. Other two variants caused slight increase in the period length, which is consistent with previous findings

indicating that mutation of residues on the surface of the a-helical domain have a tendency to change the repressor activity of mammalian CRYs (McCarthy et al., 2009). Despite earlier studies suggested that as the stability of CRY increases by either mutation or chemicals, period of circadian rhythm becomes longer; however, recent findings unveiled that not the stability but the ability of CRY to bind BMAL1/CLOCK is the primary factor in determining the period length (Hirano, Shi, et al., 2016; Patke et al., 2017; Rosensweig et al., 2018b; H. Xu et al., 2015). Interestingly, functional characterization of p.Arg293His, which is located in the a12-helix and possibly interacts with the secondary pocket, revealed different properties than the other CRY1 variants. That is to say, t1/2 of the p.Arg293His CRY1 was longer than WT CRY1. Second, functional complementation with this variant in DKO-MEF resulted in a short circadian period phenotype with increased luminescence. Third, biochemical studies showed that this variant had reduced affinity to CLOCK. Interestingly, these features are more similar to CRY2 than CRY1 (Rosensweig et al., 2018b). Thus, WT and p.Arg293His CRY1 and WT CRY2 in the same experimental set-up were tested to determine the differences and similarities among these proteins. Although p.Arg293His CRY1 and WT CRY2 had comparable t1/2 (Fig. 4A), repression capacity, and binding to BMAL1/CLOCK in pulldown assays (**Fig. 4.2D**), p.Arg293His caused a longer rhythm than WT CRY1 but shorter than WT CRY2 (Fig. 4.2C). Despite similarities between p.Arg293His CRY1 variant and WT CRY2 in various aspects, rescue assay exhibited that they have slight functionality differences in the circadian clock mechanism (**Fig. 4.2B**). To understand the dramatic change in the function of CRY1 upon Arg-293 to His-293 mutation and to assess the role of Arg-293 in CRY1, I employed molecular dynamics simulations. Computational analysis suggested that Arg-293 might be a critical residue for the regulation of the serine loop in CRY1, which is known to be important for CLOCK binding to the secondary pocket (Fribourgh et al., 2020). Replacing Arg-293 with His changes a highly dynamic serine loop into a less dynamic state and closes the gate of the secondary pocket (**Fig. 4.5**), which may be re sponsible for the reduced binding of CLOCK to the mutant CRY1. Further analysis of our MD simulations of both variant and WT CRY1 in terms of the communication pathways suggested that mutation of Arg-293 to His changes the path to serine loop, which shows the allosteric regulation of secondary pocket availability by the primary pocket (**Fig. 4.5F and G**). The rare variants characterized in this study were selected from published human SNPs,

which are all in heterozygous state and, to our knowledge, have not yet been associated with any disease phenotype. It is possible that these variants may exhibit a disease phenotype in recessive state. Their effects can be further analyzed in mouse models by reverse phenotyping studies. My findings suggest that Arg-293 is important for the allosteric regulation in CRY1 and has impact on the molecular clock.

To further understand importance of Arg-293 and whether both mammalian CRYs share a common regulatory mechanism or not; I subjected wild type CRY2 and CRY2 R311H (homolog residue of R293) to molecular dynamic simulations (**Fig 4.4A**). Wild type CRY1 and CRY2 dynamics were similar to that has been reported previously (Fribourgh et al., 2020). When I compare wild type CRY2 and CRY2 R311H; overall RMSF values other than p-loop, secondary pocket volumes, serine loop opening distances, number of hydrogen bonds that serine loop were indifferent. Only difference was pathway length between R/H 311 and A61(homolog of G43 in CRY1) (**Fig 4.4C and 4.5A-D**). Although pathway lengths changes, secondary pocket volume mainly affected by the position of highly dynamic unstructured serine loop in CRY1, however, serine loop in CRY2 has a turn of alpha helix that increases its rigidity. Because of the rigidity of serine loop in CRY2, effect of mutation might not alter its dynamics as drastically as in the CRY1.

Thus, I decided to further study CRYs with mutations that has shown to be deficient repression activity in order to explain underlying mechanism of allostery. In a prior study by (McCarthy et al., 2009) multiple mutations in CRYs were reported, resulting in diminished repression activity on CLOCK:BMAL1 transactivation(**Fig. S5**) The study identified CRY mutants that exhibited loss of function and attenuated repression activity, primarily governed by the interaction between the secondary pocket of CRYs and CLOCK. I subsequently pinpointed the following mutations in the modeled structures of CRYs: A217V/L218F, C259Y, E214K, and G288R in CRY1 alongside R293H. For CRY2; I selected A235T, E312K, and G230R mutations.

Mutations that are not in close proximity (within 4Å) of the serine loop (G43), to prevent direct interaction, are selected for further characterization. These mutant structures were then subjected to molecular dynamics simulations (MD) for a total of 2 μs (**Fig 4.6A**) In this study, I demonstrated that mutations, altering the repressor capacity of CRY1, selectively regulate the dynamicity of the serine loop. The serine loop in wild type CRY1

and CRY2 exhibited distinct levels of dynamic flexibility, as indicated by RMSF values consistent with a previous study (Fribourgh et al., 2020). I have identified specific dynamic properties of the serine loop that are crucial for the interaction between CLOCK and CRY1. Among these properties, the changes in interaction energies of S44 and S45 with neighboring amino acid residues in the serine loop determine the loop state in CRY1 (**Table 4.2**). I have found that these energies mainly arise from the formation of hydrogen bonds between E382 and S44/S45. As the hydrogen bond frequencies between these residues increase, the serine loop adopts a closed state in CRY1 systems due to a change in the correlated motion of residues (**Table 4.4**). Furthermore, in CRY1 mutants, the node degeneracy near the serine loop, where S44 and S45 are present in every subset of pathways between different source and sink residues in wild type CRY1, is reduced. However, the frequency of S44 and S45 in suboptimal pathways decreases in CRY1 mutants. Additionally, the frequency of F41 and A42 further increases in mutant suboptimal pathways. These changes suggested that the regulation of the serine loop is decreased in mutants compared to wild type, resulting in a change in the loop states in CRY1 but not in CRY2. I further examined the conformations of residues that were observed in the shortest pathways or involved in hydrogen bonds to probe the role of key amino acid residues and address how they model the serine loop of CRY1. In addition to changes in the node frequencies, some residues undergo conformational changes when mutations are introduced. For example, in the wild type, R256 extends towards the serine loop, whereas in C259Y, it is oriented away from the serine loop of CRY1 ($\chi 1 \sim 60$ vs -90). This alteration in sidechain orientation allows for the avoidance of steric clash with A42 in the closed state. Overall, the consistent presence of the same residues in suboptimal pathways and the consistent changes in the composition of these high-frequency nodes among various mutations suggest the presence of a preceding regulatory pathway. Finally, I discovered that the dynamics of E382 play a crucial role in regulating the serine loop in CRY1. The side chain orientation of E382 differed between the open and closed loop states (**Fig. 4.11D**). While the closed-state mutants favored a trans conformation in the $\chi 2$ dihedral angle, the open-state conformations favored a minus conformation. In fact, previous studies involving E382 and N393 have indicated the significance of these residues in CRY1 repression activity (Hirano, Shi, et al., 2016). The E382R/E383R double mutation was found to decrease the transcriptional repression activity by disrupting the negatively charged region

adjacent to the secondary pocket, despite increasing interaction with PER2 and decreasing interaction with FBXL3 in CRY1 (Czarna et al., 2013b). Similarly, the N393C and N393D mutants of CRY1 exhibited attenuated repression activity on CLOCK/BMAL1-driven transactivation (Hitomi et al., n.d.).

Cryptochromes play a pivotal role in orchestrating circadian rhythms. A multitude of studies highlights how disruptions in these rhythms, caused by single nucleotide variations in clock genes or circadian misalignment, are associated with various disorders, such as sleep and mood disorders (Baris et al., 2023b). Notably, two single nucleotide polymorphisms (SNPs) on CRY1 are associated with delayed sleep phase disorder (Patke et al., 2017) and attention deficit/hyperactivity disorder(Emre Onat et al., 2020a). Functional analyses of these SNPs have revealed that the deletion of exon 11 from the C-terminal end of CRY1 results in reduced affinity between CRY1 and CLOCK (Parico & Partch, 2020). In addition, a missense mutation in the human CRY2 gene was associated with familial advanced sleep phase disorder (Hirano, Shi, et al., 2016). This CRY2 variation (p.Ala260Thr) was expressed in mice, leading to a shortened circadian period when these animals were kept in constant darkness. Furthermore, I have showed a rare CRY1 SNP (p.Arg293His) to disrupt binding to CLOCK due to allosteric regulation of the secondary pocket (Gul et al., 2020).

Given the importance of SNPs on CRYs function, this paper provides mechanism insight on allosteric regulation of serine loop by the primary pocket in CRY1.

Although, discovering a new regulatory mechanism for yet to be shown be an allosteric protein is exciting; these findings bring another question. Primary pocket of CRYs is used as a target site for small molecule binding to regulate their half-life (S. Gul et al., 123 C.E.; Hirota, Lee, St. John, et al., 2012; Kavakli et al., 2022a; J. W. Lee et al., n.d.; Miller et al., 2020, 2022b; Oshima, Yamanaka, Kumar, Yamaguchi, Nishiwaki-Ohkawa, et al., 2015). Since allosteric regulation of serine loop and secondary pocket is possible; is it possible to regulate secondary pocket a small molecule? To test this hypothesis, I utilized known small moles are known to interacting with CRY1. Two different CRY stabilizer, KL001 and GO200, that have opposite effects on circadian period. However, both of them dampens circadian amplitude (Oshima, Yamanaka, Kumar, Yamaguchi, Nishiwaki-Ohkawa, et al., 2015). KL001 and GO200 docked into initial wild-type CRY1 homology and simulated for total of 700 ns (KL001 two independent replicates). I, then, analyzed the RSMF values of the

each system (**Fig. 4.13B**). Interestingly, KL001 decreased the fluctuation of serine loop while GO200 increased fluctuation of C-lid. Next, I calculated the secondary poket volumes and loop opening distances (**Fig. 4.13C, D**). Wild type Cry1 and CRY1-GO200 was similar to each other compared to CRY1-KL001. Interestingly, KL001 increased both secondary pocket volume and loop opening distance. So far, stabilized serine loops were resulted in close state loop conformation, hence, inaccessible secondary pocket. However, unlike mutations KL001 caused a stabilization at an open state serin loop without causing over-fluctuating serine loop as in G288R. Thus, allowed a constantly accessible secondary pocket which may affect the affinity between CRY1 and CLOCK. To test this hypothesis, I conducted co-IP of CLOCK with CRY1(**Fig 4.14**). Surprisingly, in presence of KL001 CLOCK affinity for CRY1 increased. These findings may change how we understand CYR1 stability affects CRY1 and CLOCK interaction as well as how it affects circadian phenotype and amplitude. However, as exciting as it is, it brings another question. Majority of small molecules that are targeting CRY1 as a matter of fact modulating CRYs half-life, which in turn modulates CRY1s role in other pathways such as gluconeogenesis. My findings add another layer of regulation to consider to already existing one. Even though an interaction partner of CRY1 can tolerate alterations on CRY1s stochiometric ratio, it may be susceptible to changes in serine loop and secondary pocket.

Multiple sequence alignment shows that CRYs have variable extended C-terminal domains that range from 30 to 300 amino acids depending on the species (Kavakli et al., 2017b; Partch et al., 2005). N-terminal domain exhibits high homology to photolyases and is called the photolyase homology region (PHR) domain. Even though photolyases have natural co-factor in their secondary pocket, mammalian CRYs doesn't have such cofactor(Cakilkaya et al., 2023). However, this increases likelihood of secondary pocket being a druggable site. There is yet to be a known small molecule that targets secondary pocket of CRYs. Considering all my previous findings and novelty of such candidate molecule, I decided to tackle this issue. To address this, I did a virtual screening study against secondary pocket of CRY1 using Ambinter's library. Approximately 7 million molecules filtered and 1.2 million of them docked in secondary pocket of CRY1 (**Fig 4.16D**). Out of molecules that have top 75 binding affinity, 43 of them was commercially available. After determining solubility, cytotoxicity of these molecules, effect of them on luciferase half-life 26 of them were ready

to assess their effect on circadian phenotype. U2OS cells that are harboring luciferase in control of *Bmal1* promoter (U2OS *Bmal1:dLuc*) used to monitor real-time bioluminescence(**APPENDIX D**). Interestingly, molecules exhibited 5 different phenotypes (**Fig 4.23, Table 4.8**). Five molecues, decreased amplitude and lengthen the period. 4 molecules increased amplitude and lengthen the period. Seven molecules increased amplitude without a dose dependent effect on period. One molecule slightly decreased the period without a dose dependent effect on amplitude. Six molecules lengthen the period without a dose dependent effect on amplitude. Three of them didn't have any effect on circadian period or amplitude which I expect to be non-interactors. Given the complexity of interactions between core clock proteins and to some degree contradictory findings in literature, I have yet to have concreate evidence to claim what will happen to circadian period when interaction between CRY1 and CLOCK altered. However, it is a question can be answered if physical interaction of these molecules with CRY1 pocket can be shown in upcoming experiments. Currently, previous studies consistent on that if amount CRYs increase, by stabilization or increased amount of expression, circadian amplitudes decrease. Another common agreement is if CRY1 lose function or lose their ability to bind CLOCK, average intensity of bioluminescence, which is not same with amplitude, increases. Therefore, amplitude enhancer small molecules here have higher likelihood of being an CRY1 antagonist by inhibiting interactions of secondary pocket. This can potentially solve all the aforementioned caveats of small molecules that target CRYs primary pocket. Which also can be tool to deeply understand underlying mechanism behind core clock protein interactions and how they affect circadian phenotype.

BIBLIOGRAPHY

Akashi, M., & Takumi, T. (2005). The orphan nuclear receptor RORα regulates circadian transcription of the mammalian core-clock Bmal1. *Nature Structural and Molecular Biology*, *12*(5), 441–448. https://doi.org/10.1038/NSMB925

Alabadí, D., Oyama, T., Yanovsky, M. J., Harmon, F. G., Más, P., & Kay, S. A. (2001). Reciprocal Regulation Between TOC1 and LHY/CCA1 Within the Arabidopsis Circadian Clock. *Science*, *293*(5531), 880–883. https://doi.org/10.1126/science.1061320

Allada, R., & Bass, J. (2021). Circadian Mechanisms in Medicine. *New England Journal of Medicine*, *384*(6), 550–561. https://doi.org/10.1056/NEJMRA1802337

Allada, R., White, N. E., So, W. V., Hall, J. C., & Rosbash, M. (1998). A Mutant Drosophila Homolog of Mammalian Clock Disrupts Circadian Rhythms and Transcription of period and timeless. *Cell*, *93*(5), 791–804. https://doi.org/10.1016/S0092-8674(00)81440-3

Allebrandt, K. V., Teder-Laving, M., Akyol, M., Pichler, I., Müller-Myhsok, B., Pramstaller, P., Merrow, M., Meitinger, T., Metspalu, A., & Roenneberg, T. (2010). CLOCK Gene Variants Associate with Sleep Duration in Two Independent Populations. *Biological Psychiatry*, *67*(11), 1040–1047. https://doi.org/10.1016/J.BIOPSYCH.2009.12.026

Amponsah, P. S., Yahya, G., Zimmermann, J., Mai, M., Mergel, S., Mühlhaus, T., Storchova, Z., & Morgan, B. (2021). Peroxiredoxins couple metabolism and cell division in an ultradian cycle. *NATuRe CheMiCAl BioloGY*, *17*. https://doi.org/10.1038/s41589-020-00728-9

Anafi, R. C., Lee, Y., Sato, T. K., Venkataraman, A., Ramanathan, C., Kavakli, I. H., Hughes, M. E., Baggs, J. E., Growe, J., Liu, A. C., Kim, J., & Hogenesch, J. B. (2014). Machine Learning Helps Identify CHRONO as a Circadian Clock Component. *PLoS Biology*, *12*(4). https://doi.org/10.1371/JOURNAL.PBIO.1001840

Astiz, M., Heyde, I., & Oster, H. (2019). Mechanisms of communication in the Mammalian Circadian timing system. *International Journal of Molecular Sciences*, *20*(2). https://doi.org/10.3390/IJMS20020343

Auton, A., Abecasis, G. R., Altshuler, D. M., Durbin, R. M., Bentley, D. R., Chakravarti, A., Clark, A. G., Donnelly, P., Eichler, E. E., Flicek, P., Gabriel, S. B., Gibbs, R. A., Green, E. D., Hurles, M. E., Knoppers, B. M., Korbel, J. O., Lander, E. S., Lee, C., Lehrach, H., … Schloss, J. A. (2015). A global reference for human genetic variation. *Nature*, *526*(7571), 68–74. https://doi.org/10.1038/NATURE15393

Baker, C. L., Loros, J. J., & Dunlap, J. C. (2012). The circadian clock of Neurospora crassa. *FEMS Microbiology Reviews*, *36*(1), 95–110. https://doi.org/10.1111/j.1574-6976.2011.00288.x

Baris, I., Ozcan, O., & Kavakli, I. H. (2023a). Single nucleotide polymorphisms (SNPs) in circadian genes: Impact on gene function and phenotype. *Advances in Protein Chemistry and Structural Biology*, *137*, 17–37. https://doi.org/10.1016/BS.APCSB.2023.03.002

Baris, I., Ozcan, O., & Kavakli, I. H. (2023b). Single nucleotide polymorphisms (SNPs) in circadian genes: Impact on gene function and phenotype. In *Advances in Protein Chemistry and Structural Biology*. Academic Press. https://doi.org/https://doi.org/10.1016/bs.apcsb.2023.03.002

Barnard, A. R., & Nolan, P. M. (2008). When clocks go bad: Neurobehavioural consequences of disrupted circadian timing. *PLoS Genetics*, *4*(5). https://doi.org/10.1371/JOURNAL.PGEN.1000040

Bass, J., & Lazar, M. A. (2016). Circadian time signatures of fitness and disease. *Science*, *354*(6315), 994–999. https://doi.org/10.1126/SCIENCE.AAH4965

Bass, J., & Takahashi, J. S. (2010). Circadian integration of metabolism and energetics. *Science*, *330*(6009), 1349–1354. https://doi.org/10.1126/SCIENCE.1195027

Belden, W. J., Loros, J. J., & Dunlap, J. C. (2007). Execution of the Circadian Negative Feedback Loop in Neurospora Requires the ATP-Dependent Chromatin-Remodeling Enzyme CLOCKSWITCH. *Molecular Cell*, *25*(4), 587–600. https://doi.org/10.1016/J.MOLCEL.2007.01.010

Benna, C., Helfrich-Förster, C., Rajendran, S., Monticelli, H., Pilati, P., Nitti, D., & Mocellin, S. (2017). Genetic variation of clock genes and cancer risk: A field synopsis and meta-analysis. *Oncotarget*, *8*(14), 23978–23995. https://doi.org/10.18632/ONCOTARGET.15074

Busino, L., Bassermann, F., Maiolica, A., Lee, C., Nolan, P. M., Godinho, S. I. H., Draetta, G. F., & Pagano, M. (2007). SCFFbxl3 controls the oscillation of the circadian clock by directing the degradation of cryptochrome proteins. *Science*, *316*(5826), 900–904. https://doi.org/10.1126/SCIENCE.1141194

Cakilkaya, B., Kavakli, I. H., & DeMirci, H. (2023). The crystal structure of Vibrio cholerae (6-4) photolyase reveals interactions with cofactors and a DNA-binding region. *Journal of Biological Chemistry*, *299*(1), 102794. https://doi.org/10.1016/J.JBC.2022.102794

Cal-Kayitmazbatir, S., Kulkoyluoglu-Cotul, E., Growe, J., Selby, C. P., Rhoades, S. D., Malik, D., Oner, H., Asimgil, H., Francey, L. J., Sancar, A., Kruger, W. D., Hogenesch, J. B., Weljie, A., Anafi, R. C., & Kavakli, I. H. (2021). CRY1-CBS binding regulates circadian clock function and metabolism. *FEBS Journal*, *288*(2), 614–639. https://doi.org/10.1111/febs.15360

Cao, X., Yang, Y., Selby, C. P., Liu, Z., & Sancar, A. (n.d.). *Molecular mechanism of the repressive phase of the mammalian circadian clock*. https://doi.org/10.1073/pnas.2021174118/-/DCSupplemental

Carlo, G., Parico, G., Perez, I., Fribourgh, J. L., Hernandez, B. N., Lee, H.-W., Partch, C. L., & Takahashi, J. S. (n.d.). *The human CRY1 tail controls circadian timing by regulating its association with CLOCK:BMAL1*. https://doi.org/10.1073/pnas.1920653117/-/DCSupplemental

Chan, A. B., Parico, G. C. G., Fribourgh, J. L., Ibrahim, L. H., Bollong, M. J., Partch, C. L., & Lamia, K. A. (2021). CRY2 missense mutations suppress P53 and enhance cell growth. *Proceedings of the National Academy of Sciences of the United States of America*, *118*(27). https://doi.org/10.1073/PNAS.2101416118

Charrier, A., Olliac, B., Roubertoux, P., & Tordjman, S. (2017). Clock genes and altered sleep–wake rhythms: Their role in the development of psychiatric disorders. *International Journal of Molecular Sciences*, *18*(5). https://doi.org/10.3390/IJMS18050938

Crosthwaite, S. K., Loros, J. J., & Dunlap, J. C. (1995). Light-induced resetting of a circadian clock is mediated by a rapid increase in frequency transcript. *Cell*, *81*(7), 1003–1012. https://doi.org/10.1016/S0092-8674(05)80005-4

Czarna, A., Berndt, A., Singh, H. R., Grudziecki, A., Ladurner, A. G., Timinszky, G., Kramer, A., & Wolf, E. (2013a). XStructures of drosophila cryptochrome and mouse cryptochrome1 provide insight into circadian function. *Cell*, *153*(6), 1394. https://doi.org/10.1016/j.cell.2013.05.011

Czarna, A., Berndt, A., Singh, H. R., Grudziecki, A., Ladurner, A. G., Timinszky, G., Kramer, A., & Wolf, E. (2013b). XStructures of drosophila cryptochrome and mouse cryptochrome1 provide insight into circadian function. *Cell*, *153*(6), 1394. https://doi.org/10.1016/j.cell.2013.05.011

Dashti, H. S., Smith, C. E., Lee, Y.-C., Parnell, L. D., Lai, C.-Q., Arnett, D. K., Ordovás, J. M., & Garaulet, M. (2014). CRY1 circadian gene variant interacts with carbohydrate intake for insulin resistance in two independent populations: Mediterranean and North American. *Chronobiology International*, *31*(5), 660–667. https://doi.org/10.3109/07420528.2014.886587

Dolinsky, T. J., Nielsen, J. E., Mccammon, J. A., & Baker, N. A. (n.d.). *PDB2PQR: an automated pipeline for the setup of Poisson-Boltzmann electrostatics calculations*. https://doi.org/10.1093/nar/gkh381

Dubowy, C., & Sehgal, A. (2017). Circadian Rhythms and Sleep in Drosophila melanogaster. *Genetics*, *205*(4), 1373–1397. https://doi.org/10.1534/genetics.115.185157

E, C. S., & S, G. S. (2015). Circadian Rhythms in Cyanobacteria. *Microbiology and Molecular Biology Reviews*, *79*(4), 373–385. https://doi.org/10.1128/mmbr.00036-15

Edgar, R. S., Green, E. W., Zhao, Y., van Ooijen, G., Olmedo, M., Qin, X., Xu, Y., Pan, M., Valekunja, U. K., Feeney, K. A., Maywood, E. S., Hastings, M. H., Baliga, N. S., Merrow, M., Millar, A. J., Johnson, C. H., Kyriacou, C. P., O, J. S., & Reddy, A. B. (2012). *Peroxiredoxins are conserved markers of circadian rhythms*. https://doi.org/10.1038/nature11088

Eide, E. J., Woolf, M. F., Kang, H., Woolf, P., Hurst, W., Camacho, F., Vielhaber, E. L., Giovanni, A., & Virshup, D. M. (2005). Control of Mammalian Circadian Rhythm by CKIε-Regulated Proteasome-Mediated PER2 Degradation. *Molecular and Cellular Biology*, *25*(7), 2795–2807. https://doi.org/10.1128/MCB.25.7.2795-2807.2005

Emery, P., So, W. V., Kaneko, M., Hall, J. C., & Rosbash, M. (1998). CRY, a Drosophila Clock and Light-Regulated Cryptochrome, Is a Major Contributor to Circadian Rhythm Resetting and Photosensitivity. *Cell*, *95*(5), 669–679. https://doi.org/10.1016/S0092-8674(00)81637-2

Emre Onat, O., Ece Kars, M., Gül, Ş., Bilguvar, K., Wu, Y., Özhan, A., Aydın, C., Nazlı Başak, A., Allegra Trusso, M., Goracci, A., Fallerini, C., Renieri, A., Casanova, J. L., Itan, Y., Atbaşoğlu, C. E., Saka, M. C., Halil Kavaklı, & Özçelik, T. (2020a). Human CRY1 variants associate with attention deficit/hyperactivity disorder. *Journal of Clinical Investigation*, *130*(7), 3885–3900. https://doi.org/10.1172/JCI135500

Emre Onat, O., Ece Kars, M., Gül, Ş., Bilguvar, K., Wu, Y., Özhan, A., Aydın, C., Nazlı Başak, A., Allegra Trusso, M., Goracci, A., Fallerini, C., Renieri, A., Casanova, J. L., Itan, Y., Atbaşoğlu, C. E., Saka, M. C., Halil Kavaklı, & Özçelik, T. (2020b). Human CRY1 variants associate with attention deficit/hyperactivity disorder. *Journal of Clinical Investigation*, *130*(7), 3885–3900. https://doi.org/10.1172/JCI135500

Emre Onat, O., Ece Kars, M., Gül, Ş., Bilguvar, K., Wu, Y., Özhan, A., Aydın, C., Nazlı Başak, A., Allegra Trusso, M., Goracci, A., Fallerini, C., Renieri, A., Casanova, J. L., Itan, Y., Atbaşoğlu, C. E., Saka, M. C., Halil Kavaklı, & Özçelik, T. (2020c). Human CRY1 variants associate with attention deficit/hyperactivity disorder. *Journal of Clinical Investigation*, *130*(7), 3885–3900. https://doi.org/10.1172/JCI135500

Fribourgh, J. L., Srivastava, A., Sandate, C. R., Michael, A. K., Hsu, P. L., Rakers, C., Nguyen, L. T., Torgrimson, M. R., Parico, G. C. G., Tripathi, S., Zheng, N., Lander, G. C., Hirota, T., Tama, F., & Partch, C. L. (2020). Dynamics at the serine loop underlie differential affinity of cryptochromes for CLOCK:BMAL1 to control circadian timing. *ELife*, *9*. https://doi.org/10.7554/eLife.55275

Fu, L., Pelicano, H., Liu, J., Huang, P., & Lee, C. C. (2002). The circadian gene Period2 plays an important role in tumor suppression and DNA damage response in vivo. *Cell*, *111*(1), 41–50. https://doi.org/10.1016/S0092-8674(02)00961-3

Gallego, M., & Virshup, D. M. (2007). Post-translational modifications regulate the ticking of the circadian clock. *Nature Reviews Molecular Cell Biology*, *8*(2), 139–148. https://doi.org/10.1038/NRM2106

Gekakis, N., Staknis, D., Nguyen, H. B., Davis, F. C., Wilsbacher, L. D., King, D. P., Takahashi, J. S., & Weitz, C. J. (1998). Role of the CLOCK Protein in the Mammalian Circadian Mechanism. *Science*, *280*(5369), 1564–1569. https://doi.org/10.1126/science.280.5369.1564

Godinho, S. I. H., Maywood, E. S., Shaw, L., Tucci, V., Barnard, A. R., Busino, L., Pagano, M., Kendall, R., Quwailid, M. M., Romero, M. R., O'Neill, J., Chesham, J. E., Brooker, D., Lalanne, Z., Hastings, M. H., & Nolan, P. M. (2007). The After-Hours Mutant Reveals a Role for Fbxl3 in Determining Mammalian Circadian Period. *Science*, *316*(5826), 897–900. https://doi.org/10.1126/science.1141138

Gul, H., Selvi, S., Yilmaz, F., Ozcelik, G., Olfaz-Aslan, S., Yazan, S., Tiryaki, B., Gul, S., Yurtseven, A., Kavakli, I. H., Ozlu, N., & Ozturk, N. (2022). Proteome analysis of the circadian clock protein PERIOD2. *Proteins: Structure, Function and Bioinformatics*, *90*(6), 1315–1330. https://doi.org/10.1002/PROT.26314

Gul, S., Akyel, Y. K., Gul, Z. M., Isin, S., Ozcan, O., Korkmaz, T., Selvi, S., Danis, I., Ipek, O. S., Aygenli, F., Taskin, A. C., Akarlar, B. A., Ozlu, N., Ozturk, N., Ozturk, N., Ünal, D. Ö., Guzel, M., Turkay, M., Okyar, A., & Kavakli, I. H. (2022a). Discovery of a small molecule that selectively destabilizes Cryptochrome 1 and enhances life span in p53 knockout mice. *Nature Communications*, *13*(1). https://doi.org/10.1038/S41467-022-34582-1

Gul, S., Akyel, Y. K., Gul, Z. M., Isin, S., Ozcan, O., Korkmaz, T., Selvi, S., Danis, I., Ipek, O. S., Aygenli, F., Taskin, A. C., Akarlar, B. A., Ozlu, N., Ozturk, N., Ozturk, N., Ünal, D. Ö., Guzel, M., Turkay, M., Okyar, A., & Kavakli, I. H. (2022b). Discovery of a small molecule that selectively destabilizes Cryptochrome 1 and enhances life span in p53 knockout mice. *Nature Communications*, *13*(1), 6742. https://doi.org/10.1038/s41467-022-34582-1

Gul, S., Aydin, C., Ozcan, O., Gurkan, B., Surme, S., Baris, I., & Kavakli, I. H. (2020). The Arg-293 of Cryptochrome1 is responsible for the allosteric regulation of CLOCK-CRY1 binding in circadian rhythm. *Journal of Biological Chemistry*, *295*(50), 17187–17199. https://doi.org/https://doi.org/10.1074/jbc.RA120.014333

Gul, S., Rahim, F., Isin, S., Yilmaz, F., Ozturk, N., Turkay, M., & Kavakli, I. H. (123 C.E.). Structure-based design and classifications of small molecules regulating the circadian

rhythm period. *Scientific Reports* |, *11*, 18510. https://doi.org/10.1038/s41598-021-97962-5

Gul, S., Rahim, F., Isin, S., Yilmaz, F., Ozturk, N., Turkay, M., & Kavakli, I. H. (2021). Structure-based design and classifications of small molecules regulating the circadian rhythm period. *Scientific Reports*, *11*(1). https://doi.org/10.1038/S41598-021-97962-5

HANDLER, A. M., & KONOPKA, R. J. (1979). Transplantation of a circadian pacemaker in Drosophila. *Nature*, *279*(5710), 236–238. https://doi.org/10.1038/279236a0

Haydon, M. J., Mielczarek, O., Robertson, F. C., Hubbard, K. E., & Webb, A. A. R. (2013). Photosynthetic entrainment of the Arabidopsis thaliana circadian clock. *Nature*. https://doi.org/10.1038/nature12603

He, Q., Cheng, P., Yang, Y., He, Q., Yu, H., & Liu, Y. (2003). FWD1‐mediated degradation of FREQUENCY in *Neurospora* establishes a conserved mechanism for circadian clock regulation. *The EMBO Journal*, *22*(17), 4421–4430. https://doi.org/https://doi.org/10.1093/emboj/cdg425

Heintzen, C., Loros, J. J., & Dunlap, J. C. (2001). The PAS Protein VIVID Defines a Clock-Associated Feedback Loop that Represses Light Input, Modulates Gating, and Regulates Clock Resetting. *Cell*, *104*(3), 453–464. https://doi.org/10.1016/S0092-8674(01)00232-X

Hirano, A., Fu, Y. H., & Ptáek, L. J. (2016). The intricate dance of post-translational modifications in the rhythm of life. *Nature Structural and Molecular Biology*, *23*(12), 1053–1060. https://doi.org/10.1038/NSMB.3326

Hirano, A., Shi, G., Jones, C. R., Lipzen, A., Pennacchio, L. A., Xu, Y., Hallows, W. C., Mcmahon, T., Yamazaki, M., Ptá, L. J., & Fu, Y.-H. (2016). *A Cryptochrome 2 mutation yields advanced sleep phase in humans*. https://doi.org/10.7554/eLife.16695.001

Hirano, A., Yumimoto, K., Tsunematsu, R., Matsumoto, M., Oyama, M., Kozuka-Hata, H., Nakagawa, T., Lanjakornsiripan, D., Nakayama, K. I., & Fukada, Y. (2013). FBXL21 regulates oscillation of the circadian clock through ubiquitination and stabilization of cryptochromes. *Cell*, *152*(5), 1106–1118. https://doi.org/10.1016/j.cell.2013.01.054

Hirota, T., Lee, J. W., st. John, P. C., Sawa, M., Iwaisako, K., Noguchi, T., Pongsawakul, P. Y., Sonntag, T., Welsh, D. K., Brenner, D. A., Doyle, F. J., Schultz, P. G., & Kay, S. A. (2012). Identification of small molecule activators of cryptochrome. *Science*, *337*(6098), 1094–1097. https://doi.org/10.1126/science.1223710

Hirota, T., Lee, J. W., St. John, P. C., Sawa, M., Iwaisako, K., Noguchi, T., Pongsawakul, P. Y., Sonntag, T., Welsh, D. K., Brenner, D. A., Doyle, F. J., Schultz, P. G., & Kay, S. A. (2012). Identification of small molecule activators of cryptochrome. *Science*, *337*(6098), 1094–1097. https://doi.org/10.1126/science.1223710

Hitomi, K., Ditacchio, L., Arvai, A. S., Yamamoto, J., Kim, S.-T., Todo, T., Tainer, J. A., Iwai, S., Panda, S., & Getzoff, E. D. (n.d.). *Functional motifs in the (6-4) photolyase crystal structure make a comparative framework for DNA repair photolyases and clock cryptochromes*. www.pnas.org/cgi/content/full/

Hoang, N., Yuen, R. K. C., Howe, J., Drmic, I., Ambrozewicz, P., Russell, C., Vorstman, J., Weiss, S. K., Anagnostou, E., Malow, B. A., & Scherer, S. W. (2021). Sleep phenotype of individuals with autism spectrum disorder bearing mutations in the PER2 circadian rhythm gene. *American Journal of Medical Genetics, Part A*, *185*(4), 1120–1130. https://doi.org/10.1002/AJMG.A.62086

Honma, S., Kawamoto, T., Takagi, Y., Fujimoto, K., Sato, F., Noshiro, M., Kato, Y., & Honma, K. I. (2002). Dec1 and Dec2 are regulators of the mammalian molecular clock. *Nature*, *419*(6909), 841–844. https://doi.org/10.1038/NATURE01123

Horst, G. T. J. van der, Muijtjens, M., Kobayashi, K., Takano, R., Kanno, S., Takao, M., Wit, J. de, Verkerk, A., Eker, A. P. M., Leenen, D. van, Buijs, R., Bootsma, D., Hoeijmakers, J. H. J., & Yasui, A. (1999a). Mammalian Cry1 and Cry2 are essential for maintenance of circadian rhythms. *Nature*, *398*(6728), 627–630. https://doi.org/10.1038/19323

Horst, G. T. J. van der, Muijtjens, M., Kobayashi, K., Takano, R., Kanno, S., Takao, M., Wit, J. de, Verkerk, A., Eker, A. P. M., Leenen, D. van, Buijs, R., Bootsma, D., Hoeijmakers, J. H. J., & Yasui, A. (1999b). Mammalian Cry1 and Cry2 are essential for maintenance of circadian rhythms. *Nature*, *398*(6728), 627–630. https://doi.org/10.1038/19323

Hua, P., Liu, W., Chen, D., Zhao, Y., Chen, L., Zhang, N., Wang, C., Guo, S., Wang, L., Xiao, H., & Kuo, S. H. (2014). Cry1 and Tef gene polymorphisms are associated with major depressive disorder in the Chinese population. *Journal of Affective Disorders*, *157*, 100–103. https://doi.org/10.1016/J.JAD.2013.11.019

Huang, J., Rauscher, S., Nawrocki, G., Ran, T., Feig, M., de Groot, B. L., Grubmüller, H., & MacKerell, A. D. (2017). CHARMM36m: an improved force field for folded and intrinsically disordered proteins. *Nature Methods*, *14*(1), 71–73. https://doi.org/10.1038/nmeth.4067

Ingram, K. K. (2020). Circadian rhythm sleep-wake disorders (CRSWDs): Linking circadian misalignment to adverse health outcomes. *EBioMedicine*, *62*. https://doi.org/10.1016/J.EBIOM.2020.103142

Iwasaki, H., Williams, S. B., Kitayama, Y., Ishiura, M., Golden, S. S., & Kondo, T. (2000). A KaiC-Interacting Sensory Histidine Kinase, SasA, Necessary to Sustain Robust Circadian Oscillation in Cyanobacteria. *Cell*, *101*(2), 223–233. https://doi.org/10.1016/S0092-8674(00)80832-6

Jagannath, A., Taylor, L., Wakaf, Z., Vasudevan, S. R., & Foster, R. G. (2017). The genetics of circadian rhythms, sleep and health. *Human Molecular Genetics*, *26*(R2), R128–R138. https://doi.org/10.1093/HMG/DDX240

Kaasik, K., Kivimäe, S., Allen, J. J., Chalkley, R. J., Huang, Y., Baer, K., Kissel, H., Burlingame, A. L., Shokat, K. M., Ptáček, L. J., & Fu, Y. H. (2013). Glucose sensor O-GlcNAcylation coordinates with phosphorylation to regulate circadian clock. *Cell Metabolism*, *17*(2), 291–302. https://doi.org/10.1016/J.CMET.2012.12.017

Karatsoreos, I. N. (2014). Links between circadian rhythms and psychiatric disease. *Frontiers in Behavioral Neuroscience*, *8*(MAY). https://doi.org/10.3389/FNBEH.2014.00162

Kavakli, I. H., Baris, I., Tardu, M., Gül, Ş., Öner, H., Çal, S., Bulut, S., Yarparvar, D., Berkel, Ç., Ustaoğlu, P., & Aydın, C. (2017a). The Photolyase/Cryptochrome Family of Proteins as DNA Repair Enzymes and Transcriptional Repressors. In *Photochemistry and Photobiology* (Vol. 93, Issue 1, pp. 93–103). Blackwell Publishing Inc. https://doi.org/10.1111/php.12669

Kavakli, I. H., Baris, I., Tardu, M., Gül, Ş., Öner, H., Çal, S., Bulut, S., Yarparvar, D., Berkel, Ç., Ustaoğlu, P., & Aydın, C. (2017b). The Photolyase/Cryptochrome Family of Proteins as DNA Repair Enzymes and Transcriptional Repressors. *Photochemistry and Photobiology*, *93*(1), 93–103. https://doi.org/https://doi.org/10.1111/php.12669

Kavakli, I. H., Gul, S., & Turkay, M. (2022a). Identification of novel small molecules targeting core clock proteins to regulate circadian rhythm. In *Current Opinion in Chemical Engineering* (Vol. 35). Elsevier Ltd. https://doi.org/10.1016/j.coche.2021.100730

Kavakli, I. H., Gul, S., & Turkay, M. (2022b). Identification of novel small molecules targeting core clock proteins to regulate circadian rhythm. In *Current Opinion in Chemical Engineering* (Vol. 35). Elsevier Ltd. https://doi.org/10.1016/j.coche.2021.100730

Kavakli, I. H., & Sancar, A. (2002). Circadian photoreception in humans and mice. *Molecular Interventions*, *2*(8), 484–492. https://doi.org/10.1124/MI.2.8.484

Kelly, M. A., Rees, S. D., Hydriem, Z. L., Shera, A. S., Bellary, S., O'Hare, J. P., Kumar, S., Taheri, S., Basit, A., & Barnett, A. H. (2012). Circadian gene variants and susceptibility to type 2 diabetes: A pilot study. *PLoS ONE*, *7*(4). https://doi.org/10.1371/JOURNAL.PONE.0032670

Kennaway, D. J., Owens, J. A., Voultsios, A., Boden, M. J., & Varcoe, T. J. (2007). Metabolic homeostasis in mice with disrupted Clock gene expression in peripheral tissues. *American Journal of Physiology - Regulatory Integrative and Comparative Physiology*, *293*(4). https://doi.org/10.1152/AJPREGU.00018.2007

Khan, S. K., Xu, H., Ukai-Tadenuma, M., Burton, B., Wang, Y., Ueda, H. R., & Liu, A. C. (2012a). Identification of a Novel Cryptochrome Differentiating Domain Required for Feedback Repression in Circadian Clock Function*. *Journal of Biological Chemistry*, *287*(31), 25917–25926. https://doi.org/https://doi.org/10.1074/jbc.M112.368001

Khan, S. K., Xu, H., Ukai-Tadenuma, M., Burton, B., Wang, Y., Ueda, H. R., & Liu, A. C. (2012b). Identification of a Novel Cryptochrome Differentiating Domain Required for Feedback Repression in Circadian Clock Function *. *Journal of Biological Chemistry*, *287*(31), 25917–25926. https://doi.org/10.1074/jbc.M112.368001

Kimiwada, T., Sakurai, M., Ohashi, H., Aoki, S., Tominaga, T., & Wada, K. (2009). Clock genes regulate neurogenic transcription factors, including NeuroD1, and the neuronal differentiation of adult neural stem/progenitor cells. *Neurochemistry International*, *54*(5–6), 277–285. https://doi.org/10.1016/J.NEUINT.2008.12.005

King, D. P., Zhao, Y., Sangoram, A. M., Wilsbacher, L. D., Tanaka, M., Antoch, M. P., Steeves, T. D. L., Vitaterna, M. H., Kornhauser, J. M., Lowrey, P. L., Turek, F. W., & Takahashi, J. S. (n.d.). *Positional Cloning of the Mouse Circadian Clock Gene*.

Kloss, B., Price, J. L., Saez, L., Blau, J., Rothenfluh, A., Wesley, C. S., & Young, M. W. (1998). The Drosophila Clock Gene double-time Encodes a Protein Closely Related to Human Casein Kinase Iε *Cell*, *94*(1), 97–107. https://doi.org/10.1016/S0092-8674(00)81225-8

Koike, N., Yoo, S. H., Huang, H. C., Kumar, V., Lee, C., Kim, T. K., & Takahashi, J. S. (2012a). Transcriptional architecture and chromatin landscape of the core circadian clock in mammals. *Science*, *338*(6105), 349–354. https://doi.org/10.1126/science.1226339

Koike, N., Yoo, S.-H., Huang, H.-C., Kumar, V., Lee, C., Kim, T.-K., & Takahashi, J. S. (2012b). Transcriptional Architecture and Chromatin Landscape of the Core Circadian Clock in Mammals. *Science*, *338*(6105), 349–354. https://doi.org/10.1126/science.1226339

Kolarski, D., Miller, S., Oshima, T., Nagai, Y., Aoki, Y., Kobauri, P., Srivastava, A., Sugiyama, A., Amaike, K., Sato, A., Tama, F., Szymanski, W., Feringa, B. L., Itami,

K., & Hirota, T. (2021). Photopharmacological Manipulation of Mammalian CRY1 for Regulation of the Circadian Clock. *Journal of the American Chemical Society*, *143*(4), 2078–2087. https://doi.org/10.1021/jacs.0c12280

Konopka, R. J., & Benzer, S. (1971). Clock Mutants of Drosophila melanogaster. *Proceedings of the National Academy of Sciences*, *68*(9), 2112–2116. https://doi.org/10.1073/pnas.68.9.2112

Kovanen, L., Donner, K., Kaunisto, M., & Partonen, T. (2015). CRY1, CRY2 and PRKCDBP genetic variants in metabolic syndrome. *Hypertension Research*, *38*, 186–192. https://doi.org/10.1038/hr.2014.157

Kovanen, L., Donner, K., Kaunisto, M., & Partonen, T. (2016). CRY1 and CRY2 genetic variants in seasonality: A longitudinal and cross-sectional study. *Psychiatry Research*, *242*, 101–110. https://doi.org/10.1016/J.PSYCHRES.2016.05.044

Kume, K., Zylka, M. J., Sriram, S., Shearman, L. P., Weaver, D. R., Jin, X., Maywood, E. S., Hastings, M. H., & Reppert, S. M. (1999). mCRY1 and mCRY2 Are Essential Components of the Negative Limb of the Circadian Clock Feedback Loop. *Cell*, *98*(2), 193–205. https://doi.org/https://doi.org/10.1016/S0092-8674(00)81014-4

Lane, J. M., Tare, A., Cade, B. E., Chen, T. H., Punjabi, N. M., Gottlieb, D. J., Scheer, F. A. J. L., Redline, S., & Saxena, R. (2013). Common variants in CLOCK are not associated with measures of sleep duration in people of European ancestry from the sleep heart health study. *Biological Psychiatry*, *74*(12). https://doi.org/10.1016/J.BIOPSYCH.2013.06.006

Lee, J. H., Gaddameedhi, S., Ozturk, N., Ye, R., & Sancar, A. (2013). DNA damage-specific control of cell death by cryptochrome in p53-mutant ras-transformed cells. *Cancer Research*, *73*(2), 785–791. https://doi.org/10.1158/0008-5472.CAN-12-1994

Lee, J. W., Ts Uyoshi Hirota,], Kumar, A., Kim, N.-J., Irle, S., & Kay, S. A. (n.d.). *Development of Small-Molecule Cryptochrome Stabilizer Derivatives as Modulators of the Circadian Clock*. https://doi.org/10.1002/cmdc.201500260:s

Lee, K., Loros, J. J., & Dunlap, J. C. (2000). Interconnected Feedback Loops in the Neurospora Circadian System. *Science*, *289*(5476), 107–110. https://doi.org/10.1126/science.289.5476.107

Lee, Y., Shen, Y., Francey, L. J., Ramanathan, C., Sehgal, A., Liu, A. C., & Hogenesch, J. B. (2019). The NRON complex controls circadian clock function through regulated PER and CRY nuclear translocation. *Scientific Reports*, *9*(1). https://doi.org/10.1038/s41598-019-48341-8

Li, Y., Xiong, W., & Zhang, E. E. (2016). The ratio of intracellular CRY proteins determines the clock period length. *Biochemical and Biophysical Research Communications*, *472*(3), 531–538. https://doi.org/10.1016/j.bbrc.2016.03.010

Lin, Y., Stormo, G. D., & Taghert, P. H. (2004). The Neuropeptide Pigment-Dispersing Factor Coordinates Pacemaker Interactions in the Drosophila Circadian System. *The Journal of Neuroscience*, *24*(36), 7951. https://doi.org/10.1523/JNEUROSCI.2370-04.2004

Liu, N., & Zhang, E. E. (2016). Phosphorylation regulating the ratio of intracellular CRY1 protein determines the circadian period. *Frontiers in Neurology*, *7*(SEP). https://doi.org/10.3389/fneur.2016.00159

Machicao, F., Peter, A., Machann, J., Konigsrainer, I., Bohm, A., Lutz, S. Z., Heni, M., Fritsche, A., Schick, F., Konigsrainer, A., Stefan, N., Haring, H. U., & Staiger, H. (2016). Glucose-raising polymorphisms in the human clock gene cryptochrome 2

(CRY2) affect hepatic lipid content. *PLoS ONE*, *11*(1). https://doi.org/10.1371/JOURNAL.PONE.0145563

Martinek, S., Inonog, S., Manoukian, A. S., & Young, M. W. (2001). A Role for the Segment Polarity Gene shaggy/GSK-3 in the Drosophila Circadian Clock. *Cell*, *105*(6), 769–779. https://doi.org/10.1016/S0092-8674(01)00383-X

McCarthy, E. V., Baggs, J. E., Geskes, J. M., Hogenesch, J. B., & Green, C. B. (2009). Generation of a Novel Allelic Series of Cryptochrome Mutants via Mutagenesis Reveals Residues Involved in Protein-Protein Interaction and CRY2-Specific Repression. *Molecular and Cellular Biology*, *29*(20), 5465–5476. https://doi.org/10.1128/mcb.00641-09

Michael, A. K., Fribourgh, J. L., Chelliah, Y., Sandate, C. R., Hura, G. L., Schneidman-Duhovny, D., Tripathi, S. M., Takahashi, J. S., & Partch, C. L. (2017). Formation of a repressive complex in the mammalian circadian clock is mediated by the secondary pocket of CRY1. *Proceedings of the National Academy of Sciences of the United States of America*, *114*(7), 1560–1565. https://doi.org/10.1073/pnas.1615310114

Mieda, M. (2019). The network mechanism of the central circadian pacemaker of the SCN: Do AVP neurons play a more critical role than expected? *Frontiers in Neuroscience*, *13*(FEB). https://doi.org/10.3389/FNINS.2019.00139

Miller, S., Aikawa, Y., Sugiyama, A., Nagai, Y., Hara, A., Oshima, T., Amaike, K., Kay, S. A., Itami, K., & Hirota, T. (2020). An Isoform-Selective Modulator of Cryptochrome 1 Regulates Circadian Rhythms in Mammals. *Cell Chemical Biology*, *27*(9), 1192-1198.e5. https://doi.org/10.1016/j.chembiol.2020.05.008

Miller, S., Kesherwani, M., Chan, P., Nagai, Y., Yagi, M., Cope, J., Tama, F., Kay, S. A., Hirota, T., & by Louis Pt cek, E. (2022a). *CRY2 isoform selectivity of a circadian clock modulator with antiglioblastoma efficacy*. https://doi.org/10.1073/pnas

Miller, S., Kesherwani, M., Chan, P., Nagai, Y., Yagi, M., Cope, J., Tama, F., Kay, S. A., Hirota, T., & by Louis Pt cek, E. (2022b). *CRY2 isoform selectivity of a circadian clock modulator with antiglioblastoma efficacy*. https://doi.org/10.1073/pnas

Miller, S., Srivastava, A., Nagai, Y., Aikawa, Y., Tama, F., & Hirota, T. (2021). *Structural differences in the FAD-binding pockets and lid loops of mammalian CRY1 and CRY2 for isoform-selective regulation*. *118*(26). https://doi.org/10.1073/pnas.2026191118/-/DCSupplemental

Mocellin, S., Tropea, S., Benna, C., & Rossi, C. R. (2018). Circadian pathway genetic variation and cancer risk: Evidence from genome-wide association studies. *BMC Medicine*, *16*(1). https://doi.org/10.1186/S12916-018-1010-1

Mohawk, J. A., Green, C. B., & Takahashi, J. S. (2012). Central and peripheral circadian clocks in mammals. *Annual Review of Neuroscience*, *35*, 445–462. https://doi.org/10.1146/ANNUREV-NEURO-060909-153128

Nakamichi, N., Kiba, T., Henriques, R., Mizuno, T., Chua, N.-H., & Sakakibara, H. (2010). PSEUDO-RESPONSE REGULATORS 9, 7, and 5 Are Transcriptional Repressors in the Arabidopsis Circadian Clock . *The Plant Cell*, *22*(3), 594–605. https://doi.org/10.1105/tpc.109.072892

Nangle, S. N., Rosensweig, C., Koike, N., Tei, H., Takahashi, J. S., Green, C. B., & Zheng, N. (2014). Molecular assembly of the period-cryptochrome circadian transcriptional repressor complex. *ELife*, *3*(August2014), 1–14. https://doi.org/10.7554/eLife.03674

Oakenfull, R. J., & Davis, S. J. (2017). Shining a light on the Arabidopsis circadian clock. *Plant, Cell & Environment*, *40*(11), 2571–2585. https://doi.org/https://doi.org/10.1111/pce.13033

Ode, K. L., Ukai, H., Susaki, E. A., Narumi, R., Matsumoto, K., Hara, J., Koide, N., Abe, T., Kanemaki, M. T., Kiyonari, H., & Ueda, H. R. (2017). Knockout-Rescue Embryonic Stem Cell-Derived Mouse Reveals Circadian-Period Control by Quality and Quantity of CRY1. *Molecular Cell*, *65*(1), 176–190. https://doi.org/10.1016/j.molcel.2016.11.022

O'Donnell, A. J., Prior, K. F., & Reece, S. E. (2020). Host circadian clocks do not set the schedule for the within-host replication of malaria parasites. *Proceedings of the Royal Society B: Biological Sciences*, *287*(1932), 20200347. https://doi.org/10.1098/rspb.2020.0347

Okamoto-Uchida, Y., Izawa, J., Nishimura, A., Hattori, A., Suzuki, N., & Hirayama, J. (2019). Post-translational Modifications are Required for Circadian Clock Regulation in Vertebrates. *Current Genomics*, *20*(5), 332–339. https://doi.org/10.2174/1389202919666191014094349

O'neill, J. S., & Reddy, A. B. (2011). Circadian clocks in human red blood cells. *Nature*. https://doi.org/10.1038/nature09702

O'neill, J. S., Van Ooijen, G., Dixon, L. E., Troein, C., Corellou, F., Bouget, F.-Y., Reddy, A. B., & Millar, A. J. (2011). Circadian rhythms persist without transcription in a eukaryote. *Nature*. https://doi.org/10.1038/nature09654

Oshima, T., Yamanaka, I., Kumar, A., Yamaguchi, J., Nishiwaki-Ohkawa, T., Muto, K., Kawamura, R., Hirota, T., Yagita, K., Irle, S., Kay, S. A., Yoshimura, T., & Itami, K. (2015). C□H Activation Generates Period-Shortening Molecules That Target Cryptochrome in the Mammalian Circadian Clock. *Angewandte Chemie*, *127*(24), 7299–7303. https://doi.org/10.1002/ange.201502942

Oshima, T., Yamanaka, I., Kumar, A., Yamaguchi, J., Nishiwaki-Ohkawa, T., Muto, K., Kawamura, R., Hirota, T., Yagita, K., Irle, S., Kay, S. A., Yoshimura, T., & Itami, K. (2015). C□H Activation Generates Period-Shortening Molecules That Target Cryptochrome in the Mammalian Circadian Clock. *Angewandte Chemie*, *127*(24), 7299–7303. https://doi.org/10.1002/ange.201502942

Ozber, N., Baris, I., Tatlici, G., Gur, I., Kilinc, S., Unal, E. B., & Kavakli, I. H. (2010). Identification of two Amino Acids in the C-terminal Domain of Mouse CRY2 Essential for PER2 Interaction. *BMC Molecular Biology*, *11*. https://doi.org/10.1186/1471-2199-11-69

Ozburn, A. R., Purohit, K., Parekh, P. K., Kaplan, G. N., Falcon, E., Mukherjee, S., Cates, H. M., & McClung, C. A. (2016). Functional implications of the CLOCK3111T/C single-nucleotide polymorphism. *Frontiers in Psychiatry*, *7*(APR). https://doi.org/10.3389/FPSYT.2016.00067

Ozcan, O., Gul, S., & Kavakli, I. H. (2021a). Allosteric Regulation of CRYs in Mammalian Circadian Clock. In M. Türkay & R. Gani (Eds.), *Computer Aided Chemical Engineering* (Vol. 50, pp. 2025–2031). Elsevier. https://doi.org/https://doi.org/10.1016/B978-0-323-88506-5.50313-2

Ozcan, O., Gul, S., & Kavakli, I. H. (2021b). Allosteric Regulation of CRYs in Mammalian Circadian Clock. In M. Türkay & R. Gani (Eds.), *Computer Aided Chemical Engineering* (Vol. 50, pp. 2025–2031). Elsevier. https://doi.org/https://doi.org/10.1016/B978-0-323-88506-5.50313-2

Ozdemir, E. S., Jang, H., Gursoy, A., Keskin, O., Li, Z., Sacks, D. B., & Nussinov, R. (2018). Unraveling the molecular mechanism of interactions of the Rho GTPases Cdc42 and Rac1 with the scaffolding protein IQGAP2. *Journal of Biological Chemistry*, *293*(10), 3685–3699. https://doi.org/10.1074/jbc.RA117.001596

Parico, G. C. G., & Partch, C. L. (2020). The tail of cryptochromes: an intrinsically disordered cog within the mammalian circadian clock. *Cell Communication and Signaling*, *18*(1). https://doi.org/10.1186/s12964-020-00665-z

Parlak, G. C., Camur, B. B., Gul, S., Ozcan, O., Baris, I., & Kavakli, I. H. (2022a). The secondary pocket of cryptochrome 2 is important for the regulation of its stability and localization. *Journal of Biological Chemistry*, *298*(9), 102334. https://doi.org/10.1016/j.jbc.2022.102334

Parlak, G. C., Camur, B. B., Gul, S., Ozcan, O., Baris, I., & Kavakli, I. H. (2022b). The secondary pocket of cryptochrome 2 is important for the regulation of its stability and localization. *Journal of Biological Chemistry*, *298*(9), 102334. https://doi.org/https://doi.org/10.1016/j.jbc.2022.102334

Partch, C. L., Clarkson, M. W., Özgür, S., Lee, A. L., & Sancar, A. (2005). Role of Structural Plasticity in Signal Transduction by the Cryptochrome Blue-Light Photoreceptor. *Biochemistry*, *44*(10), 3795–3805. https://doi.org/10.1021/bi047545g

Patke, A., Murphy, P. J., Onat, O. E., Krieger, A. C., Özçelik, T., Campbell, S. S., & Young, M. W. (2017). Mutation of the Human Circadian Clock Gene CRY1 in Familial Delayed Sleep Phase Disorder. *Cell*, *169*(2), 203-215.e13. https://doi.org/10.1016/j.cell.2017.03.027

Pellegrino, R., Kavakli, I. H., Goel, N., Cardinale, C. J., Dinges, D. F., Kuna, S. T., Maislin, G., Van Dongen, H. P. A., Tufik, S., Hogenesch, J. B., Hakonarson, H., & Pack, A. I. (2014). A novel BHLHE41 variant is associated with short sleep and resistance to sleep deprivation in humans. *Sleep*, *37*(8), 1327–1336. https://doi.org/10.5665/sleep.3924

Price, J. L., Blau, J., Rothenfluh, A., Abodeely, M., Kloss, B., & Young, M. W. (1998). double-time Is a Novel Drosophila Clock Gene that Regulates PERIOD Protein Accumulation. *Cell*, *94*(1), 83–95. https://doi.org/10.1016/S0092-8674(00)81224-6

Reischl, S., Vanselow, K., Westermark, P. O., Thierfelder, N., Maier, B., Herzel, H., & Kramer, A. (2007). β-TrCP1-mediated degradation of PERIOD2 is essential for circadian dynamics. *Journal of Biological Rhythms*, *22*(5), 375–386. https://doi.org/10.1177/0748730407303926

Richards, S., Aziz, N., Bale, S., Bick, D., Das, S., Gastier-Foster, J., Grody, W. W., Hegde, M., Lyon, E., Spector, E., Voelkerding, K., & Rehm, H. L. (2015). Standards and guidelines for the interpretation of sequence variants: a joint consensus recommendation of the American College of Medical Genetics and Genomics and the Association for Molecular Pathology. *Genetics in Medicine*, *17*(5), 405–424. https://doi.org/https://doi.org/10.1038/gim.2015.30

Rijo-Ferreira, F., & Takahashi, J. S. (2019). Genomics of circadian rhythms in health and disease. *Genome Medicine*, *11*(1). https://doi.org/10.1186/S13073-019-0704-0

Roenneberg, T., & Merrow, M. (2016). The Circadian Clock and Human Health. *Current Biology*, *26*(10), R432–R443. https://doi.org/10.1016/J.CUB.2016.04.011

Roenneberg, T., Wirz-Justice, A., & Merrow, M. (2003). Life between clocks: Daily temporal patterns of human chronotypes. *Journal of Biological Rhythms*, *18*(1), 80–90. https://doi.org/10.1177/0748730402239679

Rosensweig, C., & Green, C. B. (2020). Periodicity, repression, and the molecular architecture of the mammalian circadian clock. *European Journal of Neuroscience*, *51*(1), 139–165. https://doi.org/https://doi.org/10.1111/ejn.14254

Rosensweig, C., Reynolds, K. A., Gao, P., Laothamatas, I., Shan, Y., Ranganathan, R., Takahashi, J. S., & Green, C. B. (2018a). An evolutionary hotspot defines functional differences between CRYPTOCHROMES. *Nature Communications*, *9*(1). https://doi.org/10.1038/s41467-018-03503-6

Rosensweig, C., Reynolds, K. A., Gao, P., Laothamatas, I., Shan, Y., Ranganathan, R., Takahashi, J. S., & Green, C. B. (2018b). An evolutionary hotspot defines functional differences between CRYPTOCHROMES. *Nature Communications*, *9*(1). https://doi.org/10.1038/s41467-018-03503-6

Rudic, R. D., McNamara, P., Curtis, A. M., Boston, R. C., Panda, S., Hogenesch, J. B., & FitzGerald, G. A. (2004). BMAL1 and CLOCK, two essential components of the circadian clock, are involved in glucose homeostasis. *PLoS Biology*, *2*(11). https://doi.org/10.1371/JOURNAL.PBIO.0020377

Rutila, J. E., Suri, V., Le, M., So, W. V., Rosbash, M., & Hall, J. C. (1998). CYCLE Is a Second bHLH-PAS Clock Protein Essential for Circadian Rhythmicity and Transcription of Drosophila period and timeless. *Cell*, *93*(5), 805–814. https://doi.org/10.1016/S0092-8674(00)81441-5

Sancar, A. (2003). Structure and function of DNA photolyase and cryptochrome blue-light photoreceptors. *Chemical Reviews*, *103*(6), 2203–2237. https://doi.org/10.1021/CR0204348

Sato, T. K., Panda, S., Miraglia, L. J., Reyes, T. M., Rudic, R. D., McNamara, P., Naik, K. A., Fitzgerald, G. A., Kay, S. A., & Hogenesch, J. B. (2004). A functional genomics strategy reveals rora as a component of the mammalian circadian clock. *Neuron*, *43*(4), 527–537. https://doi.org/10.1016/J.NEURON.2004.07.018

Sato, T. K., Yamada, R. G., Ukai, H., Baggs, J. E., Miraglia, L. J., Kobayashi, T. J., Welsh, D. K., Kay, S. A., Ueda, H. R., & Hogenesch, J. B. (2006). Feedback repression is required for mammalian circadian clock function. *Nature Genetics*, *38*(3), 312–319. https://doi.org/10.1038/ng1745

Schibler, U., & Sassone-Corsi, P. (2002). A web of circadian pacemakers. *Cell*, *111*(7), 919–922. https://doi.org/10.1016/S0092-8674(02)01225-4

Schmalen, I., Reischl, S., Wallach, T., Klemz, R., Grudziecki, A., Prabu, J. R., Benda, C., Kramer, A., & Wolf, E. (2014). Interaction of circadian clock proteins CRY1 and PER2 is modulated by zinc binding and disulfide bond formation. *Cell*, *157*(5), 1203–1215. https://doi.org/10.1016/j.cell.2014.03.057

Schmitz, O., Katayama, M., Williams, S. B., Kondo, T., & Golden, S. S. (2000). CikA, a Bacteriophytochrome That Resets the Cyanobacterial Circadian Clock. *Science*, *289*(5480), 765–768. https://doi.org/10.1126/science.289.5480.765

Schuch, J. B., Genro, J. P., Bastos, C. R., Ghisleni, G., & Tovo-Rodrigues, L. (2018). The role of CLOCK gene in psychiatric disorders: Evidence from human and animal research. *American Journal of Medical Genetics, Part B: Neuropsychiatric Genetics*, *177*(2), 181–198. https://doi.org/10.1002/AJMG.B.32599

Schwarz, J. M., Cooper, D. N., Schuelke, M., & Seelow, D. (2014). MutationTaster2: mutation prediction for the deep-sequencing age. *Nature Methods*, *11*(4), 361–362. https://doi.org/10.1038/nmeth.2890

Sehgal, A., Price, J. L., Man, B., & Young, M. W. (1994). Loss of Circadian Behavioral Rhythms and per RNA Oscillations in the Drosophila Mutant timeless. *Science*, *263*(5153), 1603–1606. https://doi.org/10.1126/science.8128246

Soria, V., Martínez-Amoró, rika, rgia Escaramís, G., Valero, J., Pé rez-Egea, R., García, C., Gutié rrez-Zotes, A., Puigdemont, D., nica Bayé, M., Crespo, J. M., Martorell, L., Vilella, E., Labad, A., Vallejo, J., Pé rez, V., Menchó, J. M., Estivill, X., nica Gratacò, M., & Urretavizcaya, M. (2010). *Differential Association of Circadian Genes with Mood Disorders: CRY1 and NPAS2 are Associated with Unipolar Major Depression and CLOCK and VIP with Bipolar Disorder*. https://doi.org/10.1038/npp.2009.230

Staels, B. (2006). When the Clock stops ticking, metabolic syndrome explodes. *Nature Medicine*, *12*(1), 54–55. https://doi.org/10.1038/NM0106-54

Stanewsky, R., Kaneko, M., Emery, P., Beretta, B., Wager-Smith, K., Kay, S. A., Rosbash, M., & Hall, J. C. (1998). The cry^{b} Mutation Identifies Cryptochrome as a Circadian Photoreceptor in Drosophila. *Cell*, *95*(5), 681–692. https://doi.org/10.1016/S0092-8674(00)81638-4

Surme, S., Ergun, C., Gul, S., Akyel, Y. K., Gul, Z. M., Ozcan, O., Ipek, O. S., Akarlar, B. A., Ozlu, N., Taskin, A. C., Turkay, M., Gören, A. C., Baris, I., Ozturk, N., Guzel, M., Aydin, C., Okyar, A., & Kavakli, I. H. (2023). TW68, cryptochromes stabilizer, regulates fasting blood glucose levels in diabetic ob/ob and high fat-diet-induced obese mice. *Biochemical Pharmacology*, *218*, 115896. https://doi.org/https://doi.org/10.1016/j.bcp.2023.115896

Swan, J. A., Golden, S. S., LiWang, A., & Partch, C. L. (2018). Structure, function, and mechanism of the core circadian clock in cyanobacteria. *Journal of Biological Chemistry*, *293*(14), 5026–5034. https://doi.org/10.1074/jbc.TM117.001433

Takahashi, J. S. (2017). Transcriptional architecture of the mammalian circadian clock. In *Nature Reviews Genetics* (Vol. 18, Issue 3, pp. 164–179). Nature Publishing Group. https://doi.org/10.1038/nrg.2016.150

Takai, N., Nakajima, M., Oyama, T., Kito, R., Sugita, C., Sugita, M., Kondo, T., & Iwasaki, H. (2006). A KaiC-associating SasA–RpaA two-component regulatory system as a major circadian timing mediator in cyanobacteria. *Proceedings of the National Academy of Sciences*, *103*(32), 12109–12114. https://doi.org/10.1073/pnas.0602955103

Thresher, R. J., Vitaterna, M. H., Miyamoto, Y., Kazantsev, A., Hsu, D. S., Petit, C., Selby, C. P., Dawut, L., Smithies, O., Takahashi, J. S., & Sancar, A. (1998). Role of Mouse Cryptochrome Blue-Light Photoreceptor in Circadian Photoresponses. *Science*, *282*(5393), 1490–1494. https://doi.org/10.1126/science.282.5393.1490

Toh, K. L., Jones, C. R., He, Y., Eide, E. J., Hinz, W. A., Virshup, D. M., Ptáček, L. J., & Fu, Y. H. (2001). An hPer2 phosphorylation site mutation in familial advanced sleep phase syndrome. *Science*, *291*(5506), 1040–1043. https://doi.org/10.1126/SCIENCE.1057499

Turek, F. W., Joshu, C., Kohsaka, A., Lin, E., Ivanova, G., McDearmon, E., Laposky, A., Losee-Olson, S., Easton, A., Jensen, D. R., Eckel, R. H., Takahashi, J. S., & Bass, J. (2005). Obesity and metabolic syndrome in circadian Clock mutant nice. *Science*, *308*(5724), 1043–1045. https://doi.org/10.1126/SCIENCE.1108750

Ueda, H. R., Hayashi, S., Chen, W., Sano, M., Machida, M., Shigeyoshi, Y., Iino, M., & Hashimoto, S. (2005). System-level identification of transcriptional circuits underlying mammalian circadian clocks. *Nature Genetics*, *37*(2), 187–192. https://doi.org/10.1038/ng1504

Ukai-Tadenuma, M., Yamada, R. G., Xu, H., Ripperger, J. A., Liu, A. C., & Ueda, H. R. (2011). Delay in feedback repression by cryptochrome 1 Is required for circadian clock function. *Cell*, *144*(2), 268–281. https://doi.org/10.1016/J.CELL.2010.12.019

Valladares, M., Obregón, A. M., & Chaput, J. P. (2015). Association between genetic variants of the clock gene and obesity and sleep duration. *Journal of Physiology and Biochemistry*, *71*(4), 855–860. https://doi.org/10.1007/S13105-015-0447-3

Vanselow, J. T., & Kramer, A. (2010). Posttranslational regulation of circadian clocks. *Protein Reviews*, *12*, 79–104. https://doi.org/10.1007/978-1-4419-1262-6_3

Vanselow, K., Vanselow, J. T., Westermark, P. O., Reischl, S., Maier, B., Korte, T., Herrmann, A., Herzel, H., Schlosser, A., & Kramer, A. (2006). Differential effects of PER2 phosphorylation: Molecular basis for the human familial advanced sleep phase syndrome (FASPS). *Genes and Development*, *20*(19), 2660–2672. https://doi.org/10.1101/GAD.397006

Vitaterna, M. H., Selby, C. P., Todo, T., Niwa, H., Thompson, C., Fruechte, E. M., Hitomi, K., Thresher, R. J., Ishikawa, T., Miyazaki, J., Takahashi, J. S., & Sancar, A. (1999). Differential regulation of mammalian Period genes and circadian rhythmicity by cryptochromes 1 and 2. *Proceedings of the National Academy of Sciences*, *96*(21), 12114–12119. https://doi.org/10.1073/pnas.96.21.12114

Wang, H., Wang, S., Peng, J., Wang, Z., Lu, H., & Xu, J. (2012). Template-based protein structure modeling using the RaptorX web server. *Nature Protocols*. https://doi.org/10.1038/nprot.2012.085

Wang, M., Jiang, Y.-Y., Kim, K. M., Qu, G., Ji, H.-F., Mittenthal, J. E., Zhang, H.-Y., & Caetano-Anollés, G. (2010). *A Universal Molecular Clock of Protein Folds and Its Power in Tracing the Early History of Aerobic Metabolism and Planet Oxygenation*. https://doi.org/10.1093/molbev/msq232

Woon, P. Y., Kaisaki, P. J., Bragança, J., Bihoreau, M. T., Levy, J. C., Farrall, M., & Gauguier, D. (2007). Aryl hydrocarbon receptor nuclear translocator-like (BMAL1) is associated with susceptibility to hypertension and type 2 diabetes. *Proceedings of the National Academy of Sciences of the United States of America*, *104*(36), 14412–14417. https://doi.org/10.1073/PNAS.0703247104

Xing, W., Busino, L., Hinds, T. R., Marionni, S. T., Saifee, N. H., Bush, M. F., Pagano, M., & Zheng, N. (2013). SCF FBXL3 ubiquitin ligase targets cryptochromes at their cofactor pocket. *Nature*, *496*(7443), 64–68. https://doi.org/10.1038/nature11964

Xu, H., Gustafson, C. L., Sammons, P. J., Khan, S. K., Parsley, N. C., Ramanathan, C., Lee, H.-W., Liu, A. C., & Partch, C. L. (2015). Cryptochrome 1 regulates the circadian clock through dynamic interactions with the BMAL1 C terminus. *Nature Structural & Molecular Biology*, *22*(6), 476–484. https://doi.org/10.1038/nsmb.3018

Xu, Y., Toh, K. L., Jones, C. R., Shin, J. Y., Fu, Y. H., & Ptáček, L. J. (2007). Modeling of a Human Circadian Mutation Yields Insights into Clock Regulation by PER2. *Cell*, *128*(1), 59–70. https://doi.org/10.1016/J.CELL.2006.11.043

Yagi, M., Miller, S., Nagai, Y., Inuki, S., Sato, A., & Hirota, T. (2022). A methylbenzimidazole derivative regulates mammalian circadian rhythms by targeting

Cryptochrome proteins. *F1000Research*, *11*, 1016. https://doi.org/10.12688/f1000research.124658.1

Yagita, K., Yamaguchi, S., Tamanini, F., van der Horst, G. T. J., Hoeijmakers, J. H. J., Yasui, A., Loros, J. J., Dunlap, J. C., & Okamura, H. (2000). Dimerization and nuclear entry of mPER proteins in mammalian cells. *Genes & Development*, *14*(11), 1353–1363. https://doi.org/10.1101/gad.14.11.1353

Ye, R., Selby, C. P., Chiou, Y. Y., Ozkan-Dagliyan, I., Gaddameedhi, S., & Sancar, A. (2014). Dual modes of CLOCK:BMAL1 inhibition mediated by Cryptochrome and period proteins in the mammalian circadian clock. *Genes and Development*, *28*(18), 1989–1998. https://doi.org/10.1101/GAD.249417.114

Ye, Y., Xiang, Y., Ozguc, F. M., Kim, Y., Liu, C. J., Park, P. K., Hu, Q., Diao, L., Lou, Y., Lin, C., Guo, A. Y., Zhou, B., Wang, L., Chen, Z., Takahashi, J. S., Mills, G. B., Yoo, S. H., & Han, L. (2018). The Genomic Landscape and Pharmacogenomic Interactions of Clock Genes in Cancer Chronotherapy. *Cell Systems*, *6*(3), 314-328.e2. https://doi.org/10.1016/J.CELS.2018.01.013

Yoo, S. H., Mohawk, J. A., Siepka, S. M., Shan, Y., Huh, S. K., Hong, H. K., Kornblum, I., Kumar, V., Koike, N., Xu, M., Nussbaum, J., Liu, X., Chen, Z., Chen, Z. J., Green, C. B., & Takahashi, J. S. (2013). Competing E3 ubiquitin ligases govern circadian periodicity by degradation of CRY in nucleus and cytoplasm. *Cell*, *152*(5), 1091–1105. https://doi.org/10.1016/j.cell.2013.01.055

Zerbino, D. R., Achuthan, P., Akanni, W., Amode, M. R., Barrell, D., Bhai, J., Billis, K., Cummins, C., Gall, A., Girón, C. G., Gil, L., Gordon, L., Haggerty, L., Haskell, E., Hourlier, T., Izuogu, O. G., Janacek, S. H., Juettemann, T., To, J. K., … Flicek, P. (2018). Ensembl 2018. *Nucleic Acids Research*, *46*(D1), D754–D761. https://doi.org/10.1093/nar/gkx1098

Zhang, E. E., Liu, Y., Dentin, R., Pongsawakul, P. Y., Liu, A. C., Hirota, T., Nusinow, D. A., Sun, X., Landais, S., Kodama, Y., Brenner, D. A., Montminy, M., & Kay, S. A. (2010). Cryptochrome mediates circadian regulation of cAMP signaling and hepatic gluconeogenesis. *Nature Medicine*, *16*(10), 1152–1156. https://doi.org/10.1038/nm.2214

APPENDICES

Appendix A. Adepted Figures

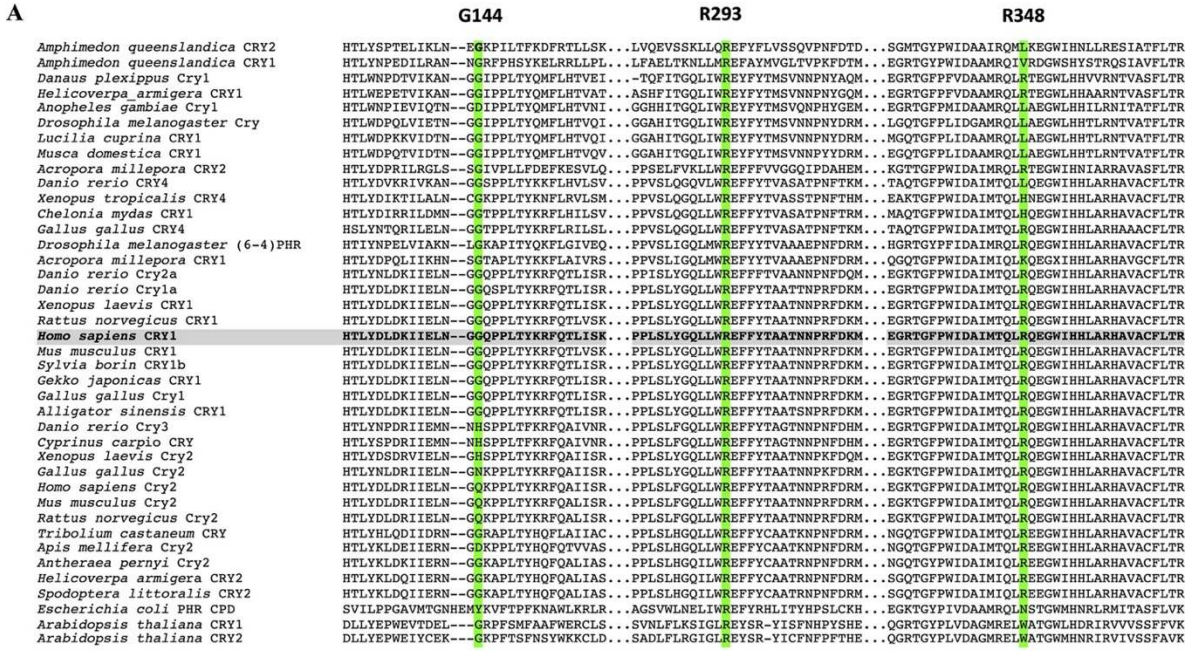

Supplementary Figure 1. Three rare SNPs affect highly conserved amino acid residues in CRY1. The figure is adapted from (S. Gul et al., 2020). A) alignments of selected each class of the cryptochrome/photolyase family proteins from the phylogenetic tree recently constructed by Kavakli et al. (66). Human CRY1 was indicated highlighted in gray color and in bold. Protein accession number organisms are as follows: Amphimedon queenslandica CRY1 (accession number: XP_003386582.1), Danaus plexippus Cry1 (accession num- ber: AAX58599.1), Helicoverpa armigera CRY1 (accession number: XP_021184243.1), Anopheles gambiae CRY1 (accession number: NP_034093), Drosophila melanogaster Cry (accession number: BAA05042.1), Lucilia cuprina CRY1 (accession number: XP_023306440.1), Musca domestica CRY1 (accession number: XP_005178207), Drosophila melanogaster (6-4)PHR (accession number: NP_001260633.1), Acropora millepora CRY1 (accession number: ABP97098.1), Danio rerio Cry1a (accession number: BAA96846.1), Xenopus laevis CRY1 (accession number: NP_001081129.1), Rattus norvegicus CRY1 (accession number: NP_942045.2), Homosapiens CRY1 (accession number: NP_004066.1 3), Mus musculus CRY1 (accession number: NP_031797.1), Sylvia

borin CRY1b (accession number: ABH03083.1), Gekko japonicas CRY1 (accession number: XP_015283074.1), Gallus gallus Cry1 (accession number: NP_989576.1), Alligator sinensis CRY1 (accession number: XP_006024339.1), Tribolium castaneum CRY (accession number: NP_001076794.1), Escherichia coli PHR CPD (accession number: WP_032176081.1), Arabidopsis thaliana CRY1 (accession number: NP_567341.1), and Solanum lycopersicum CRY1 (accession number: AAF72555.1).

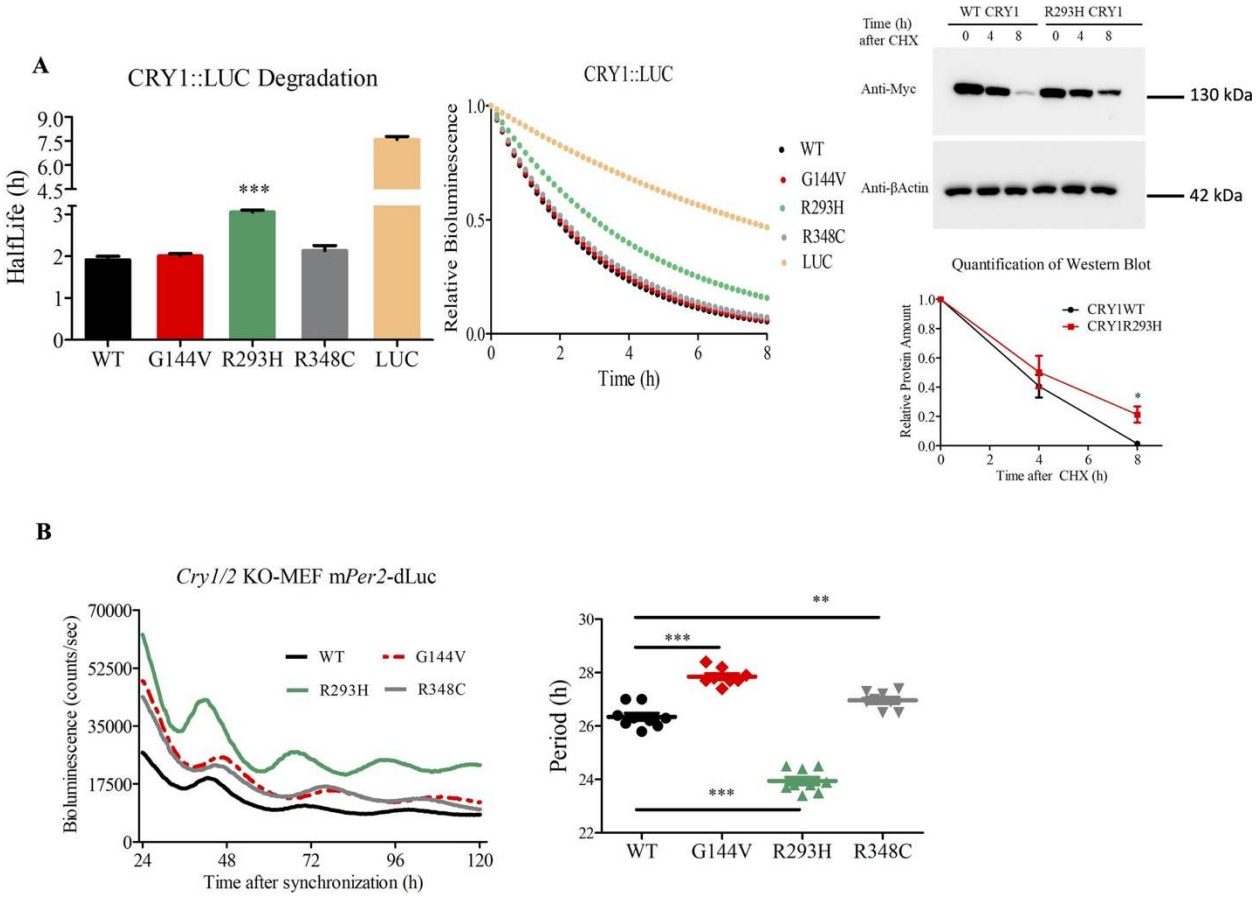

Supplementary Figure 2. t1/2 and rescue analysis of the WT and CRY1 variants. The figure is adapted from (S. Gul et al., 2020). A, the half-lives of WT and variant CRY1 were determined by monitoring CRY1::LUC degradation. Half-lives were calculated using a one-phase exponential decay function. Average t1/2 values 6 S.E. from three independent experiments (with quadruplicate samples) relative to WT CRY1::LUC were reported. Statistical significance was determined as in (B) (G144V, p = 0.427; R293H, p = 0.013;

R348C, p = 0.227). Statistical analysis for Western blot was performed with student's t-test *, (p , 0.0297). B, WT or variant CRY rescued circadian rhythms in Cry12/2Cry22/2 MEF cells with varying effects on period and amplitude. DKO MEF cells transiently transfected with pGL3-Per2-dLuc and Cry rescue plasmids (WT or variant). After 72 h, cells were synchronized with dexamethasone (0.1 mM) and luminescence values were recorded for 5 days. CRY1 rhythm was representative bioluminescence of four independent experiments with eight plates. The circadian period from all plates were determined. Statistical analysis was per- formed using an unpaired t test with a Welch’s correction (***, p , 0.0001; **, p , 0.005; *, p , 0.05; G144V, p , 0.0001; R293H, p , 0.0001; R348C, p , 0.0044).

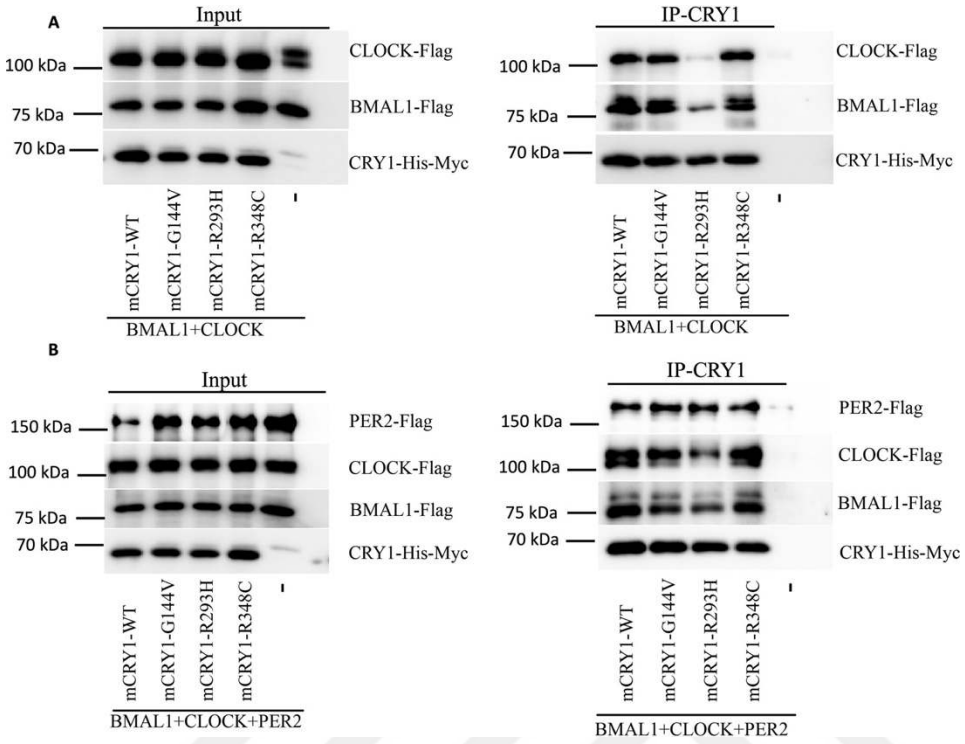

Supplementary Figure 3. Pulldown analysis. The figure is adapted from (S. Gul et al., 2020). A and B, physical interaction between WT/p.Arg293His CRY1variant with (A) BMAL1/CLOCK and (B) BMAL1/CLOCK/PER2. HEK293T cells were transfected with plasmids expressing Bmal1-FLAG, CLOCK-FLAG, and WT or variant Cry1-His-Myc. Proteins were isolated with a Ni-NTA aga- rose resin and analyzed by Western blotting. The blot shown is representative of three independent experiments. Multiple bands in BMAL1 and CLOCK are a result of posttranslational modifications. Results are shown here are representations of three independent experiments.

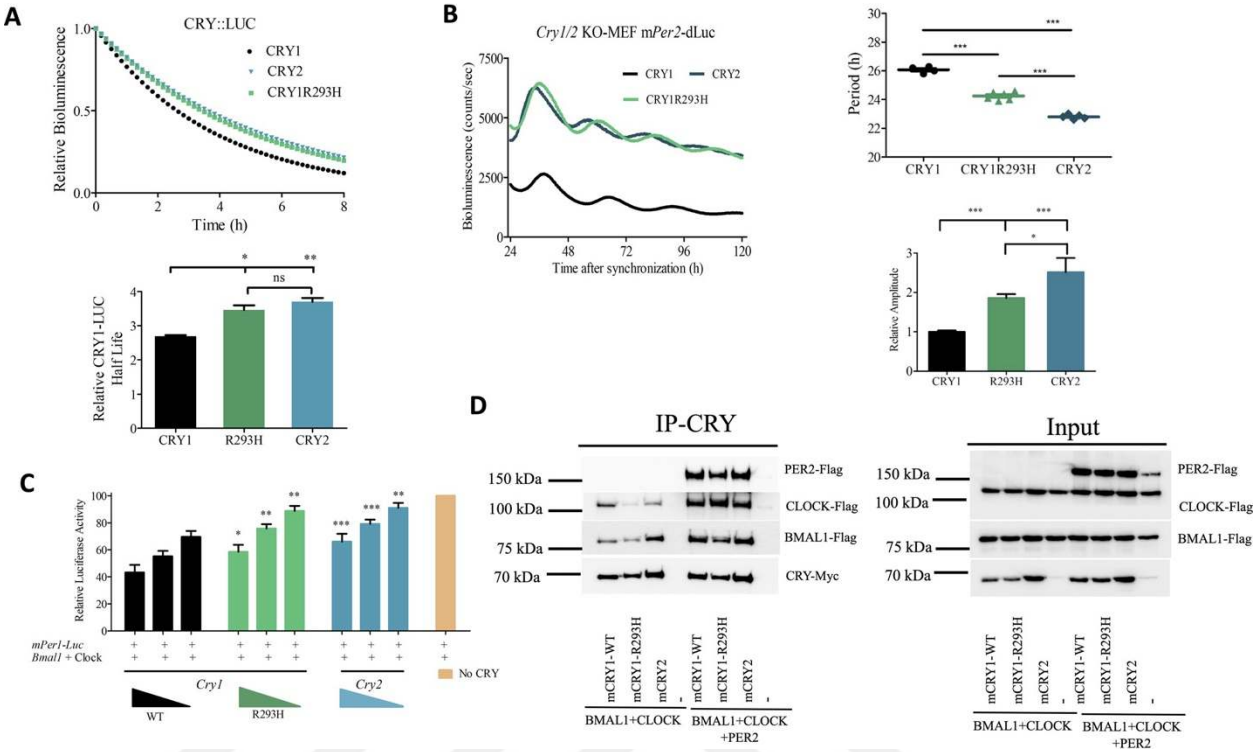

Supplementary Figure 4. Comparison of protein t1/2 and analysis of rescue of CRY1 and CRY2. The figure is adapted from (S. Gul et al., 2020). A, The half-lives of WT, R293H CRY1, and CRY2 were determined as in Fig. 2. Average t1/2 values 6 S.E. from three independent experiments (with triplicate samples) relative to WT CRY1::dLUC were reported (left panel). Statistical anal- ysis was performed using an unpaired t test with a Welch's correction (***, p , 0.0001; **, p , 0.005; *, p , 0.05; WT CRY1 versus R293H, p = 0.0226; WT CRY1 versus CRY2, p = 0.0034; R293H CRY1 versus CRY2, p = 0.4854). Degradation of WT CRY1 and R293H CRY1 was analyzed by immunoblot using anti-Myc for CRYs and anti-b-actin for loading controls (right panel). Degradation of LUC was compared with WT and R293H CRY1::LUC. B, pArg293His CRY1 and CRY2 rescued the rhythm similarly, although periods are still significantly different. Rescue assays were performed as described in Fig. 3. Representative rhythms of three in- dependent experiments are shown. Periods and amplitudes of all plates were reported (4-WT, 6-R293H CRY1, and 6-CRY2). Significance analysis was per- formed using unpaired t test with Welch's correction (***, p , 0.0001; **, p , 0.005; *, p , 0.05; WT CRY1 versus R293H, p , 0.0001; WT CRY1 versus CRY2, p , 0.0001; R293H CRY1 versus CRY2, p , 0.0001). C, repression

analysis. Cry12/2Cry22/2 MEF cells were transfected with plasmids encoding Bmal1 (50 ng), Clock (125 ng), and different amounts of WT Cry1, Cry2, and Cry1R293H, along with the pGL3-mPer1:luc (50 ng) reporter plasmid and pRLTK Renilla (4 ng) as a transfection control. Comparisons were made between WT CRY1 and CRY1R293H and WT CRY1 and CRY2 (***, p , 0.0001; **, p , 0.005; *, p , 0.05). D, pulldown analysis of WT or pArg293His CRY1, CRY2 with BMAL1, CLOCK, and PER2. HEK293T cells were transfected with plasmids expressing Bmal1-FLAG, CLOCK-FLAG, and Cry-His-Myc. Proteins were pull downed with Ni-NTA agarose resin and analyzed with Western blotting. This blot is the representation of three independent experiments.

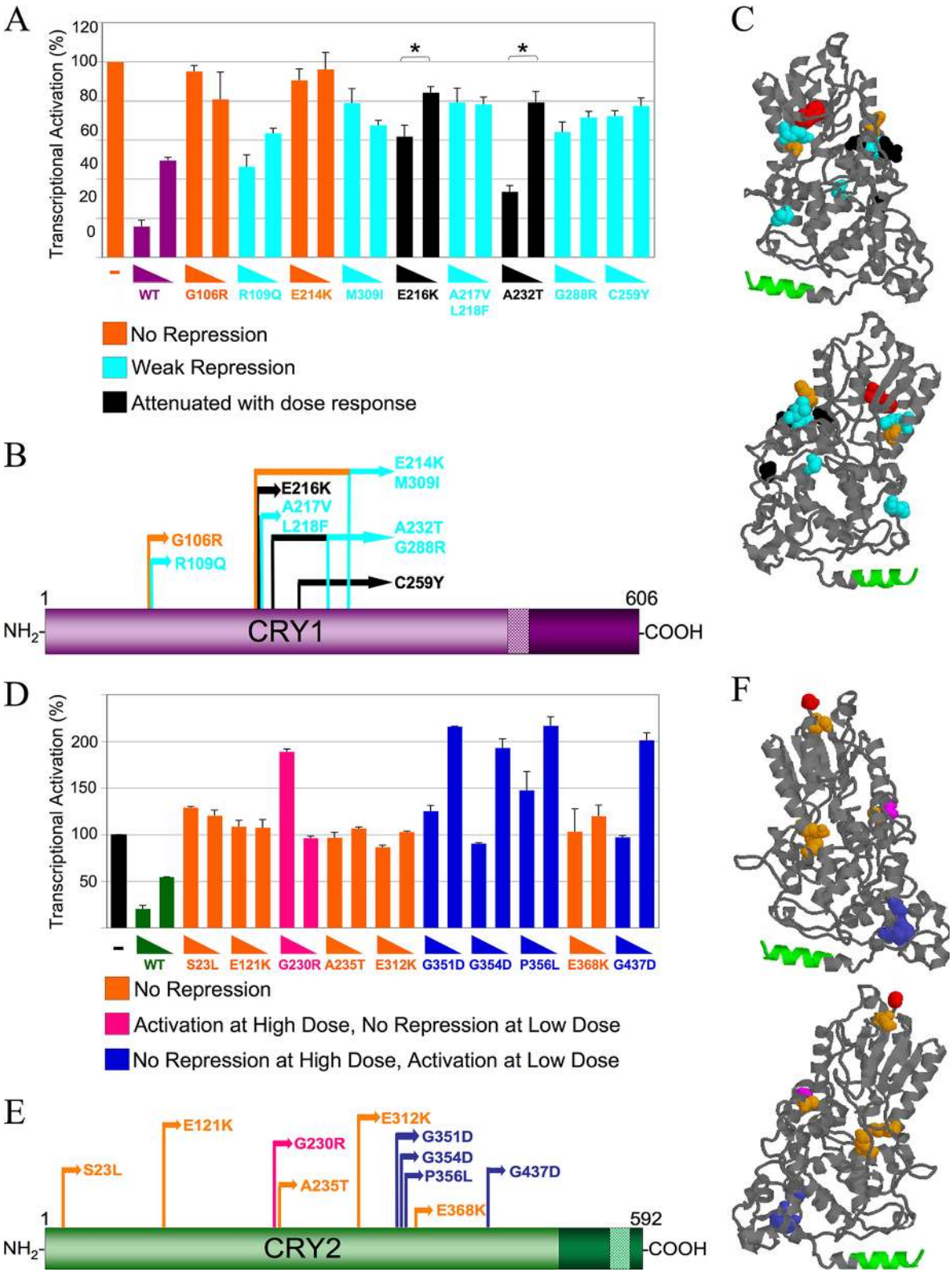
A
Transcriptional Activation (%)
120
100
80
60
40
20
0
*
*
-
WT
G106R
R109Q
E214K
M309I
E216K
A217V
L218F
A232T
G288R
C259Y
No Repression
Weak Repression
Attenuated with dose response
B
E214K
M309I
E216K
A217V
L218F
A232T
G288R
G106R
R109Q
C259Y
1
606
NH2-
CRY1
-COOH
C
D
Transcriptional Activation (%)
200
150
100
50
-
WT
S23L
E121K
G230R
A235T
E312K
G351D
G354D
P356L
E368K
G437D
No Repression
Activation at High Dose, No Repression at Low Dose
No Repression at High Dose, Activation at Low Dose
E
S23L
E121K
G230R
A235T
E312K
G351D
G354D
P356L
G437D
E368K
1
592
NH2-
CRY2
-COOH
F

Supplementary Figure 5. Some CRY mutants display loss of repression dose-response profiles, while some CRY2 mutants cause increases in CLOCK-BMAL1- mediated transcription. The figure is adapted from (McCarthy et al., 2009) (A) CRY1 dose-response assay. HEK293 cells were transfected with Per2-luciferase reporter, Clock, Bmal1, and 25 or 5 ng of either mutant or wild-type (WT) Cry1-Renilla Luciferase. Each data point is averaged from results of three to six replicates, with the error bars representing the standard errors of the means (SEM). The mutants exhibited three general dose-response profiles: no repression, weak repression, and attenuated repression with a significant dose response (P 0.01). (B) Schematic of CRY1 mutants' primary structure. The domains are indicated as described in the legend of Fig. 1. Each mutant's profile is color coded (see the key for panel A). (C) Homology model of the CRY1 PHR. This model was generated using the SWISS-MODEL protein homology-modeling server (10; http://swissmodel.expasy.org/workspace/) based on the structure of A. nidulans photolyase (Protein Data Bank code 1OWL) (11) and visualized using Protein Explorer (14). The N-terminal-most residue (red) and the coiled-coil domain (green) are shown. The mutations are color coded by repression profile (see the key in panel A). (D) CRY2 dose-response assay. This experiment was performed as described for panel A, except that 150 or 20 ng of either mutant or wild-type Cry2-GFP was used. The mutants exhibited three different dose-response profiles: no repression, no repression at the low dose with activation at a high dose, and no repression at the high dose with activation at a low dose. (E) Schematic of CRY2 protein with mutant profiles indicated. (F) CRY2 3D homology model with mutant repression profiles. This model was generated as described for panel C but using the CRY2 sequence. The mutant residues are color coded as described in panel D.

Appendix B. Ambinter IDs, binding energies, structure and interacting residues of top ranked small molecules

Table S1

Ambinter ID	Score Kcal/mol	Structure	Interacting Residues
Amb576480	-10.2	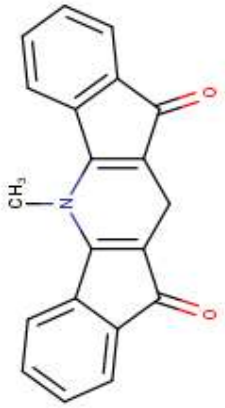	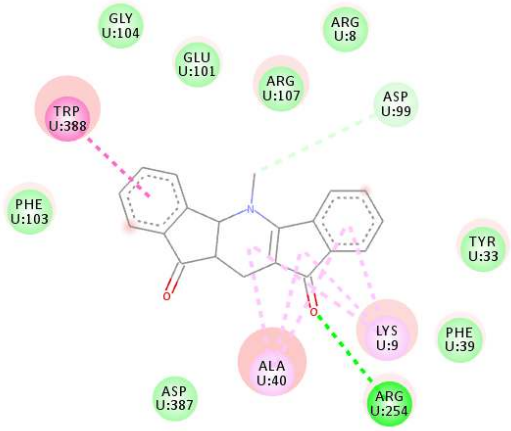
Amb19400263	-10.2	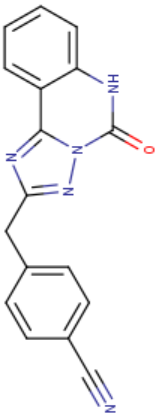	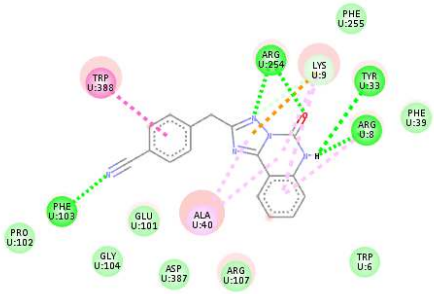

Amb6601020	-10.1	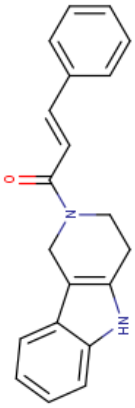	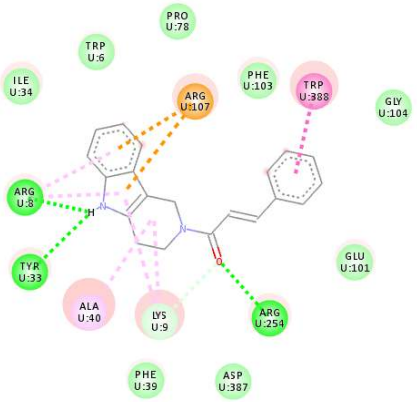
Amb9129122	-10	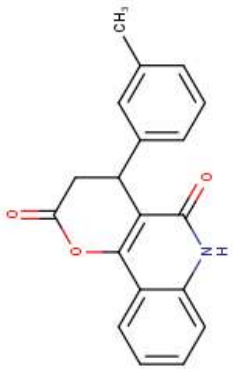	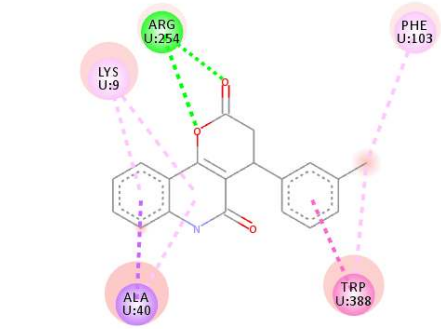
Amb33827062	-10	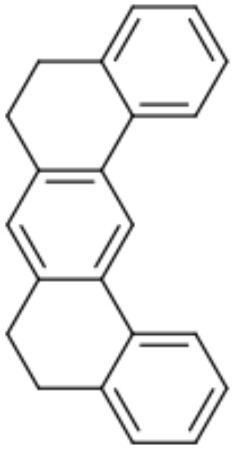	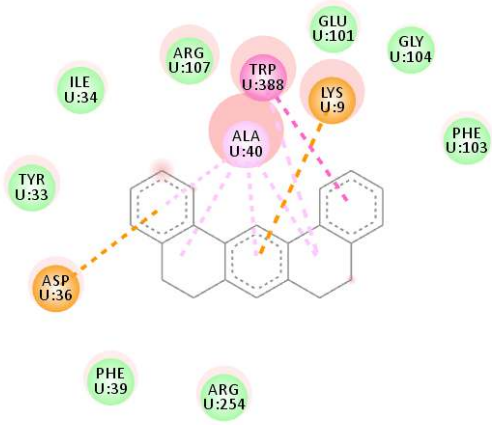

Amb240135	-10	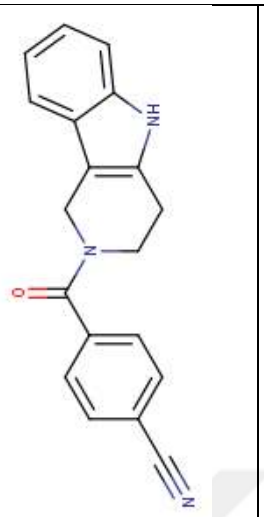	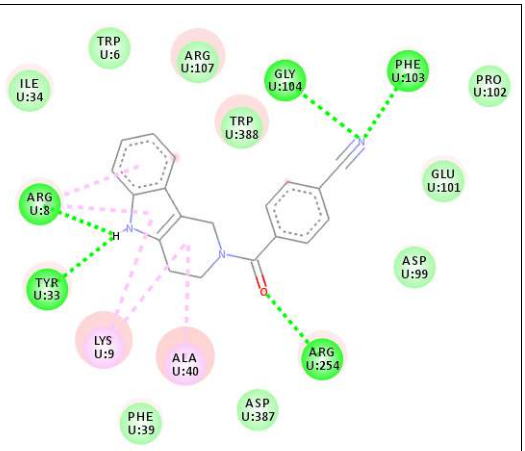
Amb6323295	-9.9	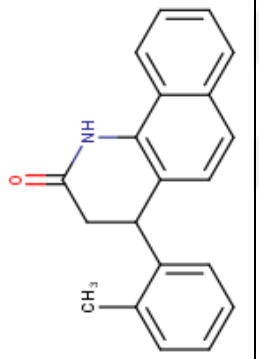	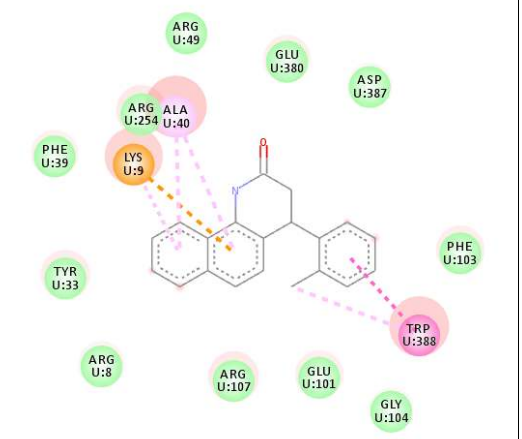
Amb2239008	-9.9	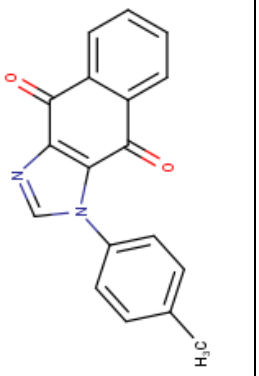	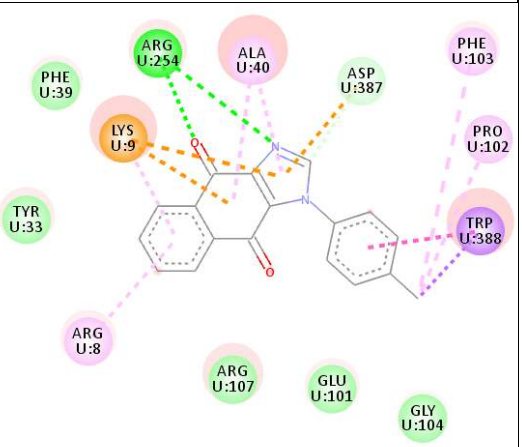

Amb20466614	-9.9	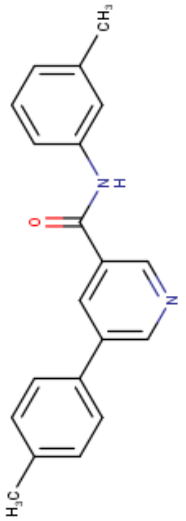	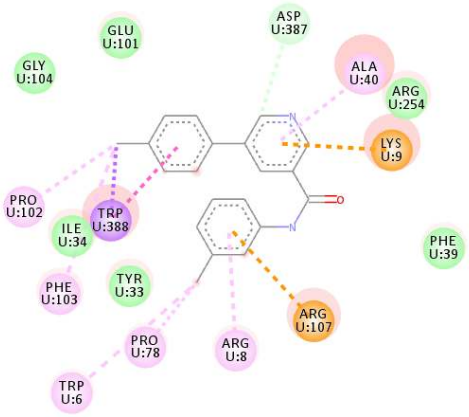
Amb21990000	-9.9	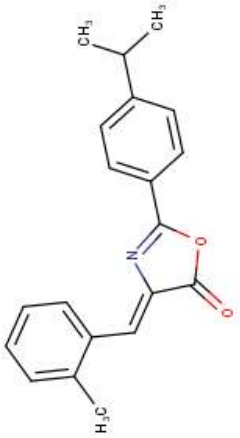	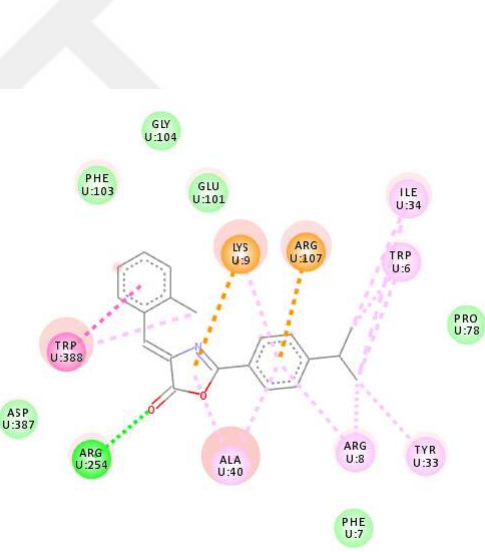
Amb318014	-9.9	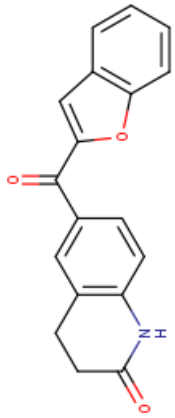	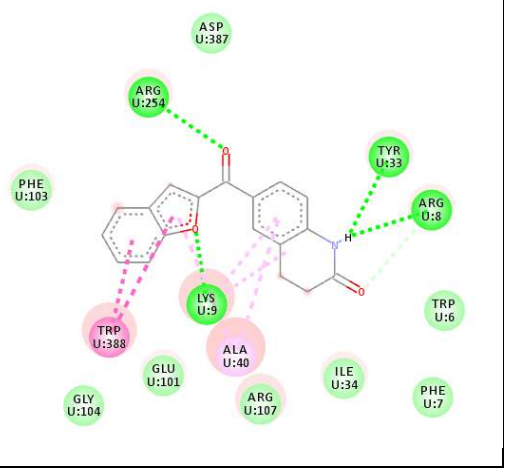

Amb33826633	-9.9	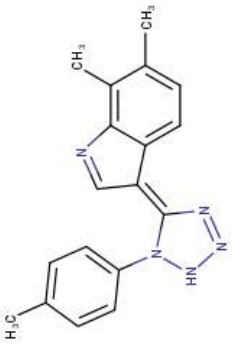	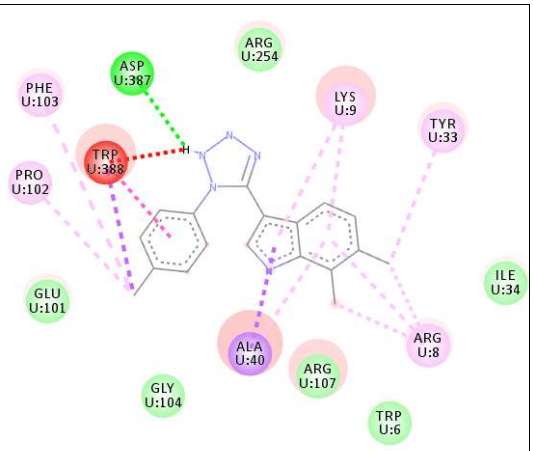
Amb16710891	-9.9	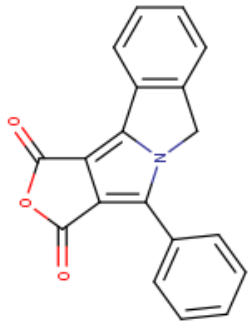	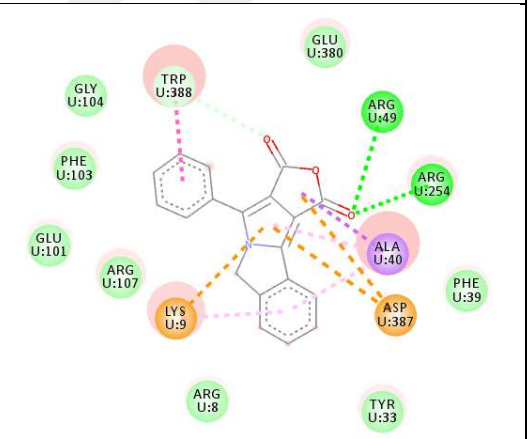
Amb16754394	-9.9	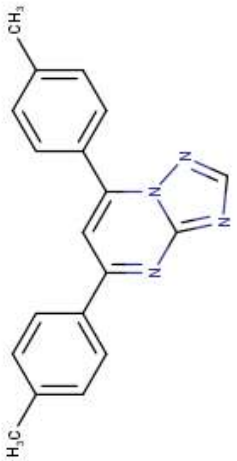	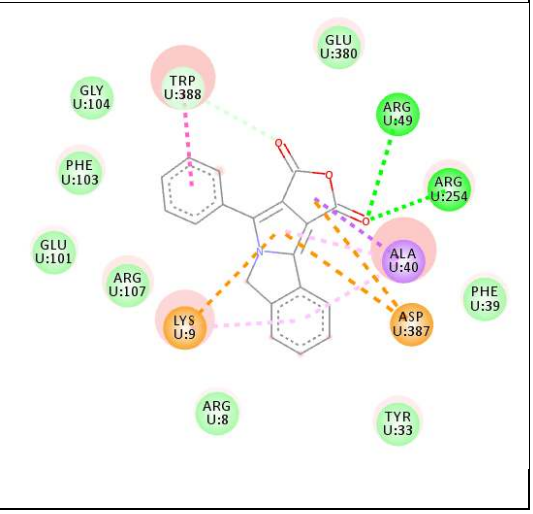

Amb20426308	-9.9	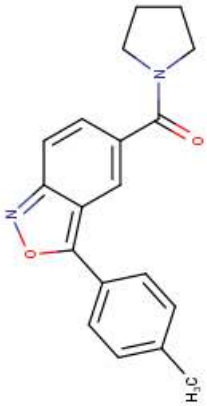	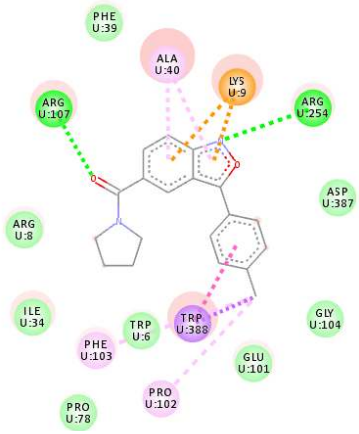
Amb20265354	-9.9	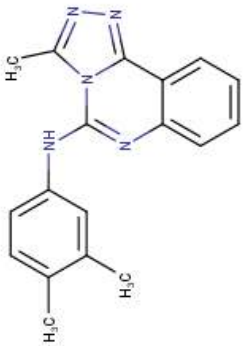	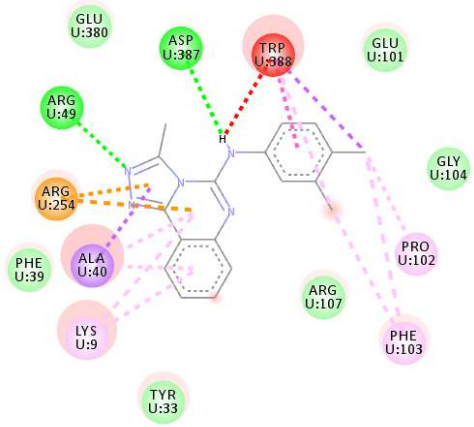
Amb541441	-9.8	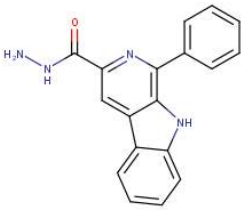	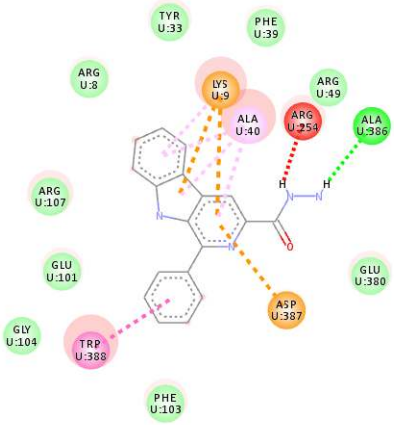

Amb6239602	-9.8	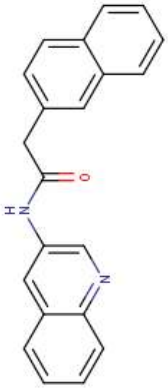	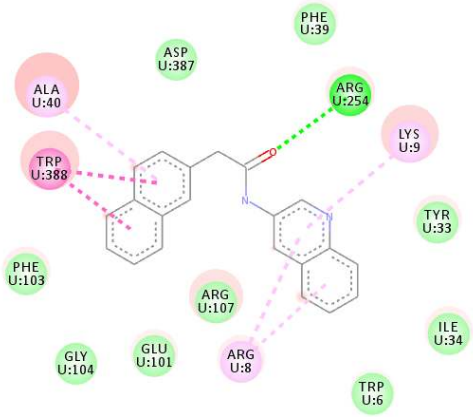
Amb542259	-9.8		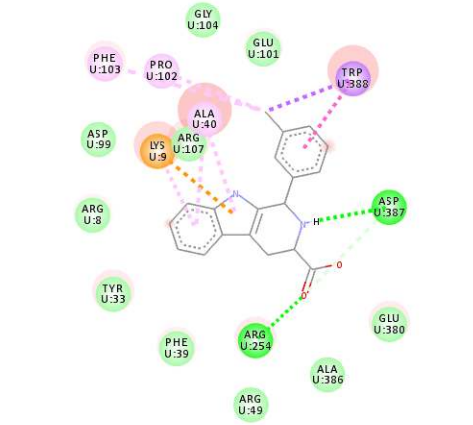
Amb35161609	-9.8	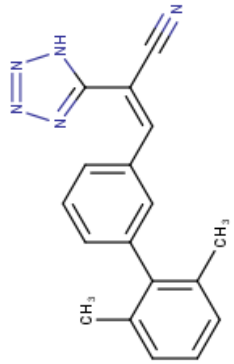	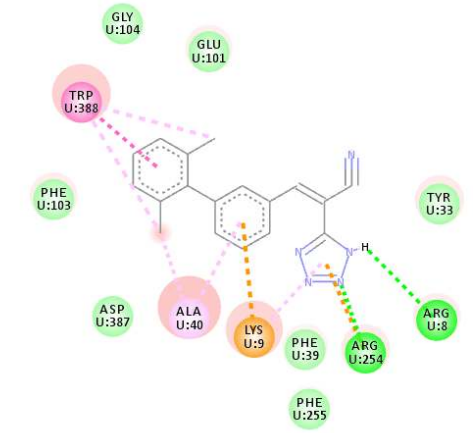

Amb22364410	-9.8	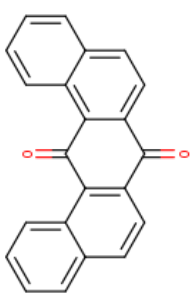	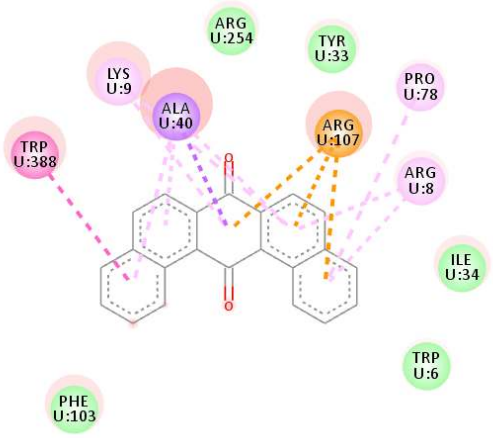
Amb30659880	-9.8	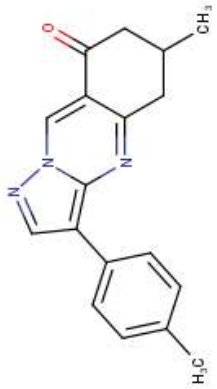	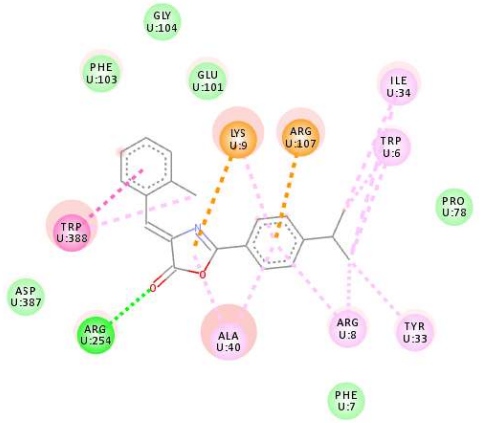
Amb30879368	-9.8	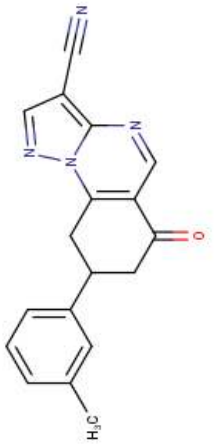	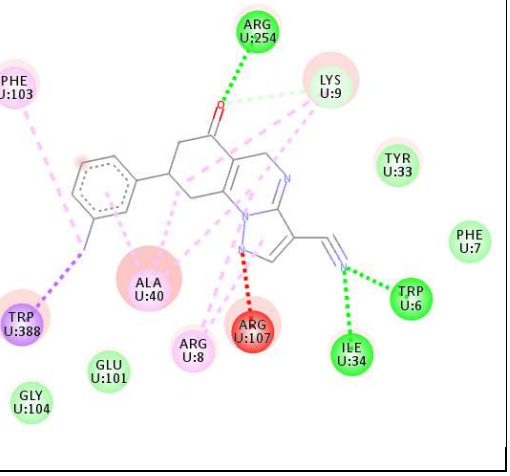

Amb1840740	-9.8	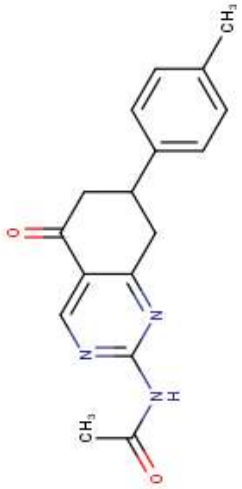	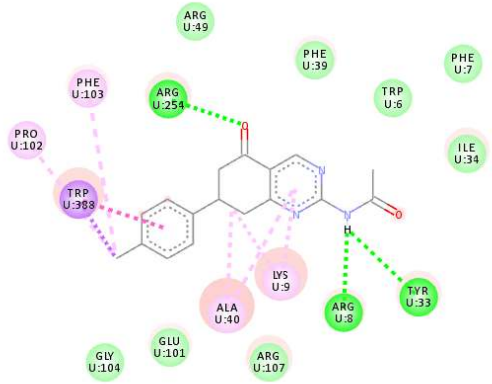
Amb16650433	-9.8	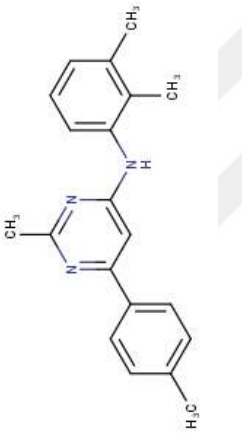	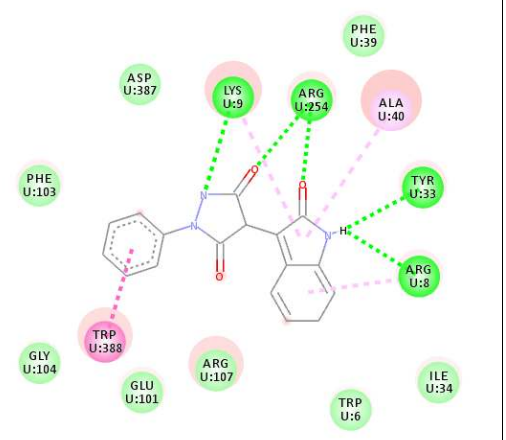
Amb22903052	-9.8	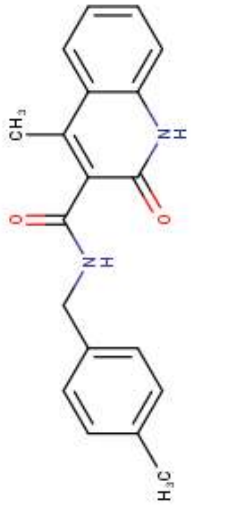	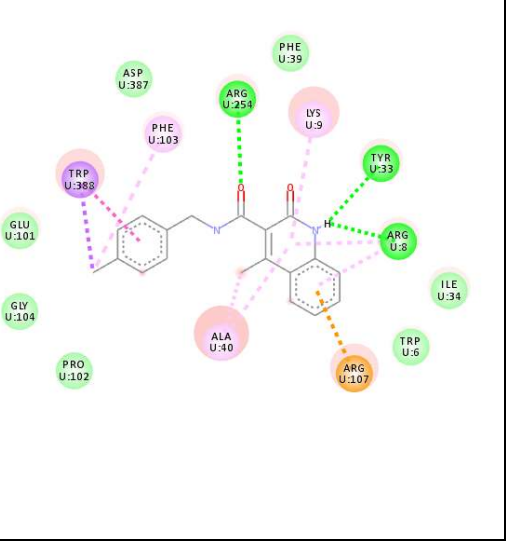

Amb10820824	-9.7		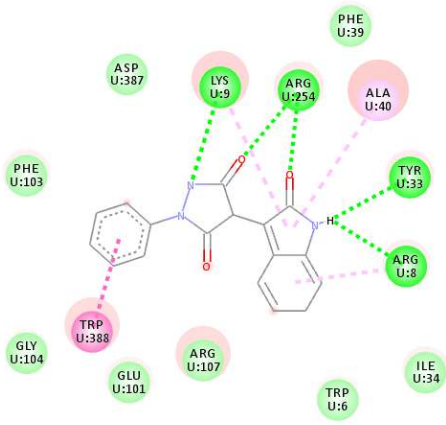
Amb10811567	-9.7	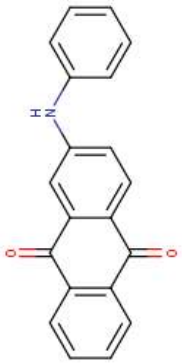	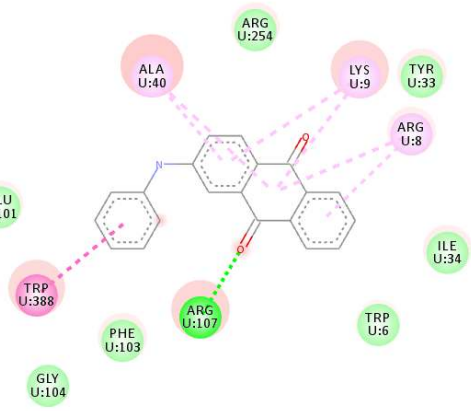
Amb8625600	-9.7	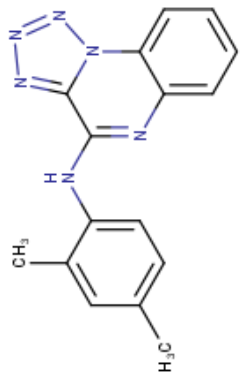	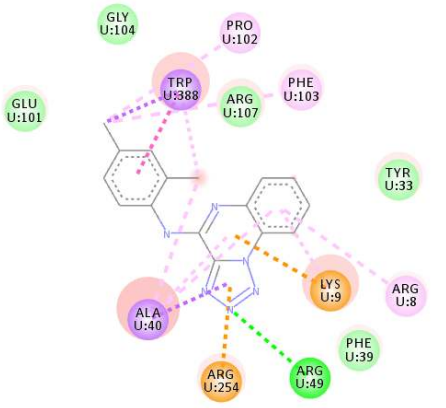

Amb698445	-9.7	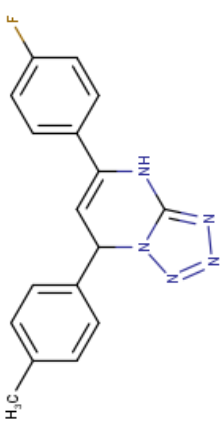	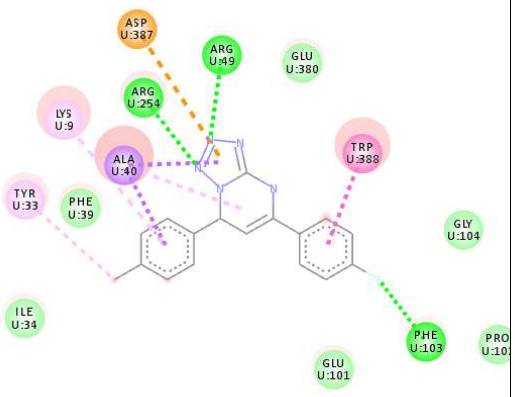
DMRL	-7.0	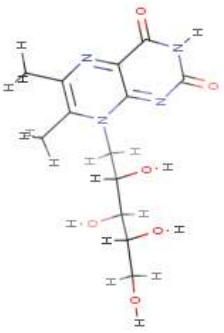	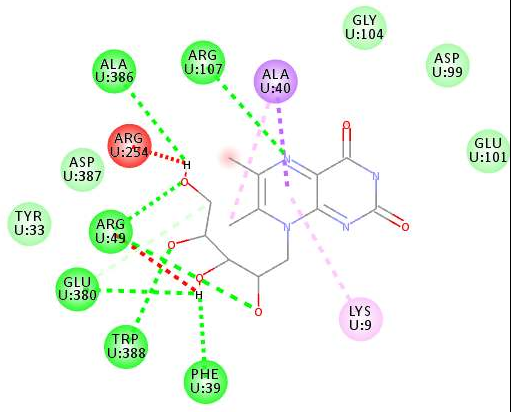

Table S2

Ambinter ID	**Structure**	**Binding Energy** (kcal/mol)	**Ambinter ID**	**Structure**	**Binding Energy** (kcal/mol)
Amb20487371	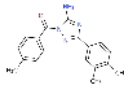	-9.7	Amb19818010	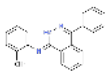	-9.7
Amb19713814	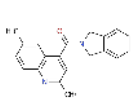	-9.7	Amb19266767	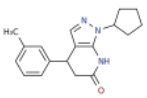	-9.7
Amb19660681	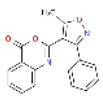	-9.7	Amb19535321	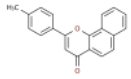	-9.7

Amb19524272	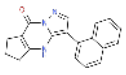	-9.7	Amb20369121	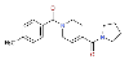	-9.7
Amb20252864	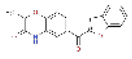	-9.7	Amb19287162	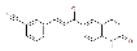	-9.7
Amb16740385	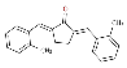	-9.7	Amb1149932	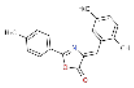	-9.6
Amb10831942	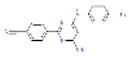	-9.6	Amb1288607	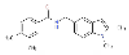	-9.6
Amb8552150	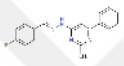	-9.6	Amb6554073	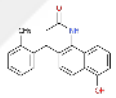	-9.6
Amb613488	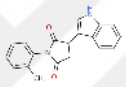	-9.6	Amb5387194	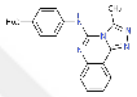	-9.6
Amb22546608	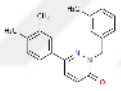	-9.7	Amb30662190	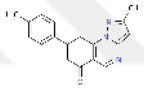	-9.7
Amb30662162	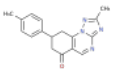	-9.7	Amb23586088	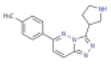	-9.7
Amb22583969	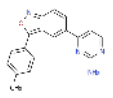	-9.7	Amb23552706	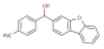	9.7
Amb687398	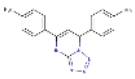	-9.6	Amb686339	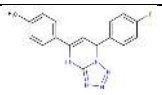	-9.7
Amb552620	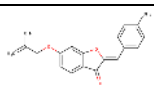	-9.7	Amb22555791	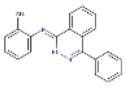	-9.7

Table S3

Box Position	Ambinter ID	Moleculer Weight	Arrived Quantity (mg)
A1	Amb687398	303.36	5.00
A2	Amb552620	306.36	5.00
A3	Amb613488	304.34	5.00
A4	Amb6554073	303.35	5.00
A5	Amb19818010	311.38	5.00
A6	Amb686339	307.33	5.00
A7	Amb1149932	291.34	5.00
A8	Amb19713814	302.37	1.00
A9	Amb19672626	295.38	5.00
A10	Amb19535321	286.32	5.00
A11	Amb19524272	301.34	1.00
B1	Amb8552150	306.34	5.00
B2	Amb19287162	302.33	5.00
B3	Amb20252864	307.30	5.00
B4	Amb19660681	304.30	5.00
B5	Amb16740385	288.38	5.00
B6	Amb20369121	298.38	2.00
B7	Amb5387194	289.34	2.00
B8	Amb20487371	306.36	5.00
B9	Amb1288607	306.40	5.00
B10	Amb22665408	304.39	5.00
C1	Amb16650433	303.40	5.00
C2	Amb3923625	299.32	3.00
C3	Amb20491902	304.35	5.00
C4	Amb20466614	302.37	2.00
C5	Amb20426308	306.36	2.00

C6	Amb16754394	300.36	5.00
C7	Amb16710891	301.30	5.00
C8	Amb20547507	296.32	2.00
C9	Amb2239008	288.30	5.00
C10	Amb6239602	312.37	5.00
C11	Amb318014	291.30	5.00
C12	Amb240135	301.34	5.00
D1	Amb21990000	305.37	33.00
D2	Amb10820824	305.29	5.00
D3	Amb10811567	299.32	5.00
D4	Amb1840740	295.34	5.00
D5	Amb8625600	290.22	5.00
D6	Amb22355645	310.35	5.00
D7	Amb22364410	308.33	1.10
D8	Amb22364410	308.33	1.10
D9	Amb22364410	308.33	1.10
D10	Amb22364410	308.33	1.10
D11	Amb22364410	308.33	1.10
D12	Amb6323295	287.36	5.00
E1	Amb21913478	305.28	5.00
E2	Amb542259	306.36	5.00
E3	Amb541441	302.33	5.00
E4	Amb6601020	302.37	5.00
E5	Amb22903052	306.36	5.00

APPENDIX C. Bioluminescence of U2OS *Bmal1:dLuc* cells via Synergy H1

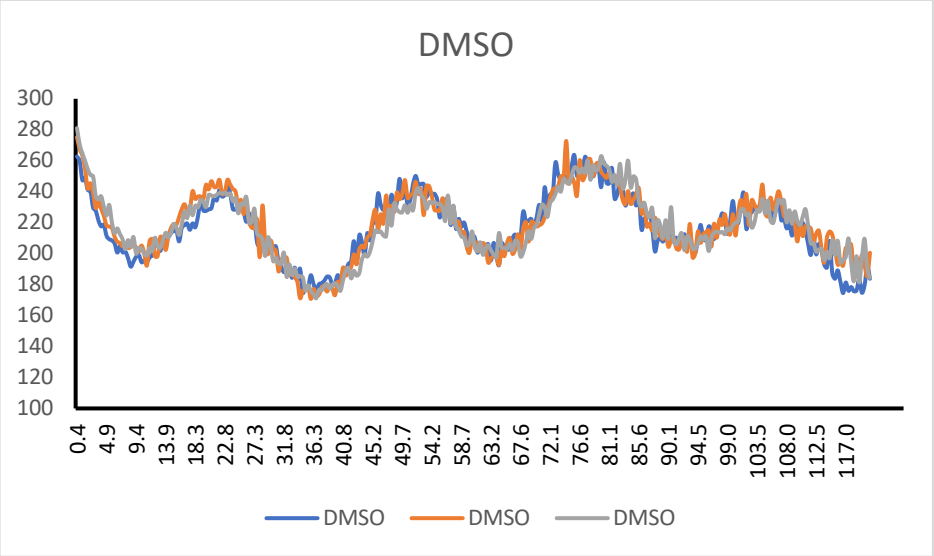

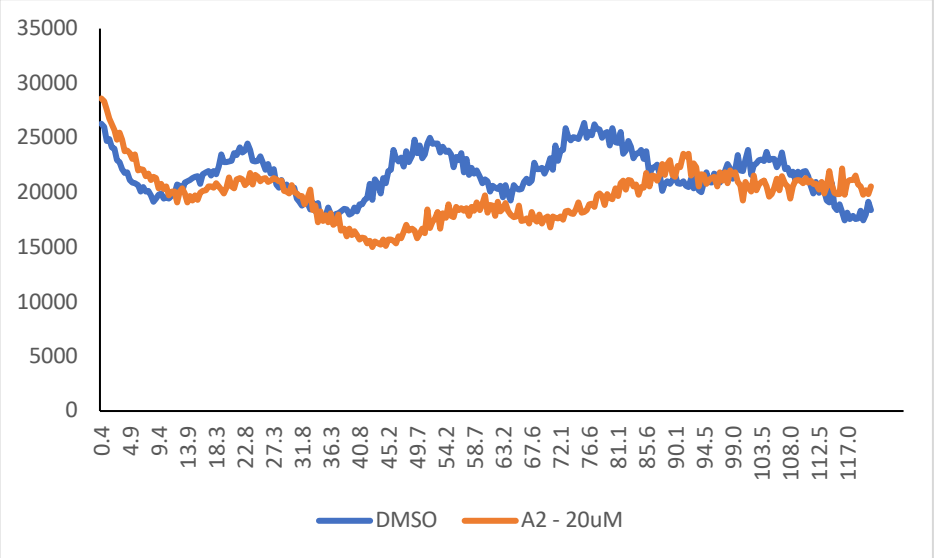

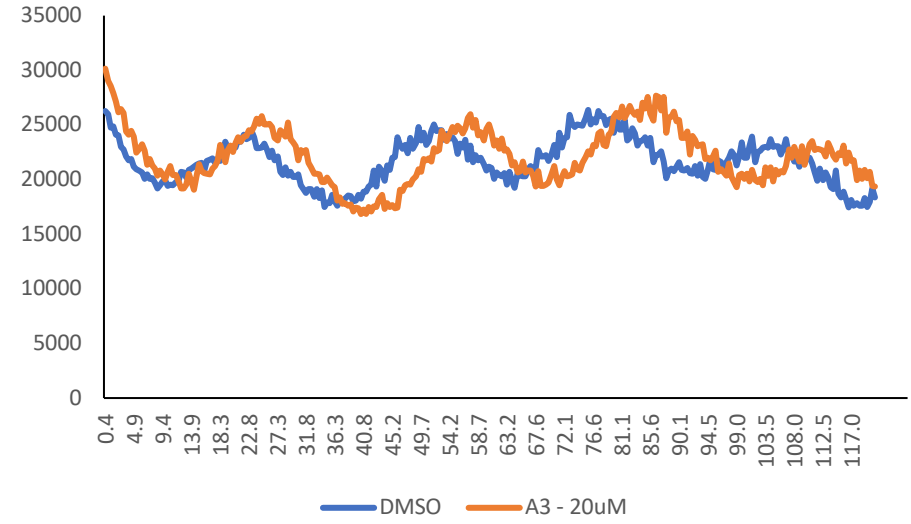
35000
30000
25000
20000
15000
10000
5000
0
0.4 4.9 9.4 13.9 18.3 22.8 27.3 31.8 36.3 40.8 45.2 49.7 54.2 58.7 63.2 67.6 72.1 76.6 81.1 85.6 90.1 94.5 99.0 103.5 108.0 112.5 117.0
DMSO
A3 - 20uM

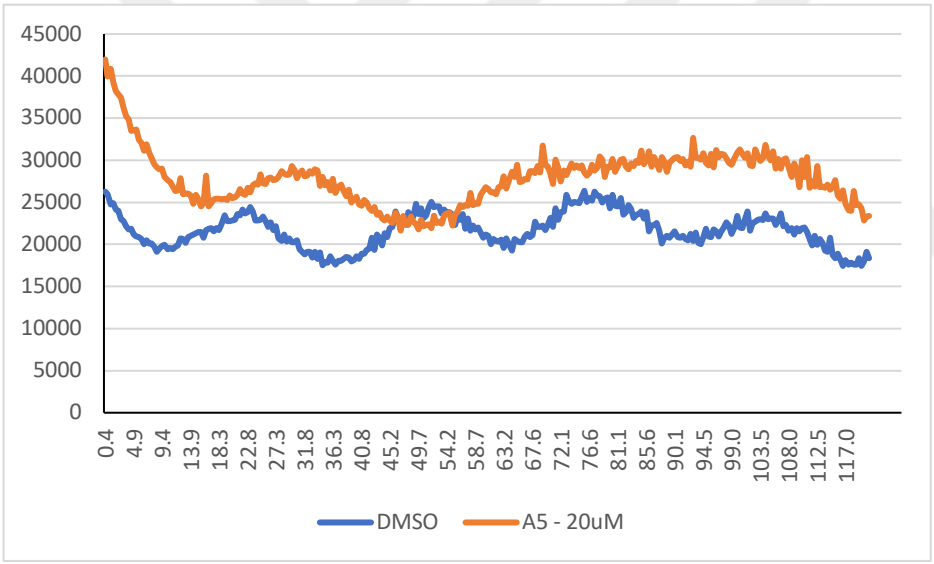
45000
40000
35000
30000
25000
20000
15000
10000
5000
0
0.4 4.9 9.4 13.9 18.3 22.8 27.3 31.8 36.3 40.8 45.2 49.7 54.2 58.7 63.2 67.6 72.1 76.6 81.1 85.6 90.1 94.5 99.0 103.5 108.0 112.5 117.0
DMSO
A5 - 20uM

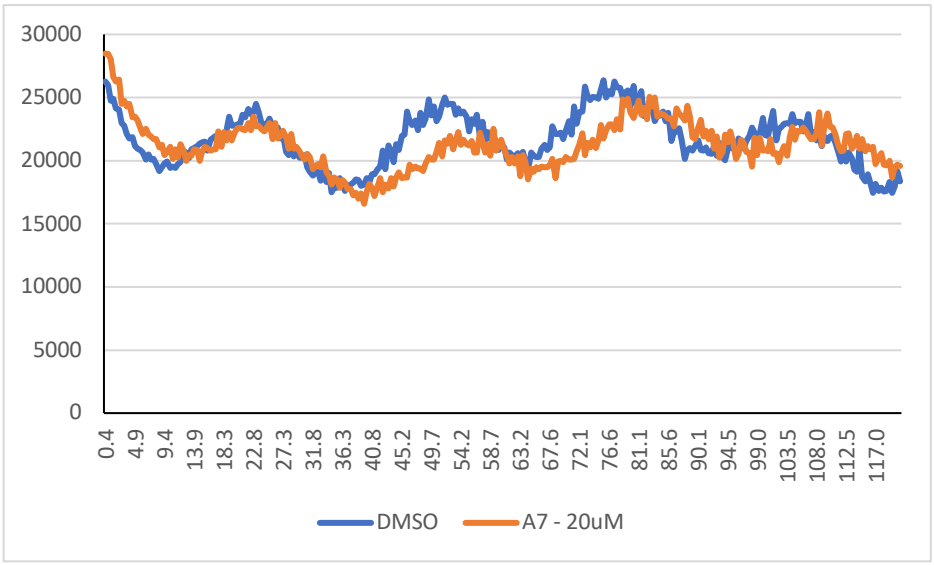
30000
25000
20000
15000
10000
5000
0
0.4 4.9 9.4 13.9 18.3 22.8 27.3 31.8 36.3 40.8 45.2 49.7 54.2 58.7 63.2 67.6 72.1 76.6 81.1 85.6 90.1 94.5 99.0 103.5 108.0 112.5 117.0
DMSO
A7 - 20uM

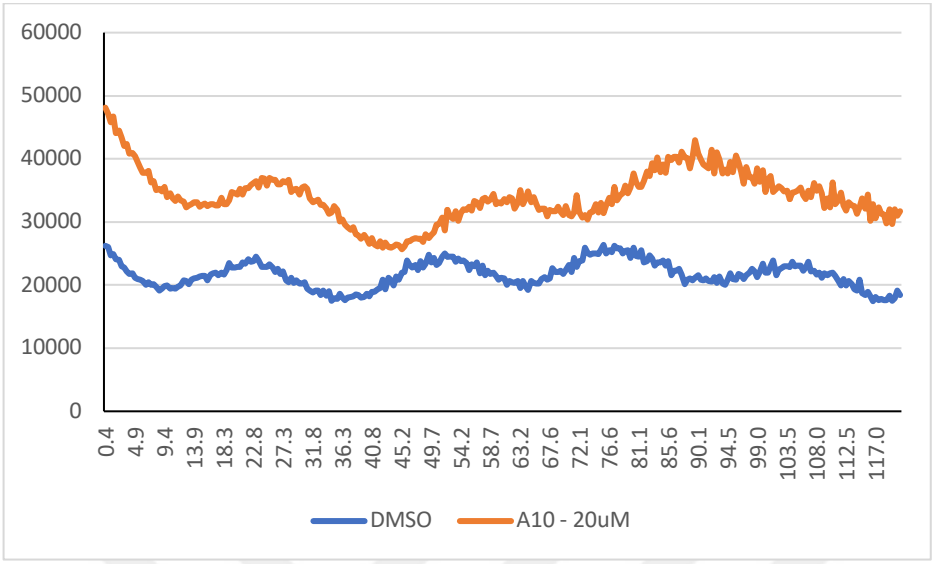
60000
50000
40000
30000
20000
10000
0
0.4
4.9
9.4
13.9
18.3
22.8
27.3
31.8
36.3
40.8
45.2
49.7
54.2
58.7
63.2
67.6
72.1
76.6
81.1
85.6
90.1
94.5
99.0
103.5
108.0
112.5
117.0
DMSO
A10 - 20uM

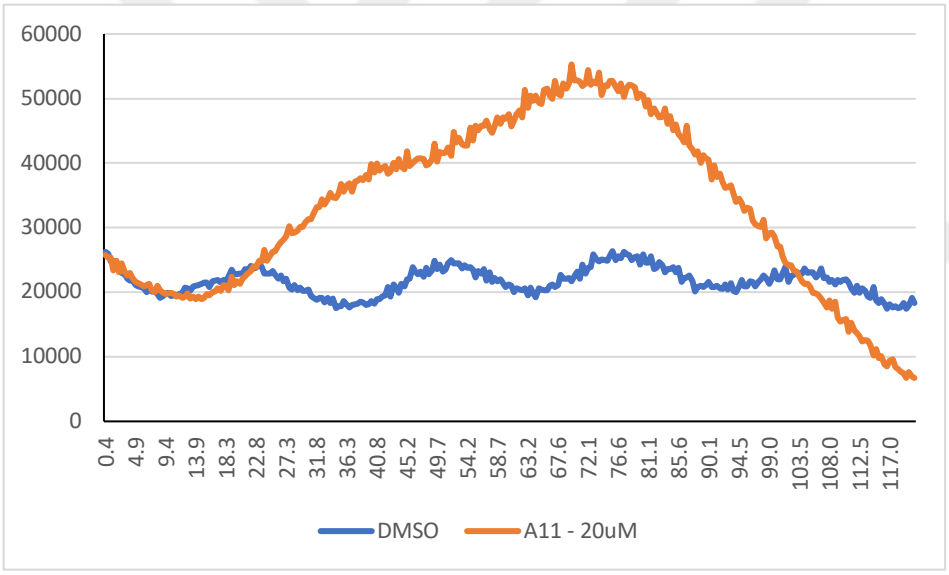
60000
50000
40000
30000
20000
10000
0
0.4
4.9
9.4
13.9
18.3
22.8
27.3
31.8
36.3
40.8
45.2
49.7
54.2
58.7
63.2
67.6
72.1
76.6
81.1
85.6
90.1
94.5
99.0
103.5
108.0
112.5
117.0
DMSO
A11 - 20uM

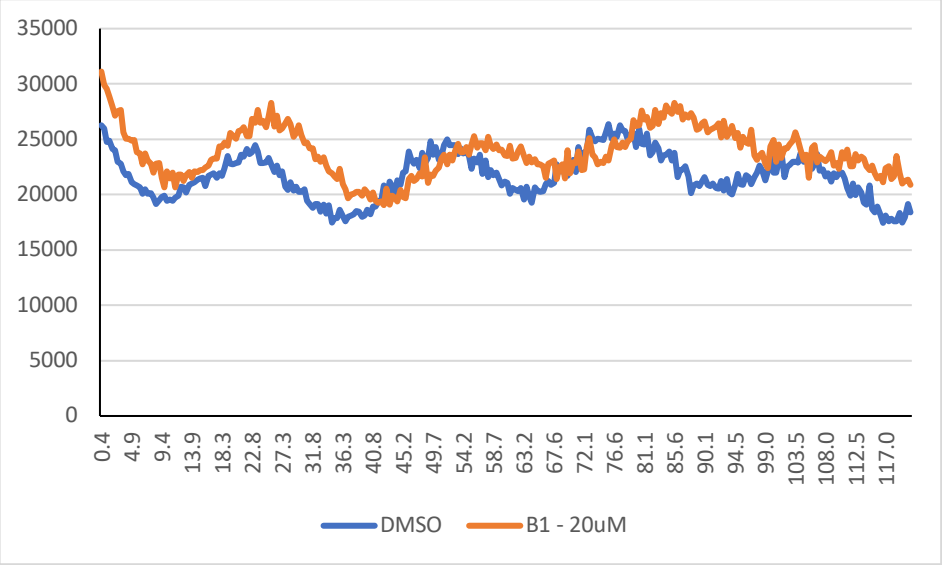
35000
30000
25000
20000
15000
10000
5000
0
0.4
4.9
9.4
13.9
18.3
22.8
27.3
31.8
36.3
40.8
45.2
49.7
54.2
58.7
63.2
67.6
72.1
76.6
81.1
85.6
90.1
94.5
99.0
103.5
108.0
112.5
117.0
DMSO
B1 - 20uM

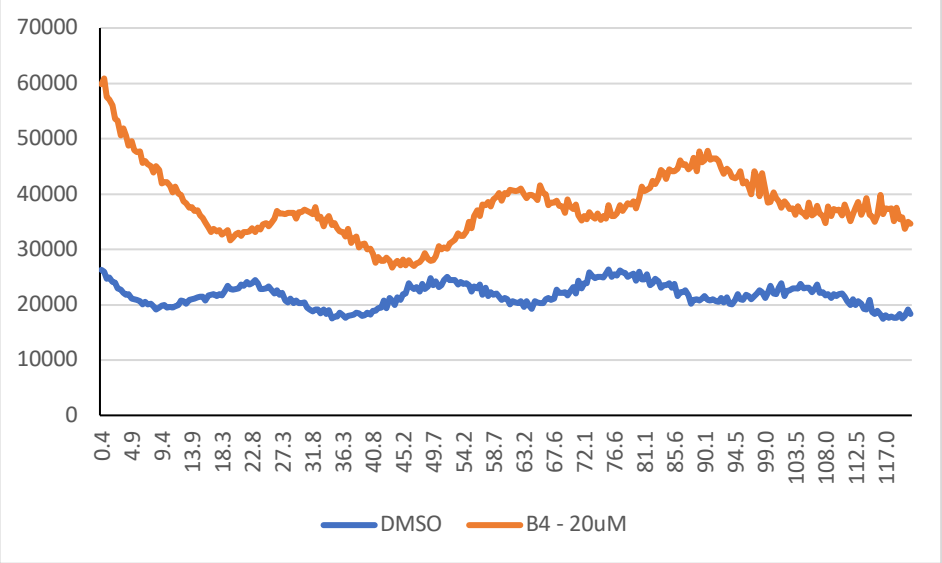
70000
60000
50000
40000
30000
20000
10000
0
0.4
4.9
9.4
13.9
18.3
22.8
27.3
31.8
36.3
40.8
45.2
49.7
54.2
58.7
63.2
67.6
72.1
76.6
81.1
85.6
90.1
94.5
99.0
103.5
108.0
112.5
117.0
DMSO
B4 - 20uM

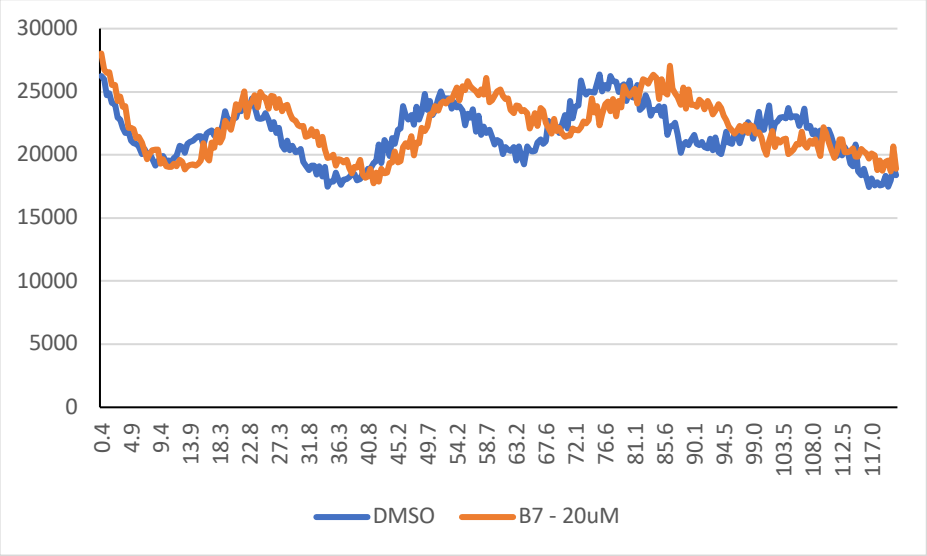
30000
25000
20000
15000
10000
5000
0
0.4 4.9 9.4 13.9 18.3 22.8 27.3 31.8 36.3 40.8 45.2 49.7 54.2 58.7 63.2 67.6 72.1 76.6 81.1 85.6 90.1 94.5 99.0 103.5 108.0 112.5 117.0
DMSO
B7 - 20uM

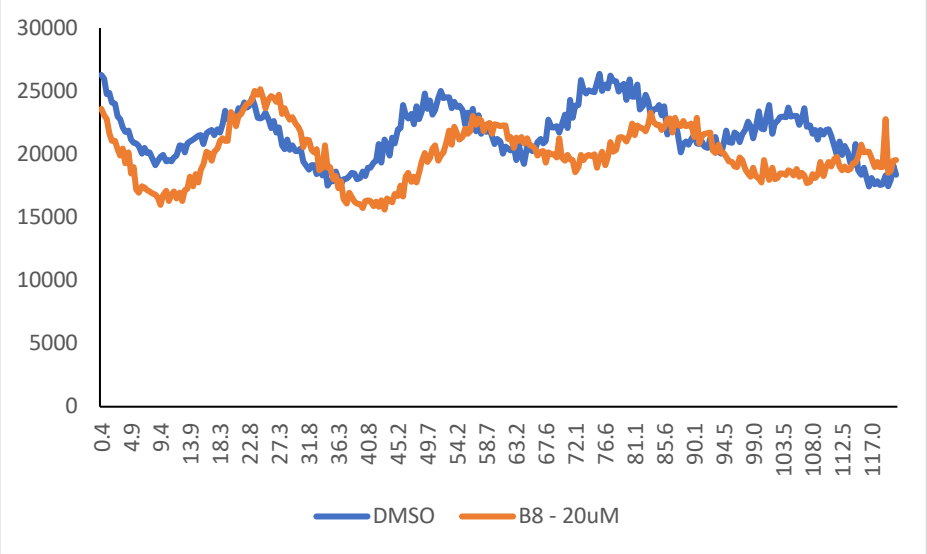
30000
25000
20000
15000
10000
5000
0
0.4 4.9 9.4 13.9 18.3 22.8 27.3 31.8 36.3 40.8 45.2 49.7 54.2 58.7 63.2 67.6 72.1 76.6 81.1 85.6 90.1 94.5 99.0 103.5 108.0 112.5 117.0
DMSO
B8 - 20uM

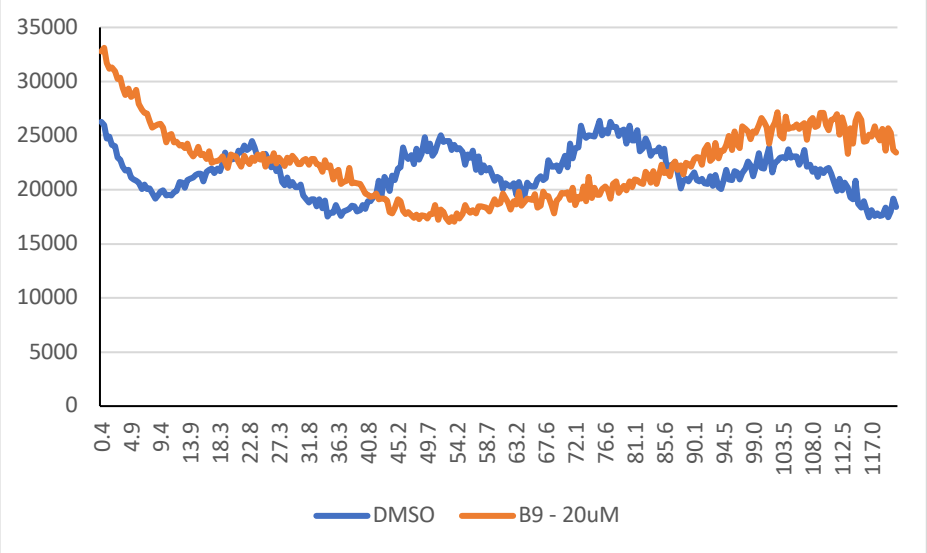
35000
30000
25000
20000
15000
10000
5000
0
0.4 4.9 9.4 13.9 18.3 22.8 27.3 31.8 36.3 40.8 45.2 49.7 54.2 58.7 63.2 67.6 72.1 76.6 81.1 85.6 90.1 94.5 99.0 103.5 108.0 112.5 117.0
DMSO
B9 - 20uM

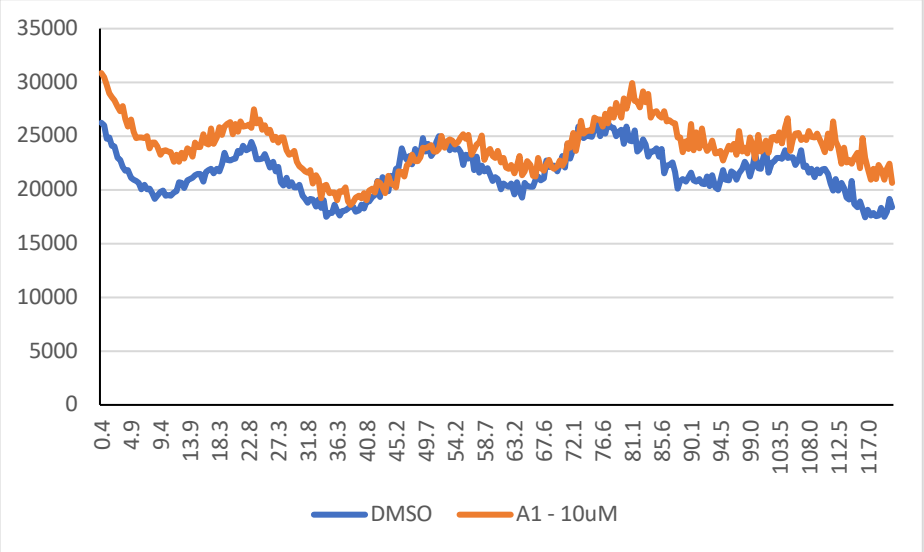
35000
30000
25000
20000
15000
10000
5000
0
0.4 4.9 9.4 13.9 18.3 22.8 27.3 31.8 36.3 40.8 45.2 49.7 54.2 58.7 63.2 67.6 72.1 76.6 81.1 85.6 90.1 94.5 99.0 103.5 108.0 112.5 117.0
DMSO
A1 - 10uM

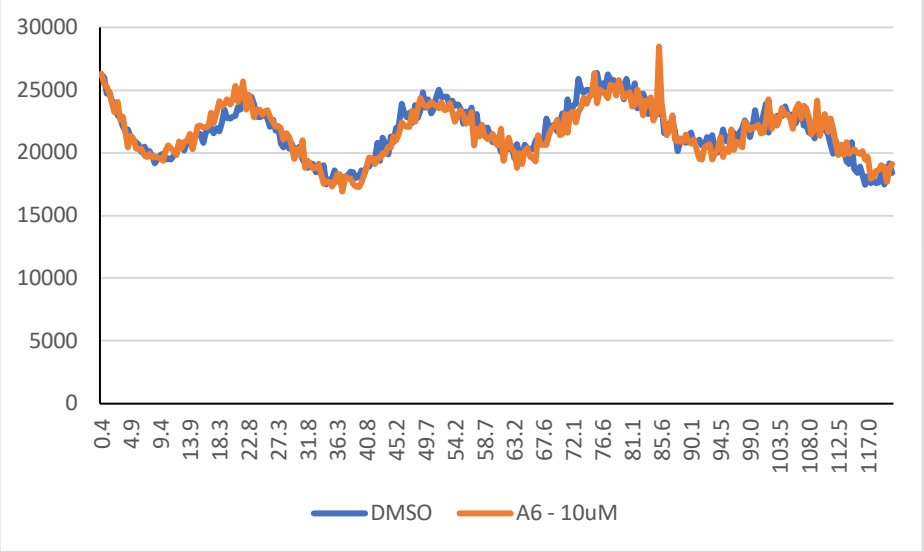
30000
25000
20000
15000
10000
5000
0
0.4 4.9 9.4 13.9 18.3 22.8 27.3 31.8 36.3 40.8 45.2 49.7 54.2 58.7 63.2 67.6 72.1 76.6 81.1 85.6 90.1 94.5 99.0 103.5 108.0 112.5 117.0
DMSO
A6 - 10uM

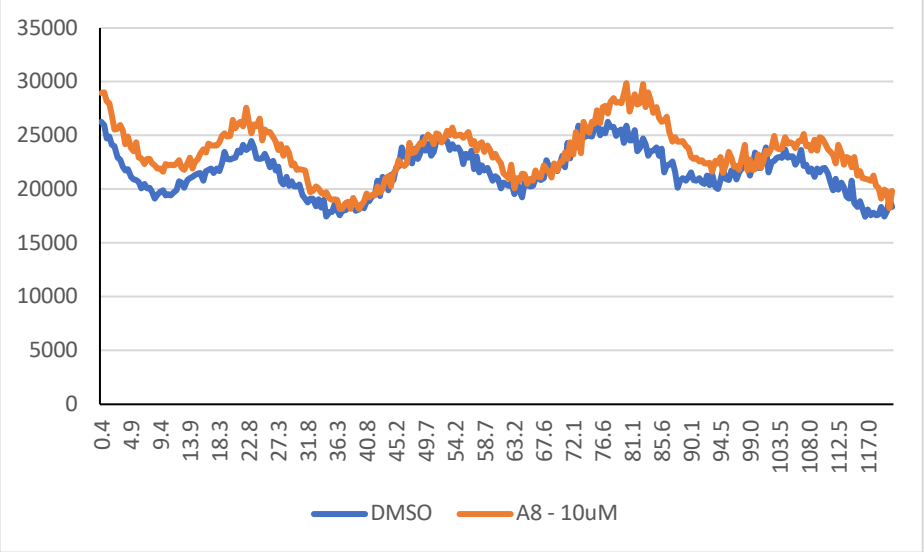
35000
30000
25000
20000
15000
10000
5000
0
0.4 4.9 9.4 13.9 18.3 22.8 27.3 31.8 36.3 40.8 45.2 49.7 54.2 58.7 63.2 67.6 72.1 76.6 81.1 85.6 90.1 94.5 99.0 103.5 108.0 112.5 117.0
DMSO
A8 - 10uM

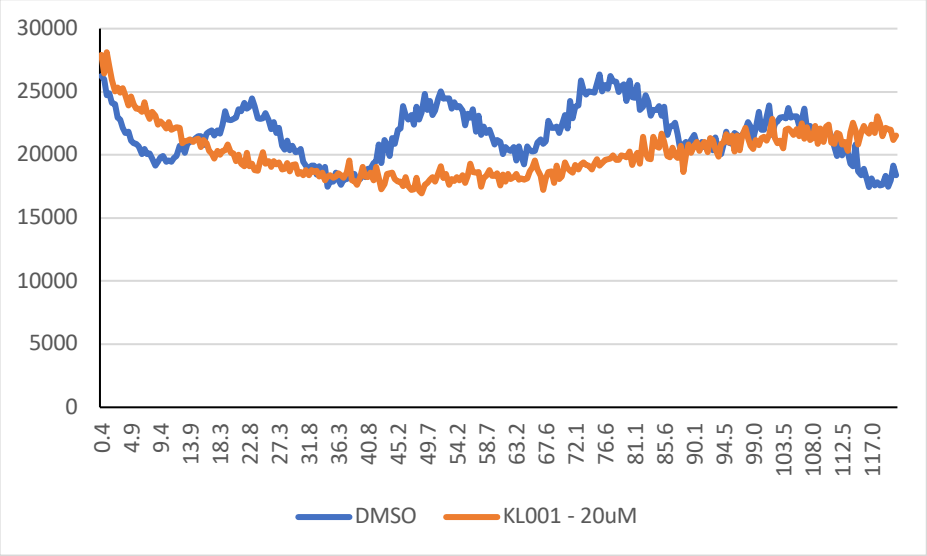
30000
25000
20000
15000
10000
5000
0
0.4
4.9
9.4
13.9
18.3
22.8
27.3
31.8
36.3
40.8
45.2
49.7
54.2
58.7
63.2
67.6
72.1
76.6
81.1
85.6
90.1
94.5
99.0
103.5
108.0
112.5
117.0
DMSO
KL001 - 20uM

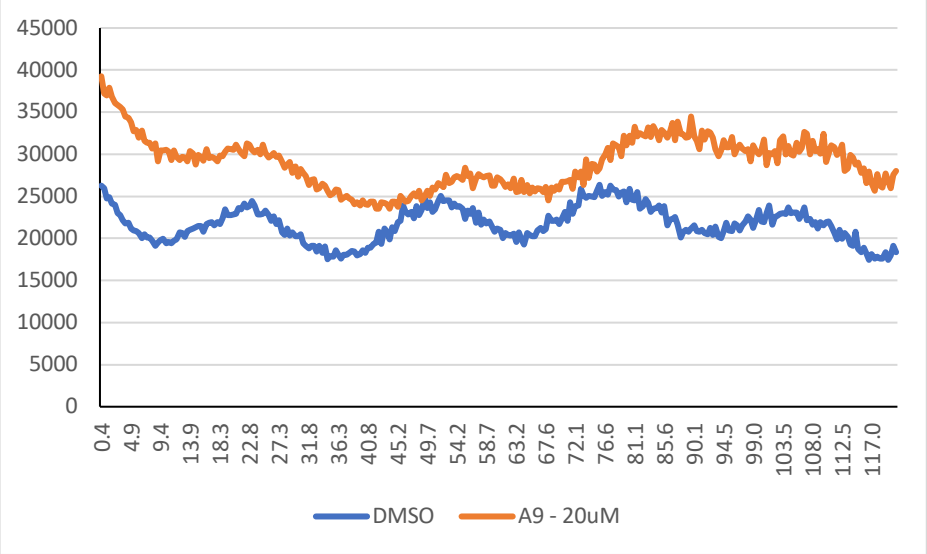
45000
40000
35000
30000
25000
20000
15000
10000
5000
0
0.4
4.9
9.4
13.9
18.3
22.8
27.3
31.8
36.3
40.8
45.2
49.7
54.2
58.7
63.2
67.6
72.1
76.6
81.1
85.6
90.1
94.5
99.0
103.5
108.0
112.5
117.0
DMSO
A9 - 20uM

APPENDIX D: Bioluminescence of U2OS *Bmal1:dLuc* cells via Lumicycle

KL001

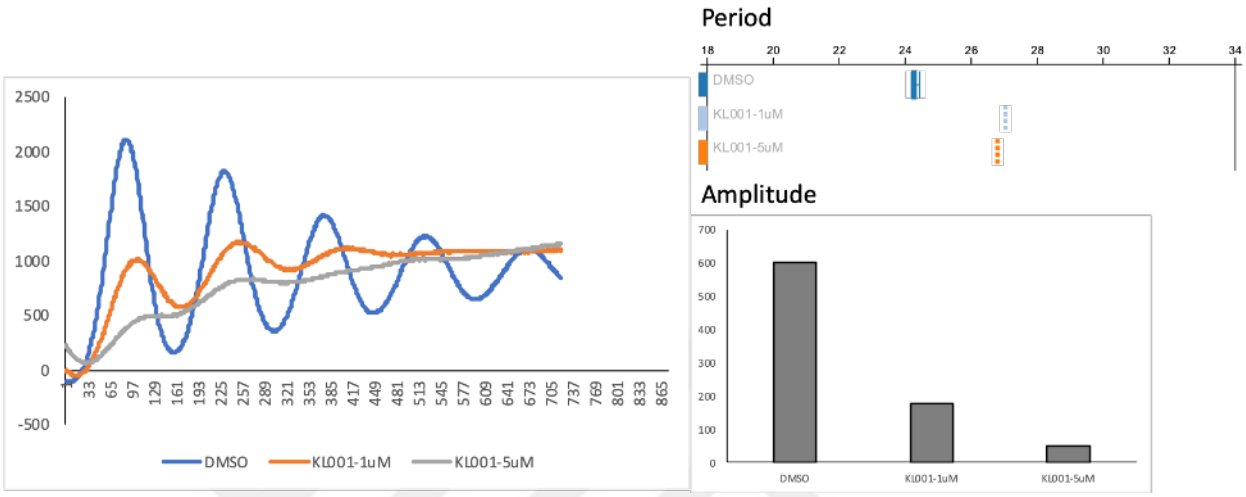

A2

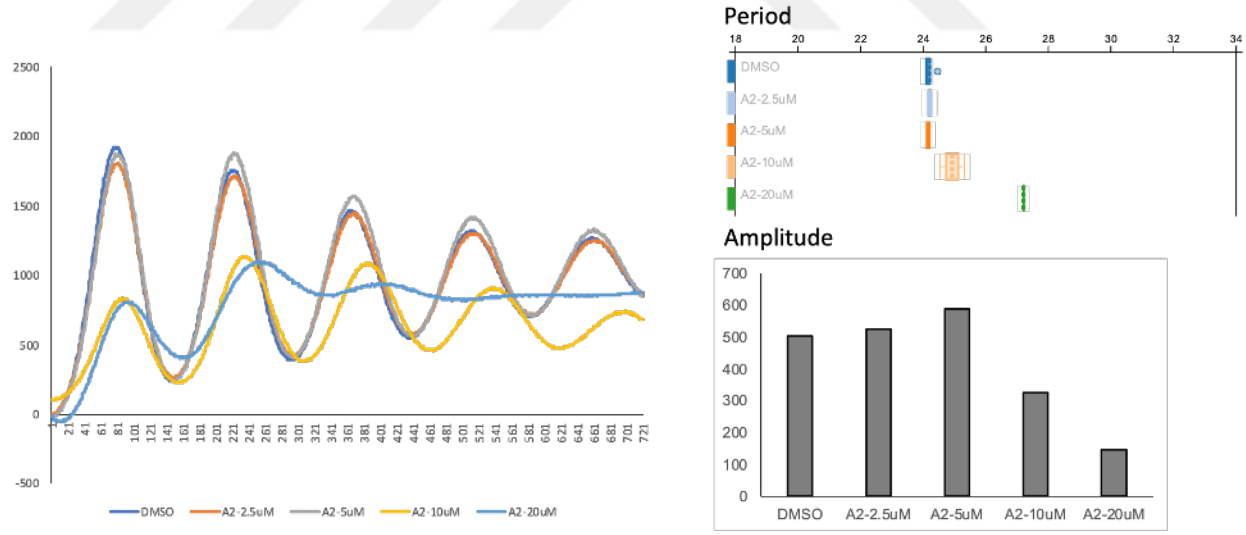

A11

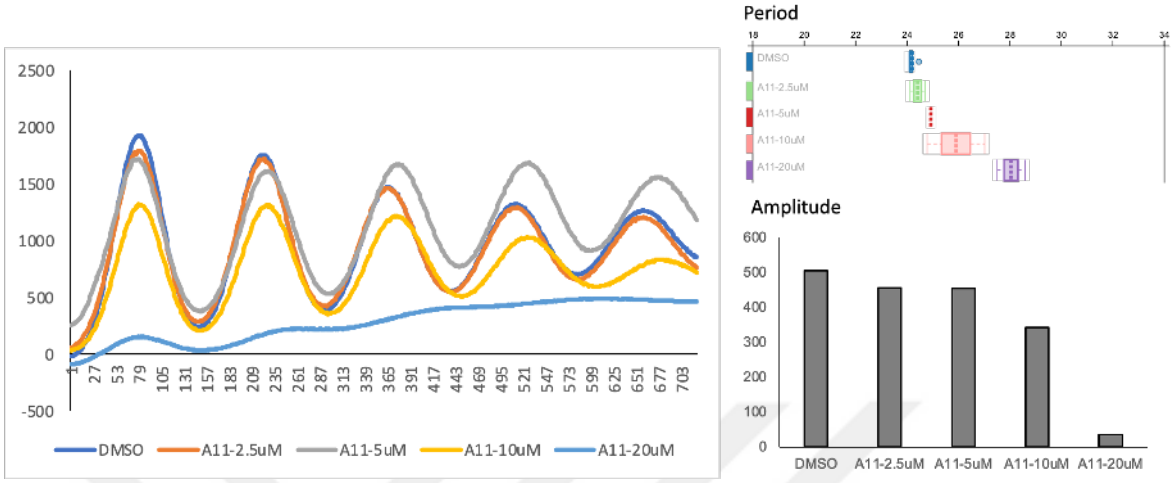
Period
DMSO
A11-2.5uM
A11-5uM
A11-10uM
A11-20uM
Amplitude
DMSO A11-2.5uM A11-5uM A11-10uM A11-20uM

C4

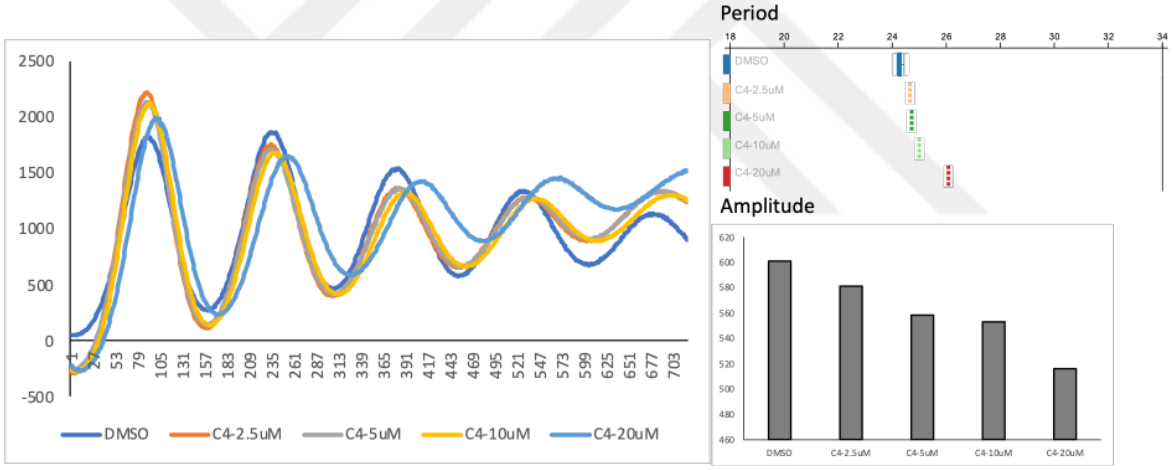
Period
DMSO
C4-2.5uM
C4-5uM
C4-10uM
C4-20uM
Amplitude

E4

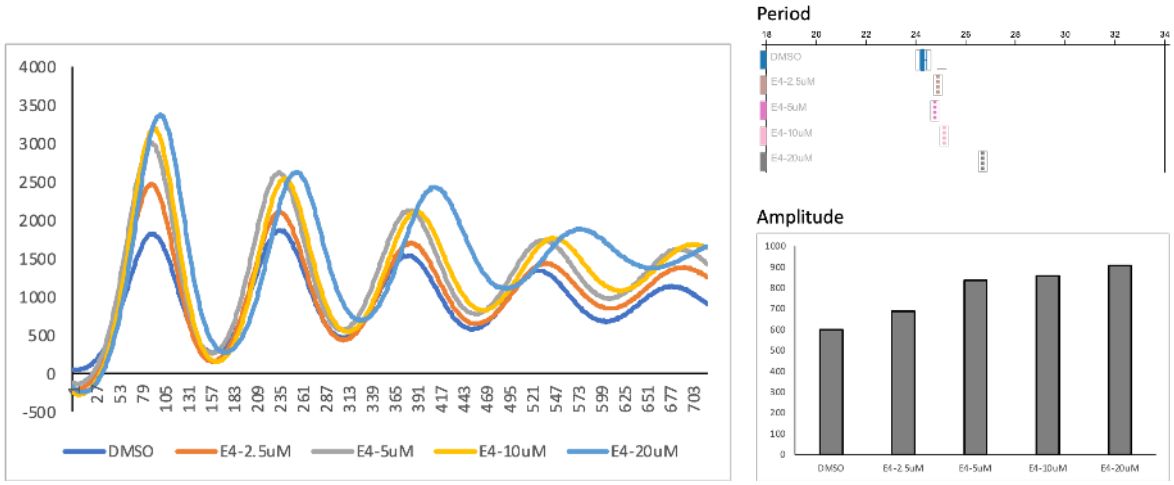
Period
DMSO
E4-2.5uM
E4-5uM
E4-10uM
E4-20uM
Amplitude

D2

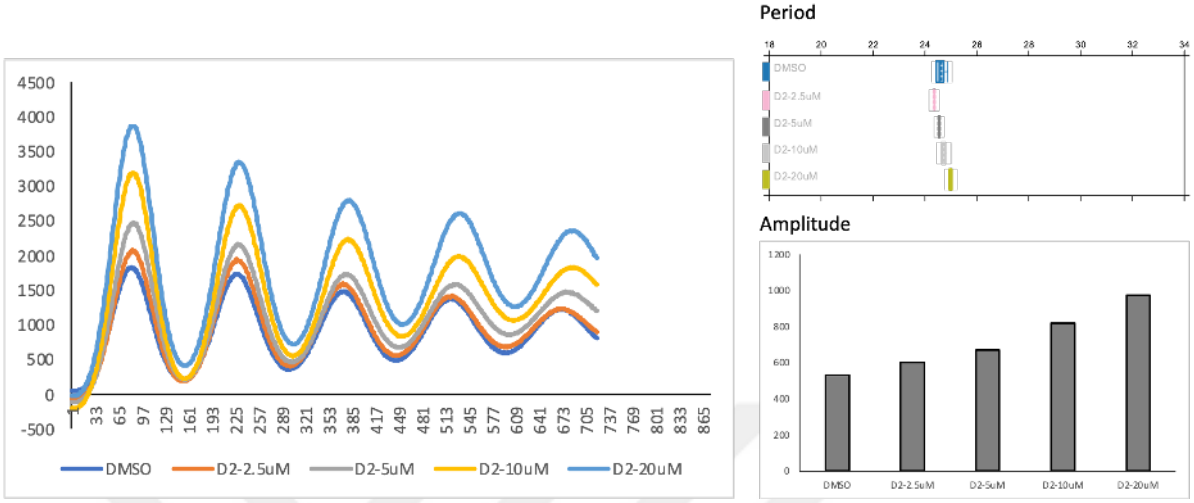
Period
DMSO
D2-2.5uM
D2-5uM
D2-10uM
D2-20uM
Amplitude
DMSO
D2-2.5uM
D2-5uM
D2-10uM
D2-20uM

B8

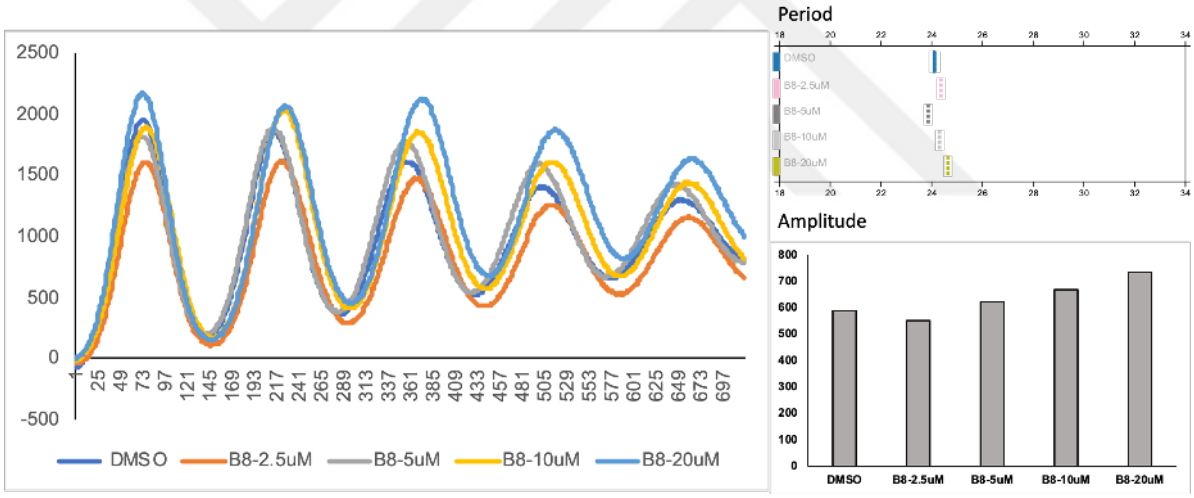
Period
DMSO
B8-2.5uM
B8-5uM
B8-10uM
B8-20uM
Amplitude
DMSO
B8-2.5uM
B8-5uM
B8-10uM
B8-20uM

A7

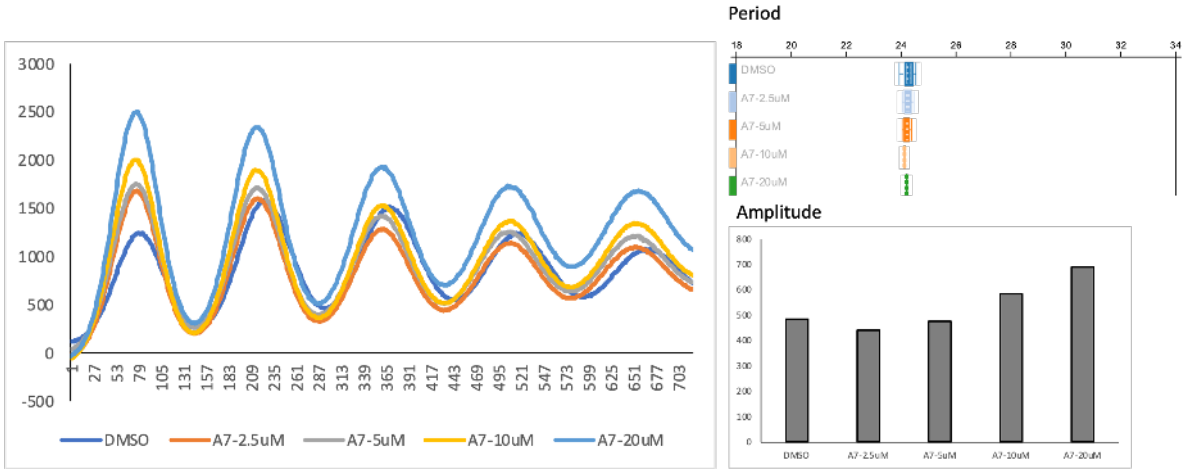
Period
DMSO
A7-2.5uM
A7-5uM
A7-10uM
A7-20uM
Amplitude
DMSO
A7-2.5uM
A7-5uM
A7-10uM
A7-20uM

A8

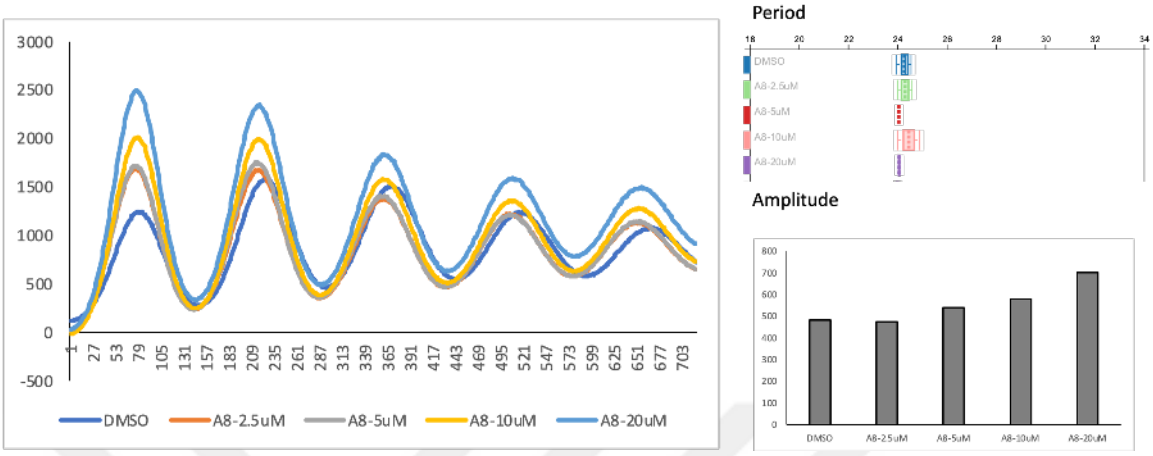
Period
Amplitude
DMSO
A8-2.5uM
A8-5uM
A8-10uM
A8-20uM

A9

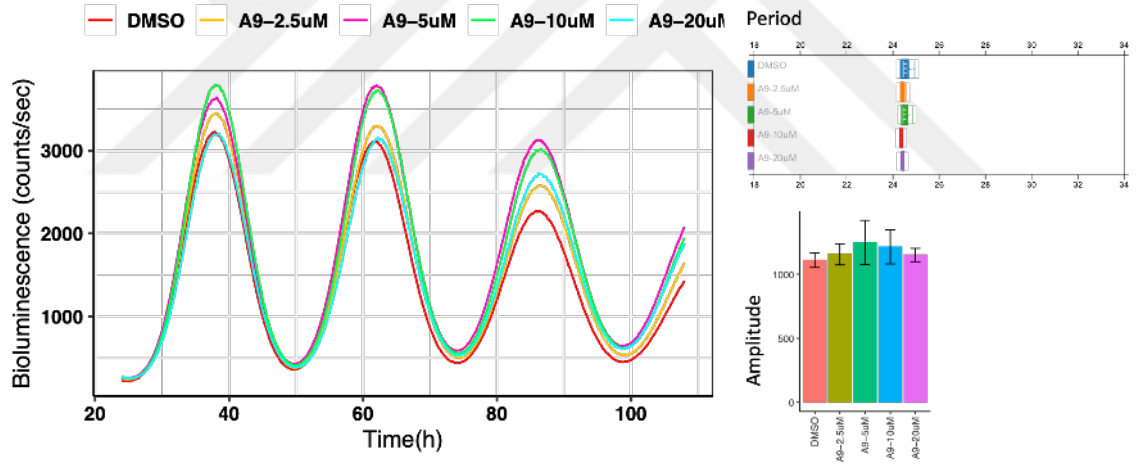
DMSO
A9–2.5uM
A9–5uM
A9–10uM
A9–20uM
Bioluminescence (counts/sec)
Time(h)
Period
Amplitude

B4

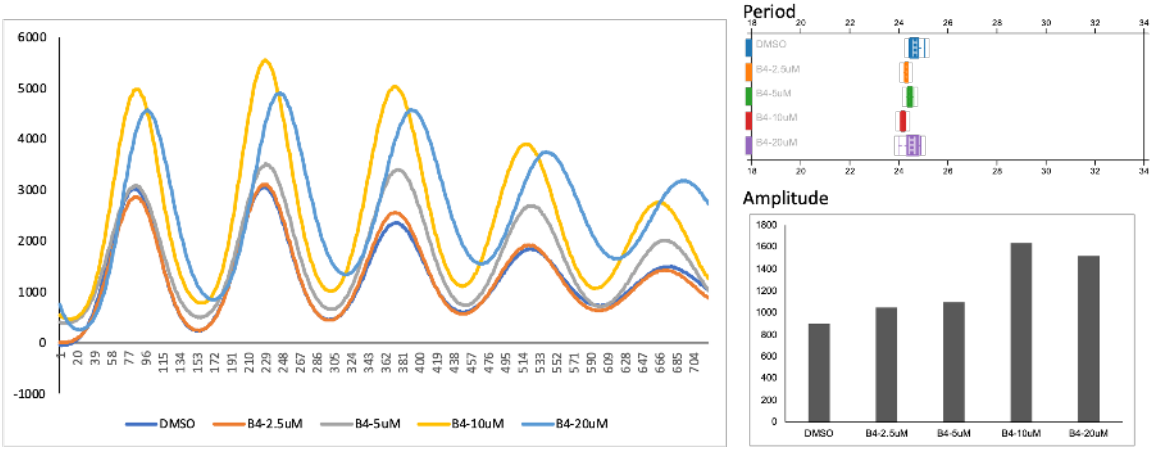
Period
Amplitude
DMSO
B4-2.5uM
B4-5uM
B4-10uM
B4-20uM

B9

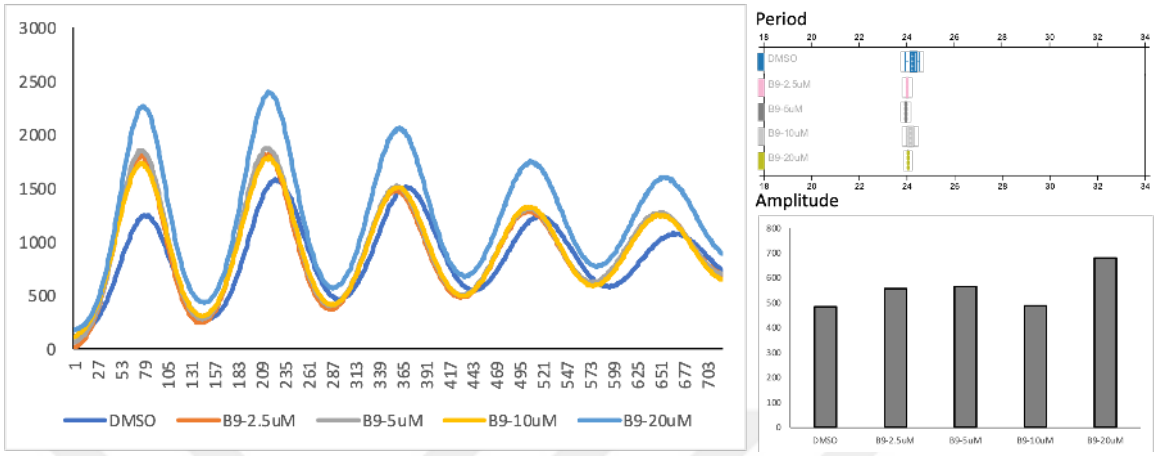
Period
Amplitude
DMSO
B9-2.5uM
B9-5uM
B9-10uM
B9-20uM

C10

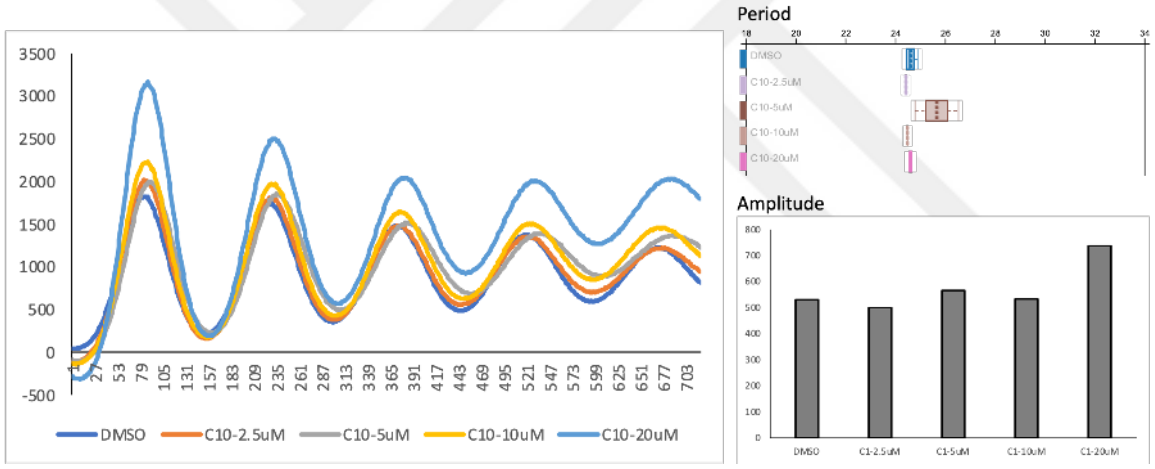
Period
Amplitude
DMSO
C10-2.5uM
C10-5uM
C10-10uM
C10-20uM

A3

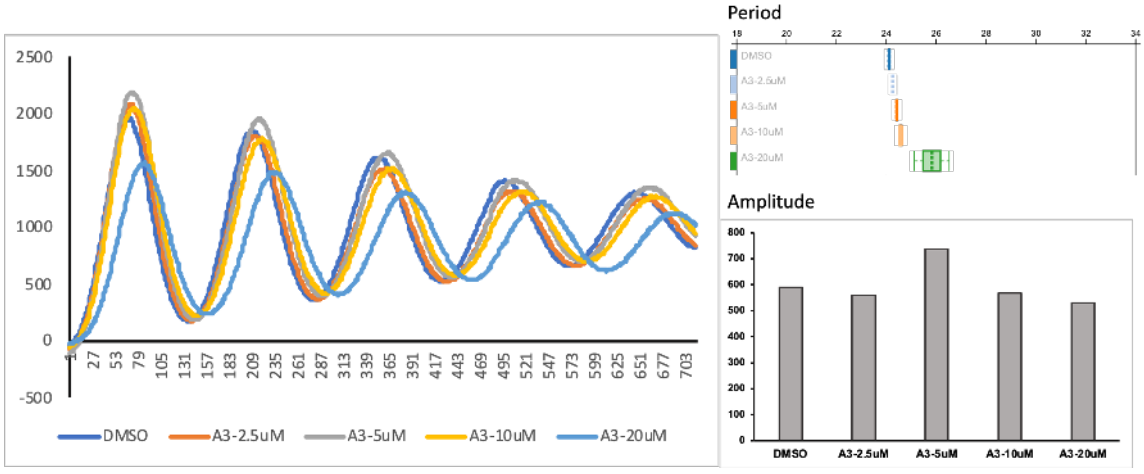
Period
Amplitude
DMSO
A3-2.5uM
A3-5uM
A3-10uM
A3-20uM

A1 / A6

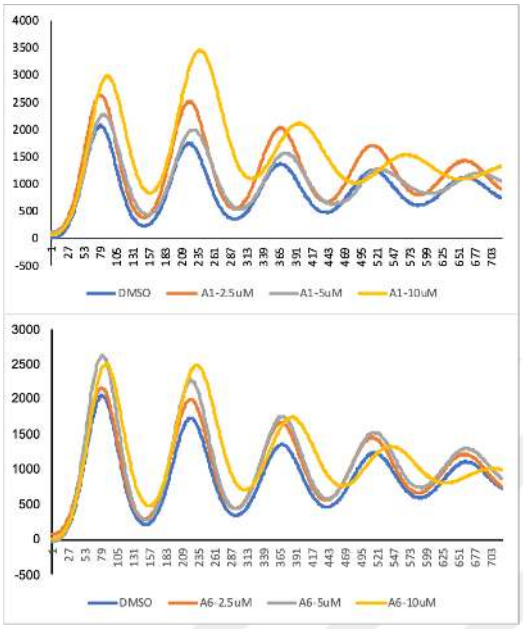
DMSO
A1-2.5uM
A1-5uM
A1-10uM
DMSO
A6-2.5uM
A6-5uM
A6-10uM

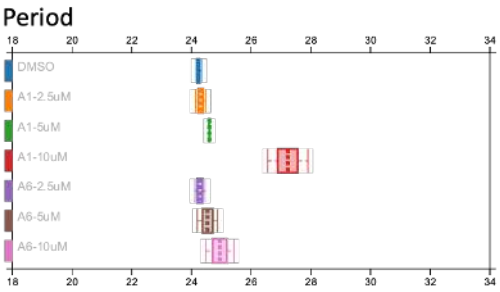
Period
DMSO
A1-2.5uM
A1-5uM
A1-10uM
A6-2.5uM
A6-5uM
A6-10uM

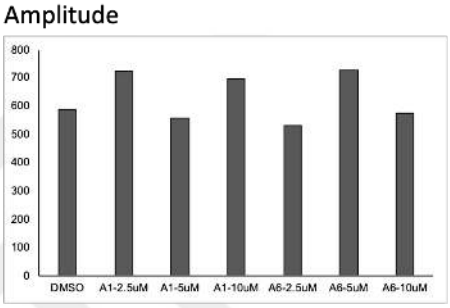
Amplitude
DMSO
A1-2.5uM
A1-5uM
A1-10uM
A6-2.5uM
A6-5uM
A6-10uM

A5

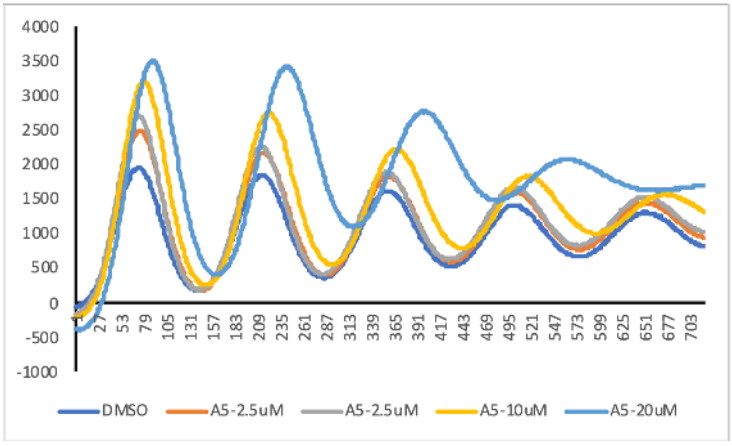
DMSO
A5-2.5uM
A5-2.5uM
A5-10uM
A5-20uM

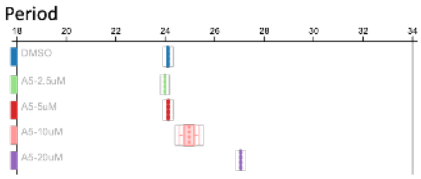
Period
DMSO
A5-2.5uM
A5-5uM
A5-10uM
A5-20uM

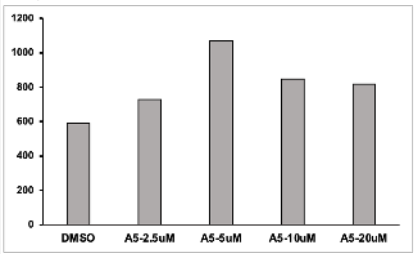
Amplitude
DMSO
A5-2.5uM
A5-5uM
A5-10uM
A5-20uM

B1

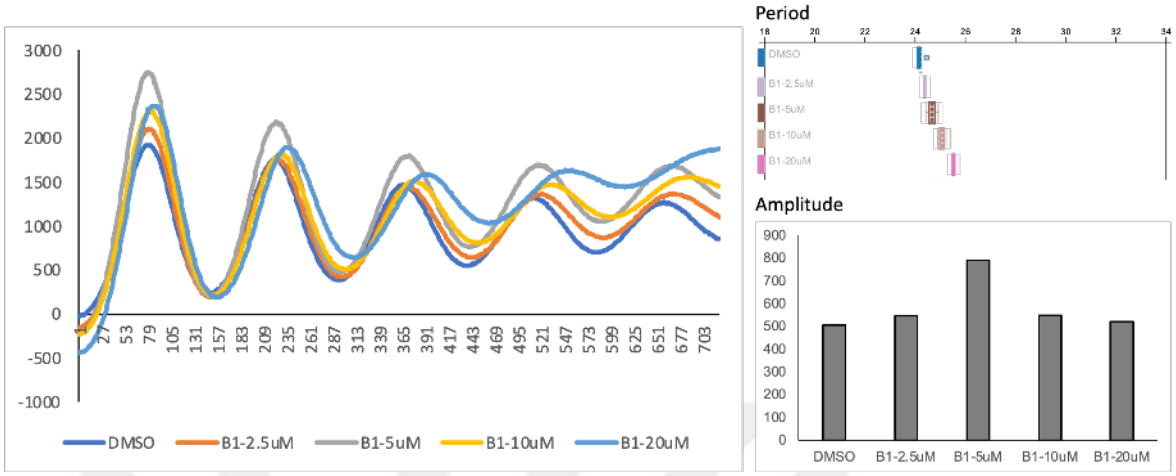
Period
DMSO
B1-2.5uM
B1-5uM
B1-10uM
B1-20uM
Amplitude
DMSO
B1-2.5uM
B1-5uM
B1-10uM
B1-20uM

B7

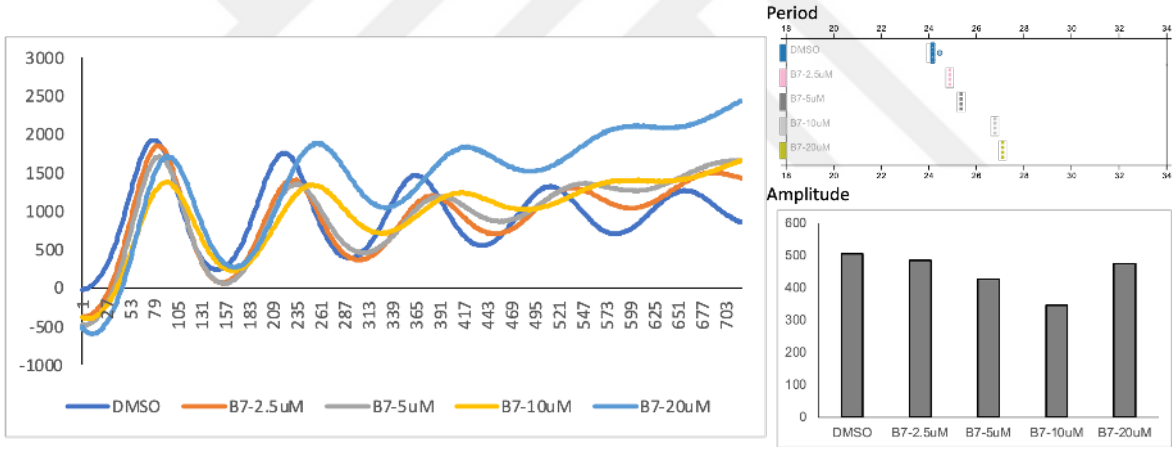
Period
DMSO
B7-2.5uM
B7-5uM
B7-10uM
B7-20uM
Amplitude
DMSO
B7-2.5uM
B7-5uM
B7-10uM
B7-20uM

C1

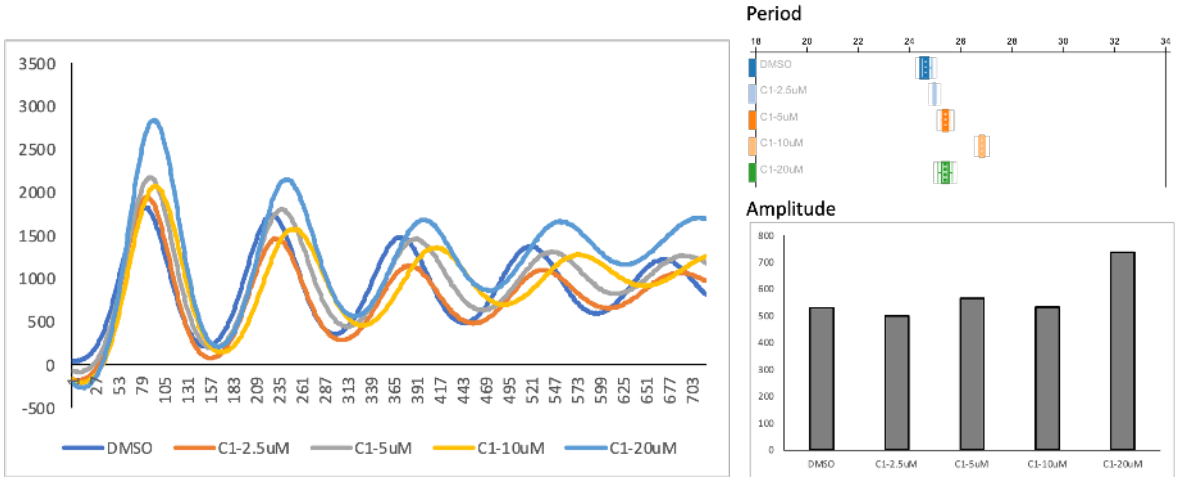
Period
DMSO
C1-2.5uM
C1-5uM
C1-10uM
C1-20uM
Amplitude
DMSO
C1-2.5uM
C1-5uM
C1-10uM
C1-20uM

A10

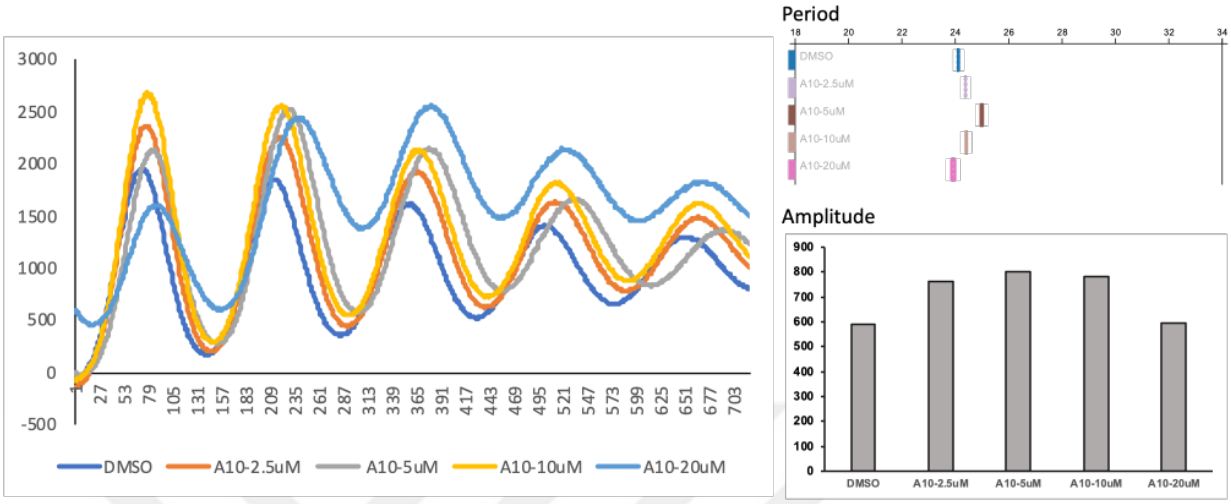
Period
DMSO
A10-2.5uM
A10-5uM
A10-10uM
A10-20uM
Amplitude
DMSO
A10-2.5uM
A10-5uM
A10-10uM
A10-20uM

C2

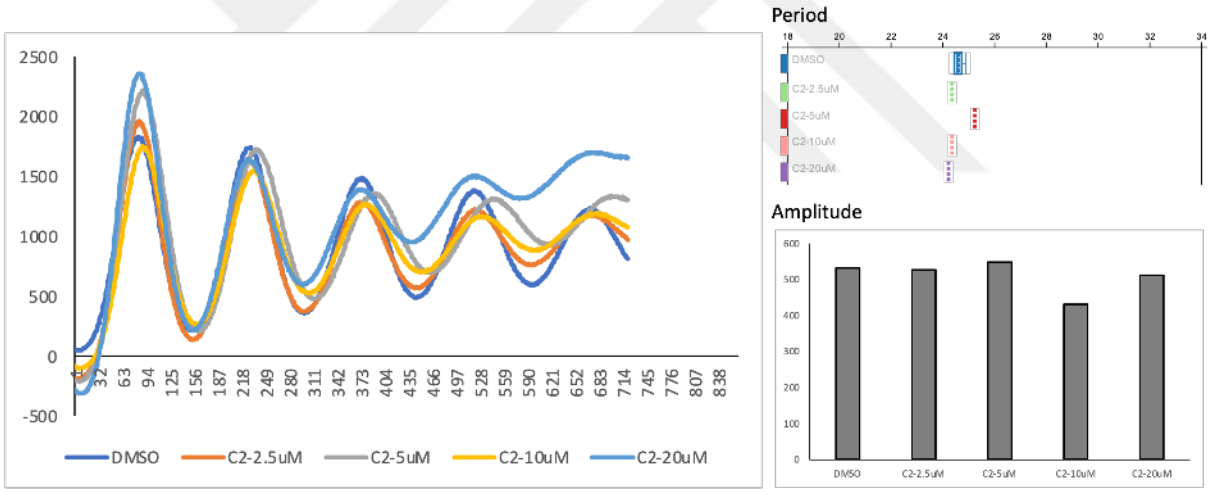
Period
DMSO
C2-2.5uM
C2-5uM
C2-10uM
C2-20uM
Amplitude
DMSO
C2-2.5uM
C2-5uM
C2-10uM
C2-20uM

C5

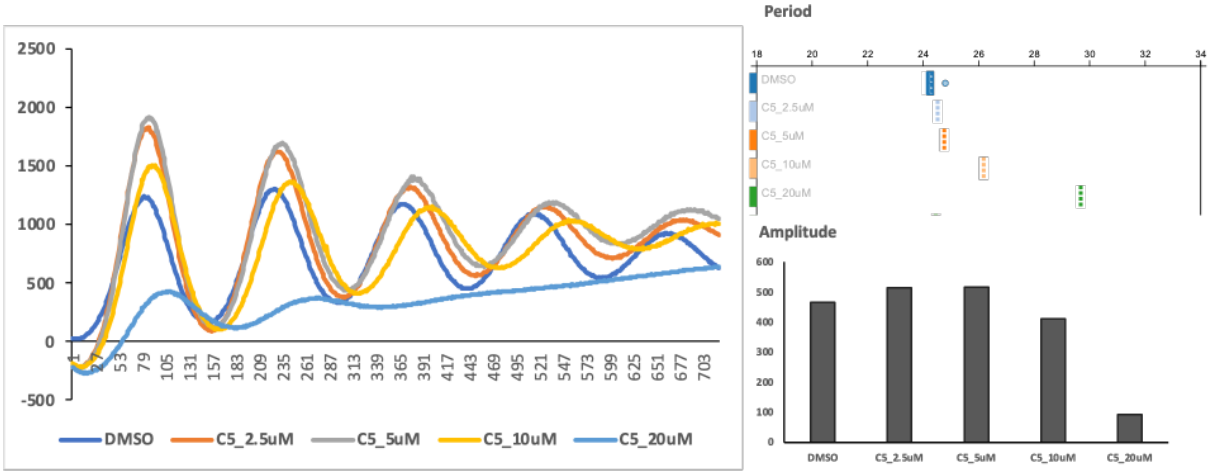
Period
DMSO
C5_2.5uM
C5_5uM
C5_10uM
C5_20uM
Amplitude
DMSO
C5_2.5uM
C5_5uM
C5_10uM
C5_20uM

C6

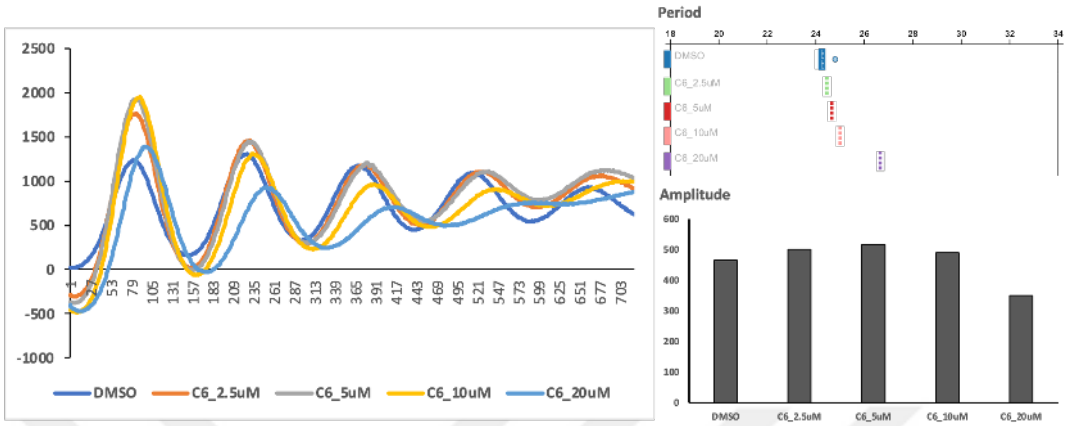
Period
Amplitude
DMSO
C6_2.5uM
C6_5uM
C6_10uM
C6_20uM

C8

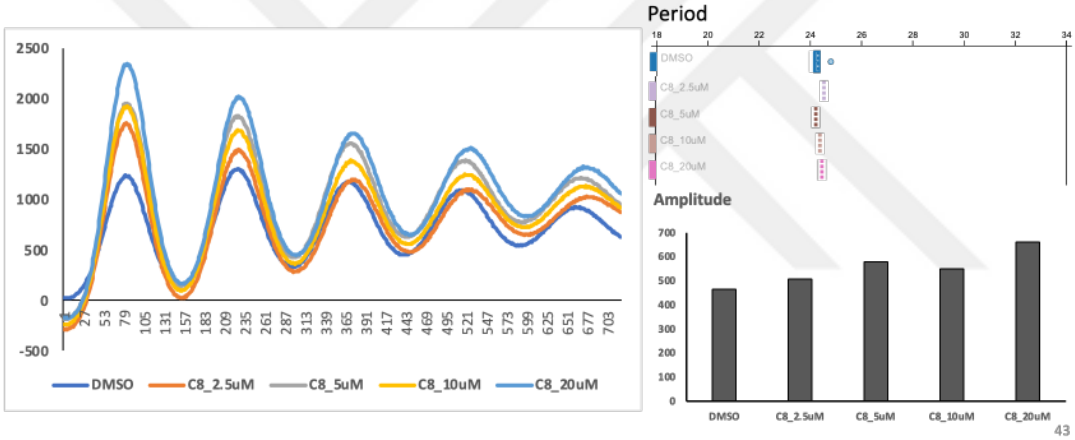
Period
Amplitude
DMSO
C8_2.5uM
C8_5uM
C8_10uM
C8_20uM

43

C12

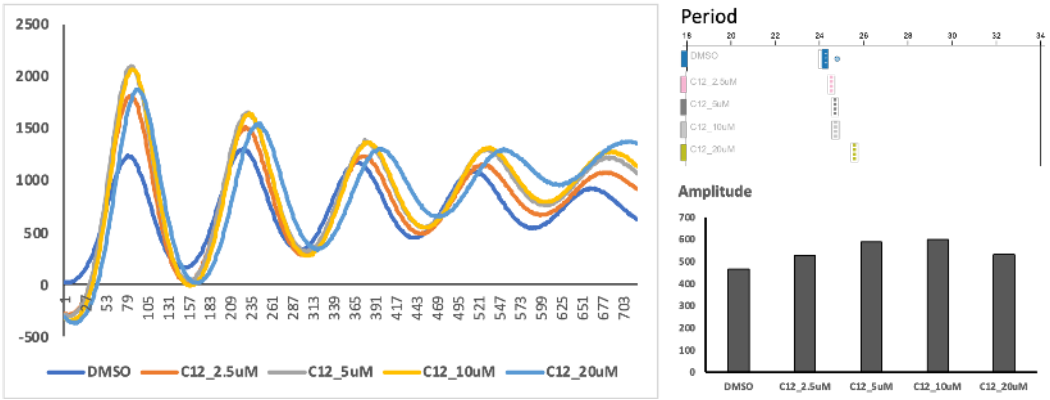
Period
Amplitude
DMSO
C12_2.5uM
C12_5uM
C12_10uM
C12_20uM

E2

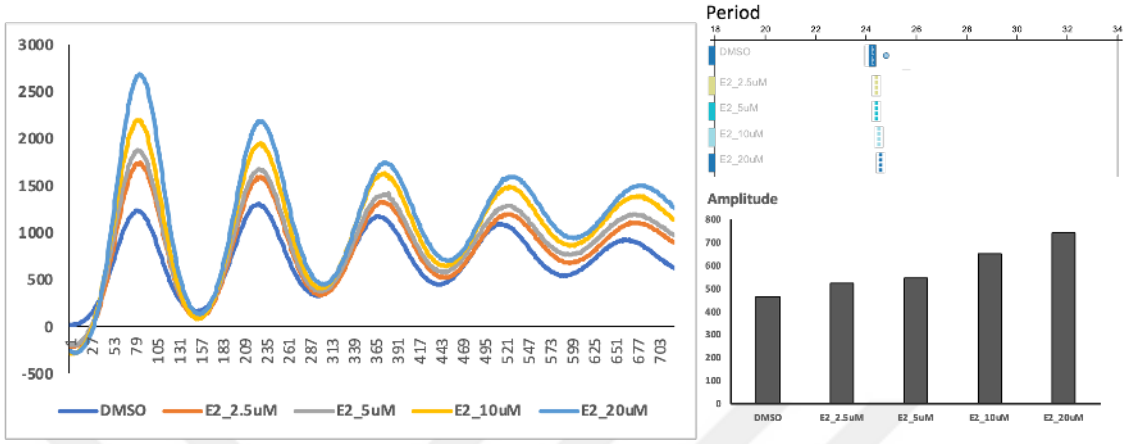
3000
2500
2000
1500
1000
500
0
-500
1
27
53
79
105
131
157
183
209
235
261
287
313
339
365
391
417
443
469
495
521
547
573
599
625
651
677
703
DMSO
E2_2.5uM
E2_5uM
E2_10uM
E2_20uM
Period
18
20
22
24
26
28
30
32
34
DMSO
E2_2.5uM
E2_5uM
E2_10uM
E2_20uM
Amplitude
800
700
600
500
400
300
200
100
0
DMSO
E2_2.5uM
E2_5uM
E2_10uM
E2_20uM

APPENDIX E: Permissions to Reproduce Figures

Generation of a Novel Allelic Series of Cryptochrome Mutants via Mutagenesis Reveals Residues Involved in Protein-Protein Interaction and CRY2-Specific Repression

Author:

Ellena V. McCarthy, Julie E. Baggs, Jeanne M. Geskes, et al

Publication:

Molecular and Cellular Biology

Publisher:

Taylor & Francis

Date:

Mar 21, 2023

Thesis/Dissertation Reuse Request

Taylor & Francis is pleased to offer reuses of its content for a thesis or dissertation free of charge contingent on resubmission of permission request if work is published.

An evolutionary hotspot defines functional differences between CRYPTOCHROMES

Author:

Clark Rosensweig et al

Publication:

Nature Communications

Publisher:

Springer Nature

Date:

Mar 19, 2018

SPRINGER NATURE LICENSE
TERMS AND CONDITIONS

Jan 10, 2025

This Agreement between Onur OZCAN ("You") and Springer Nature ("Springer Nature") consists of your license details and the terms and conditions provided by Springer Nature and Copyright Clearance Center.

License Number	5945290127306
License date	Jan 10, 2025
Licensed Content Publisher	Springer Nature
Licensed Content Publication	Nature
Licensed Content Title	Peroxiredoxins are conserved markers of circadian rhythms
Licensed Content Author	Rachel S. Edgar et al
Licensed Content Date	May 16, 2012
Type of Use	Thesis/Dissertation
Requestor type	academic/university or research institute
Format	print and electronic
Portion	figures/tables/illustrations
Number of figures/tables/illustrations	1
Would you like a high resolution image with your order?	no
Will you be translating?	no
Circulation/distribution	1 - 29
Author of this Springer Nature content	no
Title of new work	Allosteric Regulation and Functional Dynamics of CRY1 in the Mammalian Circadian Clock: Insights from Mutational and Small Molecule Interactions
Institution name	Koc University
Expected presentation date	Jan 2025
Portions	Figure 6
The Requesting Person / Organization to Appear on the License	Onur OZCAN
Requestor Location	Mr. Onur Ozcan Koc University Istanbul, 34440 Turkey
Billing Type	Invoice
Billing Address	Mr. Onur Ozcan Koc University Istanbul, Turkey 34440
Total	0.00 USD

Structure, function, and mechanism of the core circadian clock in cyanobacteria

Author:
Jeffrey A. Swan,Susan S. Golden,Andy LiWang,Carrie L. Partch
Publication:
Journal of Biological Chemistry
Publisher:
Elsevier
Date:
6 April 2018

OXFORD UNIVERSITY PRESS LICENSE
TERMS AND CONDITIONS

Jan 10, 2025

This Agreement between Onur OZCAN ("You") and Oxford University Press ("Oxford University Press") consists of your license details and the terms and conditions provided by Oxford University Press and Copyright Clearance Center.

License Number	5945290827817
License date	Jan 10, 2025
Licensed content publisher	Oxford University Press
Licensed content publication	FEMS Microbiology Reviews
Licensed content title	The circadian clock of *Neurospora crassa*
Licensed content author	Baker, Christopher L.; Loros, Jennifer J.
Licensed content date	Jan 1, 2012
Type of Use	Thesis/Dissertation
Institution name	
Title of your work	Allosteric Regulation and Functional Dynamics of CRY1 in the Mammalian Circadian Clock: Insights from Mutational and Small Molecule Interactions
Publisher of your work	Koc University
Expected publication date	Jan 2025
Permissions cost	0.00 USD
Value added tax	0.00 USD
Total	0.00 USD
Title of new work	Allosteric Regulation and Functional Dynamics of CRY1 in the Mammalian Circadian Clock: Insights from Mutational and Small Molecule Interactions
Institution name	Koc University
Expected presentation date	Jan 2025
Portions	Figure 1
The Requesting Person / Organization to Appear on the License	Onur OZCAN
Requestor Location	Mr. Onur Ozcan Koc University Istanbul, 34440 Turkey
Publisher Tax ID	GB125506730
Billing Type	Invoice
Billing Address	Mr. Onur Ozcan Koc University Istanbul, Turkey 34440
Total	0.00 USD

SPRINGER NATURE LICENSE
TERMS AND CONDITIONS

Jan 10, 2025

This Agreement between Onur OZCAN ("You") and Springer Nature ("Springer Nature") consists of your license details and the terms and conditions provided by Springer Nature and Copyright Clearance Center.

License Number	5945291030257
License date	Jan 10, 2025
Licensed Content Publisher	Springer Nature
Licensed Content Publication	Nature
Licensed Content Title	Photosynthetic entrainment of the Arabidopsis thaliana circadian clock
Licensed Content Author	Michael J. Haydon et al
Licensed Content Date	Oct 23, 2013
Type of Use	Thesis/Dissertation
Requestor type	academic/university or research institute
Format	print and electronic
Portion	figures/tables/illustrations
Number of figures/tables/illustrations	1
Would you like a high resolution image with your order?	no
Will you be translating?	no
Circulation/distribution	1 - 29
Author of this Springer Nature content	no
Title of new work	Allosteric Regulation and Functional Dynamics of CRY1 in the Mammalian Circadian Clock: Insights from Mutational and Small Molecule Interactions
Institution name	Koc University
Expected presentation date	Jan 2025
Portions	Extended Data Figure 1
The Requesting Person / Organization to Appear on the License	Onur OZCAN
Requestor Location	Mr. Onur Ozcan Koc University Istanbul, 34440 Turkey
Billing Type	Invoice
Billing Address	Mr. Onur Ozcan Koc University Istanbul, Turkey 34440
Total	0.00 USD

OXFORD UNIVERSITY PRESS LICENSE
TERMS AND CONDITIONS

Jan 10, 2025

This Agreement between Onur OZCAN ("You") and Oxford University Press ("Oxford University Press") consists of your license details and the terms and conditions provided by Oxford University Press and Copyright Clearance Center.

License Number	5945330627615
License date	Jan 10, 2025
Licensed content publisher	Oxford University Press
Licensed content publication	Genetics
Licensed content title	Circadian Rhythms and Sleep in *Drosophila melanogaster*
Licensed content author	Dubowy, Christine; Sehgal, Amita
Licensed content date	Apr 1, 2017
Type of Use	Thesis/Dissertation
Institution name	
Title of your work	Allosteric Regulation and Functional Dynamics of CRY1 in the Mammalian Circadian Clock: Insights from Mutational and Small Molecule Interactions
Publisher of your work	Koc University
Expected publication date	Jan 2025
Permissions cost	0.00 USD
Value added tax	0.00 USD
Total	0.00 USD
Title of new work	Allosteric Regulation and Functional Dynamics of CRY1 in the Mammalian Circadian Clock: Insights from Mutational and Small Molecule Interactions
Institution name	Koc University
Expected presentation date	Jan 2025
Portions	Figure 2
The Requesting Person / Organization to Appear on the License	Onur OZCAN Mr. Onur Ozcan Koc University
Requestor Location	Istanbul, 34440 Turkey
Publisher Tax ID	GB125506730
Billing Type	Invoice
Billing Address	Mr. Onur Ozcan Koc University Istanbul, Turkey 34440
Total	0.00 USD

ELSEVIER LICENSE
TERMS AND CONDITIONS

Jan 10, 2025

This Agreement between Onur OZCAN ("You") and Elsevier ("Elsevier") consists of your license details and the terms and conditions provided by Elsevier and Copyright Clearance Center.

License Number	5945340413247
License date	Jan 10, 2025
Licensed Content Publisher	Elsevier
Licensed Content Publication	Elsevier Books
Licensed Content Title	Advances in Protein Chemistry and Structural Biology
Licensed Content Author	Ibrahim Baris,Onur Ozcan,Ibrahim Halil Kavakli
Licensed Content Date	Jan 1, 2023
Licensed Content Pages	21
Start Page	17
End Page	37
Type of Use	reuse in a thesis/dissertation
Portion	full chapter
Circulation	5
Format	both print and electronic
Are you the author of this Elsevier chapter?	Yes
How many pages did you author in this Elsevier book?	20
Will you be translating?	No
Title of new work	Allosteric Regulation and Functional Dynamics of CRY1 in the Mammalian Circadian Clock: Insights from Mutational and Small Molecule Interactions
Institution name	Koc University
Expected presentation date	Jan 2025
The Requesting Person / Organization to Appear on the License	Onur OZCAN
Requestor Location	Mr. Onur Ozcan Koc University Istanbul, 34440 Turkey
Publisher Tax ID	GB 494 6272 12
Total	0.00 USD

The Arg-293 of Cryptochrome1 is responsible for the allosteric regulation of CLOCK-CRY1 binding in circadian rhythm

Author:
Seref Gul,Cihan Aydin,Onur Ozcan,Berke Gurkan,Saliha Surme,Ibrahim Baris,Ibrahim Halil Kavakli
Publication:
Journal of Biological Chemistry
Publisher:
Elsevier
Date:
11 December 2020

ELSEVIER LICENSE
TERMS AND CONDITIONS

Jan 10, 2025

This Agreement between Onur OZCAN ("You") and Elsevier ("Elsevier") consists of your license details and the terms and conditions provided by Elsevier and Copyright Clearance Center.

License Number	5945341203158
License date	Jan 10, 2025
Licensed Content Publisher	Elsevier
Licensed Content Publication	Elsevier Books
Licensed Content Title	Computer Aided Chemical Engineering
Licensed Content Author	Onur Ozcan,Seref Gul,Ibrahim Halil Kavakli
Licensed Content Date	Jan 1, 2021
Licensed Content Pages	7
Start Page	2025
End Page	2031
Type of Use	reuse in a thesis/dissertation
Portion	full chapter
Circulation	5
Format	both print and electronic
Are you the author of this Elsevier chapter?	Yes
How many pages did you author in this Elsevier book?	6
Will you be translating?	No
Title of new work	Allosteric Regulation and Functional Dynamics of CRY1 in the Mammalian Circadian Clock: Insights from Mutational and Small Molecule Interactions
Institution name	Koc University
Expected presentation date	Jan 2025
The Requesting Person / Organization to Appear on the License	Onur OZCAN
Requestor Location	Mr. Onur Ozcan Koc University Istanbul, 34440 Turkey
Publisher Tax ID	GB 494 6272 12
Total	0.00 USD

Dynamic regulation of the serine loop by distant mutations reveals allostery in cryptochrome1

OHN WILEY AND SONS LICENSE
TERMS AND CONDITIONS

Jan 16, 2025

This Agreement between Onur OZCAN ("You") and John Wiley and Sons ("John Wiley and Sons") consists of your license details and the terms and conditions provided by John Wiley and Sons and Copyright Clearance Center.

License Number	5951101353045
License date	Jan 16, 2025
Licensed Content Publisher	John Wiley and Sons
Licensed Content Publication	FEBS Journal
Licensed Content Title	CRY1-CBS binding regulates circadian clock function and metabolism
Licensed Content Author	Sibel Cal-Kayitmazbatir, Eylem Kulkoyluoglu-Cotul, Jacqueline Growe, et al
Licensed Content Date	Jun 9, 2020
Licensed Content Volume	288
Licensed Content Issue	2
Licensed Content Pages	26
Type of use	Dissertation/Thesis
Requestor type	University/Academic
Format	Electronic
Portion	Figure/table
Number of figures/tables	1
Will you be translating?	No
Title of new work	Allosteric Regulation and Functional Dynamics of CRY1 in the Mammalian Circadian Clock: Insights from Mutational and Small Molecule Interactions
Institution name	Koc University
Expected presentation date	Jan 2025
Portions	Figure 5
The Requesting Person / Organization to Appear on the License	Onur OZCAN Mr. Onur Ozcan Koc University
Requestor Location	 Istanbul, 34440 Turkey
Publisher Tax ID	EU826007151
Total	0.00 USD

ELSEVIER LICENSE
TERMS AND CONDITIONS

Jan 17, 2025

This Agreement between Onur OZCAN ("You") and Elsevier ("Elsevier") consists of your license details and the terms and conditions provided by Elsevier and Copyright Clearance Center.

License Number	5951521276477
License date	Jan 17, 2025
Licensed Content Publisher	Elsevier
Licensed Content Publication	Cell Chemical Biology
Licensed Content Title	Metabolic and chemical architecture of the mammalian circadian clock
Licensed Content Author	Isara Laothamatas,Emil Sjulstok Rasmussen,Carla B. Green,Joseph S. Takahashi
Licensed Content Date	Sep 21, 2023
Licensed Content Volume	30
Licensed Content Issue	9
Licensed Content Pages	20
Start Page	1033
End Page	1052
Type of Use	reuse in a thesis/dissertation
Portion	figures/tables/illustrations
Number of figures/tables/illustrations	1
Format	electronic
Are you the author of this Elsevier article?	No
Will you be translating?	No
Title of new work	Allosteric Regulation and Functional Dynamics of CRY1 in the Mammalian Circadian Clock: Insights from Mutational and Small Molecule Interactions
Institution name	Koc University
Expected presentation date	Jan 2025
Portions	Figure 1
The Requesting Person / Organization to Appear on the License	Onur OZCAN
Requestor Location	Mr. Onur Ozcan Koc University Istanbul, 34440 Turkey
Publisher Tax ID	GB 494 6272 12
Total	0.00 USD
Terms and Conditions	

SPRINGER NATURE LICENSE
TERMS AND CONDITIONS

Jan 18, 2025

This Agreement between Onur OZCAN ("You") and Springer Nature ("Springer Nature") consists of your license details and the terms and conditions provided by Springer Nature and Copyright Clearance Center.

License Number	5951980663898
License date	Jan 18, 2025
Licensed Content Publisher	Springer Nature
Licensed Content Publication	Nature Reviews Genetics
Licensed Content Title	Transcriptional architecture of the mammalian circadian clock
Licensed Content Author	Joseph S. Takahashi
Licensed Content Date	Dec 19, 2016
Type of Use	Thesis/Dissertation
Requestor type	academic/university or research institute
Format	electronic
Portion	figures/tables/illustrations
Number of figures/tables/illustrations	1
Would you like a high resolution image with your order?	no
Will you be translating?	no
Circulation/distribution	1 - 29
Author of this Springer Nature content	no
Title of new work	Allosteric Regulation and Functional Dynamics of CRY1 in the Mammalian Circadian Clock: Insights from Mutational and Small Molecule Interactions
Institution name	Koc University
Expected presentation date	Jan 2025
Portions	Figure 1
The Requesting Person / Organization to Appear on the License	Onur OZCAN
Requestor Location	Mr. Onur Ozcan Koc University Istanbul, 34440 Turkey
Billing Type	Invoice
Billing Address	Mr. Onur Ozcan Koc University Istanbul, Turkey 34440
Total	0.00 USD

Terms and Conditions